Understanding the subcellular regulation of the NLRP3 inflammasome and IL-1α

A thesis submitted to the University of Manchester for the degree of Doctor of Philosophy in the Faculty of Biology, Medicine, and Health

2023

Rose Wellens

School of Biological Sciences

Table of contents

Word Count: 45,015

List of figures

List of tables

Abbreviations

AIM2	Absent in Melanoma 2
ALR	AIM2-like receptor
ASC	Apoptosis-associated speck-like protein containing a CARD
ATP	Adenosine Triphosphate
BMDMs	Bone Marrow-Derived Macrophages
Ca2+	Calcium
CAPS	Cryopyrin-associated periodic syndromes
CARD	Caspase recruitment domain
cGAS	Cyclic GMP-AMP synthase
CLIC	Cl- channel intracellular protein
CLRs	C-type lectin receptors
CRISPR-Cas9	Clustered Regularly Interspaced Short Palindromic Repeats/CRISPR-associated protein 9
dA:dT	Double-stranded DNA composed of deoxyadenosine and deoxythymidine
DAMP	Damage-associated molecular pattern
DAPI	4',6-Diamidino-2-Phenylindole, Dihydrochloride
DMEM	Dulbecco's Modified Eagle Medium
DMSO	Dimethyl Sulfoxide
DNA	Deoxyribose nucleic acid
dTGN	Dispersed trans-Golgi network
EEA1	Early endosome antigen 1
ER	Endoplasmic reticulum
FBS	Foetal bovine serum
FISNA	FIIND and NACHT associated
GBPs	Guanylate-binding proteins
GCN5	General control of amino acid synthesis protein 5
gDNA	Genomic DNA
GO	Gene ontology
GSDMD	Gasdermin D

$GSDMD^{NT}$	Gasdermin-D N-terminal fragment
HAT	Histone acetyltransferase
HAX-1	HCLS1-associated protein X-1
HDAC6	Histone deacetylase 6
HRP	Horseradish peroxidase
HS1	Hematopoietic lineage cell-specific protein-1
HSV-1	Herpes simplex virus type 1
ICC	Immunocytochemistry
ICE	Inference of CRISPR Edits
IFNs	Interferons
IKKβ	Inhibitor of nuclear factor kappa-B kinase subunit beta
IL-1	Interleukin-1
IL-18	Interleukin-18
IL-1R1	Interleukin-1 receptor type 1
IL-1α	Interleukin-1 alpha
IL-1β	Interleukin-1 beta
INV	Intracellular nanovesicle
IP3	Inositol 1,4,5-trisphosphate
IP3R	IP3 receptor
IPA	Ingenuity pathway analysis
K+	Potassium
KD	Knockdown
KO	Knockout
LAMP1	Lysosomal-associated membrane protein 1
LDH	Lactate dehydrogenase
Lenti-HEK	Lentivirus-transduced Human Embryonic Kidney cell line
LeuLeu-OMe	Leu-Leu methyl ester
LPS	Lipopolysaccharide
LPS	Lipopolysaccharide
LRRC8A	Leucine-rich repeat-containing protein 8A
MAC	Membrane attack complex

MAMs	Mitochondrial-associated membranes
MARK4	Microtubule-affinity regulating kinase 4
MAVS	Mitochondrial antiviral signalling protein
mL	Millilitre
mM	Millimolar
MSU	Monosodium urate
mtDNA	Mitochondrial DNA
MTOC	Microtubule organizing centre
mtROS	Mitochondrial reactive oxygen species
Na+	Sodium
NEK7	NIMA Related Kinase 7.
NETs	Neutrophil extracellular traps
NF-κB	Nuclear factor kappa-light-chain-enhancer of activated B cells
NINJ1	Ninjurin-1
NLR	NOD-like receptor
NLRC4	NLR family CARD domain-containing protein 4
NLRP3	NOD-like receptor family, pyrin domain-containing protein 3
NLR	Nucleotide-binding oligomerization domain-like receptor
NLS	Nuclear localization sequence
oxPAPC	Oxidized phospholipid 1-palmitoyl-2-arachidonoyl-sn-glycero-3-phosphorylcholine
PAMP	Pathogen-associated molecular pattern
PAO	Phenyl Arsine Oxide
PBS	Phosphate-buffered saline
PCAF	P300/CBP-associated factor
PCC	Pearson's correlation coefficient
PCR	Polymerase Chain Reaction
PI	Phosphoinositide
PI4K	Phosphatidylinositol 4-kinase
PI4P	Phosphatidylinositol 4-phosphate
PIP2	Phosphatidylinositol 4,5-bisphosphate

PKD	Protein kinase D
PKD2	Polycystic kidney disease-2/polycystin-2
PMA	Phorbol 12-myristate 13-acetate
pMD2.G	Envelope plasmid for lentivirus production
PMR	Plasma membrane rupture
Pro-IL-1α	Pro-interleukin-1 alpha
PRR	Pattern recognition receptor
psPAX2	Packaging plasmid for lentivirus production
PYD	Pyrin domain
RIG-I	Retinoic acid-inducible gene I
ROS	Reactive oxygen species
RPMI-1640	Roswell Park Memorial Institute 1640
RVD	Regulatory volume decrease
SASP	Senescence-associated secretory phenotype
SCAP-SREBP2	Sterol regulatory element-binding protein 2
sgRNA	Single guide RNA
STING	Stimulator of interferon genes
Tf	Transferrin
TfR	Transferrin receptor
TGN	Trans-Golgi network
TGN46	Trans-Golgi Network Integral Membrane Protein 2
THP-1	Human acute monocytic leukaemia cell line
TLR	Toll-like receptor
UPR	Unfolded protein response
VRAC	Volume regulated anion channel
WB	Western blot
µg	Microgram
µl	Microliter
µM	Micromolar

Abstract

NLRP3 inflammasome activation and subsequent inflammation is an essential line of defence to protect against infectious organisms or other potential threats to the host. However, NLRP3 inflammasome activation can contribute to the chronic inflammation observed in disease. The NLRP3 inflammasome indirectly regulates the activation of the pro-inflammatory cytokine IL-1α, which is a key player in driving harmful inflammation. Therefore, the activation of the NLRP3 inflammasome and IL-1α must be tightly regulated to avoid disease. IL-1α is produced in a precursor form (pro-IL-1α), with a highly conserved pro-domain and nuclear localisation sequence (NLS). Therefore, pro-IL-1α is thought to have an intracellular function, in addition to its secreted pro-inflammatory role. The aim of this thesis was to investigate the subcellular regulation of the NLRP3 inflammasome and pro-IL-1α. Firstly, this thesis reports that NLRP3-activating stimuli cause a disruption in endocytic traffic. It characterises the subcellular localisation of NLRP3 with respect to organelles involved in endocytic traffic and suggests that localisation of NLRP3 to endolysosomal compartments containing the phosphatidylinositol, PI4P, may be an important common step in activation of the NLRP3 inflammasome. Additionally, this research reveals a protein interactome for NLRP3, highlighting novel interactors of NLRP3 that are involved in endocytic trafficking. This study suggests that the trafficking protein TPD54, interacts with NLRP3 following nigericin stimulation, and genetic deletion of TPD54 in a THP-1 monocyte cell line potentiates NLRP3 inflammasome activation. These data suggest that a disruption in endocytic traffic may be a common cellular event in the activation of the NLRP3 inflammasome. This thesis also characterises the pro-IL-1α interactome, and through bioinformatic analysis suggests a novel role of pro-IL-1α inside the cell. The interaction of pro-IL-1α with histone acetyltransferase

proteins may point to the intracellular function of pro-IL-1α. These findings build on our current understanding of the subcellular regulation of the NLRP3 inflammasome and IL-1α. Developing this work further will allow greater insight into the fundamental biology of inflammation and may prove beneficial in identifying new targets for the treatment of inflammatory disease.

Declaration

I declare that no portion of the work referred to in the thesis has been submitted in support of an application for another degree or qualification of this or any other university or other institute of learning.

Copyright statement

1 The author of this thesis (including any appendices and/or schedules to this thesis) owns certain copyright or related rights in it (the "Copyright") and they have given the University of Manchester certain rights to use such Copyright, including for administrative purposes.

2 Copies of this thesis, either in full or in extracts and whether in hard or electronic copy, may be made only in accordance with the Copyright, Designs and Patents Act 1988 (as amended) and regulations issued under it or, where appropriate, in accordance with licensing agreements which the University has from time to time. This page must form part of any such copies made.

3 The ownership of certain Copyright, patents, designs, trademarks and other intellectual property (the "Intellectual Property") and any reproductions of copyright works in the thesis, for example graphs and tables ("Reproductions"), which may be described in this thesis, may not be owned by the author and may be owned by third parties. Such Intellectual Property and Reproductions cannot and must not be made available for use without the prior written permission of the owner(s) of the relevant Intellectual Property and/or Reproductions

4 Further information on the conditions under which disclosure, publication and commercialisation of this thesis, the Copyright and any Intellectual Property and/or Reproductions described in it may take place is available in the University IP Policy (see http://documents.manchester.ac.uk/DocuInfo.aspx?DocID=2442 0), in any relevant Thesis restriction declarations deposited in the University Library, the University Library's regulations (see http://www.library.manchester.ac.uk/about/regulations/) and in the University's policy on Presentation of Theses.

Acknowledgements

During the writing of this thesis there have been many parts that I have found challenging, but to do justice to the wonderful people who have supported me throughout these past three years is the greatest challenge of all. I would like to begin by thanking my primary supervisor, David Brough, not only for giving me this amazing opportunity but for being a voice of calm throughout this crazy journey. It goes without saying that none of us anticipated the storm that was ahead at the start of the Covid-19 pandemic, but during this time, Dave led with kindness and compassion and for that I am truly grateful. Dave is a fantastic researcher with an incredible vision for how experiments can come together to form exciting and important stories. But it is also his vision in the people he chooses to be part of his lab that I am so thankful for; the Brough lab has been the most amazing working and social environment to be part of and I would be lost without everyone in it. I would also like to thank the rest of my co-supervisory team Jack Green, Gloria López-Castejón, Martin Lowe and Stuart Allan for their invaluable contributions and direction throughout my PhD.

I would like to thank my funders, The British Heart Foundation, for allowing me to do this PhD and for the amazing work they do in funding important and necessary research.

A super special thanks goes out to my supervisors, counsellors, sounding boards and friends: Jack, Paula, Chris, Sarah, and Victor. As they say, it takes a village to raise a PhD student and their guidance, thoughtfulness and humour has carried me throughout these three years. An extra super special thanks must go to Jack Green, who had the absolute pleasure (his words not mine) of training and supporting me throughout. Jack, it is safe to say that without you these past three years would have been a lot more stressful and a lot less fun, thank you for

always being the voice of reason. Whether it's as a PI or not, you are all going to be such wonderful leaders and role models to the people you supervise in the future, and I'm very lucky to have been one of them.

Thank you to the incredible PhD students that make up the Brough lab, Billie, Tara, Grace, and Susie. At the start of my PhD, the pandemic had knocked us all sideways and naturally we were all a little weary from the trials that lockdown had brought. But when you guys arrived shortly after, without even knowing you breathed new life back into the lab with your gorgeous personalities and positive attitudes. Thank you for all our chats from science to menstrual cycles; I'm so very grateful for you all and wish you all the luck in the future, PhD and beyond.

I would like to thank everyone in the Brain Inflammation Group. BIG is an environment that knows how to get the best out of everyone and instils in each person that the highest quality work must be met with an even higher quality of fun. I'm beyond grateful to be able to come to AV Hill every day and be at work with my friends. Mary, Jill, Alba and Will, wow I am so lucky to have you all. I knew I would get a lot out of doing this PhD but to have gained four incredible friends that bring me so much joy is a bigger prize than any.

I would also like to thank my incredible friends in the magical land outside of AV Hill. Tess and Nella, thank you for your support through the start of my PhD and in lockdown, and for listening to my ramblings about the NLRP3 (Nella Learns Rose's Project 3) inflammasome. To Eve, Jose, and Tara, I'm pretty sure that you guys made me think science was cool, so thank you. We are bonded by our foot brains/cauliflowers forever no matter where in the world we

all are. Thank you to my oldest friends, Becky, Will, Ev and Elise for your unwavering friendship. I treasure you all so much and am so privileged have you in my life.

My final thanks go to my mum, dad, Tom, and Sophie. You have had the unenviable task of keeping me on the straight and narrow and dealing with my wobbles throughout the past three years. I'm so grateful for our little team and the constant support and love that you give to me. LIAV.

I would like to dedicate this thesis to my niece Lily who has brought an immeasurable amount of light to my life. By the time you're old enough to read this properly, these flashy illustrator figures will probably look a bit old and dusty, but at least I hope that you think your auntie Rose was pretty cool for doing a PhD!

Chapter 1:

General Introduction

Chapter 1. General Introduction

1.1 Inflammation

Inflammation is a host's primary response to microbial infection or tissue damage. Inflammation is typically a protective response that initiates the process of pathogen clearance and tissue repair and is characterised by vasodilation and permeation of the vascular endothelium, recruitment and activation of immune cells and the release of cytotoxic compounds to fight infection and clear debris. A controlled inflammatory response results in removal of detrimental stimuli and the restoration of homeostatic repair mechanisms, protecting against further infection or injury. Insufficient inflammation, however, can result in persistent unresolved infection, whilst excessive or dysregulated inflammation contributes to multiple chronic inflammatory diseases. Therefore, it is important that the signalling mechanisms that contribute to the overall inflammatory response are tightly regulated to avoid disease. Here, I will review the literature regarding subcellular inflammatory signalling mechanisms, providing particular focus on the regulation of inflammation by the canonical NLRP3 inflammasome. I will also review the current understanding of the inflammatory protein interleukin (IL)-1α and discuss its potential nuclear role in addition to its characterised function as a secreted, pro-inflammatory cytokine.

1.2 The inflammatory response

Inflammation is a response of the innate immune system to protect against damage, injury, or infection. The innate immune response occurs rapidly upon detection of non-specific patterns found either on pathogenic organisms (pathogen-associated molecular patterns; PAMPs) or expelled from damaged or stressed cells (damage-associated molecular patterns;

DAMPs), examples of which include lipopolysaccharide (LPS) and extracellular adenosine triphosphate (ATP), respectively. PAMPs and DAMPs are detected by pattern recognition receptors (PRRs), expressed by virtually all cell types, immune cells of which include blood-circulating monocytes and tissue-resident macrophages (Janeway and Medzhitov, 2002).

Currently, five classes of PRR have been identified which can be broadly categorised into two main groups: membrane-bound receptors and unbound intracellular receptors (Brubaker et al., 2015). Toll-like receptors (TLRs) and C-type lectin receptors (CLRs) are membrane-bound and are located either at the plasma membrane or on intracellular compartments such as endosomes (Kumar et al., 2011). Nucleotide-binding oligomerisation domain-like receptors (NLRs), retinoic acid-inducible gene (Grossman et al.)-I-like receptors (RLRs) and absent in melanoma (AIM)2-like receptors (ALRs) are free in the cytoplasm and recognise intracellular PAMPs and DAMPs (Schroder and Tschopp, 2010). Once activated, PRRs initiate a series of downstream signalling cascades including the production and release of inflammatory cytokines and chemokines that play a pivotal role in antimicrobial and inflammatory responses (Chen and Nunez, 2010). A diverse range of PRRs evolved to allow appropriate response to many different threats invoked by pathogens and other types of cellular stress (Mushegian and Medzhitov, 2001).

1.3 Sterile inflammation

The inflammatory response evolved as a mechanism to protect against microbial infection and disease. However, inflammation can occur in the absence of a foreign, infectious agent and in response to sterile stimuli such as amyloid beta, cholesterol crystals and DNA (Chen and Nunez, 2010). The response to sterile threats and associated chronic sterile inflammation

is suggested to be a fallout of Western lifestyle and increased lifespan (Furman et al., 2019, Christ et al., 2019). Mounting an immune response to sterile signs of danger and damage allows the innate immune system to respond quickly to resolve infection or damage without having to identify a specific threat (Rock et al., 2010). However, this represents a paradox for innate immunity. Mounting an inappropriate innate immune response to sterile stimuli can lead to extensive tissue damage and injury to the surrounding tissue (Brough et al., 2015). Therefore, the initiation of sterile inflammation can be extremely dangerous and is implicated in pathogenesis of major non-communicable diseases including stroke, Alzheimer's disease, diabetes, atherosclerosis and cancer (Denes et al., 2011; Weiner et al., 2006; Boni-Schnetzler et al., 2008; Ridker et al., 2017; Coussens et al., 2002). Non-communicable diseases such as these contribute to the majority of mortality and disability worldwide (GBD, 2019), therefore it is of great importance to understand the cellular mechanisms that drive the sterile inflammatory response.

1.4 IL-1 signalling

There has been a wealth of research regarding the mechanisms that initiate and propagate sterile inflammatory responses. The IL-1 family of cytokines are key drivers of sterile inflammation. IL-1α and IL-1β are pro-inflammatory members of the IL-1 family and blockade of their signalling has demonstrated the crucial role of IL-1 in a number of inflammatory and non-communicable diseases (Lukens et al., 2012). IL-1α and IL-1β both bind independently to the type I IL-1 receptor (IL-1R1), which is ubiquitously expressed on immune and non-immune cell types (REF). IL-1 receptor antagonist (IL-1Ra) is the third specific ligand for IL-1R1 and binds with similar affinity as the IL-1 cytokines but blocks downstream signal transduction (Dunn et al., 2001; Schreuder et al., 1997). Binding of IL-1α or IL-1β to their receptor results

in a ligand-induced conformational change of the IL-1R1 and allows its association with the IL-1 receptor accessory protein (IL-1RAcP) (Wesche et al., 1997). Via conserved cytosolic Toll- and IL-1R-like (TIR) domains, the IL-1 receptor complex quickly recruits two intracellular signalling proteins, myeloid differentiation primary response gene 88 (MYD88) and interleukin-1 receptor–activated protein kinase (IRAK) 4 (Li et al., 2002; Brikos et al., 2007). The IL-1, IL-1R1, IL-RAcP, MYD88, and IRAK4 complex form a stable cytokine induced signalling unit, and following its assembly, IRAK4 self phosphorylates and subsequently phosphorylates IRAK1 and IRAK2, leading to recruitment and oligomerisation of tumour necrosis factor–associated factor (TRAF) 6. IRAK1, IRAK2 and TRAF6 then dissociate from the initial receptor complex and activate downstream signalling via NFκB, as well as p38, c-Jun N-terminal kinases (JNKs), extracellular signal-regulated kinases (ERKs) and mitogen-activated protein kinases (MAPKs) (Dunne et al., 2003).

IL-1 cytokines have been implicated in the pathogenesis of many diseases including stroke, atherosclerosis, type 2 diabetes, and cancer, and blockade of IL-1 signalling has been shown to be beneficial in the treatment of such disease (Gabay et al., 2010). Therapeutically targeting IL-1 began with the use of anakinra, a recombinant form of IL-1Ra, which successfully blocks IL-1α and IL-1β signalling at IL-1R1 (Bresnihan et al., 1998). Anakinra has since been used or is in clinical trails to target multiple diseases including join and muscle disease, type 2 diabetes, stroke and cerebrovascular disease (Sobowale et al., 2016; Emsley et al., 2005; Larsen et al., 2009; Bresnihan et al., 1998). Neutralising IL-1 with antibodies or soluble receptors has also proven effective in the treatment of disease. Canakinumab is an anti-IL-1β monoclonal antibody and played a central role in the CANTOS trail, a seminal paper that lead further research into the role of inflammation in the pathogenesis of cardiovascular

disease (Ridker et al., 2017). These studies highlight that targeting the IL-1 pathway is a promising strategy in the treatment of inflammatory-driven disease.

IL-1α and IL-1β activation is regulated, to varying degrees, by the NLRP3 inflammasome. Inflammasomes are multiprotein complexes that assemble in response to detection of infection- or stress-associated stimuli, of which the NLRP3 inflammasome is the best characterised. Here, I will review our current understanding of the NLRP3 inflammasome and its regulation of inflammatory signalling and cell death.

1.5 Inflammasomes

Canonical inflammasomes are assembled following detection of PAMPs or DAMPs by cytosolic PRRs (Martinon et al., 2002; Lamkanfi and Dixit, 2014). The recognition of PAMPs or DAMPs by PRRs results in the recruitment of the adaptor protein ASC (apoptosis-associated speck-like protein containing a CARD), and pro-caspase 1. Formation of an active inflammasome complex results in the auto-proteolytic activation of caspase-1 which then cleaves the cytokine precursors pro-IL-1β and pro-IL-18, leading to release of their active forms. Caspase-1 also cleaves gasdermin-D (GSDMD) to form a GSDMD N-terminal fragment ($GSDMD^{NT}$) with intrinsic pore-forming abilities (Shi et al., 2015; He et al., 2015). $GSDMD^{NT}$ forms pores within the plasma membrane, which allow the release of small proteins, including IL-1 cytokines, and movement of water and ions (Shi et al., 2015, He et al., 2015). Following GSDMD pore formation, plasma membrane rupture (PMR) is mediated by the clustering of cell surface protein ninjurin1 (NINJ1), facilitating the release of DAMPs and culminating in a rapid inflammatory cell death termed pyroptosis (Kayagaki et al., 2021).

Numerous inflammasome complexes have been defined, including NLR family pyrin domain-containing 1 (NLRP1), NLR family pyrin domain-containing 3 (NLRP3), NLR family CARD domain-containing protein 4 (NLRC4) and AIM2 (Broz and Dixit, 2016) each sensing and reacting to specific inflammatory stimuli. Each inflammasome is named by its associated PRR. The NLRP3 PRR consists of a leucine rich repeat (LRR) domain, NACHT binding domain (NBD) and pyrin domain (PYD) (Figure 1.1). Formation of the NLRP3 inflammasome complex involves association between PYD domains of NLRP3 and ASC, and CARD domains of ASC and pro-caspase-1 (Figure 1.1). The NLRP3 inflammasome is set apart from its fellow inflammasomes due to its well described capability of reacting to a diverse range of PAMPs and DAMPs (Table 1.1); it is suggested that NLRP3 is a broad sensor of cellular stress and dysregulation in homeostasis (Abderrazak et al., 2015).

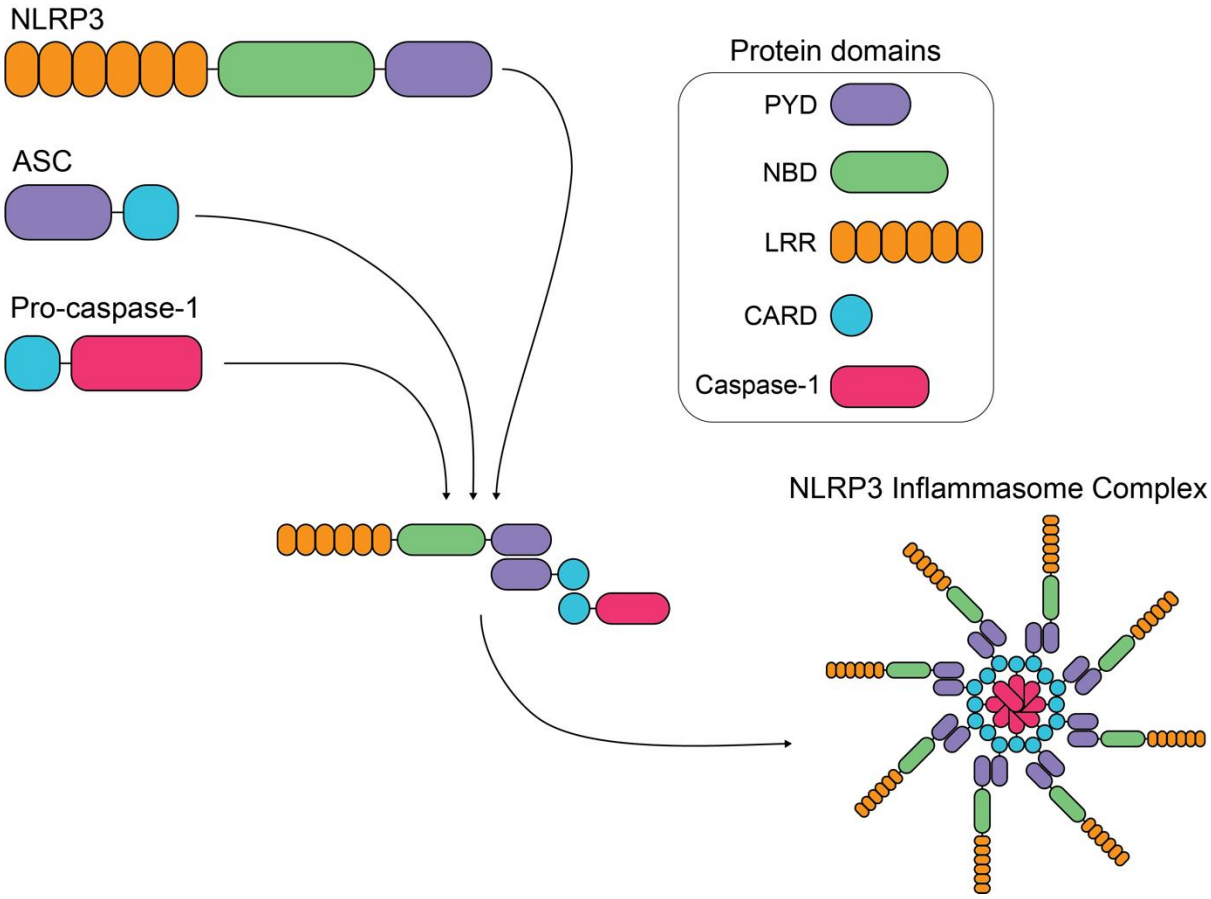

Figure 1.1 Structure of the NLRP3 inflammasome complex. The NLRP3 protein consists of three primary domains: the leucine rich repeat (LRR) domain, NACHT binding domain (NBD) and pyrin domain (PYD). The adaptor protein ASC associates with NLRP3 via their shared pyrin domains and ASC associates with pro-caspase-1 via shared caspase activation and recruitment domains (CARD). Multiple NLRP3-ASC-pro-casapse-1 structures form the NLRP3 inflammasome complex.

1.6 The NLRP3 inflammasome

Multiple pathways of NLRP3 inflammasome activation have been described, which can be broadly categorised into canonical, non-canonical and alternative activation. I will review all mechanisms of NLRP3 inflammasome activation here, although canonical activation of the NLRP3 inflammasome is the key area of focus throughout this thesis and is therefore described in greatest detail.

1.6.1 Priming

Canonical NLRP3 inflammasome activation requires both a priming and activation step to achieve full inflammasome assembly (Figure 1.2). Inflammation must be tightly regulated to avoid an inappropriate response that is damaging to the host, therefore inflammasome priming represents a regulatory step in inflammasome-driven inflammation (Lamkanfi and Dixit, 2014). Inflammasome priming serves two main purposes; (1) to transcriptionally upregulate the inflammasome components NLRP3 and pro-IL-1β, and (2) to stabilise the inflammasome into an auto-supressed yet signal competent state via post-translational modifications. Upregulation of NLRP3 and pro-IL-1β is achieved through activation of the transcription factor NF-κB (Bauernfeind et al., 2011). Experimentally, inflammasome priming is typically achieved through the action of LPS at TLR4. However, NF-κB can also be activated by a range of TLR, NLR or cytokine receptor ligands (Kelley et al., 2019). Endogenous cytokines such as tumour necrosis factor alpha (TNF-α) and IL-1α are alarmins that can act via their respective receptors, TNF receptor (TNFR) and IL-1R1, to engage NF-κB dependent gene expression of NLRP3 and pro-IL-1β (Franchi et al., 2009; Eigenbrod et al., 2008). IL-1β is not constitutively expressed but upon release can initiate priming in a paracrine manner via the IL-1R1 (McKee et al., 2020). In addition, it has been suggested that NF-κB has a functional IL-1β binding site that allows its upregulation via NF-κB signalling, in a regulatory loop that increases pro-IL-1β expression (Hiscott et al., 1993).

1.6.2 Canonical NLRP3 activation

Following transcriptional priming, a second step is required to form the active inflammasome complex to allow cytokine processing and initiation of cell death (Figure 1.2) (Bauernfeind et

al., 2009). Upon activation, multiple proteins have been reported to associate with NLRP3, including kinases NEK7 and IKKβ, which have also been shown to bind to NLRP3 to form part of the active inflammasome complex (He et al., 2016, Shi et al., 2016, Schmacke et al., 2022). The NLRP3 inflammasome is distinct in that its activation is triggered by a diverse range of stimuli (Rahman et al., 2020). These stimuli can be broadly characterised into DAMPs, which include extracellular ATP, cholesterol crystals, or oxidised mitochondrial DNA, and PAMPs which include LPS and bacterial toxins. Given that the NLRP3 inflammasome has such a diverse array of activators, it is unlikely that NLRP3 can sense these stimuli directly; instead, NLRP3 may detect the cellular stress caused by the stimuli (Lamkanfi and Kanneganti, 2010). How this cellular stress leads to NLRP3 activation is a complex and highly studied area of inflammasome research. Disturbances in ion homeostasis have been identified as one such cellular stress that regulates NLRP3 activity (Munoz-Planillo et al., 2013, Murakami et al., 2012, Katsnelson and Dubyak, 2013, Green et al., 2018). NLRP3 is also associated with various subcellular organelles, and therefore it is possible that dysfunction of these organelles might be sensed by NLRP3 (Seoane et al., 2020). These mechanisms ultimately converge on NLRP3 activation, and although they are often discussed separately, it is likely that they are highly integrated with a large degree of crosstalk between them. Thus, it is important to explore the role of each ion and each major cellular organelle that is implicated in NLRP3 regulation.

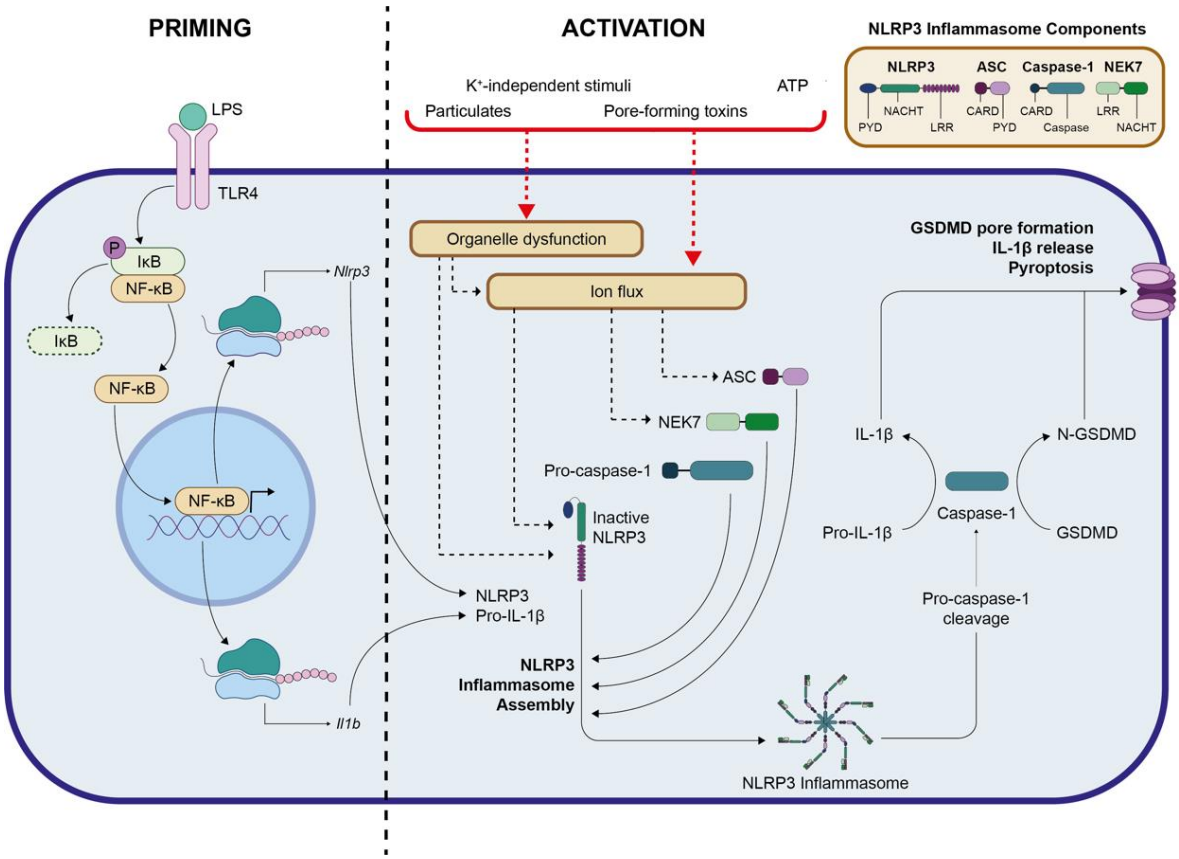

Figure 1.2 Canonical activation of the NLRP3 inflammasome. Priming stimuli such as LPS drive NF-κB-dependent expression of NLRP3 and pro-IL-1β. Following canonical activation stimuli, NLRP3 is activated and forms an active inflammasome complex with ASC, pro-caspase-1, and NEK7. Caspase-1 is then activated, which cleaves pro-IL-1β and pro-IL-18 into their mature forms. Caspase-1 also cleaves gasdermin D (GSDMD), allowing the GSDMD N-terminal fragment (N-GSDMD) to form pores in the membrane and facilitate the release of mature cytokines and pyroptotic cell death.

Table 1.1 Examples of NLRP3 inflammasome activators.

Activator	Source	Example	References
DAMP	Endogenous	ATP, mitochondrial DNA, uric acid crystals, amyloid-β, prion protein	(Perregaux and Gabel, 1994, Nakahira et al., 2011, Martinon et al., 2006, Heneka et al., 2013, Hafner-Bratkovic et al., 2012, Shi et al., 2012)
	Foreign-derived	Silica, imiquimod	(Hornung et al., 2008, Groß et al., 2016)
PAMP	Bacterial	Lipopolysaccharide, nigericin	(Gaidt et al., 2016, Gross et al., 2009)
	Fungal	β-Glucan	(Kankkunen et al., 2010)
	Viral	Double-stranded RNA	(Kanneganti et al., 2006)

1.6.2.1 Ion flux

K^+ efflux

K^+ efflux was identified as a necessary and common downstream signalling event upon which various NLRP3-activating stimuli converged to activate NLRP3 (Munoz-Planillo et al., 2013). This finding was consistent with the identification that many NLRP3-activating stimuli cause a decrease in intracellular K^+ levels, necessary for IL-1β processing. Furthermore, exposing THP1 monocytes and bone marrow-derived macrophages (BMDMs) to low extracellular K^+ is sufficient to trigger NLRP3 activation, whereas high concentrations of extracellular K^+ inhibits NLRP3 (Pétrilli et al., 2007). Gain-of-function mutations in the NLRP3 gene encoding cryopyrin results in a spectrum of rare auto-inflammatory diseases called cryopyrin-associated periodic syndromes (CAPS) (Karasawa et al., 2022, Hoffman et al., 2001). Macrophages that contain the constitutively active CAPS NLRP3 mutant no longer require K^+ efflux for NLRP3 activation

(i.e. are active immediately following priming), and the presence of high extracellular K^+ is insufficient to block NLRP3 activation here, further supporting an upstream role of K^+ efflux in NLRP3 activation (Meng et al., 2009). Despite the identification of K^+ efflux as an important trigger in the activation of NLRP3, the mechanism by which NLRP3 can sense and react to changes in K^+ remains unclear. A recent study has suggested that K^+ efflux induces a structural change in inactive NLRP3 to promote its active, open conformation. This conformational change is facilitated by a flexible linker sequence between the PYD and FISNA domain, which also allows the assembly of $NLRP3^{PYD}$ into a seed structure for ASC oligomerisation (Tapia-Abellan et al., 2021). Although K^+ efflux was accepted as a common downstream signalling event of many NLRP3 activating-stimuli, it may not be an absolute requirement as additional canonical activating stimuli, such as imiquimod, are capable of activating NLRP3 via a mechanism independent of K^+ efflux (Groß et al., 2016). In addition, K^+ efflux-independent stimuli are also described to cause a conformational change in NLRP3, suggesting that this structural mechanism is not exclusive to K^+-dependent activators of NLRP3 (Tapia-Abellan et al., 2021).

Cl^- efflux

Cl^- efflux may also be an important signalling step in the canonical activation of NLRP3. Depletion of extracellular Cl^- enhances ATP-induced IL-1β release in murine and human macrophages (Verhoef et al., 2005). Cl^- channel blockers have been shown to inhibit NLRP3 activation in response to K^+ efflux-dependent stimuli, suggesting a link between Cl^- and K^+ efflux in NLRP3 inflammasome activation (Swanton et al., 2020). WNK1 is a protein kinase that senses low intracellular Cl^-. Following Cl^- efflux, WNK1 phosphorylates downstream

targets leading to activation of cation-Cl^- co-transporters, limiting further Cl^- efflux and attenuating NLRP3 activation as a result (Mayes-Hopfinger et al., 2021).

Cl^- channel intracellular proteins (CLICs) mediate Cl^- efflux and have been shown to be necessary for NLRP3-mediated IL-1β release but dispensable in the activation of NLRC4 or AIM2. CLIC4 deficiency reduces nigericin-induced NLRP3 activation, but in *Clic4*$^{-/-}$ cells, additional knockdown of Clic1 and Clic5 further impedes NLRP3 activation, suggesting that CLIC proteins have redundant functions in NLRP3 inflammasome activation (Tang et al., 2017). A commercially available treatment for coronary heart disease, ticagrelor, has been shown to degrade CLIC proteins and prevent their translocation to the plasma membrane. Here, CLIC protein degradation attenuates Cl^- efflux and hinders ASC oligomerisation and NLRP3 activation in response K^+ efflux-dependent stimuli and particulate activators of NLRP3 (Huang et al., 2021). Cl^- efflux has also been shown to be essential in ASC oligomerisation. However, concomitant K^+ efflux was required for active ASC speck formation, recruitment of caspase-1, cytokine processing and cell death (Green et al., 2018).

Volume regulated anion channels (VRAC) facilitate Cl^- efflux to restore cell volume in response to hypo-osmotic cell swelling and have been suggested to be involved in NLRP3 inflammasome activation. Fenamate non-steroidal anti-inflammatory drugs (NSAIDs) are effective at inhibiting DAMP-mediated NLRP3 inflammasome activation through their ability to inhibit VRAC and limit subsequent Cl^- efflux. Further, numerous VRAC inhibitors have been shown to be effective NLRP3 inhibitors (Swanton et al., 2020, Daniels et al., 2016). However, LRRC8A, the essential subunit of VRAC, is dispensable for canonical NLRP3 inflammasome, except for NLRP3 activation following regulatory volume decrease (RVD). This suggests that

different Cl^- channels coordinate inflammasome activation to different stimuli, or that there may be a redundancy to in Cl^- efflux leading to DAMP-induced NLRP3 inflammasome activation.

Ca^{2+} flux

Ca^{2+} flux is implicated in the activation of the NLRP3 inflammasome (Murakami et al., 2012, Lee et al., 2012). The movement of cellular Ca^{2+} can occur across the plasma membrane or from intracellular endoplasmic reticulum (ER) stores into the cytosol. Mechanisms of Ca^{2+} flux are often linked; when Ca^{2+} channels in the plasma membrane open and Ca^{2+} enters the cell, ER-linked release of Ca^{2+} soon follows and vice versa. Calcium flux was first implicated in IL-1β processing and caspase-1 activation, following P2X7R activation by ATP and the subsequent release of calcium from ER stores (Brough et al., 2003). Ca^{2+} mobilisation from the ER, triggered by inositol 1,4,5-trisphosphate (IP3) interacting with its receptor (IP3R) on the ER has also been suggested to result in NLRP3 activation (Murakami et al., 2012). It is now known that Ca^{2+} and K^+ flux are closely related in the activation of NLRP3. For example, activation of the P2X7R by ATP allows a sustained increase in intracellular Ca^{2+} and subsequent activation of the TWIK2 channel to allow K^+ efflux (Di et al., 2018). K^+ efflux also promotes release of ER-linked intracellular Ca^{2+} stores. Excessive release of ER-stored Ca^{2+} leads to mitochondrial Ca^{2+} overload and release of mitochondrial reactive oxygen species (mtROS), a key indicator of cellular stress and leading to subsequent NLRP3 inflammasome activation. However, there has also been evidence to indicate that NLRP3 activation can occur in a Ca^{2+}-independent manner (Katsnelson and Dubyak, 2013, Baldwin et al., 2017). Although Ca^{2+} flux is suggested to be important in the activation of NLRP3, increasing intracellular Ca^{2+} is neither necessary or sufficient to trigger inflammasome activation and must occur

concomitantly with K^+ efflux or an induction of organelle stress (Munoz-Planillo et al., 2013, Katsnelson et al., 2015).

Na^+ influx

Na^+ influx is also associated with the activation of the NLRP3 inflammasome. Decreasing extracellular Na^+ inhibits K^+-dependent activators of NLRP3 such as nigericin, gramicidin, or K^+-free medium, but fails to block activation induced by ATP or silica (Munoz-Planillo et al., 2013). Phagocytosis of MSU crystals causes acidification of lysosomes and an increase in cytosolic Na^+, resulting in increased osmolarity, passive water influx through aquaporins and subsequent cell swelling. This water influx reduces the relative cytosolic K^+ concentration, leading to NLRP3 activation (Schorn et al., 2011). The Na^+ ionophore monensin causes Na^+ influx but fails to elicit NLRP3 activation alone, illustrating that Na^+ influx alone is insufficient to activate NLRP3 (Munoz-Planillo et al., 2013). However, pre-treatment with monensin sensitized macrophages to the NLRP3 activator imiquimod, driving enhanced inflammasome activation and cytokine secretion (Lee et al., 2023). Here, monensin could disrupt endosomal trafficking and enhancing NLRP3 activation as a result. However, this was only observed with K^+ efflux-independent activators of NLRP3, highlighting a further complexity in the relationship between Na^+ and K^+ flux in NLRP3 activation.

1.6.2.2 Organelle dysfunction

The role of subcellular organelles in NLRP3 inflammasome activation has become an area of increasing interest. Mechanisms underlying how NLRP3 senses and reacts to a dysregulation in typical organelle function and the role of organelles as platforms for inflammasome

activation are major overarching themes in the literature. Here, each main organelle system will be discussed with respect to NLRP3 inflammasome activation.

Lysosomes

The destabilisation of lysosomes and their location with respect to NLRP3 has been strongly implicated in the activation of the inflammasome. Phagocytosis of particulates such as cholesterol crystals, silica, and amyloid-β can activate the NLRP3 inflammasome through destabilisation of the lysosomal membrane and lysosomal rupture, causing subsequent K^+ efflux from the cell (Munoz-Planillo et al., 2013). Lysosomal cathepsin B is released into the cytoplasm following lysosomal destabilisation and is thought to contribute to K^+ efflux, although there is conflicting evidence regarding the role of cathepsins in NLRP3 activation (Hornung et al., 2008, Orlowski et al., 2015). Activation of the cyclic GMP-AMP synthase (cGAS)-STING signalling pathway initiates lysosomal cell death, resulting in K^+ efflux and subsequent activation of NLRP3 (Gaidt et al., 2017). Alzheimer's disease and prion disease are characterised by the accumulation of amyloid-β and Prion protein respectively and have an NLRP3-mediated inflammatory phenotype that has been shown to act through lysosomal destabilisation (Halle et al., 2008, Shi et al., 2012). The proximity of NLRP3 to lysosomal compartments has been shown to be important for NLRP3 activation. NLRP3-activating stimuli cause concomitant accumulation of NLRP3 and phosphatidylinositol 4-phosphate (PI4P) at compartments positive for the lysosomal marker LAMP1 (Lee et al., 2023). In fact, NLRP3 has been suggested to form a complex with the lysosomal regulator complex subunit Lamtor1 and HDAC6 at the lysosomal membrane, with Lamtor1 deficiency resulting in abrogated NLRP3 inflammasome activation (Tsujimoto et al., 2023).

Mitochondria

Mitochondrial dysfunction and the release of mitochondrial species into the cytoplasm have been implicated in the activation of the NLRP3 inflammasome (Holley and Schroder, 2020). NLRP3-activating stimuli, including K^+ efflux-independent stimuli, cause mitochondrial damage and the subsequent accumulation of ROS in the cytoplasm, activating NLRP3 as a result (Groß et al., 2016). Mitochondrial damage, downstream of NLRP3-activating stimuli, can liberate mitochondrial DNA (mtDNA) into the cytosol, promoting NLRP3 activation (Shimada et al., 2012, Zhong et al., 2018). However, it has also been suggested that release of mtDNA occurs because of NLRP3 activation, rather than as a driver of inflammasome activation (Nakahira et al., 2011). Activation of caspase-11 during non-canonical NLRP3 activation results in GSDMD cleavage and insertion of GSDMD pores into the mitochondrial membrane, facilitating mtDNA release and propagating canonical NLRP3 activation (Huang et al., 2020). Mitochondrial positioning may be important for NLRP3 activation. Mitochondria or ER-associated mitochondrial membranes have been suggested as docking sites for NLRP3 and ASC during NLRP3 inflammasome activation (Zhou et al., 2011). Further to this, NLRP3 is suggested to associate with a range of mitochondrial membrane components including cardioplin, mitochondrial antiviral signalling protein (MAVS) and mitofusin 2 (Iyer et al., 2013, Subramanian et al., 2013, Ichinohe et al., 2013).

Endoplasmic reticulum

Activation of STING via HSV-1 infection and cytosolic DNA transfection has been shown to cause recruitment of NLRP3 to the ER. Here, NLRP3-STING interaction inhibits ubiquitination of NLRP3, promoting speck formation and NLRP3 activation (Wang et al., 2020). NLRP3 is also suggested to sense ER stress, mediated by the ER unfolded protein response (UPR) (Lerner et

al., 2012). In addition to this, other studies have associated ER stress with NLRP3 activation but via an UPR-independent signalling mechanism (Menu et al., 2012).

Centrosome

The centrosome was first recognised as playing a role in NLRP3 inflammasome activation when the kinase NEK7 was identified as a key regulator of inflammasome activation (Schmid-Burgk et al., 2016). NEK7 is involved in spindle formation during mitosis and centriole duplication during interphase (O'Regan and Fry, 2009, Kim et al., 2011). In the context of NLRP3 activation, NEK7 can bind directly to NLRP3 and acts downstream of K^+ efflux, promoting NLRP3 oligomerisation and ASC speck formation (He et al., 2016). Due to the importance of NEK7 in spindle formation and cell cycle events, NLRP3 inflammasome activation during mitosis was investigated. NLRP3 activation was dampened in mitotic cells, possibly due to the limited availability of NEK7 during mitosis. Indeed, overexpression of NEK7 restored IL-1β release during mitosis but only partially, suggesting that NEK7 serves as an interface to allow mitosis and NLRP3 inflammasome activation to occur as two mutually exclusive events (Shi et al., 2016). More recently, NLRP3 has been shown to be activated proximal to the microtubule organising centre (MTOC), dependent on its interaction with the dynein adaptor protein histone deacetylase (HDAC6) (Magupalli et al., 2020). Also, the microtubule-affinity regulating kinase 4 (MARK4) has been shown to bind to NLRP3 and facilitate its localisation to the MTOC (Li et al., 2017). Whether localisation to the MTOC facilitates interaction with NEK7 is unclear, and as a NEK7-independent mechanism of NLRP3 activation has also been characterised, this requires further clarification (Schmacke et al., 2022).

Golgi apparatus

Recent literature implicates the Golgi as a platform for NLRP3 activation. Phosphorylation of NLRP3 at the Golgi by protein kinase D (PKD) was shown to be required for NLRP3 activation, and important for the translocation of inactive NLRP3 from mitochondrial-associated membranes (MAMs) (Zhang et al., 2017). Previously, NLRP3-activating stimuli were suggested to cause a dispersal of the trans-Golgi network (dTGN), which was proposed as an essential upstream signalling event in inflammasome activation (Chen and Chen, 2018). Recently, apparent dTGN has been characterised a mechanism of dysregulated endosome-to-trans-Golgi trafficking, where the TGN marker TGN46/38 is trapped in endosomes following treatment with NLRP3-activating stimuli (Lee et al., 2023, Zhang et al., 2023). NLRP3 activation has also been shown to be coupled to the maturation of the cholesterol transcription factor SCAP-SREBP2, during which NLRP3 forms a complex with SCAP-SREBP2 and is translocated to the perinuclear Golgi (Guo et al., 2018).

Endosomes

NLRP3 inflammasome activation has been associated with endosomes, their membrane components and the cellular dysfunction that occurs when their trafficking is disrupted. NLRP3 has been shown to be recruited to endosomes following endocytosis of the membrane attack complex (MAC), where NLRP3 and ASC form a speck, co-localised with the MAC at EEA1-positive endosomes (Xie et al., 2019, Diaz-Del-Olmo et al., 2021). The endosomal protein EEA1 can be cleaved by active caspase-1, suggesting a relationship and proximity between endosomes and NLRP3 inflammasome activation (Baroja-Mazo et al., 2019). The location of NLRP3 with respect to endosomal compartments is important as NLRP3 has been suggested to sense and react to a dysfunction in endosomal trafficking (Lee et al., 2023, Zhang

et al., 2023). In fact, NLRP3-activating stimuli have been shown to impair endosome-to-TGN trafficking, endosome recycling and endosome-to-lysosome trafficking (Lee et al., 2023, Zhang et al., 2023). Pharmacological disruption of endosomal traffic also enhanced inflammasome activation in response to the NLRP3-activating stimulus imiquimod (Lee et al., 2023). NLRP3-activating stimuli also triggered the re-localisation of PI4P from the Golgi to compartments positive for endosomal and lysosomal markers, colocalising too with NLRP3 on endosomes and lysosomes (Lee et al., 2023, Zhang et al., 2023). NLRP3 has been reported to interact with PI4P via the NLRP3 polybasic motif (Chen and Chen, 2018).

1.6.3 Non-canonical NLRP3 activation

As mentioned earlier, the NLRP3 inflammasome can also be activated by a mechanism described as non-canonical NLRP3 activation. In contrast to the direct activation of caspase-1 in canonical NLRP3 activation, non-canonical NLRP3 activation involves the activation of caspase-4/5 in humans and caspase-11 in mice, following detection of cytosolic LPS as a result of Gram-negative bacterial infection (Vigano et al., 2015). Initially, extracellular LPS is detected by the membrane bound TLR4, which activates the release and paracrine signalling of interferons (IFNs) resulting in the upregulation of capsase-4/5/11 (Kayagaki et al., 2011, Shi et al., 2014). IFNs also upregulate the expression of guanylate-binding proteins (GBPs), which liberate LPS into the cytosol through the recruitment and lysis of Gram-negative bacteria (Man et al., 2016, Meunier et al., 2014). GBPs have been suggested to be necessary for the recruitment and activation of human caspase-4. Here, members of the GBP family, GBP1-4, assemble a platform to allow LPS detection, caspase-4 activation, GSDMD-mediated pyroptosis and IL-18 processing (Santos et al., 2020, Wandel et al., 2020, Kutsch et al., 2020).

Activated caspase-4/5/11 cleaves GSDMD, allowing K^+ efflux through GSDMD pores (Kayagaki et al., 2015). K^+ efflux through GSDMD pores is then sufficient to activate the NLRP3 inflammasome, which enables activated caspase-1 to cleave pro-IL-1β.

Mechanisms that regulate and are affected by non-canonical activation of the NLRP3 inflammasome vary across cell types. In dendritic cells, the oxidised phospholipid 1-palmitoyl-2-arachidonoyl-sn-glycero-3-phosphorylcholine (oxPAPC) has been shown to bind caspase-11 and activate the non-canonical pathway (Zanoni et al., 2016). However, this was only observed at concentrations of oxPAPC that were not physiologically relevant. In contrast, studies in macrophages revealed that oxPAPC was readily taken up into the cell and inhibited non-canonical inflammasome activation through action at caspase-11(Chu et al., 2018). In neutrophils, the detection of cytosolic LPS triggers non-canonical NLRP3 activation, GSDMD cleavage by caspase-11, and the release of neutrophil extracellular traps (NETs) through the induction of a cell death mechanism termed NETosis (Chen et al., 2018). NETs not only have direct implications in disease, such as attenuating vascular growth post-stroke and delaying wound healing in diabetes, but also prime other immune cells to induce sterile inflammation (Kang et al., 2020, Roth Flach and Czech, 2015, Warnatsch et al., 2015).

1.6.4 Alternative NLRP3 activation

It has been well characterised that K^+ efflux, ASC speck formation and proptosis play pivotal roles in the production and release of mature IL-1β during canonical NLRP3 activation. However, the identification of an alternative pathway of inflammasome activation in human monocytes challenged this dogma and reveals how mature IL-1β can be released in response

to a single LPS stimulus at TLR4, bypassing the canonical requirement for 2-step activation and acting independently of K^+ efflux, ASC speck formation and cell death (Gaidt and Hornung, 2017). The lack of speck formation, however, does not discount the involvement of ASC in the alternative inflammasome. Upon single TLR4 stimulation, monocytes deficient in ASC are unable to effectively produce mature IL-1β (Gaidt and Hornung, 2017). This may suggest that ASC is forming soluble oligomers upon alternative inflammasome activation, rather than stable cytosolic specks (Green et al., 2018). The alternative inflammasome is species-specific and at present has only been observed in human and porcine monocytes, provoking interesting questions with regards to human disease (Gaidt and Hornung, 2017). Most studies surrounding acute infection and chronic inflammatory conditions such as sepsis and cerebrovascular disease have been carried out in murine macrophages, which lack the alternative inflammasome. Therefore, there may be a huge aspect of human vascular disease missing from our knowledge as a result. To understand the implications of the alternative inflammasome in such diseases, we must utilise human *in vitro* models in future research.

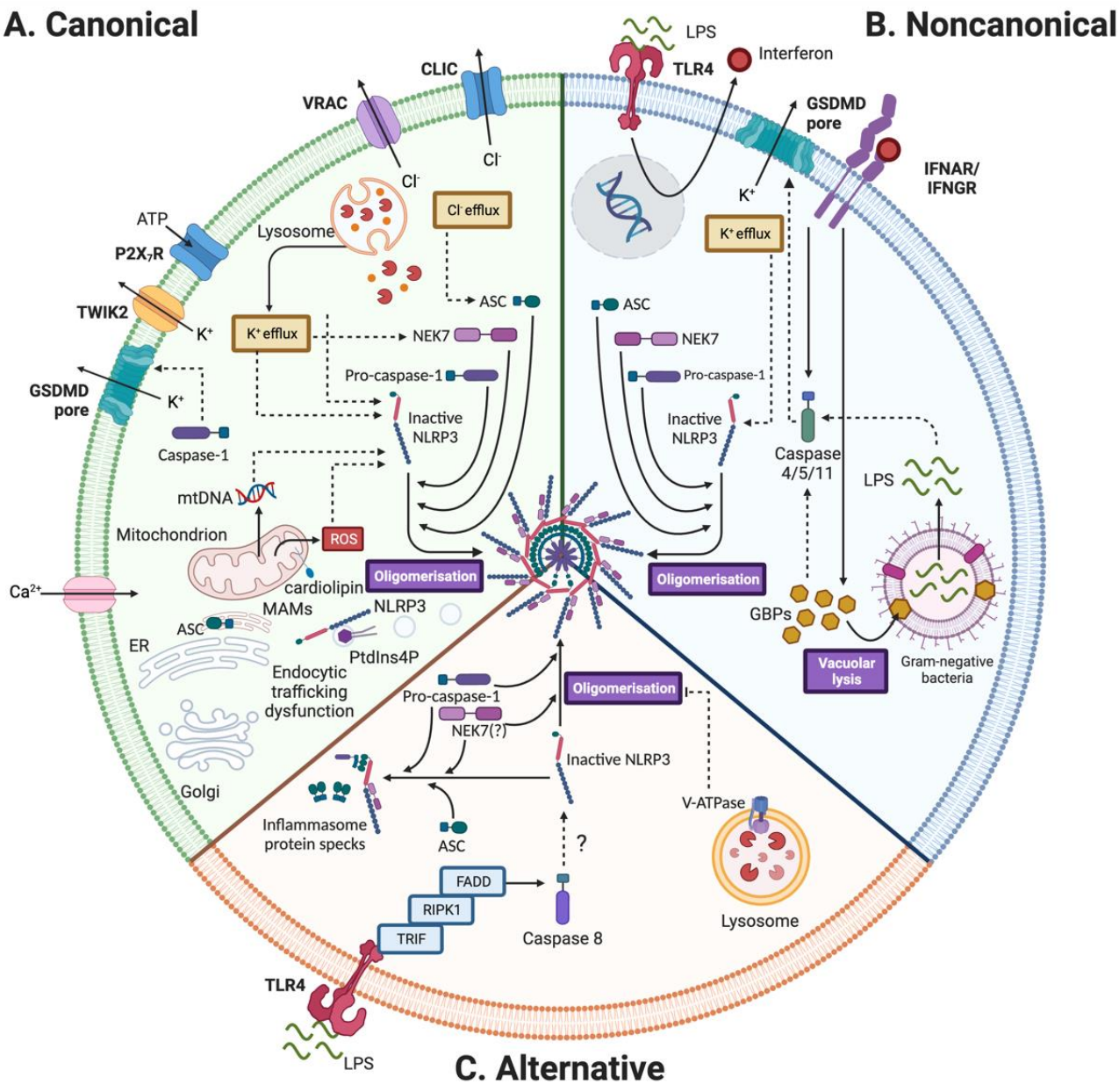
A. Canonical
B. Noncanonical
C. Alternative
LPS
TLR4
Interferon
CLIC
VRAC
Cl⁻
Cl⁻ efflux
GSDMD pore
IFNAR/ IFNGR
K⁺
K⁺ efflux
ATP
P2X7R
Lysosome
TWIK2
ASC
NEK7
Pro-caspase-1
Inactive NLRP3
Caspase-1
Caspase 4/5/11
mtDNA
Mitochondrion
ROS
Oligomerisation
cardiolipin
MAMs
NLRP3
Ca²⁺
ER
PtdIns4P
Endocytic trafficking dysfunction
GBPs
Vacuolar lysis
Gram-negative bacteria
Pro-caspase-1
NEK7(?)
Inactive NLRP3
Golgi
Inflammasome protein specks
V-ATPase
Lysosome
?
FADD
RIPK1
TRIF
Caspase 8
TLR4
LPS

Figure 1.3. Mechanisms of NLRP3 activation. A schematic detailing the canonical, noncanonical and alternative mechanisms of NLRP3 activation. **(A)** Canonical activation of the NLRP3 inflammasome relies on numerous upstream signalling events including K+ efflux, Cl- efflux, Ca2+ flux, lysosomal destabilisation and cathepsin release, release of mitochondrial DNA (mtDNA), reactive oxygen species (ROS) production, relocalisation of cardiolipin to the outer mitochondrial membrane, endoplasmic reticulum (ER) stress, endocytic trafficking dysfunction and association with PtdIns4P on endosomes and lysosomes. **(B)** Noncanonical activation of NLRP3 occurs as a result of gram-negative bacterial infection, supplying an intracellular load of lipopolysaccharide (LPS), which in turn activates caspase 4/5 (human) and caspase 11 (mice). LPS is liberated into the cytosol by granulocyte binding proteins (GBPs) which also serve as a platform for capsase-4/5/11 activation. Interferons are produced upon LPS-TLR4 binding and upregulate capase-4/5/11 and GBPs through paracrine signalling at their interferon alpha or gamma receptor (IFNAR/IFNGR). Activated caspase 4/5/11 then cleaves GSDMD. K+ efflux through GSDMD pores is then sufficient to activate the NLRP3 inflammasome. **(C)** Alternative activation of NLRP3 occurs as a result of LPS binding to TLR4. Signalling via TRIF-RIPK1-FADD capase-8 is then activated. It is unknown how caspase-8 activates the inflammasome and whether NEK7 is a component of the alternative inflammasome. The vesicular-ATPase (V- ATPase) has been shown to inhibit oligomerisation of the NLRP3 inflammasome. Alternative inflammasome activation may form smaller ASC-dependent specks, aside from the inflammasome complex.

1.7 IL-1β release and cell death

Due to its strong inflammatory activity, the processing and release of IL-1β is tightly regulated. IL-1β is produced as a precursor protein that requires cleavage of its pro-domain before it is released as a mature cytokine and can bind to its receptor, IL-1R1. The activation of the NLRP3 inflammasome culminates in the processing of pro-IL-1β by caspase-1, and therefore the activation of IL-1β is relatively well characterised. Following the discovery that IL-1β lacks a signal peptide and therefore is not released via the typical ER-Golgi route, the mechanisms that lead to its secretion have been an area of great interest (Rubartelli et al., 1990). As discussed previously, NLRP3 activation also results in the cleavage of GSDMD, formation of GSDMD pores in the plasma membrane and induction of pyroptosis. One of the best characterised mechanisms of IL-1β release is passively via GSDMD pores and subsequent cell death (He et al., 2015, Shi et al., 2015). Pyroptosis is often observed in monocytes and macrophages in response to NLRP3-activating stimuli such as nigericin and ATP (Perregaux and Gabel, 1994, Diamond et al., 2017). However, IL-1β processing and release precedes cell death, suggesting that cell lysis is not a necessary step to achieve mature IL-1β secretion (Brough and Rothwell, 2007). In fact, incubation of macrophages with glycine, an agent that protects against cell lysis, prevents ATP-induced cell death but not the release of mature IL-1β (Verhoef et al., 2005, Tapia et al., 2019).

Alternative mechanisms of IL-1β release have been proposed, facilitating the release of mature IL-1β independent of cell death. The shedding of microvesicles containing mature IL-1β from the plasma membrane, as well as the recruitment endolysosome-related organelles, have been highlighted as mechanisms of unconventional protein secretion (Rubartelli et al., 1990, Andrei et al., 1999, MacKenzie et al., 2001, Bianco et al., 2005, Pizzirani et al., 2007).

MacKenzie et al. (2001) initially observed microvesicles containing bioactive IL-1β pinching off from the plasma membrane. This was described as a rapid mechanism of IL-1β secretion from activated monocytes. Microvesicle-mediated release of IL-1β is not a mechanism exclusive to monocytes and has also been observed in activated microglia and dendritic cells (Bianco et al., 2005, Pizzirani et al., 2007). This mechanism relies upon a polybasic motif within the mature IL-1β facilitating the relocation of the cytokine to PIP2-enriched plasma membrane ruffles (Monteleone et al., 2018).

1.8 Interleukin-1α

1.8.1 IL-1α processing and release

As discussed, NLRP3 inflammasome has an important role in the regulation of IL-1β. Although indirectly, the processing and release of IL-1α can also be regulated by inflammasomes (Groß et al., 2012). Like IL-1β, IL-1α is produced as a 31kDa precursor protein that requires cleavage of its pro-domain to produce the mature cytokine. Cleavage of the IL-1α pro-domain is primarily achieved via the action of calcium-dependent proteases known as calpains (Kobayashi et al., 1990, Groß et al., 2012). Calpains detect changes in intracellular calcium and are activated upon calcium influx (Goll et al., 2003). Following inflammasome activation, the formation of GSDMD pores in the plasma membrane allows an influx of calcium and subsequent activation of calpains, explaining the indirect regulation of IL-1α by inflammasomes (Tsuchiya et al., 2021). In addition to calpains, pro-IL-1α has also been shown to be cleaved by multiple other immune cell-derived proteases, including granzyme B, elastase, cathepsin G and caspase-5/11 in human and mouse, respectively (Figure 1.4) (Afonina et al., 2011, Carroll et al., 2005, Clancy et al., 2018, Wiggins et al., 2019). Caspase-

5/11-dependent processing of IL-1α switches cells from an anti-tumorigenic, senescent state to a senescence-associated secretory phenotype (SASP), promoting a pro-inflammatory profile with the ability to drive tumour progression (Wiggins et al., 2019, Coppe et al., 2010). Like IL-1β, IL-1α does not possess a signal peptide and therefore is proposed to follow a similar unconventional secretory route (Perregaux and Gabel, 1998). However, it has also been suggested that the secretory mechanisms of IL-1α and IL-1β are distinct (Tapia et al., 2019).

In contrast to IL-1β, the IL-1α precursor is active at IL-1R1 (Mosley et al., 1987), but it is suggested that cleavage of the pro-domain results in an increase in IL-1α bioactivity (Zheng et al., 2013, Afonina et al., 2011). Pro-IL-1α is characterised as an alarmin as it can be released from cells under infectious or non-infectious threat such as hypoxia and trauma, prior to cleavage. Here, pro-IL-1α acts as a DAMP, signalling through IL-1R1 to induce the release of cytokines and chemokines from neighbouring cells (Kim et al., 2013).

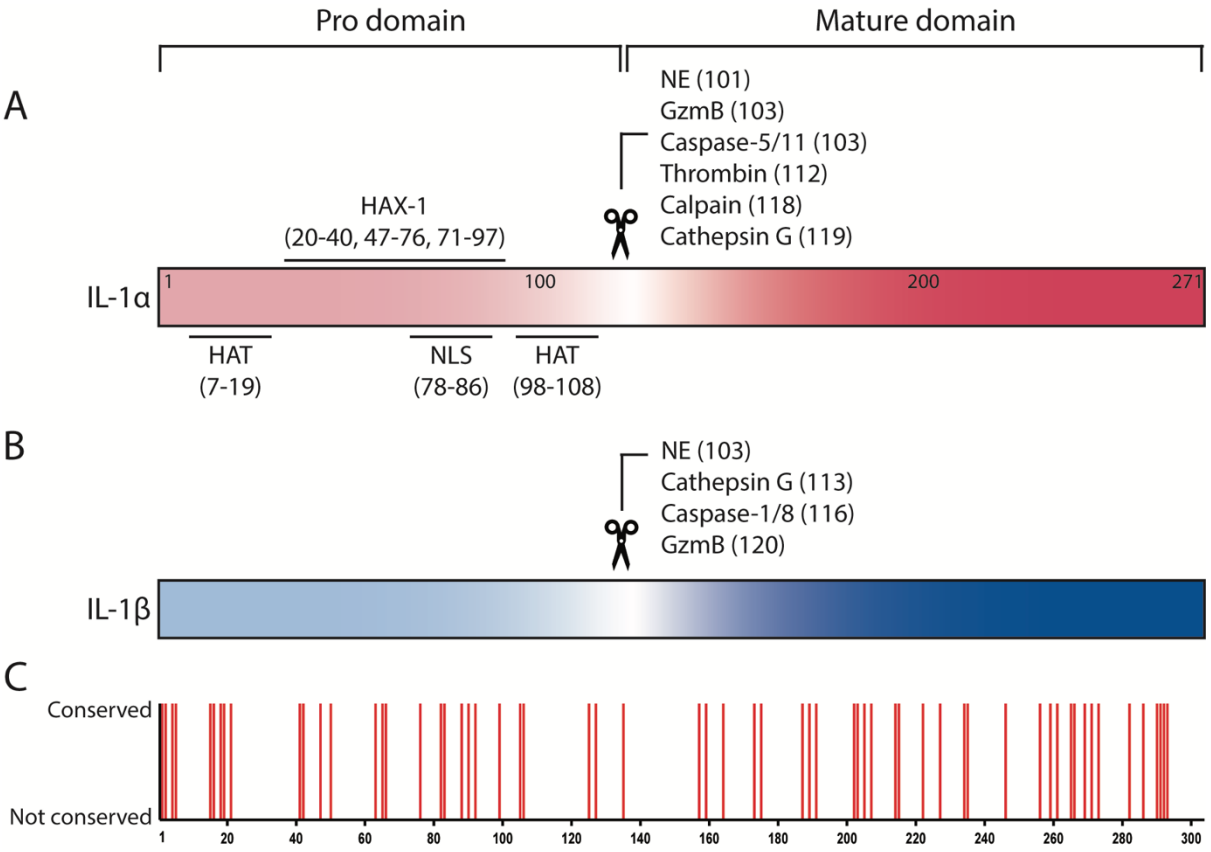

Figure 1.4. IL-1 protein domains, cleavage sites and conservation. (A) Pro-IL-1α protein with pro-domain and mature domain, labelled with HAX-1 binding domains, nuclear localisation sequence (NLS) and histone acetyltransferase (Chen et al.) binding domains. Cleavage sites and corresponding enzymes; neutrophil elastase (NE), Granzyme B (GzmB), Casapse-5/11, Thrombin, Calpain and Cathepsin G. **(B)** Pro-IL-1β cleavage and corresponding enzymes, neutrophil elastase (NE), Cathepsin G, Caspase-1/8 and Granzyme B (GzmB). Amino acid positions of binding/cleavage are in brackets. **(C)** Conservation of pro-IL-1α amino acid sequence compared to pro-IL-1β. Conserved residues are denoted by a red bar.

1.8.2 Evolution of IL-1α

Thus far, I have discussed some characteristics that are common between IL-1α and IL-1β, including their production as precursor proteins, bioactivity at IL-1R1 and lack of a signal peptide. In fact, IL-1α originated as the result of a gene duplication event of IL-1β between 320 and 160 million years ago, somewhat explaining their structural functional similarity

(Rivers-Auty et al., 2018). However, despite IL-1α and IL-1β sharing many important similarities, the pro-domains of these two cytokines appear to have evolved separate biological roles. The pro-domain of IL-1β exhibits limited conservation in mammalian species and seems to simply act as a pro-piece to prevent processing and release of IL-1β. The IL-1α pro-domain, however, is highly conserved in mammals and has several domains with particularly high conservation, indicating their potential role in functionalisation of the pro-domain, and therefore driving the divergence of IL-1α from IL-1β. Highly conserved domains within the IL-1α pro-domain include a nuclear localisation sequence (NLS), two histone acetyltransferase (Chen et al.)-binding domains and a HAX-1-binding domain (Rivers-Auty et al., 2018). As a result, the role of nuclear pro-IL-1α has been an area of interesting research and may point to a function for pro-IL-1α in addition to its well characterised role as a pro-inflammatory cytokine.

1.8.3 Nuclear pro-IL-1α

1.8.3.1 Nuclear localisation

The nuclear localisation sequence (NLS) within the IL-1α pro-domain is a KVLKKRRL motif, located between residues 78 and 86 (Figure 1.4) (Wessendorf et al., 1993). Pro-IL-1α undergoes Ran-dependent active transport into the nucleus and likely relies on the presence of an intact NLS (Luheshi et al., 2009b). We have previously shown that mutation of a single lysine residue at site 85 abolishes pro-IL-1α nuclear localisation (Luheshi et al., 2009b). Members of the toothed whale clade possess a mutation in the KKRR region of the NLS, that suggests a loss of a functional NLS (Rivers-Auty et al., 2018). However, mechanisms in addition to the presence of an intact NLS have been suggested to impact pro-IL-1α nuclear localisation.

Genotoxic stress and subsequent acetylation of Lys82 within the mammalian NLS has been shown to increase nuclear localisation of pro-IL-1α (Cohen et al., 2015). Triggering necrosis in microglial cells has been shown to cause a nuclear retention of pro-IL-1α, which may serve as a mechanism to limit inflammation (Luheshi et al., 2009a). The association of pro-IL-1α with IL-1R2 in the cytosol has also been suggested to regulate the nuclear import of pro-IL-1α (Zheng et al., 2013). The nuclear localisation of pro-IL-1α likely points to a potential nuclear role driving the divergence of IL-1α from IL-1β. However, the lack of NLS sequence homology amongst toothed whales points to other highly conserved regions, namely the HAT binding domains and HAX-1 binding domain, as potential drivers of IL-1α neofunctionalisation.

1.8.3.2 HAT-binding domains

Pro-IL-1α has two highly conserved HAT-binding domains and has previously been recorded to interact directly with HATs p300, PCAF and GCN5 (Buryskova et al., 2004, Zamostna et al., 2012). HATs were originally identified as enzymes that acetylate histones; however, multiple non-histone substrates of HATs have since been identified in both the nucleus and the cytosol, highlighting their wide-ranging role in regulating a plethora of proteins within the cell (Lee and Workman, 2007). In fact, pro-IL-1α itself has been shown to be acetylated, suggesting that HATs may not only bind to but acetylate pro-IL-1α to regulate its localisation and function (Cohen et al., 2015).

1.8.3.3 HAX-1-binding domain

The HAX-1-binding domain is a highly conserved region of the IL-1α pro-domain and HAX-1 has been shown to interact with pro-IL-1α experimentally, suggesting a role for HAX-1 in the

divergence of pro-IL-1α (Rivers-Auty et al., 2018). HAX-1 is a cytosolic protein that appears to be predominantly localised to mitochondria and has multiple binding partners including HS1 (hematopoietic lineage cell-specific protein-1), PKD2 (polycystic kidney disease-2/polycystin-2) and Bcl-2 (Fadeel and Grzybowska, 2009). The exact function of HAX-1 binding is unknown, however, it has been suggested to be involved in shuttling of proteins to the nucleus. In a skin fibroblast model of systemic sclerosis, pro-IL-1α was shown to interact with HAX-1, and inhibition of HAX-1 caused a loss of pro-IL-1α nuclear localisation, suggesting that pro-IL-1α nuclear localisation is dependent upon HAX-1 binding (Kawaguchi et al., 2006). The potential role of HAX-1 in pro-IL-1α nuclear shuttling may allow a nuclear role of pro-IL-1α to remain even in the context of a non-functional NLS.

1.9 Summary and aims

Inflammation is implicated in a wide range of diseases, therefore understanding how key inflammatory mediators are regulated is important in developing effective therapeutic interventions. In particular, the NLRP3 inflammasome and IL-1α are important players in signalling inflammation. To understand how NLRP3 and IL-1α are regulated, we must learn more about their location and protein interactomes at the subcellular level. Creating a more accurate picture of the fundamental biology of inflammation will broaden our understanding of inflammatory disease and treatment targets as a result.

The overall aim of this PhD was to investigate the intracellular regulation of NLRP3 and IL-1α. Specifically, this thesis aimed to:

1. Characterise the subcellular localisation of NLRP3 in the context of endosomal trafficking disruption
2. Identify and investigate novel interactors of NLRP3 that are associated with the endosomal trafficking pathway
3. Investigate the nuclear role of pro-IL-1α by identification of novel nuclear interacting proteins

Chapter 2:

Materials and methods

Chapter 2. Materials and methods

2.1 Reagents

Dulbecco's Modified Eagle Medium (DMEM), RPMI-1640, sodium pyruvate, Penicillin-Streptomycin, Trypsin-EDTA solution (10x) and phorbol 12-myristate 13-acetate (Chapman and Munro) were from Sigma Aldrich. Foetal bovine serum (FBS) was from Life Technologies Ltd. GibcoTM Trypan Blue Solution (0.4%) was from Thermo Fisher Scientific. Lipopolysaccharide (LPS, *Escherichia coli* 026:B6), nigericin sodium salt (N7143), L-Leucyl-L-Leucine methyl ester (hydrochloride) (G6295) and MCC950 (PZ0280) were from Sigma Aldrich. 4-Sulfonic calix[8]arene Hydrate was sourced from Tokyo Chemical Industry (S0471). Imiquimod (R837) was from InvivoGen. Monensin sodium salt (5223/500) was from BioTechne. Transferrin from Human Serum, Alexa FluorTM 488 Conjugate (T13342) was from InvitrogenTM and holo-transferrin human (T4132) was from Sigma-Aldrich. Paraformaldehyde (PFA) solution was from Sigma Aldrich. DAPI (4',6-Diamidino-2-Phenylindole, Dihydrochloride) (D1306) and ProLong Gold Antifade Mountant (P36934) were from Invitrogen^{TM}. Primary and secondary antibodies are specified in Table 2.1 and Table 2.2, respectively.

Table 2.1. Primary antibodies. Table displaying primary antibodies, their application in this thesis, target protein, host species, concentration used and manufacturer details. ICC: immunocytochemistry; WB: western blot; NLRP3 PYD: NLRP3 pyrin domain. N/A: not applicable.

Application	Target protein	Target species	Host species	Conc.	Manufacturer details
ICC	Golgin97	Human	Rabbit	2 µg/mL	Abcam, ab84340
	EEA1	Polyclonal	Mouse	2.5 µg/mL	R&D, AF8047
	CD63	Human	Mouse	1 µg/mL	Merck, CBL553
	LAMP1	Polyclonal	Mouse	1:300 (v/v)	Thermo, MA1-164
	NLRP3 PYD	Polyclonal	Mouse	2 µg/mL	Adipogen, G-20B-0014-C100
	TurboID (BirA)	Polyclonal	Rabbit	1:500 (v/v)	Sino Biological, 11582-RP01
	Biotin (Streptavidin)	Polyclonal	N/A	1 µg/mL	Thermo, N200
	GOLGA3	Polyclonal	Rabbit	250 ng/mL	Protein Tech, 21193-1-AP
	GORASP2	Polyclonal	Rabbit	225 ng/mL	Protein Tech, 10598-1-AP
	SNX3	Polyclonal	Rabbit	1.5 µg/mL	Protein Tech, 10772-1-AP
	TPD53L2	Polyclonal	Rabbit	450 ng/mL	Protein Tech, 11795-1-AP
	IL-1α	Human	Goat	2 µg/mL	R&D, AF-400-NA
WB	NLRP3 PYD	Polyclonal	Mouse	1 µg/mL	Adipogen, G-20B-0014-C100
	TurboID (BirA)	Polyclonal	Rabbit	1:1000 (v/v)	Sino Biological, 11582-RP01
	Biotin (Streptavidin)	Polyclonal	N/A	2 µg/mL	Thermo, N200
	IL-1α	Human	Goat	0.2 µg/mL	R&D, AF-400-NA

Table 2.2. Secondary antibodies. Table displaying secondary antibodies, their application in this thesis, target species/protein, host species, concentration used and manufacturer details. ICC: immunocytochemistry; WB: western blot; HRP: horse radish peroxidase.

Application	Conjugate	Target species/ protein	Host species	Conc.	Manufacturer details
ICC	Alexa Fluor 488	Rabbit	Donkey	2 µg/mL	Thermo, A-21206
	Alexa Fluor 594	Rabbit	Donkey	2 µg/mL	Thermo, A-21207
	Alexa Fluor 594	Streptavidin	Donkey	4 µg/mL	Thermo, S11227
	Alexa Fluor 647	Mouse	Donkey	2 µg/mL	Thermo, A-31571
WB	HRP	Goat	Rabbit	500 ng/mL	Agilent, P044901-2
	HRP	Rabbit	Goat	250 ng/mL	Agilent, P044801-2
	HRP	Rabbit	Mouse	1.3 µg/mL	Agilent, P016102-2

2.2 Plasmid generation and characterisation

2.2.1 Generation of NLRP3-GSW-TurboID plasmid

2.2.1.1 NLRP3-GS-TurboID digestion and purification

NLRP3-GS-TurboID lentiviral vector was created by the Genome Editing Unit (GEU) at The University of Manchester. The vector was assembled using HiFi DNA Assembly, by inserting amplified human NLRP3 from the parent vector pEF-1α-NLRP3wt-Venus-polyA into

pGS_cTurboID. NLRP3 was inserted into pGS-cTurboID at KpnI (1234) and sequence was flipped, resulting in 12,592 base pair vector pNLRP3-GS-TurboID (Figure 2.1A).

GSW (Waldo et al.) was inserted as a more flexible linker between NLRP3 and TurboID, with the aim to avoid any functional interference between NLRP3 and TurboID. The GSW linker is a class of flexible linker which is rich in glycine and serine residues; these small, polar amino acids provide flexibility, and allow for mobility of the connecting functional domains. The sequence of the Waldo linker is GSAGSAAGSGEF, and in contrast to a typical flexible linker with sequence $(GGGGS)_4$, the Waldo linker does not have high homologous repeats in its coding sequence to avoid deletion in by homologous recombination during the cloning process (Chen et al., 2013). To remove the GS linker and insert the GSW linker into our NLRP3-TurboID vector, the restriction enzymes PshAI and SalI (Table 2.3) were used to cut either side of the GS linker to produce a linearised plasmid with N-terminal TurboID and C-terminal NLRP3. NLRP3-GS-TurboID plasmid was incubated initially with PshAI (5.1 µl NLRP3-GS-TurboID (196.3 ng/µl); 1 µl PshA1; 5 µl CutSmart; 1 µl CIP; 37.9 µl Rnase free water) at 37°C for 15 minutes before incubation with SalI (1 µl SalI and 1 µl NaCl (5 mM)) for a further 15 minutes at 37°C. Single digestions with PshAI and SalI alone were carried out as controls (Figure 2.1B).

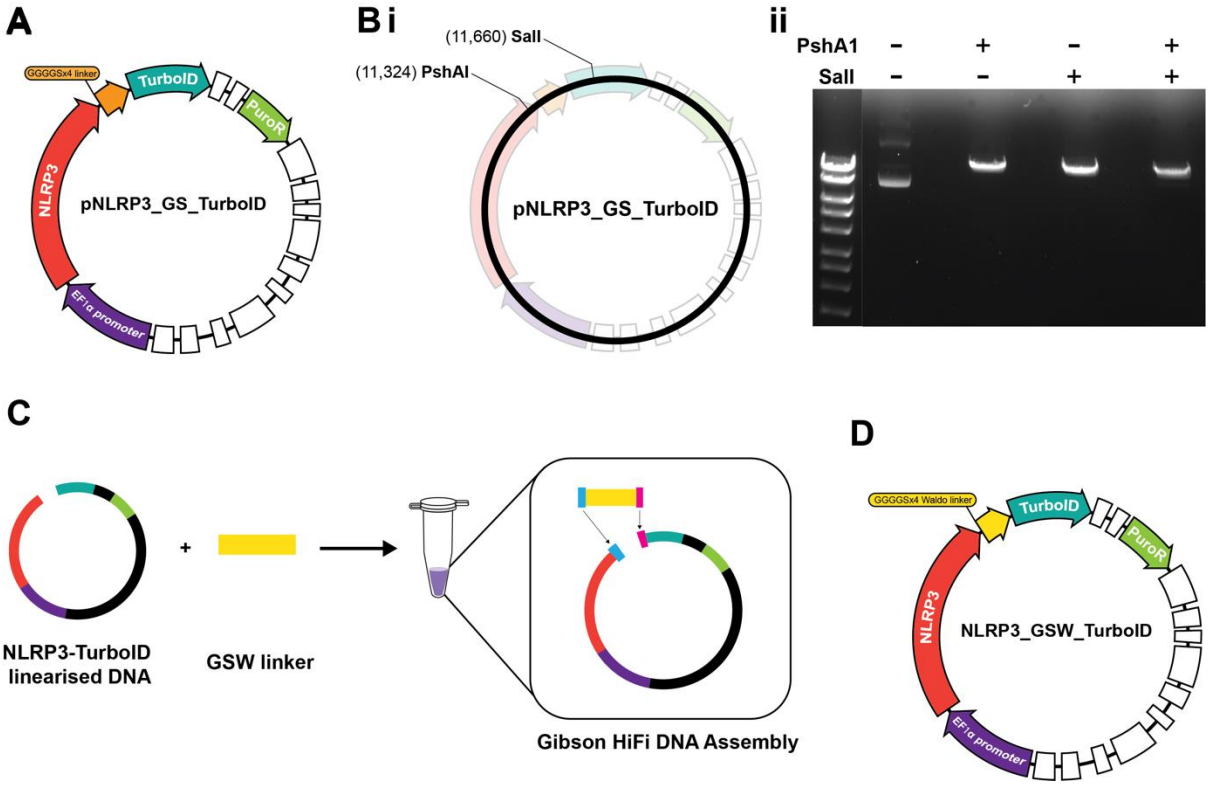

Figure 2.1. Generation of NLRP3-GSW-TurboID vector. (A) NLRP3-GS-TurboID starting vector. **(B)** Digestion of NLRP3-GS-TurboID. **(i)** Cleavage sites for restriction enzymes PshAI and SalI **(ii)** NLRP3-GS-TurboID digestion fragments following incubation with no restriction enzymes, PshA1 alone, SalI alone, and PshA1 and SalI in combination. **(C)** Insertion of GSW linker into NLRP3-TurboID linearised DNA by Gibson HiFi DNA Assembly. **(D)** NLRP3-GSW-TurboID final vector.

Table 2.3. Restriction enzymes used in restriction digestion reaction of NLRP3-GS-TurboID. Table also details the enzyme recognition sequence sourced from Snap Gene. All enzymes were purchased from New England BioLabs Inc.

Restriction enzyme	Recognition sequence (5'-3')
PshAI	GACNNNNGTC
SalI	GTCGAC

Following NLRP3-GS-TurboID digestion, linearised DNA fragments were resolved using 0.8% agarose gel prepared using 1x tris-acetate (TAE) buffer (40mM Tris, 20mM Acetate and 1mM EDTA), SYBR safe was added at 1:10000 dilution to stain the agarose gel. Gels were visualised using Bio-Rad chemidoc imaging system. DNA band digested by both PshAI and SalI was purified from the agarose gel using DNA Gel Extraction Kit (New England Biolabs), as per manufacturer's instructions.

2.2.1.2 Gibson HiFi DNA assembly

NEB Gibson HiFi assembly kit (New England BioLabs Inc. Massachusetts, USA) was used to assemble the linearised NLRP3-TurboID plasmid and the GSW linker gBlock to allow recombination of linearised DNA into a circular plasmid with the newly inserted GSW linker. This assembly reaction required a ratio of 1:2 for NLRP3-TurboID plasmid (0.012 pmols) and GSW linker (0.024 pmols) DNA, 10 µl NEBuilder HiFi DNA assembly master mix and appropriate nuclease-free water for a final reaction volume of 20 µl. The reaction was then incubated at 50°C for 15 min, before being stored at 20°C prior to bacterial transformation.

2.2.1.3 Bacterial transformation and plasmid preparation

NLRP3-GSW-TurboID plasmid DNA was then transformed using NEB C33040 stable competent *E. coli.* 100 pg-100 ng of plasmid DNA was added to the cell mixture and incubated on ice for 30 minutes. *E. coli* were heat shocked at 42°C for 30 seconds and incubated on ice for a further 5 minutes. 950 µl of room temperature NEB 10-beta/Stable Outgrowth Medium was added to the bacterial cells and rotated horizontally at 250 rpm at 30°C for 60 min. Agar selection

plates containing puromycin were warmed to 30°C before being coated with either 100 µl or 850 µl of bacterial cell mixture, plates were incubated at 37°C overnight.

Single colonies were then selected and incubated in 5 mL LB broth at 37°C overnight. Recombinant culture was centrifuged at 12,000 xg for 1 minute to pellet cells. Bacterial pellet was then resuspended and lysed in mini-prep provided solutions and mini-prep was carried out as per manufacturer's instructions (Sigma). Plasmid DNA was eluted from the final spin column using Sigma elution solution and concentration was determined by Nano drop. Sequencing was carried out with primers DB12_TID_SeqR and DB12_NLRP3_R, to verify the insertion of the GSW linker and presence of NLRP3 and TurboID domains (Figure 2.2).

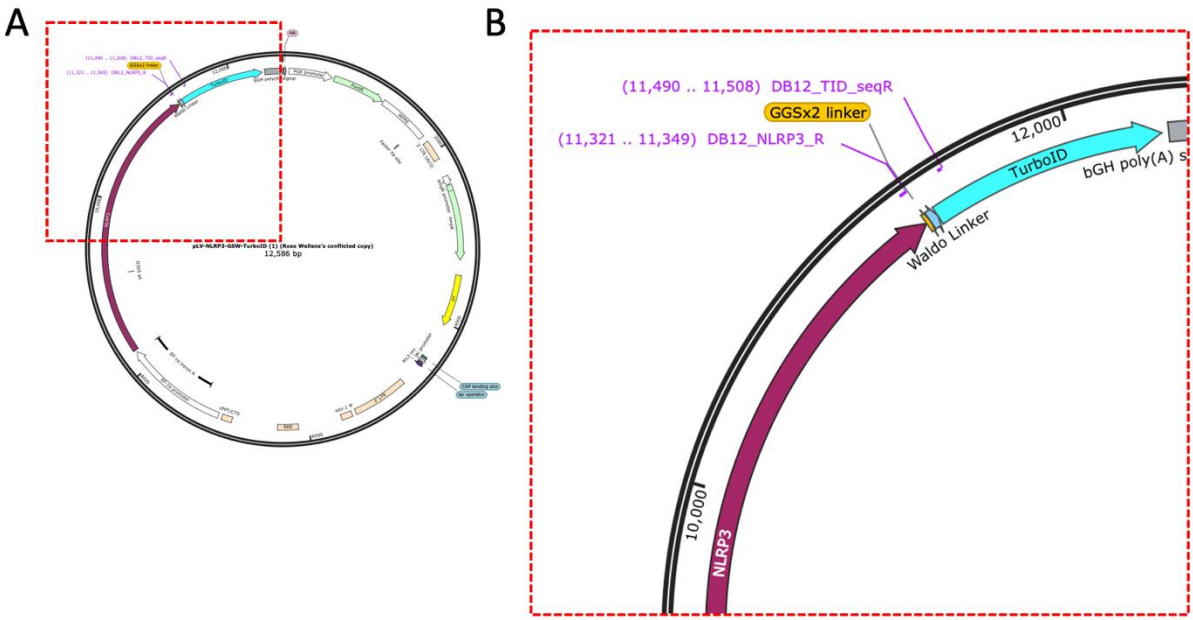

Figure 2.2 NLRP3-GSW-TurboID sequencing primers. NLRP3-GSW-TurboID plasmid map with primers DB12_TID_SeqR and DB12_NLRP3_R labelled.

2.2.2. Other plasmids

2.2.2.1 SidM-mCherry

mCherry-P4M-mCherry vector was a gift from Martin Lowe (Addgene plasmid #51471).

2.2.2.2 NLRP3-mVenus

Methods courtesy of Antony Adamson and Hayley Bennett from The University of Manchester Genome Editing Unit

A third-generation lentiviral EF1a-NLRP3-mVenus expression vector was generated by HiFi assembly [New England Biolabs (NEB)]. Briefly, a custom-built Lenti-EF1a-Multiple cloning site-pGK-Puro vector was digested with Kpn I and Not I (NEB) and column-purified (Bioline). Hifi assembly fragments were amplified with HF KOD polymerase from NLRP3 (fragments 1 and 2) or mVenus (fragment 3) template DNA using the primers detailed below (Table 2.4) and assembled into the backbone vector according to the manufacturer's instructions. Vectors were transformed into NEB C3040 cells.

Table 2.4. DNA primers used for recognition of NLRP3 (fragments 1 and 2) and mVenus (fragment 3).

Fragment number	Primer sequence (5'-3')
1	actagtccagtgtggtggtaccggtggatccgccaccatgaagatggcaagcacccg
	tcgtcaaaggcaccttgcagctcatcgaagccgtccatgag
2	tcatggacggcttcgatgagctgcaaggtgcctttgacg
	gcagcggagccagcggagccccaagaaggctcaaagacgacg
3	tcgtctttgagccttcttggggctccgctggctcc
	aacagatggctggcaactagaaggcacaggcggccgctcacttgtacagctcgtccatgc

2.2.2.3 Pro-IL-1α-TurboID and TurboID

Methods courtesy of Antony Adamson and Hayley Bennett from The University of Manchester Genome Editing Unit

Coding sequences were obtained from human *IL1A* (NCBI Gene ID: 3552).

Pro-IL-1α gene was synthesized and cloned to pcDNA3.1$^{(+)}$ vectors (Life Technologies).

To generate a pro-IL-1α-TurboID expression vector, the pro IL-1α sequence was amplified from pcDNA3.1-pro-IL-1α using pF1F and pF1R, and TurboID sequence amplified from Addgene plasmid #107173 using primers tF2F and tF2R. The vector was assembled by HiFi assembly (NEB) into pcDNA3.1/KpnI/NotI. To generate the TID expression vector, the TurboID sequence was amplified from Addgene plasmid #107173 using primers tF1F and tF1R. Followed by HiFi assembly into pLV-Ef1a-MCS/KpnI/NheI.

2.3 Generation of cell lines

2.3.1 COS7 NLRP3-mVenus

COS7 NLRP3-mVenus cells were generated by Fatima Matin-Sanchez using the protocol detailed below for the generation of HeLa NLRP3-GSW-TurboID cells.

2.3.2 HeLa NLRP3-GSW-TurboID

Lenti-HEK 293T cells (#632180, Takara) were cultured in DMEM supplemented with 10% FBS, 100 U/mL penicillin, 100 µg/mL streptomycin, and 1 mM sodium pyruvate. Lenti-HEK 293T cells were plated at $5x10^5$ cells per well in a six-well plate coated with 1% (v/v) poly-L-lysine to promote Lenti-HEK adherence. Lenti-HEK 293T cells were left to adhere for 24 h before transfection with 1.2 µg pMD2.G, 0.4 µg psPAX2 and 1.5 µg NLRP3-GSW-TurboID or 1.5 µg PBS as an untransduced control using Lipofectamine 3000 (Invitrogen). Transfection was performed following the Lipofectamine manufacturer's instructions. 24 h following transfection, media was replaced with fresh DMEM, and cells were further incubated for 48 h. Supernatants were then collected and filtered with a 0.45 µm filter to remove any intact cells from the viral particle suspension. Viral suspension was then used to transduce HeLa cells plated at $1x10^5$ in a 12-well plate. HeLa cells were incubated with viral suspension in combination with polybrene (0.8 µg/µl) for 7 h before media was replaced with fresh DMEM. HeLa cells were then left for 4 days before media was replaced with DMEM containing 15 µg/mL puromycin to begin puromycin selection.

NLRP3-GSW-TurboID transduced cells (named as HeLa NLRP3-TurboID from hereon in) and empty vector control remained in puromycin media until all empty vector control cells were

visibly dead under light microscope. HeLa cells expressing puromycin resistance were then cultured in DMEM containing puromycin for a further week.

2.3.3 THP-1 monocytes containing knockdowns of NLRP3-TurboID proteins of interest using CRISPR-Cas9

THP-1 CRISPR-Cas9 knockdown cells were generated by Wei-Hsiang Lin on behalf of The Genome Editing Unit at the University of Manchester. Below details their methodology for this process.

2.3.3.1 Target design

Three single guide RNAs (sgRNA) were designed by Wei-hsiang Lin (Genome Editing Unit, University of Manchester) to target common exons in genes GOLGA3 (DB38a), GORASP2 (DB38b), SNX3 (DB38c) and TPD52L2 (DB38d). For sgRNA design, the webtools http://www.sanger.ac.uk/htgt/wge/ and www.CRISPOR.org were used. GuideRNA predicted to have 0, 1 or 2 mismatches (MM) elsewhere in the genome are not considered. NHEJ and InDel formation at this site should frameshift and cause nonsense mediated decay of the transcript, thus knocking out the gene.

2.3.3.2 Experimental procedure

Three sgRNAs for each gene KO were co-nucleofected with Cas9 to THP-1 cells. To determine the KO efficiency of the target genes, gDNA was extracted. The relevant DNA sequences were amplified by PCR and KO efficiency was calculated using ICE analysis. Multiple runs of

nucleofection were performed when KO efficiency were not satisfied. Three rounds of nucleofection were performed for DB38a (GOLGA3), DB38c (SNX3) and DB38d (TPD52L2). Four rounds of nucleofection were done for DB38b (GORASP2). DB38e (Mariathasan et al.) line is THP-1 cells that received nucleofection with Cas9 but without sgRNAs.

Table 2.5. THP-1 CRISPR-Cas9 knockdown efficiency. Table displaying the knockdown efficiency determined by ICE analysis of four genes knockdown using CRISPR-Cas9 in THP-1 monocytes. KO efficiency denotes the proportion of cells within the pool with a non-wild type sequence.

Project	Gene	KO efficiency (%)
DB38a	GOLGA3	83
DB38b	GORASP2	56
DB38c	SNX3	61
DB38d	TPD52L2	79

2.4 Cell culture

WT HeLa, HeLa NLRP3-TurboID cells, COS7 NLRP3-mVenus cells and Lenti-X 293T cells were cultured in DMEM supplemented with 10% (v/v) foetal bovine serum (FBS), 100 U/ml penicillin 100 μg/ml streptomycin and 1 mM sodium pyruvate. Human WT, NLRP3 KO and NLRP3-TurboID THP-1 cells were cultured in RPMI-1640 medium supplemented with 10% (v/v) foetal bovine serum (FBS), 100 U/ml penicillin 100 μg/ml streptomycin and 2 mM L-glutamine (v/v). HeLa NLRP3-TurboID and THP-1 NLRP3-TurboID cells were also cultured in the presence of 10 μg/μl puromycin to maintain antibiotic selection pressure.

HeLa and COS7 cells were seeded in a 24-well plate (Corning) at 2 x 10^5 cells/ml for western blotting and on coverslips at 1 x 10^5 cells/ml for immunocytochemistry. Cells were left to adhere overnight at 37°C and 5% CO_2. To allow THP-1 cells to adhere, suspension cells were seeded at 1 x 10^6 cells/ml in a 24-well plate or 96-well plate in the presence of PMA (250 nM for 18 h), cells were seeded on coverslips for immunocytochemistry.

For TurboID experiments for mass spectrometry analysis, NLRP3-TurboID and WT (for IL-1α-TurboID transient transfection) HeLa cells were seeded in 10 cm culture dishes (Corning) at 2 x 10^5 cells/ml, 2 dishes per experimental condition were used.

Table 2.6. Examples of *in vitro* NLRP3 inflammasome activators

Activator	Proposed mechanism of action	References
ATP	P2X7 receptor activation, subsequent potassium efflux	(Perregaux and Gabel, 1994, Mariathasan et al., 2006)
Nigericin	Pore-forming toxin, subsequent potassium efflux	(Perregaux and Gabel, 1994, Mariathasan et al., 2006)
Imiquimod	Mitochondrial stress, potassium efflux-independent	(Groß et al., 2016)
Leu-LeuOMe	Lysosomal damage	(Hornung et al., 2008)
Silica	Phagosomal destabilisation	(Hornung et al., 2008)
Lipopolysaccharide	Alternative NLRP3 activation, TLR4 signalling in monocytes	(Gaidt et al., 2016)

Primary mouse BMDMs were prepared from the femurs of 3–6-month-old male and female C57BL/6 mice. Bone marrow was harvested, red blood cells were lysed with ACK lysing buffer

(Lonza, LZ10-548E), and the resulting cells passed through a 70 μm cell strainer and cultured in 70% DMEM supplemented with 30% L929 mouse fibroblast-conditioned medium for 7 days at 37°C and 5% CO_2. Cells were seeded at a density of 1 x 10^6 cells/ml and left to adhere overnight.

Human WT and KD THP-1 monocytes were cultured in RPMI-1640 medium supplemented with 10% (v/v) FBS, 100 U/ml penicillin 100 μg/ml streptomycin and 2 mM L-glutamine. For differentiation of THP-1 cells, THP-1 monocytes were seeded at 1 x10^6 cells per mL in the presence of PMA (250 nM, overnight).

2.4.1 Cell stimulation

2.4.1.1 NLRP3-activating stimuli

For stimulation of COS7 NLRP3-mVenus and HeLa cells, cell media was replaced with serum-free DMEM prior to stimulation with vehicle (ethanol, 0.5% v/v), nigericin (10 μM), Leu-Leu-OMe (1 mM), imiquimod (75 μM) or monensin (10 μM) for 90 min. When treating with monensin and imiquimod in combination, cells were stimulated with monensin for 90 min prior to imiquimod stimulation for a further 90 min.

For stimulation of primary murine BMDMs, cells were primed with LPS (1 μg/ml) in complete DMEM for 4 h. For NLRP3 inflammasome activation, the media was then replaced with serum-free DMEM containing vehicle (DMSO), MCC950 (10 μM) or phenyl arsine oxide (PAO, 1 μM). After 15 min, cells were stimulated with nigericin (10 μM, 1 h) or vehicle (ethanol; 0.5% v/v). For AIM2 inflammasome activation the media was then replaced with serum-free DMEM

containing vehicle (DMSO), 8-sulfonic calixarene (Calix[8]; 10 µM) or phenyl arsine oxide (PAO, 1 µM). After 15 minutes, cells were activated by lipofectamine-mediated transfection of poly dA:dT (1 µg/ml, 4 h) or mock (Lipofectamine alone).

2.4.1.2 Transferrin recycling and uptake

HeLa cells were washed three times in serum-free media and incubated for 30 minutes in the same media containing 5 µg/mL Transferrin Alexa Fluoro-488 and NLRP3 inflammasome-activating stimuli (nigericin 10 µM, LeuLeu-OMe 1 mM, imiquimod 75 µM), monensin (10 µM) or vehicle (ethanol, 0.5% (v/v)). Cells underwent a 3-minute ice cold acid wash (50 mM glycine, 0.1 M NaCl in dH_20, pH 3) before being washed three times in serum-free media containing 0.1 mg/ml holo-transferrin (Figure 2.2). Cells were either fixed at this point (0 min) or incubated in serum-free DMEM containing unlabelled holo-transferrin (0.1 mg/ml) for 15 or 30 minutes at 37°C before fixation (Figure 2.2). Cells were fixed on coverslips in 4% paraformaldehyde for 15 minutes at room temperature.

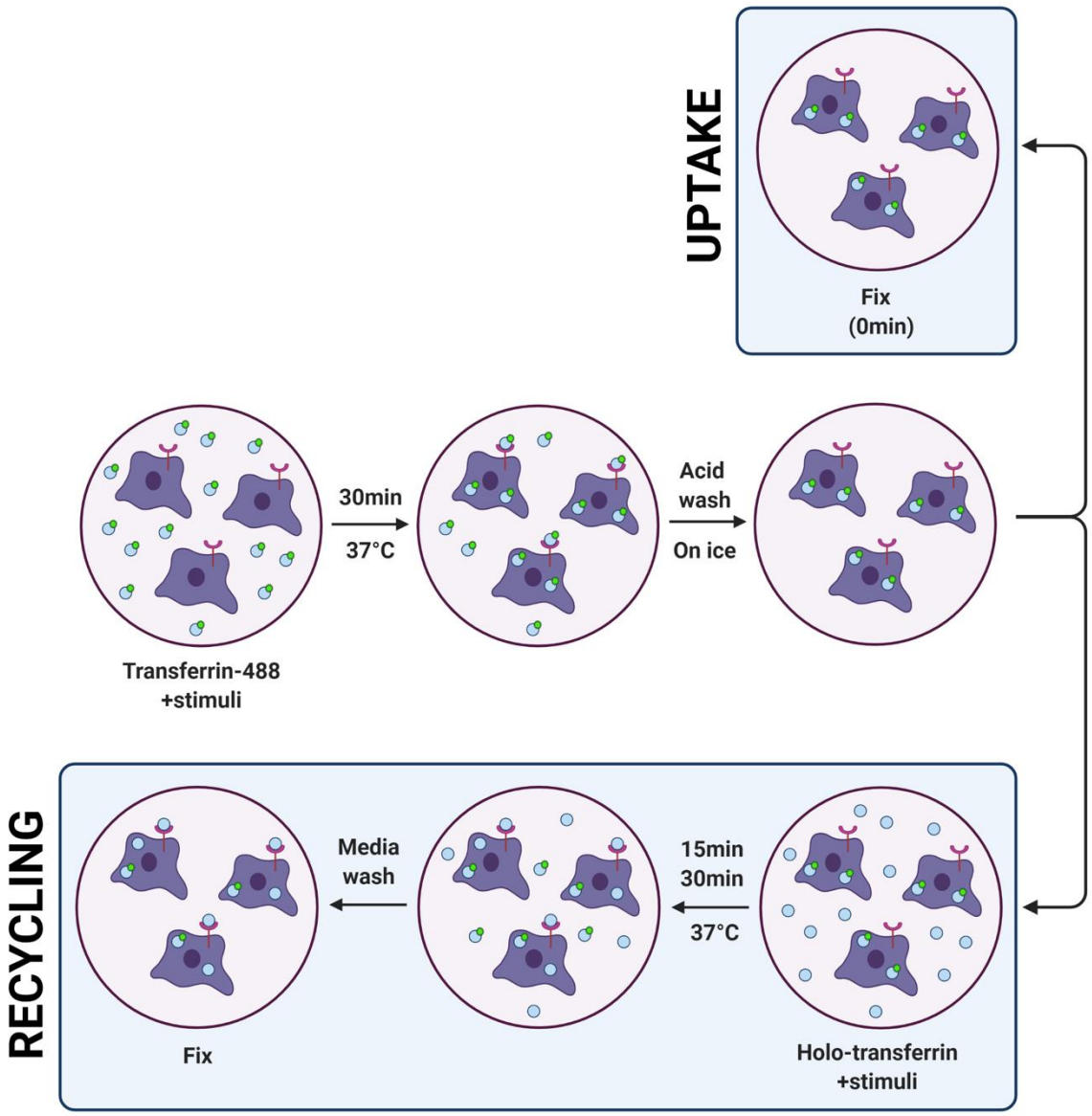

Figure 2.3. Transferrin assays. HeLa cells were incubated for 30 min at 37°C in serum-free DMEM containing fluorescent transferrin (5 µg/ml, Transferrin-488) along with treatment (vehicle (0.5% v/v) monensin (10 µM), nigericin (10 µM), Leu-Leu-OMe (1 mM) or imiquimod (75 µM)). Cells then underwent an acid wash, pH 3 on ice, to remove any surface-bound fluorescent transferrin. Media was then replaced containing holo-transferrin (0.1 mg/mL) along with treatments (vehicle (0.5% v/v) monensin (10 µM), nigericin (10 µM), Leu-Leu-OMe (1 mM) or imiquimod (75 µM)). Cells were either fixed before holo-transferrin treatment (0 min), to provide a measure of fluorescent transferrin uptake, or incubated at 37°C for 15 or 30 min before being fixed. These time points were used as a measure of fluorescent transferrin recycling.

2.4.1.3 Biotinylation experiments

NLRP3-TurboID HeLa cells were stimulated with vehicle (ethanol, 0.5% v/v) or nigericin (10 μM) for 30 minutes in serum-free DMEM. After 30 minutes, biotin (500 μM) was added and cells were left to incubate for 1 hour.

HeLa cells transfected with Pro-IL-1α-TurboID or TurboID were stimulated with vehicle (ethanol, 0.5% v/v) or ionomycin (10 μM) for 30 min and biotin (500 μM) for 30 min, simultaneously in serum-free DMEM.

In both NLRP3 and pro-IL-1α-TurboID experiments, cells were then washed 4 times in cold PBS (containing $MgCl_2$), scraped and pelleted at 1000 xg for 5 min at 4°C. Cell pellet was preserved at -80°C prior to sending off for mass spectrometry analysis.

2.4.2 Transient transfection

Transfection was carried out using Lipofectamine 3000 (Invitrogen) reagent as per the manufacturer's instructions. COS7 NLRP3 mVenus cells were transfected with 300 ng SidM-mCherry per 5 $x10^5$ cells and HeLa cells were transfected with either 500 ng Pro-IL-1α-TurboID or 12.5 ng TurboID per 5 $x10^5$ cells. Whilst the DNA-lipid complex was incubating at room temperature for 15 minutes, cell media was changed to Opti-MEM (Thermo-Fisher). DNA-lipid complex was then added to cells and left to incubate for 18 h at 37°C and 5% CO_2. In those cells transfected with Pro-IL-1α-TurboID or TurboID for mass spectrometry experiments, cell media was changed to complete DMEM 18 h following transfection and left to incubate for a further 24 h prior to stimulation to obtain an optimal cell number for stimulation and cell scraping.

2.4.3 ELISA

Supernatants were measured for human (THP-1 monocytes) or mouse (primary BMDMs) IL-1β by enzyme-linked immunosorbent assay (ELISA; DY201 (human), DY401 (mouse), DuoSet, R&D Systems) according to the manufacturer's instructions.

2.4.4 LDH

Supernatants were measured for lactate dehydrogenase (LDH) release as a determinant of cell death. LDH assay was carried out using CytoTox 96 nonradioactive cytotoxicity assay (G1780, Promega) according to the manufacturer's instructions.

2.4.5 Western blot

Supernatants were removed and HeLa cells, BMDMs or THP-1 monocyte-derived macrophages were lysed in-well with lysis buffer containing Tris/HCl (50 mM), NaCl (150 mM), Triton X-100 [1% (v/v)], and protease inhibitor cocktail [1% (v/v)]. Equal volumes of cell lysate were run on 8%, 10%, 12% or 15% SDS–polyacrylamide gel and transferred at 25 V onto PVDF membranes using a Trans-Blot Turbo Transfer System (Bio-Rad). Membranes were blocked in milk [5% (w/v)] in PBS Tween20 [PBSTw20; 0.1% (v/v)] for 1 hour at room temperature. Membranes were incubated at 4°C overnight with primary antibodies (Table 2.1) in 0.1% BSA in PBSTw20. Membranes were washed in PBSTw20 and incubated with secondary antibodies (Table 2.2) at room temperature for 1 hour. Proteins were incubated using G:BOX (Syngene) and Genesys software following incubation with Cytiva Amersham ECL Prime Western Blotting Detection Reagent (GE Healthcare, RPN2236). β-Actin was used as a loading control.

2.5 Microscopy

2.5.1 Immunocytochemistry

Cells were fixed in 4% paraformaldehyde (PFA) for 17 minutes before permeabilization with PBS 0.1% Triton X-100 (PBSTX100) for 5 min at room temperature. Cells were blocked in 5% BSA in PBSTX100 for 1 hour at room temperature to prevent non-specific antibody binding. Cells were incubated with primary antibodies (Table 2.1) in 1% BSA PBSTX100 at 4°C overnight. Cells were washed in PBS containing Mg_2 and Cl_2 and incubated secondary antibodies (Table 2.2). Nuclei were stained by 4',6-diamidino-2-phenylindole (DAPI). Coverslips were mounted on slides using ProLong Gold antifade mounting reagent (Invitrogen) and left to dry overnight at room temperature.

2.5.2 Immunofluorescent microscopy

Widefield fluorescent microscopy was used for imaging in transferrin-488 trafficking assays (Chapter 3. Figures 3.1-3.3) and HeLa NLRP3-TurboID characterisation (Chapter 4. Figure 4.1). Images were obtained via Zeiss Axioimager D2 upright microscope using a 63×/1.4 Plan Apochromat objective with a Coolsnap HQ2 camera (Photometrics) and Micromanager software (v1.4.23). Band pass filter sets FITC, Texas Red, Cy5 and DAPI were used sequentially to prevent bleed through from one channel to the next. Images were taken of at least three independent fields of view per treatment per time point within each independent experiment.

Confocal microscopy was used for imaging in NLRP3/PI4P organelle marker experiments (Chapter 3. Figures 3.5-3.14, 3.16) and IL-1α-TurboID characterisation (Chapter 5. Figure 5.1).

Images (1024x1024 pixels) were obtained using a 63×/1.40 HCS PL Apo objective on a Leica TCS SP8 AOBS inverted confocal microscope with LASX software (v3.5.1.18803). The 405 nm blue diode and white light laser with 488, 514, 594, and 647 nm laser lines were used. To prevent crosstalk between channels, images were acquired sequentially. Z-stacks were acquired with 0.3 µm steps between Z sections. Camera gain and exposure times were unchanged within each replicate. Images were taken from three independent fields of view per treatment per time point within each replicate.

2.5.3 Image analysis

2.5.3.1 Transferrin-488 fluorescence analysis

Analysis of cell fluorescence was carried out using Fiji Image J software. For each image, brightness was increased to reveal the boundaries of each cell. 10 cells from each field of view (3 fields of view per condition) were drawn around and added to the region of interest (ROI) manager. The fluorescence of each image was then gated between 1,000-10,000 and fluorescence of each ROI then measured. Background was manually calculated by taking 3 independent measurements within each image from areas where cells were absent. The averaged background value was then subtracted from its respective mean fluorescent read-out. Mean cell fluorescence was then converted into percentage change using vehicle (column analyses) or 0 minute (group analyses) as mean 100%.

2.5.3.2 Colocalisation analysis

Image analysis was carried out using Fiji Image J software. Pearson's correlation coefficient (PCC) was calculated using Coloc2 Image J plugin. Maximum intensity projections were used for confocal images.

2.5.3.3 Fluorescence line graphs

Fluorescence intensity line graphs were created using Image J software. Fluorescence intensity of each channel was plotted individually over a 10 µm line then combined for comparison between channels. Line graphs depict fluorescence intensity between 0 and 250 grey value (a.u).

2.6 Statistical analysis and bioinformatic processing

2.6.1 GraphPad prism

PCC and fluorescence intensity data are presented as median ± interquartile range with individual data points shown (representing single cells or fields of view analysed within each experiment). ELISA and cell death data are presented as mean ± SEM with individual data points representing each independent experiment. Data were assessed for normal distribution using the Shapiro-Wilk normality test and analysed using unpaired two-tailed t-test or one-way analysis of variance (Tyanova et al.) followed by Dunnett's multiple comparison test for parametric data. For non-parametric data, a Kruskal-Wallis test followed by Dunn's multiple comparison test was used. For group analysis, data were analysed by two-way ANOVA followed by Dunnett's or Šidák's multiple comparisons test.

2.6.2 Perseus Max Quant for TurboID

The Perseus software platform (Tyanova et al., 2016) was used to prepare Protein Group datasets for NLRP3-TurboID (Vehicle) and NLRP3-TurboID (Nigericin), or Pro-IL-1α-TurboID and TurboID alone obtained from MaxQuant analysis of mass spectrometry data. Protein Group data included LFQ intensities which are normalised intensities for the interaction between bait, NLRP3-TurboID, IL-1α-TurboID or TurboID, and protein groups identified by mass spectrometry. Controls for false discovery rate (FDR) during MaxQuant analysis include the identification of reverse hits and protein groups only identified by site. Protein Groups were loaded into Perseus and LFQ intensities were identified as the columns of interest in this analysis. The dataset was then filtered to remove reverse hits and proteins only identified by site.

Data were transformed using a log2(x) transformation and normal distribution was checked by plotting histograms of LFQ intensity for all repeats within each experimental group (Alfa_VEH or TID_VEH). Samples were then grouped according to biological replicates and rows were filtered so that at least one experimental group (Alfa_VEH or TID_VEH) must contain a valid value for all 4 replicates. Imputation was carried out to allow any further missing values to be replaced with values predicted from a normal distribution. Principal component analysis (PCA) was performed on each biological replicate within Alfa_VEH and TID_VEH groups.

Two sample t-test was performed to identify proteins significantly enriched in Alfa_VEH groups, compared to TID_VEH. s0 is a parameter that defines the artificial variance within

groups and was set to a value of s0=2. Values were also corrected for using a false discovery rate (FDR) of 0.01. Data were presented as -Log p-value versus Log2 Fold change (FC).

Prior to further analysis, the Contaminant Repository for Affinity Purification (CRAPome) database (https://reprint-apms.org/) was used to investigate whether any significant hits have a propensity for a protein to be a 'non-specific' hit. The CRAPome provides a qualitative and semiqualitative description based on a large database of standardised negative control from serval leading labs specialising in affinity mass spectrometry.

2.6.3 Ingenuity pathway analysis

For NLRP3-TurboID and pro-IL-1α-TurboID pathway analysis, significant proteins were inputted into IPA along with respective fold change and p-value as determined by Perseus analysis. Subcellular location is assigned to each protein based on literature reviewed on the Qiagen IPA database. Canonical pathways, biological functions and diseases and disorders were assigned a p-value of overlap which describes whether there is a significant overlap between proteins from that given interactome and all proteins in that pathway. For pro-IL-1α-TurboID pathway analysis $p<0.01$ was used as a significance threshold for the pathways shown. The predicted upregulation and downregulation of canonical pathways, biological functions and diseases and disorders can also be calculated based on the enrichment of the proteins within the given interactome. Z-score is a read-out of the upregulation or downregulation; $z>0$ highlights a predicted activation and $z<0$ highlights a predicted inhibition, these scores are represented by orange and blue respectively (Kramer et al., 2014).

2.7 Appendix 1

Methods for TurboID proximity labelling acquisition edited from Stanford Burnham Prebys Proteomics Core report

2.7.1 Sample preparation

Cells were lysed in 8 M urea, 50 mM ammonium bicarbonate (ABC) and benzonase, and the lysate was centrifuged at 14,000 x g for 15 minutes to remove cellular debris. Supernatant protein concentration was determined using a bicinchoninic acid (BCA) protein assay (Thermo Scientific). Disulfide bridges were reduced with 5 mM tris(2-carboxyethyl) phosphine (TCEP) at 30°C for 60 min, and cysteines were subsequently alkylated with 15 mM iodoacetamide (IAA) in the dark at room temperature for 30 min.

2.7.2 Affinity purification

Affinity purification was carried out in a Bravo AssayMap platform (Agilent) using AssayMap streptavidin cartridges (Agilent). Briefly, cartridges were first primed with 50 mM ammonium bicarbonate, and then proteins were slowly loaded onto the streptavidin cartridge. Background contamination was removed with 8 M urea, 50 mM ammonium bicarbonate. Finally, cartridges were washed with Rapid digestion buffer (Promega, Rapid digestion buffer kit) and proteins were subjected to on-cartridge digestion with mass spec grade Trypsin/Lys-C Rapid digestion enzyme (Promega, Madison, WI) at 70C for 1 h. Digested peptides were then desalted in the Bravo platform using AssayMap C18 cartridges, and dried down in a SpeedVac concentrator.

2.7.3 Mass spectrometry analysis

Prior to LC-MS/MS analysis, dried biotin-enriched peptides were reconstituted with 2% ACN, 0.1% FA and concentration was determined using a NanoDropTM spectrophometer (ThermoFisher). Samples were then analyzed by LC-MS/MS using a Proxeon EASY-nanoLC system (ThermoFisher) coupled to a Orbitrap Fusion Lumos Tribid mass spectrometer (Thermo Fisher Scientific). Peptides were separated using an analytical C18 Aurora column (75µm x 250 mm, 1.6 µm particles; IonOpticks) at a flow rate of 300 nL/min (60C) using a 75-min gradient: 2% to 6% B in 1 min, 6% to 23% B in 45 min, 23% to 34% B in 28 min, and 34% to 48% B in 1 min (A= FA 0.1%; B=80% ACN: 0.1% FA). The mass spectrometer was operated in positive data-dependent acquisition mode. MS1 spectra were measured in the Orbitrap in a mass-to-charge (m/z) of 375 – 1500 with a resolution of 60,000. Automatic gain control target was set to 4 x 10^5 with a maximum injection time of 50 ms. The instrument was set to run in top speed mode with 1-second cycles for the survey and the MS/MS scans. After a survey scan, the most abundant precursors (with charge state between +2 and +7) were isolated in the quadrupole with an isolation window of 0.7 m/z and fragmented with HCD at 30% normalized collision energy. Fragmented precursors were detected in the ion trap as rapid scan mode with automatic gain control target set to 1 x 10^4 and a maximum injection time set at 35 ms. The dynamic exclusion was set to 20 seconds with a 10 ppm mass tolerance around the precursor.

2.7.4 Data analysis

All mass spectra were analysed with MaxQuant software version 1.6.11.0. MS/MS spectra were searched against the Homo sapiens Uniprot protein sequence database (downloaded in

April 2022) and GPM cRAP sequences (commonly known protein contaminants). Precursor mass tolerance was set to 20 ppm and 4.5 ppm for the first search where initial mass recalibration was completed and for the main search, respectively. Product ions were searched with a mass tolerance 0.5 Da. The maximum precursor ion charge state used for searching was 7. Carbamidomethylation of cysteine was searched as a fixed modification, while oxidation of methionine and acetylation of protein N-terminal were searched as variable modifications. Enzyme was set to trypsin in a specific mode and a maximum of two missed cleavages was allowed for searching. The target-decoy-based false discovery rate (FDR) filter for spectrum and protein identification was set to 1%.

Chapter 3:

The cell biology of NLRP3 activation

Chapter 3. The cell biology of NLRP3 activation

3.1 Introduction

The canonical NLRP3 inflammasome requires a two-step activation process to achieve caspase-1 cleavage, IL-1β processing and release, and cell death (Swanson et al., 2019). The first signal known as priming, is necessary to induce expression of NLRP3 and pro-IL-1β. A further stimulus is then required for an active inflammasome to assemble; this may be a PAMP, DAMP or another activating stimulus (Kelley et al., 2019). The NLRP3 inflammasome is distinct in its ability to respond to a diverse range of stimuli (Rahman et al., 2020). It has been suggested that these diverse stimuli may cause a common disruption in cellular homeostasis that is sensed by NLRP3 (Liston and Masters, 2017). The literature has recently been reviewed highlighting the role of subcellular organelles in integrating a dysregulation in cellular homeostasis, with a particular focus on the role of endosomal trafficking dysfunction in this process (Seoane et al., 2020).

NLRP3-activating stimuli cause a dispersal of the *trans*-Golgi marker TGN38/46 (Chen and Chen, 2018). This is suggested to represent a dTGN that is important in NLRP3 recruitment, activation, and subsequent downstream inflammatory signalling. However, in addition to its presence at the TGN, TGN38/46 also cycles through the plasma membrane and endosomes before returning to the TGN (Reaves et al., 1993). Another marker of the TGN, Golgin97, does not cycle in this manner and remains localised to the TGN (Lee et al., 2023, Zhang et al., 2023). TGN38/46 co-localises with markers for endosomes and lysosomes following stimulation with NLRP3-activating stimuli (Lee et al., 2023, Zhang et al., 2023). This co-localisation is specific to TGN38/46, as Golgin97 remains localised to the TGN following NLRP3 activation. A disruption in endosomal trafficking is suggested to cause an accumulation of TGN38/46 in endosomes.

TGN38/46 cycling is most disrupted by reagents that cause alterations in endosomal pH. Interestingly, NLRP3-activating stimuli imiquimod has been shown to perturb endosomal pH (Groß et al., 2016). Therefore, NLRP3 inflammasome activation may also be associated with perturbed endosomal function and cargo trafficking.

NLRP3 interacts with the inositol lipid phosphatidylinositol 4-phosphate (PI4P) through a conserved polybasic motif (Chen and Chen, 2018). PI4P is characteristically pooled at the TGN, but both endosomal and lysosomal membranes have been shown to contain this lipid (Hammond et al., 2014, Tan and Finkel, 2022). Interestingly, PI4P is recruited to lysosomes following lysosomal damage, which can be an upstream event in NLRP3 activation (Tan and Finkel, 2022, Hornung et al., 2008). Recent studies report that NLRP3 recruitment is dependent upon NLRP3-PI4P interaction on endosomal membranes (Lee et al., 2023, Zhang et al., 2023). We therefore tested the hypothesis that endocytic traffic disruption is a common downstream effect of NLRP3-activating stimuli and therefore NLRP3 senses disrupted endocytic traffic as a trigger for its activation. We investigated whether endocytic traffic disruption causes NLRP3 to localise to endolysosomal compartments and whether this was observed to co-localise with an accumulation of PI4P.

3.2 Results

3.2.1 NLRP3-activating stimuli disrupt endocytic traffic

Dispersal of TGN38/46 following treatment with NLRP3-activating stimuli may be a consequence of a disruption in endosomal cargo trafficking. Work by our group has shown co-localisation of TGN38/46 with endolysosomal markers following stimulation with a panel

of NLRP3 activators (Lee et al., 2023). This suggested that the dTGN vesicles may be endolysosomal in nature, and that TGN38/46 is trapped in endosomes and lysosomes following stimulation. Therefore, I wanted to test the hypothesis that NLRP3 activating stimuli cause a disruption in endocytic traffic. To do this, I investigated the effect of NLRP3-activating stimuli on an endosomal cargo trafficking pathway: endosome-plasma membrane recycling. Here, I used a fluorescently tagged version of transferrin to track this pathway. Upon binding to its receptor, transferrin is endocytosed at the plasma membrane into early endosomes before being recycled back to the plasma membrane (Kauppi et al., 2002) (Figure 3.1A).

The NLRP3-activating stimuli used in these experiments were chosen as they each induce a mechanism implicated in NLRP3 activation: K^+ efflux (nigericin), lysosomal destabilisation (LeuLeu-OMe) and oxidative stress (imiquimod) (Table 1.1) (Perregaux and Gabel, 1994, Mariathasan et al., 2006, Hornung et al., 2008, Groß et al., 2016). Monensin is a monovalent ionophore, which primarily facilitates the transmembrane exchange of sodium ions for protons (Mollenhauer et al., 1990). This results in the neutralisation of acidic intracellular compartments and the disruption in intracellular traffic (Hu et al., 2015). Monensin, therefore, was included as a control for its ability to disrupt endosomal trafficking but not activate NLRP3.

3.2.1.1 Transferrin is readily recycled in vehicle-treated cells

HeLa cells were first incubated with fluorescent transferrin for 30 minutes. Cells were then placed on ice to halt transferrin trafficking and underwent an ice-cold acid wash to remove any plasma membrane bound fluorescent transferrin. A proportion of cells were fixed at this

point, 0 minutes, as a measure of fluorescent transferrin uptake. The remaining cells were saturated with unlabelled transferrin (holo-transferrin), encouraging exchange of fluorescent transferrin with holo-transferrin, and incubated for a further 15 or 30 minutes at 37°C. Functional endosome to plasma membrane recycling allows internalised fluorescent transferrin to be trafficked to the plasma membrane via endosomal compartments, where it is then replaced by saturated holo-transferrin at its receptor. Therefore, a decrease in cell fluorescence at 15 and 30 minutes is a measure of successful endosome to plasma membrane recycling. In vehicle-treated cells, intracellular fluorescent transferrin decreased by 52% following 15-minute chase with holo-transferrin (Figure 3.1B and C). Upon inspection, the remaining fluorescent transferrin at 15 minutes showed a perinuclear localisation, compared to the more diffuse spread of fluorescent transferrin at 0 minutes (Figure 3.1B), suggesting that transferrin may be retained at the endosome recycling complex, due to the disruption in endosome-plasma membrane recycling (Xie et al., 2016). At 30 minutes, intracellular fluorescent transferrin decreased by 83% compared to 0 minutes, showing that almost all fluorescent transferrin internalised after a 30-minute uptake period was recycled back out of the cell after 30 minutes holo-transferrin chase (Figure 3.1B, C). Therefore, tracking the fate of fluorescent transferrin in this way provides a model for functional endosome to plasma membrane recycling and a means to measure dysfunction in endosomal cargo trafficking.

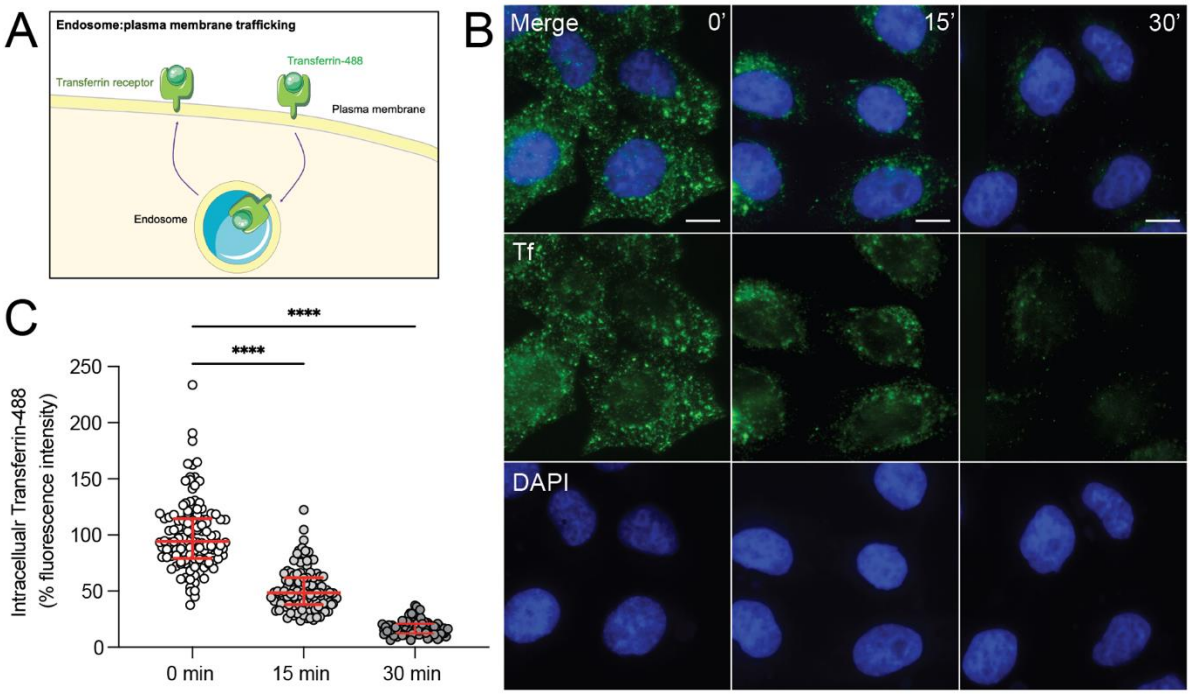

Figure 3.1. Fluorescent transferrin is readily recycled out of the cell. (A) Transferrin binds to the transferrin receptor and is endocytosed into early endosomes, where it releases bound iron, before cycling back to the plasma membrane before being released extracellularly. **(B)** HeLa cells were treated with transferrin-488 (5 ug/ml) for 30 minutes, then incubated with media containing unlabelled transferrin for 0, 15 or 30 minutes. Representative immunofluorescence images of transferrin-488 (Tf; green), blue represents nuclei staining by DAPI. **(C)** Quantification of remaining cell associated transferrin-488 was measured by intracellular transferrin-488 fluorescence intensity at 0, 15 and 30 minutes after incubation with unlabelled transferrin (n = 97 to 117 cells per group from three fields of view from four independent experiments). Scale bars are 10 µm. Values are median ± IQR. Data were analysed using Kruskal-Wallis test followed by Dunn's multiple comparison test (compared with 0 minutes). ****P ≤ 0.0001

3.2.1.2 NLRP3-activating stimuli differentially affect transferrin uptake

Before investigating the impact of NLRP3 inflammasome activating stimuli upon endosome to plasma membrane recycling, I first determined whether NLRP3 inflammasome activating stimuli had any effect on the uptake of fluorescent transferrin. HeLa cells were treated with NLRP3 inflammasome activating stimuli together with fluorescent transferrin for 30 minutes and uptake of fluorescent transferrin was measured. Fluorescent microscopy showed that following nigericin stimulation, the amount of intracellular fluorescent transferrin at 0 minutes was significantly less compared to vehicle (Figure 3.2A, B). However, following Leu-LeuLOMe and monensin stimulation, there was a significant increase in the amount of intracellular fluorescent transferrin (Figure 3.2B). Imiquimod had no impact on the amount of internalised fluorescent transferrin here (Figure 3.2B). NLRP3 inflammasome activating stimuli and monensin also had little effect upon the phenotypic distribution of fluorescent transferrin within the cell, with the slight exception of the nigericin treated cells which show a more rounded cell morphology and greater concentration of fluorescent transferrin around the perinuclear region (Figure 3.2A). These data suggest that NLRP3 inflammasome activating stimuli affect the amount of internalised transferrin, and therefore may impact endocytosis. However, as there is variation between how these stimuli affect uptake in this assay, this suggests that perturbation of endocytosis is not a global effect of NLRP3 inflammasome activating stimuli observed here.

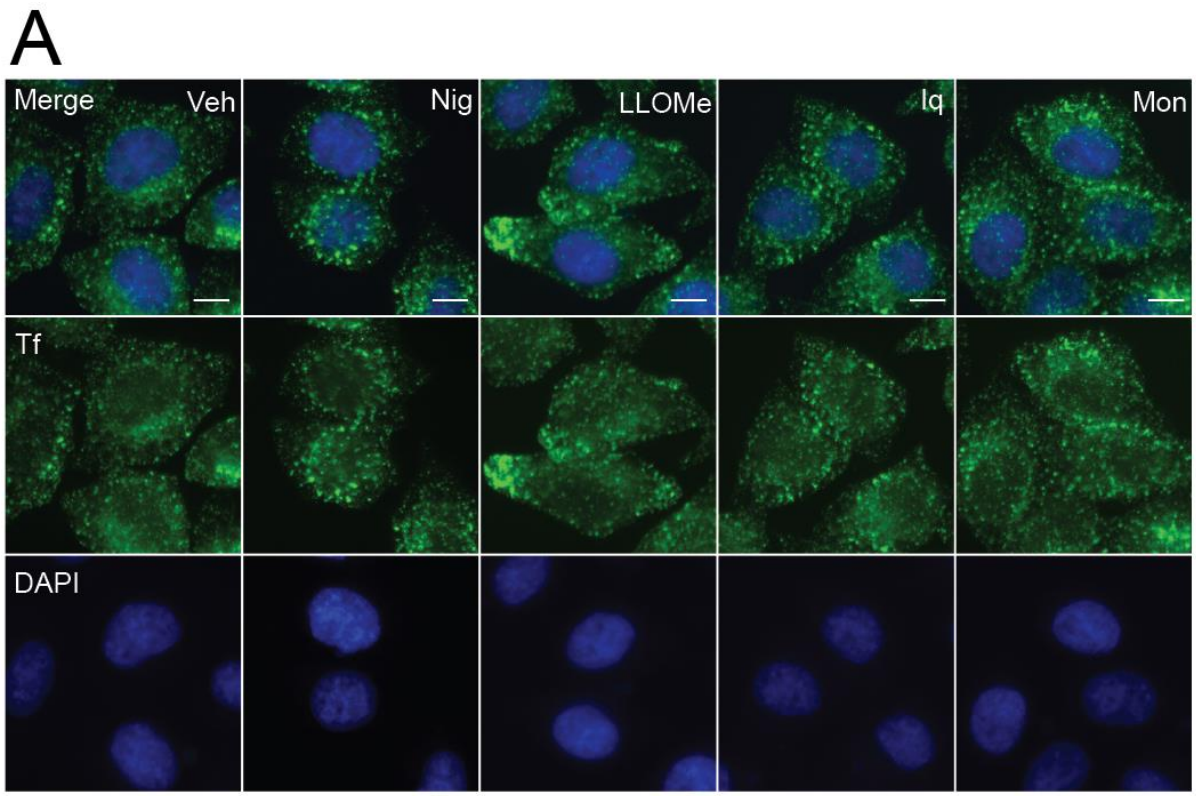
A
Merge
Veh
Nig
LLOMe
Iq
Mon
Tf
DAPI

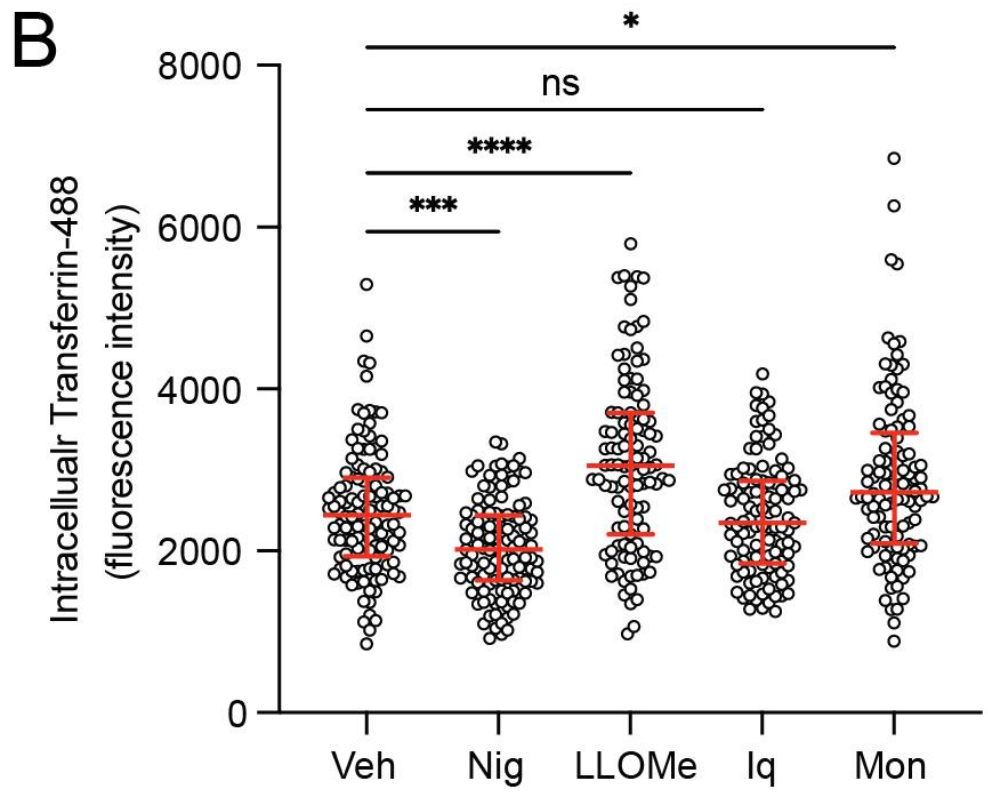
B
*
ns
****
***
8000
6000
4000
2000
0
Intracelluair Transferrin-488
(fluorescence intensity)
Veh
Nig
LLOMe
Iq
Mon

Figure 3.2. Transferrin uptake in the presence of NLRP3 inflammasome activating stimuli. **(A)** HeLa cells were treated with transferrin-488 (5 ug/ml) and with either vehicle (Veh), nigericin (Nig, 10 µM), LeuLeu-OMe (LLOMe, 1 mM), imiquimod (Iq, 75 µM), or monensin (Mon, 10 µM) for 30 minutes. Representative immunofluorescence images of transferrin-488 (Tf; green), blue represents nuclei staining by DAPI. **(B)** Quantification of remaining cell associated transferrin-488 was measured by intracellular transferrin-488 fluorescence intensity following 30 minutes incubation with trasnferrin-488 and respective stimuli. (n = 107-120 cells per group from 3 fields of view from 4 independent experiments). Scale bars are 10 µm. Values are median ± IQR. Data were analysed using Kruskal-Wallis test followed by Dunn's multiple comparison test (compared to vehicle). *, P≤0.05; ***, P≤0.001, ****, P≤0.0001, ns= not significant.

3.2.1.3 NLRP3-activating stimuli disrupt endosomal recycling

I proceeded to investigate the impact of NLRP3 inflammasome activating stimuli on endosome to plasma membrane recycling. I treated HeLa cells with vehicle, nigericin, LeuLeu-OMe, imiquimod, or monensin, simultaneously with fluorescent transferrin for 30 minutes at 37°C. Cells were then put on ice to halt endosomal recycling and underwent an acid wash to remove any surface bound fluorescent transferrin. Cells were then incubated at 37°C in media saturated with holo-transferrin along with vehicle, nigericin, LeuLeu-OMe, imiquimod, or monensin for 15 or 30 minutes. When endosome to plasma membrane recycling is impaired, fluorescent transferrin cannot be readily recycled out of the cell and remains trapped within endosomal compartments. Therefore, the amount of fluorescent transferrin maintained within the cell after 15 and 30 minutes is proportional to the degree of endosomal recycling disruption. Vehicle-treated cells showed a time-dependent loss of transferrin fluorescence by fluorescent microscopy, with 52% loss at 15 minutes and 83% loss at 30 minutes confirming recycling of transferrin receptors to the plasma membrane (Figure 3.3A and B). All treatments caused a retention of transferrin in the cell after 15- and 30-minute holo-transferrin chase. This effect on transferrin recycling was most evident in nigericin and monensin treated cells, although Leu-Leu-OMe and imiquimod too caused a disruption in transferrin recycling (Figure 3.3A and B). These data suggest that endosome to plasma membrane recycling is perturbed by NLRP3-activating stimuli and monensin.

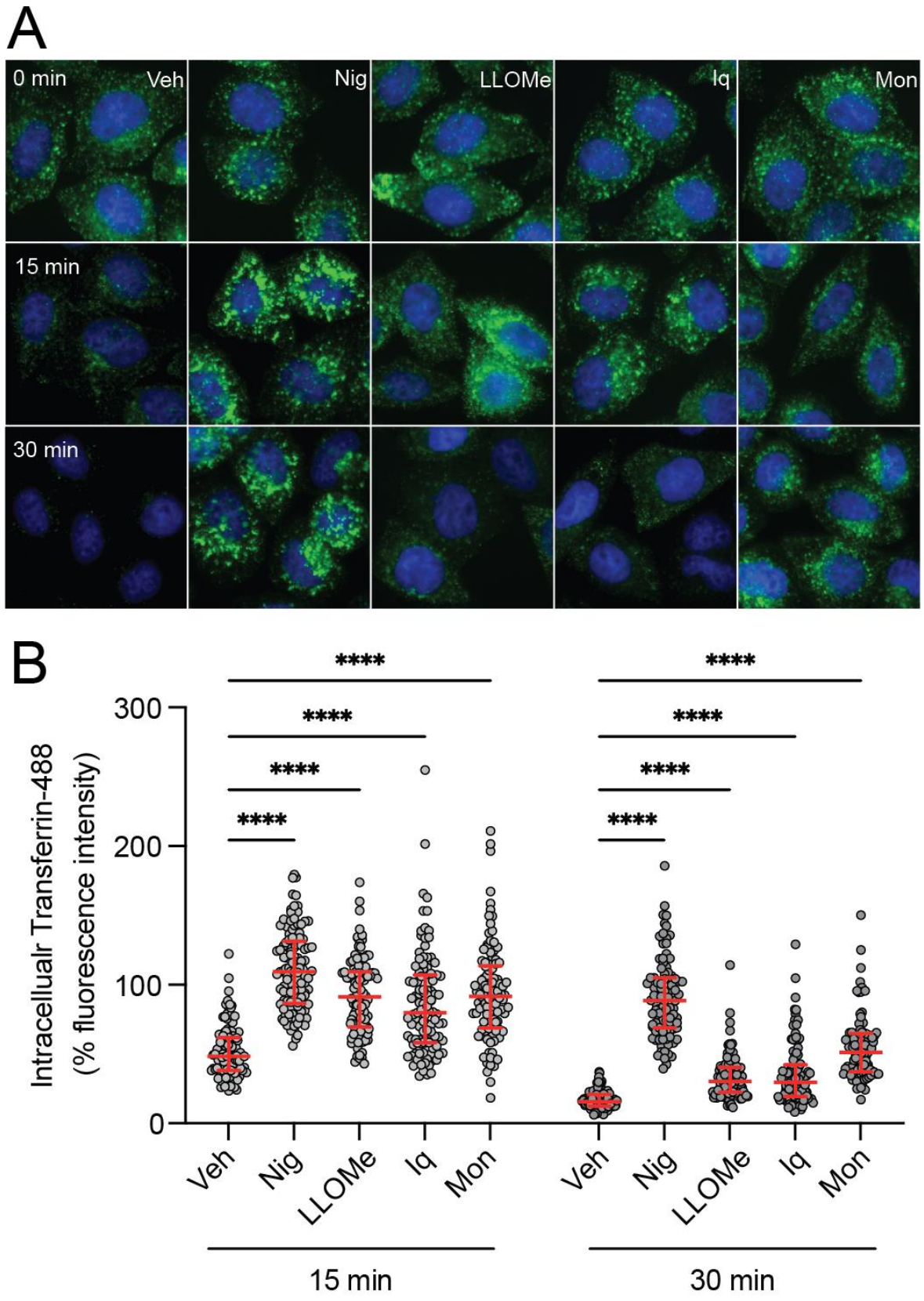
A
0 min
Veh
Nig
LLOMe
Iq
Mon
15 min
30 min
B
Intracellualr Transferrin-488
(% fluorescence intensity)
300
200
100
0
****
****
****
****
****
****
****
****
Veh
Nig
LLOMe
Iq
Mon
Veh
Nig
LLOMe
Iq
Mon
15 min
30 min

Figure 3.3. Endosome to plasma membrane recycling is disrupted by NLRP3-activating stimuli. (A) HeLa cells were treated with transferrin-488 (5 ug/ml) and with either vehicle (Veh), nigericin (Nig, 10 µM), LeuLeu-OMe (LLOMe, 1 mM), imiquimod (Iq, 75 µM), or monensin (Mon, 10 µM) for 30 minutes, then incubated with media containing unlabelled transferrin for 0, 15 or 30 minutes in the presence of indicated stimuli. Representative immunofluorescence images of transferrin-488 (Tf; green), blue represents nuclei staining by DAPI. **(B)** Quantification of remaining cell-associated transferrin-488 was measured by the fluorescence intensity of transferrin-488 at 15 and 30 min after removal of extracellular transferrin-488 (n = 97 to 117 cells per group from three fields of view from four independent experiments). Scale bars are 10 µm. Values are median ± IQR. Data were analysed using Kruskal-Wallis test followed by Dunn's multiple comparison test (compared to vehicle). ****, P≤0.0001.

3.2.2 NLRP3 puncta characterisation and localisation

The data thus far suggested a link between NLRP3 inflammasome activation and endosomal cargo trafficking dysfunction. Therefore, I next wanted to assess whether NLRP3 could localise to endolysosomal membranes following stimulation. To do this, I used COS7 cells stably expressing low levels of NLRP3-mVenus to assess NLRP3 localisation. Prior to co-staining with a panel of endolysosomal and TGN markers (Figure 3.4), I first wanted to characterise the behaviour of NLRP3-mVenus in these cells following stimulation.

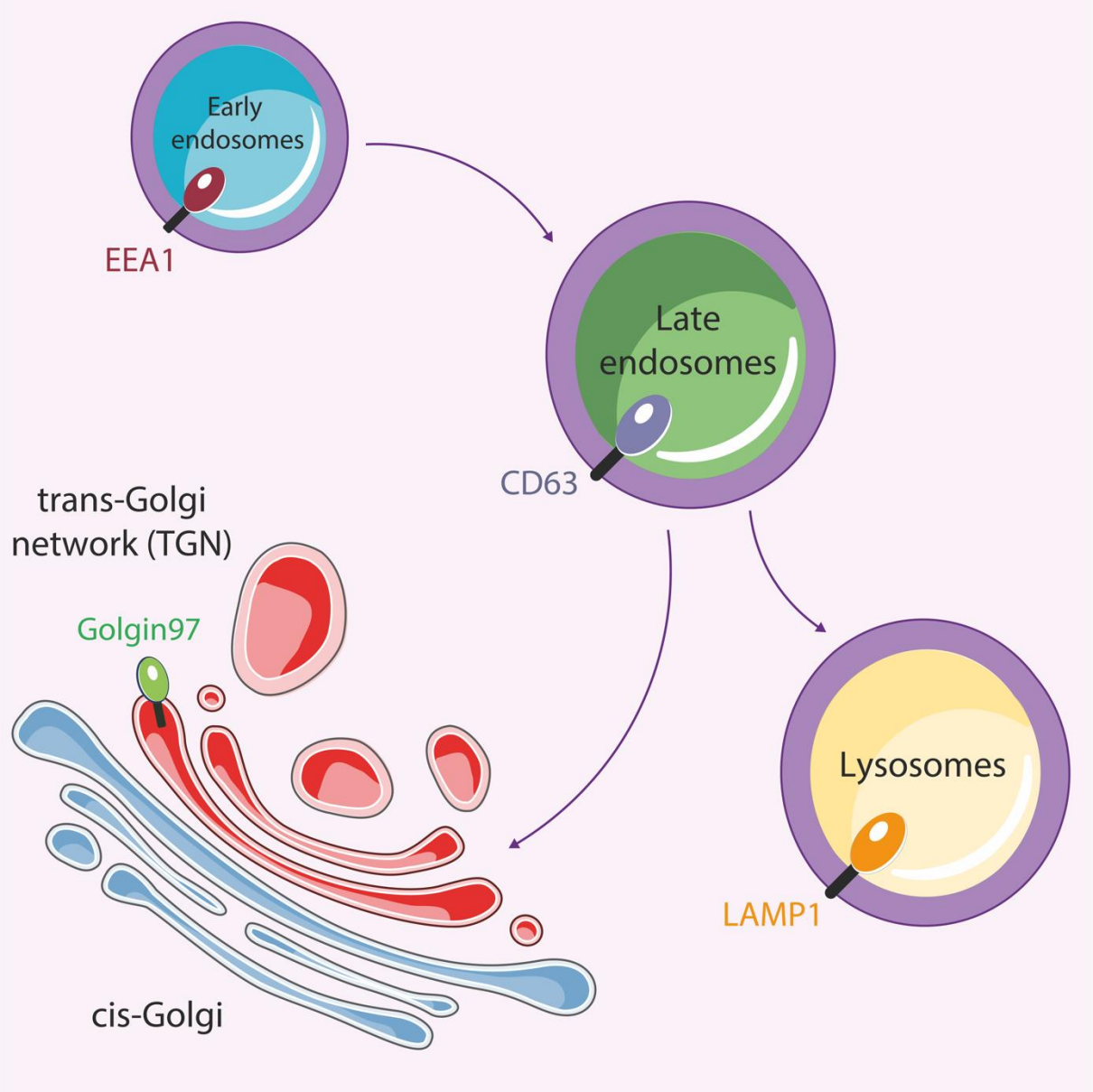

Figure 3.4. Schematic of endolysosomal trafficking with relevant compartment markers. Early endosomes mature to late endosomes. Late endosomes can mature to lysosomes or cycle to the *trans*-Golgi network. Membrane bound organelles are depicted with their common membrane marker proteins; early endosomes: EEA1 (red), late endosomes: CD63 (purple), lysosomes: LAMP1 (orange) and the *trans*-Golgi network (TGN): Golgin97 (green).

3.2.2.1 NLRP3-mVenus forms puncta after treatment with NLRP3-activating stimuli

COS7 cells stably expressing low levels of NLRP3-mVenus were used as a model to characterise the distribution of NLRP3 following treatment with NLRP3-activating stimuli. In the absence of stimulation, NLRP3-mVenus was predominantly diffuse across the cytosol and with some perinuclear localisation (Figure 3.5). Stimulation with the NLRP3 inflammasome activating stimuli, nigericin and Leu-LeuOMe, caused a redistribution of NLRP3-mVenus to cytoplasmic puncta and a relocation away from the perinuclear region. In contrast, stimulation with imiquimod caused NLRP3-mVenus to remain localised to the perinuclear region, like that observed in vehicle-treated cells (Figure 3.5). Interestingly, monensin, although not an NLRP3 inflammasome activator, also induced a punctate distribution of NLRP3-mVenus (Figure 3.5).

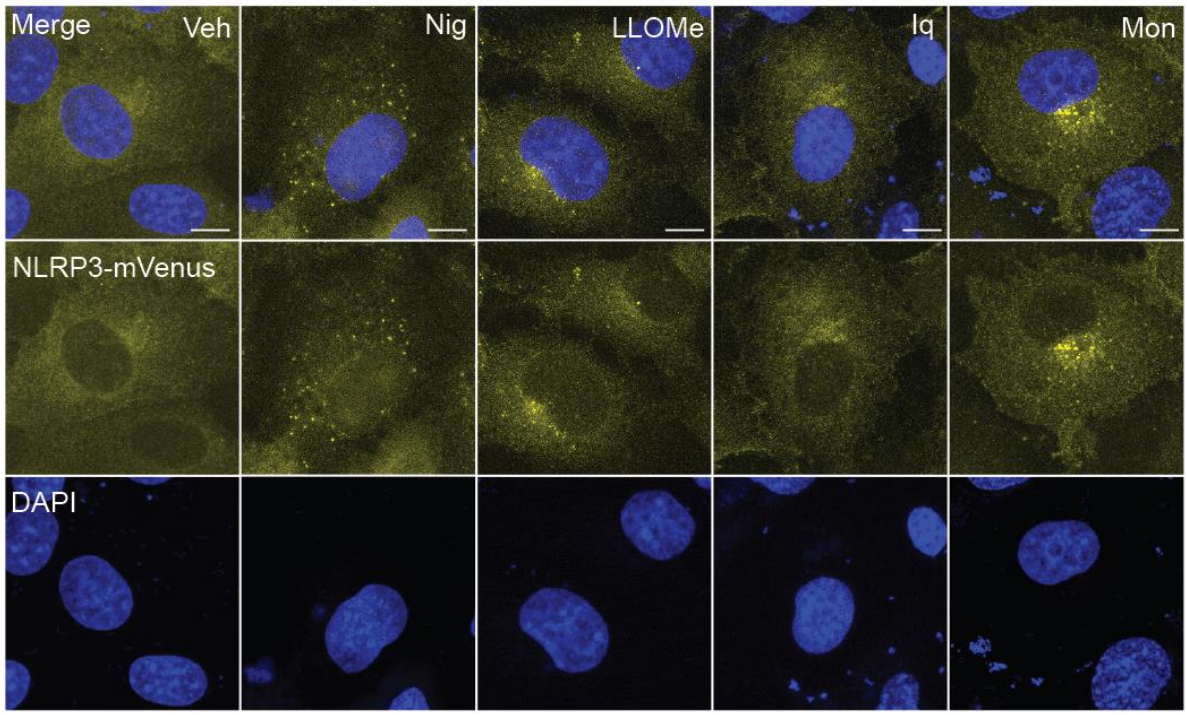

Figure 3.5. NLRP3-mVneus subcellular localisation following stimulation with NLRP3-activating stimuli. COS7 NLRP3-mVenus cells were treated with either vehicle (Veh), nigericin (Nig, 10 µM), LeuLeu-OMe (LLOMe, 1 mM), imiquimod (Iq, 75 µM), or monensin (Mon, 10 µM) for 90 minutes. Representative immunofluorescence images of NLRP3-mVenus (yellow), blue represents nuclei staining by DAPI. Scale bars are 10 µm. Images are representative of eight independent experiments.

3.2.2.2 NLRP3-mVenus can co-localise on endolysosomal membranes

To assess whether NLRP3 puncta co-localised with compartments positive for endosomal and lysosomal markers following stimulation, I co-stained COS7 NLRP3-mVenus cells with the resident *trans*-Golgi marker Golgin97 (Figure 3.6), early endosomal marker EEA1 (Figure 3.7), CD63 for late endosomes (Figure 3.8), and lysosomal marker LAMP1 (Figure 3.9). Stimulation with the NLRP3-activating stimulus nigericin caused a redistribution of NLRP3-mVenus to cytoplasmic puncta that co-localised with EEA1-, CD63- and LAMP1-positive compartments. Stimulation with Leu-LeuOMe too caused a redistribution of NLRP3-mVenus that co-localised with EEA1- and LAMP1-positive compartments (Figure 3.7 and 3.9). In contrast, NLRP3-mVenus rarely co-localised with the *trans*-Golgi marker, Golgin97, following stimulation with nigericin or Leu-LeuOMe (Figure 3.6). Interestingly, imiquimod did not cause a drastic redistribution of NLRP3-mVenus; NLRP3-mVenus remained perinuclear and co-localised with Golgin97 (Figure 3.6) and showed co-localisation with EEA1-positive compartments only (Figures 3.7). Following monensin stimulation, NLRP3-mVenus remained largely localised to the TGN (Figure 3.6) but did show some cytoplasmic puncta formation that co-localised with the late endosome marker, CD63 (Figure 3.8). These data suggest that NLRP3-mVenus can localise to multiple endolysosomal membranes following stimulation with NLRP3-activating stimuli. However, the characteristics of NLRP3-mVenus localisation following stimulation varies between stimuli, therefore another common signal may be involved to trigger NLRP3 inflammasome activation.

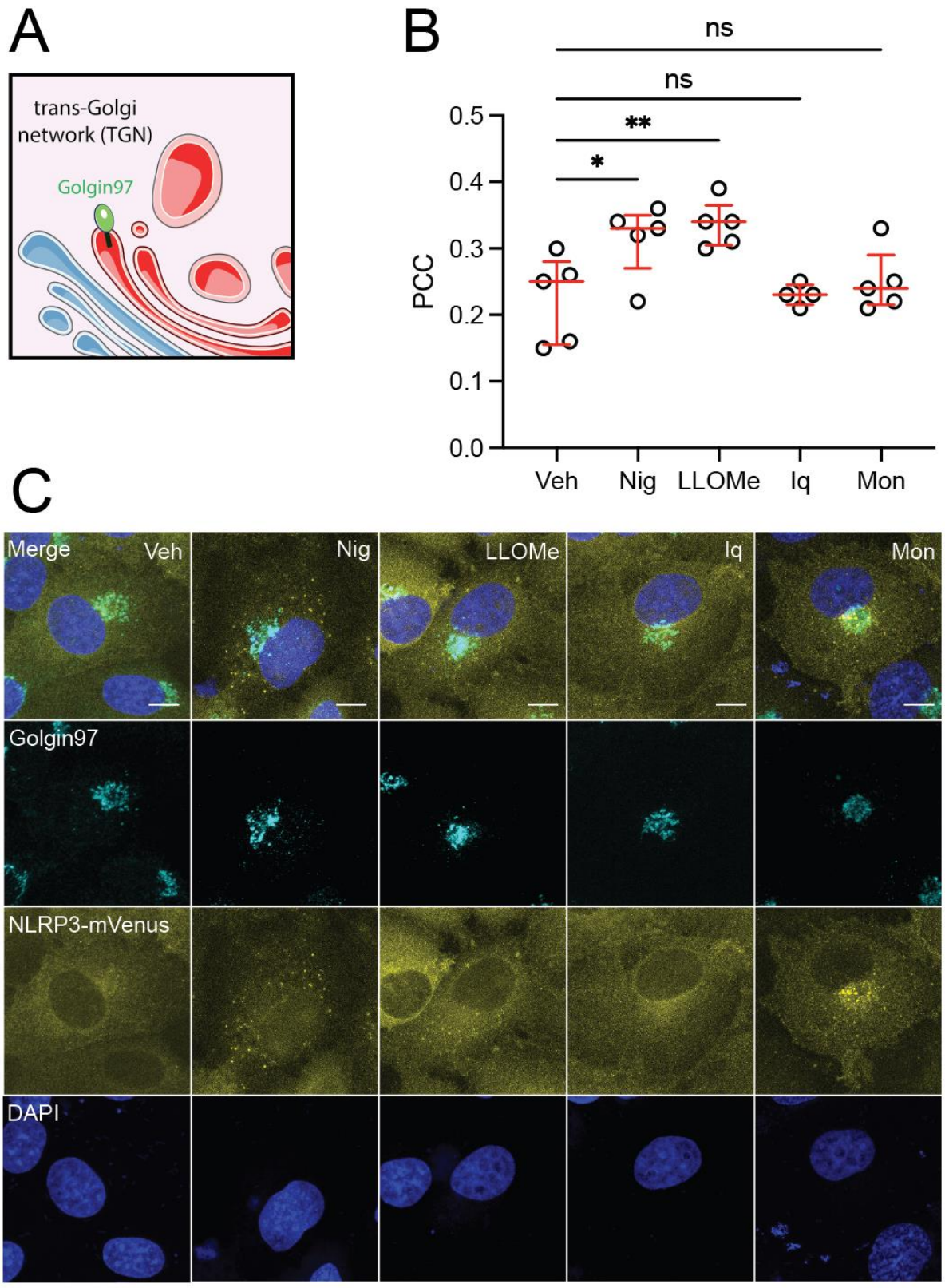
A
trans-Golgi
network (TGN)
Golgin97
B
ns
ns
**
*
PCC
0.5
0.4
0.3
0.2
0.1
0.0
Veh
Nig
LLOMe
Iq
Mon
C
Merge
Veh
Nig
LLOMe
Iq
Mon
Golgin97
NLRP3-mVenus
DAPI

Figure 3.6. Localisation of NLRP3-mVenus with Golgin97 following stimulation with NLRP3-activating stimuli. (A) Schematic of trans-Golgi network (TGN) with resident TGN marker Golgin97 (green). **(B)** Quantification of stimulus-induced co-localisation of NLRP3-mVenus and Golgin97 with the Pearson's correlation coefficient (PCC) in COS7 NLRP3-mVenus cells treated with either vehicle (Veh), nigericin (Nig, 10 µM), LeuLeu-OMe (LLOMe, 1 mM), imiquimod (Iq, 75 µM), or monensin (Mon, 10 µM) for 90 minutes. Data are n=4-5 fields of view across 3 independent experiments. Values are median ± IQR. Data were analysed using one-way ANOVA followed by Dunnett's multiple comparison test (compared to vehicle). *, P≤0.05; **, P≤0.01, ns= not significant. **(C)** Representative immunofluorescence images of NLRP3-mVenus (yellow) and Golgin97 (cyan). Blue represents nuclei staining by DAPI. Scale bars are 10 µm. Images are representative of three independent experiments.

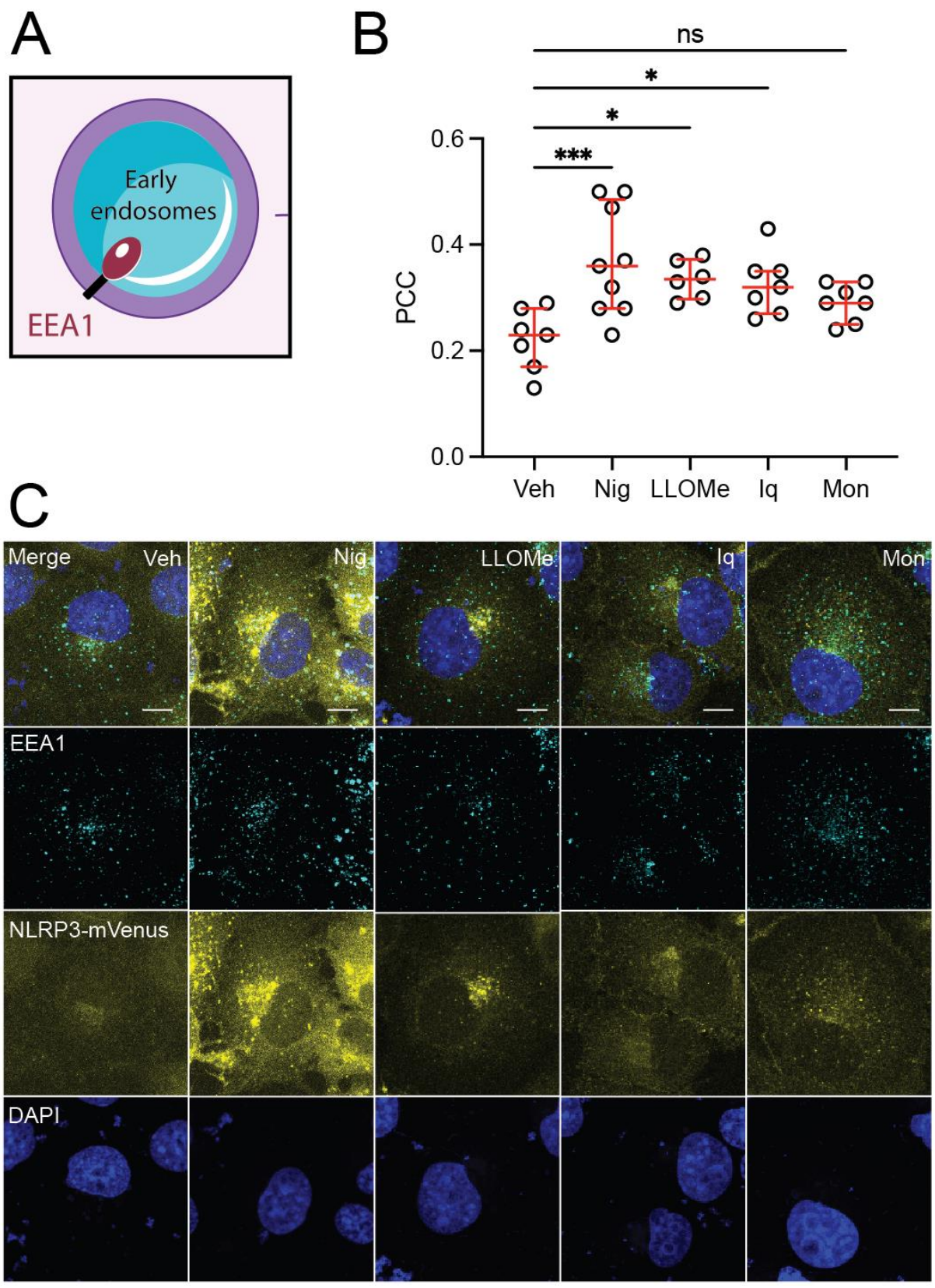
A
Early endosomes
EEA1
B
ns
*
*
***
0.6
0.4
0.2
0.0
PCC
Veh
Nig
LLOMe
Iq
Mon
C
Merge
Veh
Nig
LLOMe
Iq
Mon
EEA1
NLRP3-mVenus
DAPI

Figure 3.7. Localisation of NLRP3-mVenus with EEA1 following stimulation with NLRP3-activating stimuli. (A) Schematic an early endosome with marker EEA1 (red). **(B)** Quantification of stimulus-induced co-localisation of NLRP3-mVenus and EEA1 with the Pearson's correlation coefficient (PCC) in COS7 NLRP3-mVenus cells treated with either vehicle (Veh), nigericin (Nig, 10 µM), LeuLeu-OMe (LLOMe, 1 mM), imiquimod (Iq, 75 µM), or monensin (Mon, 10 µM) for 90 minutes. Data are n=6-9 fields of view across 3 independent experiments. Values are median ± IQR. Data were analysed using one-way ANOVA followed by Dunnett's multiple comparison test (compared to vehicle). *, P≤0.05; ***, P≤0.001, ns= not significant. **(C)** Representative immunofluorescence images of NLRP3-mVenus (yellow) and EEA1 (cyan). Blue represents nuclei staining by DAPI. Scale bars are 10 µm. Images are representative of three independent experiments.

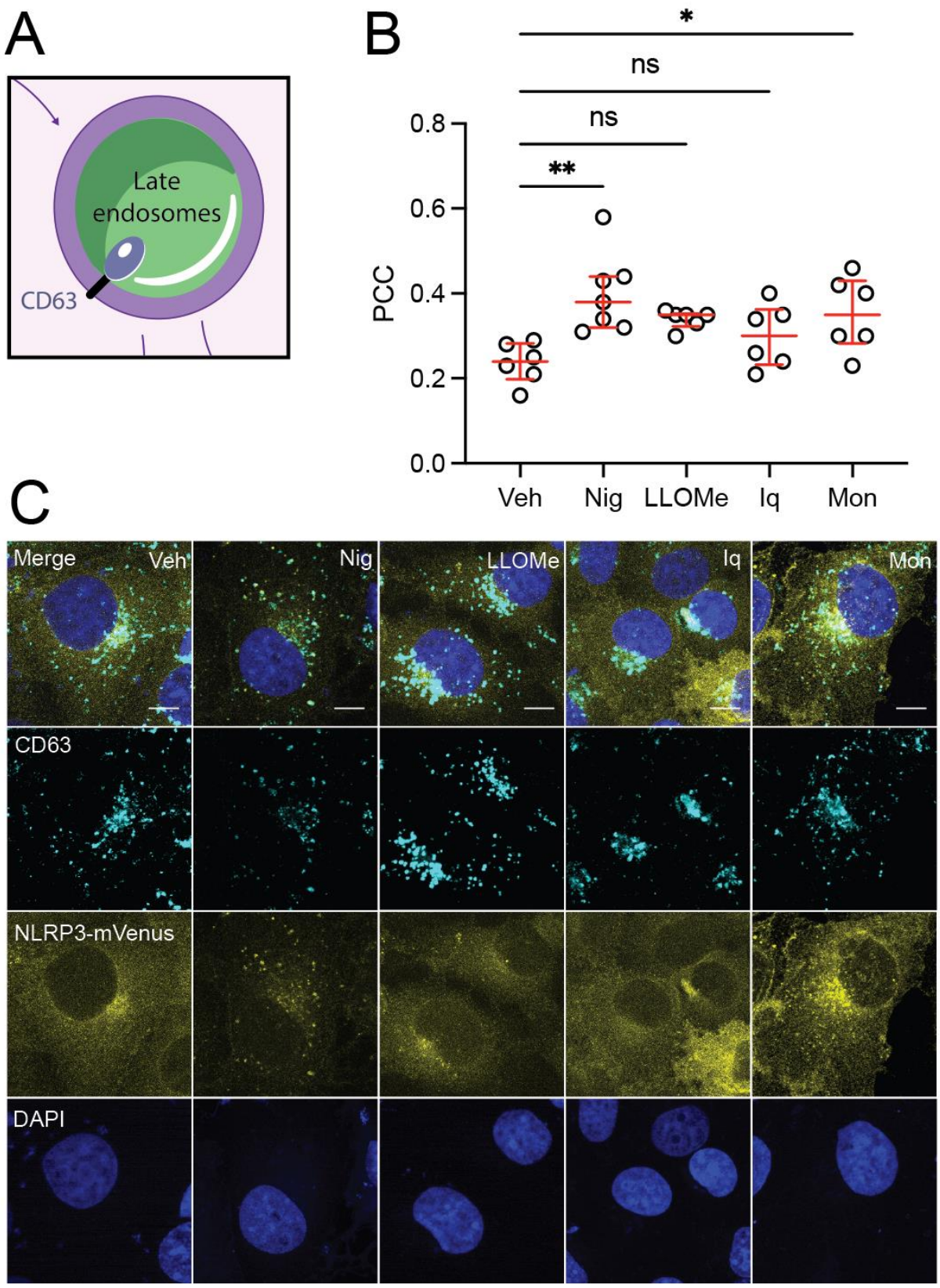
A
Late endosomes
CD63
B
*
ns
ns
**
PCC
0.8
0.6
0.4
0.2
0.0
Veh
Nig
LLOMe
Iq
Mon
C
Merge
Veh
Nig
LLOMe
Iq
Mon
CD63
NLRP3-mVenus
DAPI

Figure 3.8. Localisation of NLRP3-mVenus with CD63 following stimulation with NLRP3-activating stimuli. (A) Schematic an early endosome with marker CD63 (red). **(B)** Quantification of stimulus-induced co-localisation of NLRP3-mVenus and CD63 with the Pearson's correlation coefficient (PCC) in COS7 NLRP3-mVenus cells treated with either vehicle (Veh), nigericin (Nig, 10 µM), LeuLeu-OMe (LLOMe, 1 mM), imiquimod (Iq, 75 µM), or monensin (Mon, 10 µM) for 90 minutes. Data are n=6-7 fields of view across 3 independent experiments. Values are median ± IQR. Data were analysed using one-way ANOVA followed by Dunnett's multiple comparison test (compared to vehicle). *, P≤0.05; **, P≤0.01, ns= not significant. **(C)** Representative immunofluorescence images of NLRP3-mVenus (yellow) and CD63 (cyan). Blue represents nuclei staining by DAPI. Scale bars are 10 µm. Images are representative of three independent experiments.

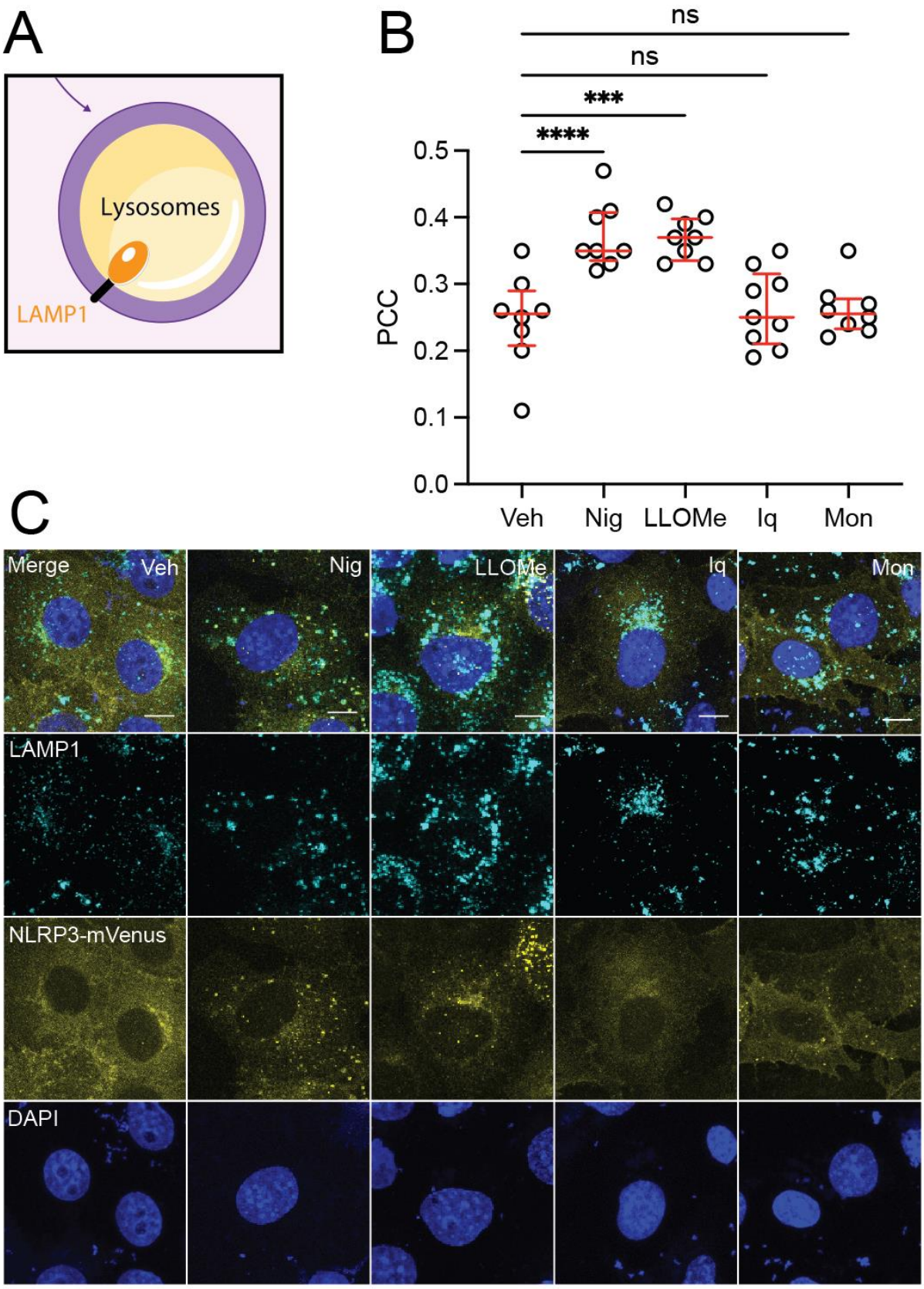
A
Lysosomes
LAMP1
B
ns
ns
***
****
PCC
0.5
0.4
0.3
0.2
0.1
0.0
Veh
Nig
LLOMe
Iq
Mon
C
Merge
Veh
Nig
LLOMe
Iq
Mon
LAMP1
NLRP3-mVenus
DAPI

Figure 3.9. Localisation of NLRP3-mVenus with LAMP1 following stimulation with NLRP3-activating stimuli. (A) Schematic an early endosome with marker LAMP1 (red). **(B)** Quantification of stimulus-induced co-localisation of NLRP3-mVenus and LAMP1 with the Pearson's correlation coefficient (PCC) in COS7 NLRP3-mVenus cells treated with either vehicle (Veh), nigericin (Nig, 10 µM), LeuLeu-OMe (LLOMe, 1 mM), imiquimod (Iq, 75 µM), or monensin (Mon, 10 µM) for 90 minutes. Data are n=8-9 fields of view across 3 independent experiments. Values are median ± IQR. Data were analysed using one-way ANOVA followed by Dunnett's multiple comparison test (compared to vehicle). ***, P≤0.001, ****, P≤0.0001 ns= not significant. **(C)** Representative immunofluorescence images of NLRP3-mVenus (yellow) and LAMP1 (cyan). Blue represents nuclei staining by DAPI. Scale bars are 10 µm. Images are representative of three independent experiments.

3.2.3 PI4P puncta characterisation and localisation

NLRP3 is reported to associate with PI4P on the membranes of TGN38/46-positive vesicles (Chen and Chen, 2018). Recent reports have suggested that TGN38/46-positive vesicles can also be endolysosomal in nature (Lee et al., 2023, Zhang et al., 2023). I have reported here that NLRP3 localises to compartments positive for endolysosomal markers. Therefore, I wanted to characterise the localisation of PI4P with respect to NLRP3-mVenus and a panel of organelle markers, to test the hypothesis that NLRP3 co-localised with PI4P on vesicles of endolysosomal origin.

3.2.3.1 PI4P co-localised with NLRP3-mVenus following stimulation with NLRP3 inflammasome activating stimuli

To verify previous literature reporting the interaction between NLRP3 and PI4P during NLRP3 inflammasome activation, I first assessed the localisation of PI4P and NLRP3-mVenus following stimulation with a panel of NLRP3 inflammasome activating stimuli and monensin. To do this, I transiently transfected COS7 NLRP3-mVenus cells with the PI4P probe, SidM-mCherry (Hammond et al., 2014), and cells were then imaged using a fluorescence microscope. In the absence of stimulation, PI4P showed a similar perinuclear localisation to NLRP3-mVenus (Figure 3.10A). Upon stimulation with the NLRP3 inflammasome activators, nigericin and LLOMe, PI4P formed cytoplasmic puncta (Figure 3.10A). Colocalisation analysis between PI4P and NLRP3-mVenus only showed a significant increase under LLOMe stimulation, however, nigericin stimulation also caused an increased trend in colocalisation between PI4P and NLRP3-mVenus (Figure 3.10B). Imiquimod treatment caused both NLRP3 and PI4P to remain perinuclear, however, this co-localisation was not significant following

Pearson's correlation analysis (Figure 3.10B). Here, NLRP3 inflammasome activating stimuli caused PI4P localisation to behave in a similar fashion to that of NLRP3. Interestingly, monensin caused vesiculation of the NLRP3-mVenus signal (as described earlier) but did not affect the distribution of the PI4P signal, which remained perinuclear, and thus the NLRP3 and PI4P signals under this condition were separated (Figure 3.10A). These data suggest that the co-localisation between PI4P and NLRP3 is an important, common stimulus brought about by NLRP3 inflammasome activating stimuli. I proceeded to investigate the subcellular location of NLRP3 and PI4P relative to my panel of organelle markers.

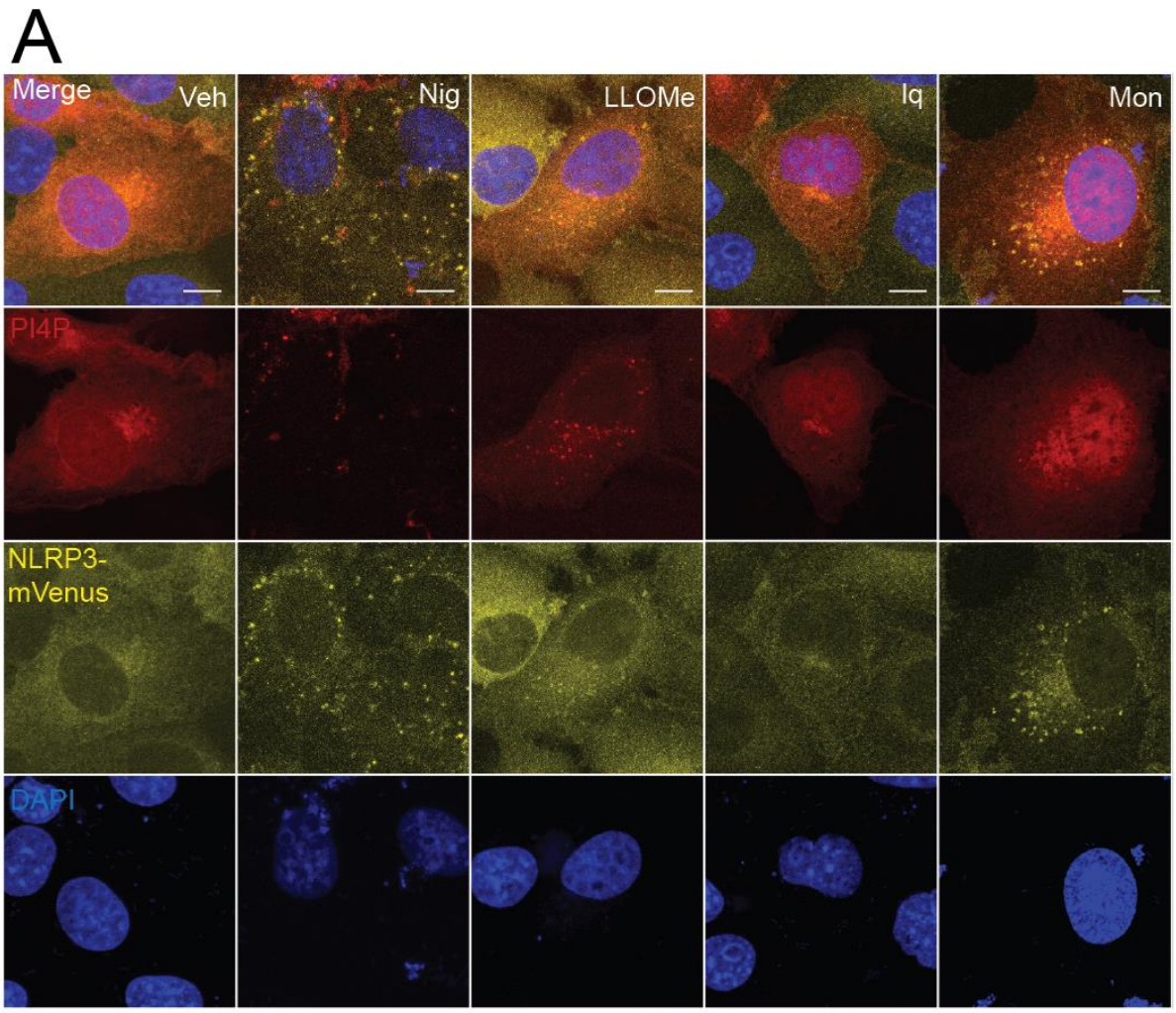
A
Merge
Veh
Nig
LLOMe
Iq
Mon
PI4P
NLRP3-
mVenus
DAPI

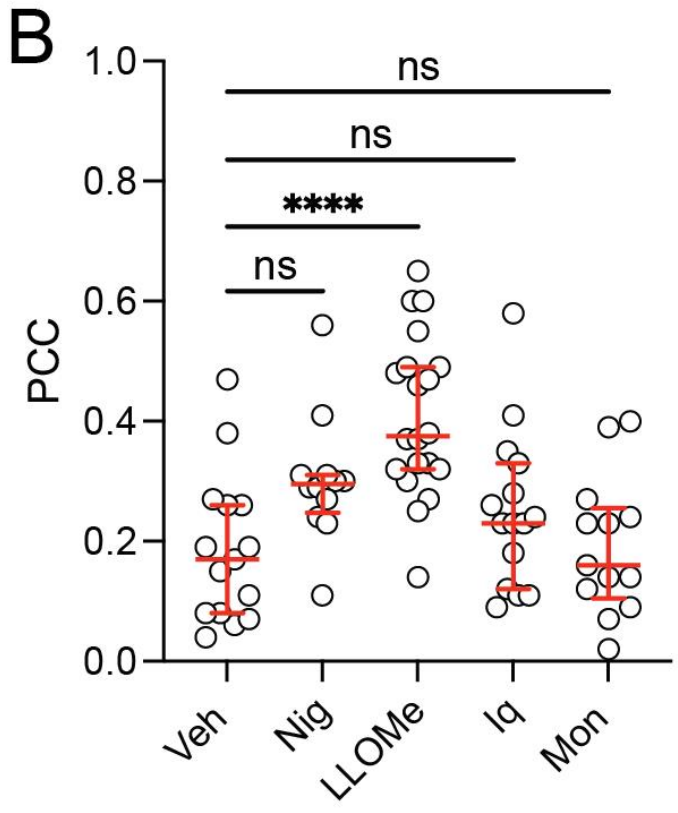
B
PCC
1.0
0.8
0.6
0.4
0.2
0.0
ns
ns
****
ns
Veh
Nig
LLOMe
Iq
Mon

Figure 3.10. Localisation of PI4P with NLRP3-mVenus following stimulation with NLRP3-activating stimuli. (A) Fluorescence and immunofluorescence images of COS7 cells stably expressing NLRP3-mVenus (yellow), transfected with PI4P probe SidM-mCherry (red), and stimulated for 90 minutes with either vehicle (Veh), nigericin (Nig, 10 µM), LeuLeu-OMe (LLOMe, 1 mM), imiquimod (Iq, 75 µM), or monensin (Mon, 10 µM). Blue represents nuclei staining by DAPI. Scale bars are 10 µm. Images are representative of three independent experiments **(B)** Quantification of stimulus-induced co-localisation of NLRP3-mVenus and PI4P with the Pearson's correlation coefficient (PCC) (n = 12 to 20 cells per group from three random fields of view from three independent experiments). Values are median ± IQR. Data were analysed using One-way ANOVA followed by Dunnett's multiple comparison test (compared to vehicle). ****, P≤0.0001 ns= not significant.

3.2.3.2 PI4P co-localised with NLRP3-mVenus on endolysosomal membranes

As observed previously, in resting conditions NLRP3-mVenus was diffuse throughout the cell with some concentration in the perinuclear region and at the TGN (Figure 3.5). PI4P also concentrated at the TGN, co-localising with Golgin97 (Figure 3.11). Upon nigericin stimulation, discrete PI4P cytoplasmic puncta co-localised with EEA1- (Figure 3.12 and 3.15B), CD63- (Figure 3.13 and 3.15C) and LAMP1-positive (Figure 3.14 and 3.15D) compartments, many of which also co-localised with NLRP3-mVenus (Figure 3.12-3.14). Stimulation with Leu-LeuOMe caused PI4P to co-localise with CD63- (Figure 3.13 and 3.15C) and LAMP1-positive (Figure 3.14 and 3.15D) vesicles, many of which showed co-localisation with NLRP3-mVenus (Figure 3.13 and 3.14). As described previously, imiquimod caused PI4P to remain largely perinuclear, however, co-localisation between PI4P and LAMP1-positive compartments were observed (Figure 3.14 and 3.15D). This may be explained in part as an artefact of Pearson's colocalisation analysis due to the largely perinuclear localisation of LAMP1. Monensin stimulation caused a loss of localisation from the TGN marker Golgin97 compared to vehicle but failed to localise PI4P to endolysosomal compartments (Figure 3.11 and 3.15). This may partially explain why monensin, although an active disruptor of endocytic trafficking, fails to trigger NLRP3 inflammasome activation. These data suggest that localisation of NLRP3, together with PI4P on endolysosomal membranes may be important for NLRP3 inflammasome activation, as this occurs following stimulation with NLRP3-actibating stimuli but not monensin.

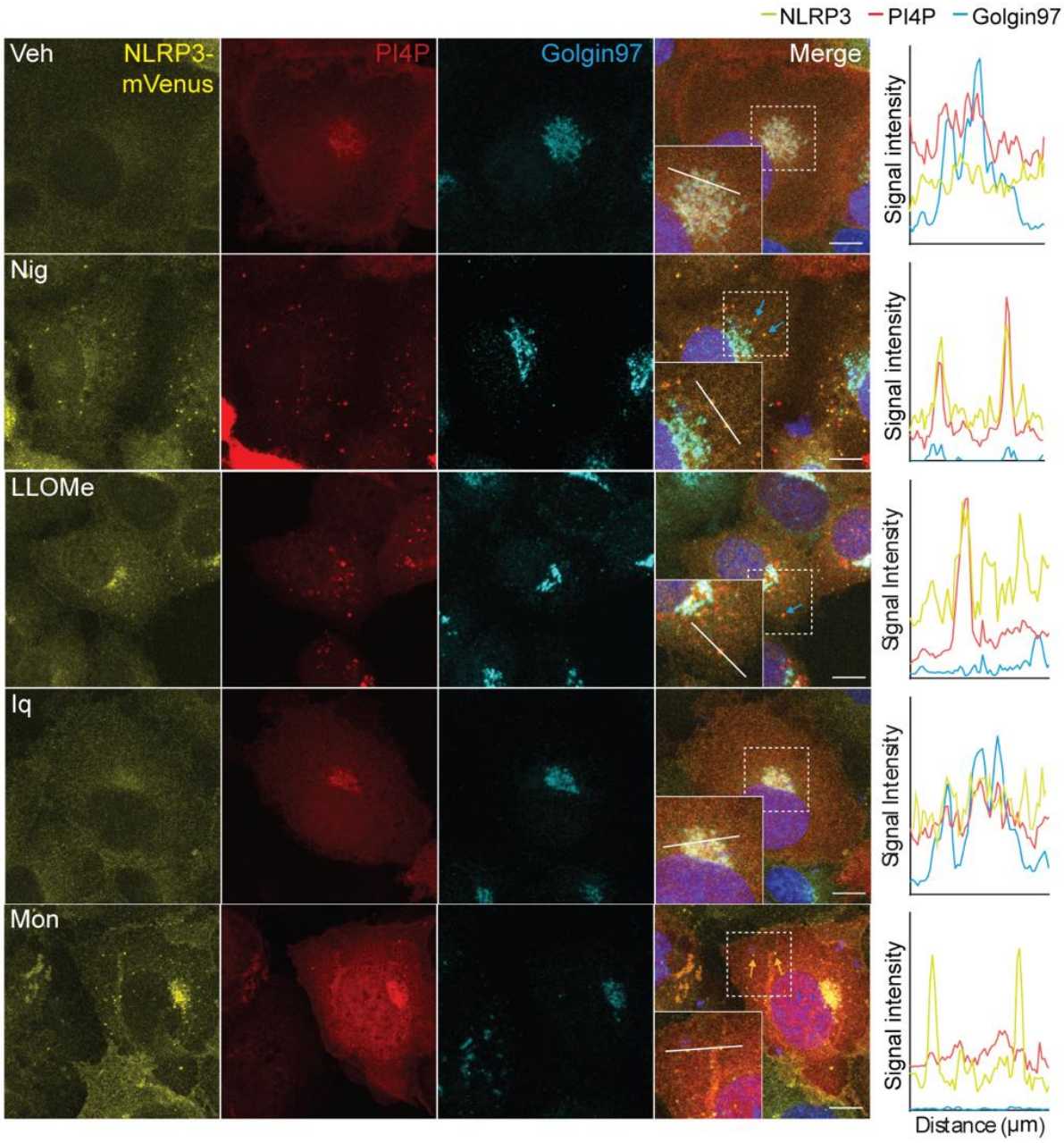

Figure 3.11. Localisation of NLRP3-mVenus with PI4P and Golgin97 following stimulation with NLRP3-activating stimuli. Fluorescence and immunofluorescence images of COS7 cells stably expressing NLRP3-mVenus (yellow), transiently transfected with PI4P probe SidM-mCherry (red) and stimulated for 90 minutes with either vehicle (Veh), nigericin (Nig, 10 µM), LeuLeu-OMe (LLOMe, 1 mM), imiquimod (Iq, 75 µM), or monensin (Mon, 10 µM). Co-stained for Golgin97 (cyan). Blue represents nuclei staining by DAPI. Scale bars are 10 µm. Images are representative of three independent experiments. Line graphs depicting changes in fluorescence intensity (min = 0 and max = 250) over 10 µm for each stimulus and stain are shown.

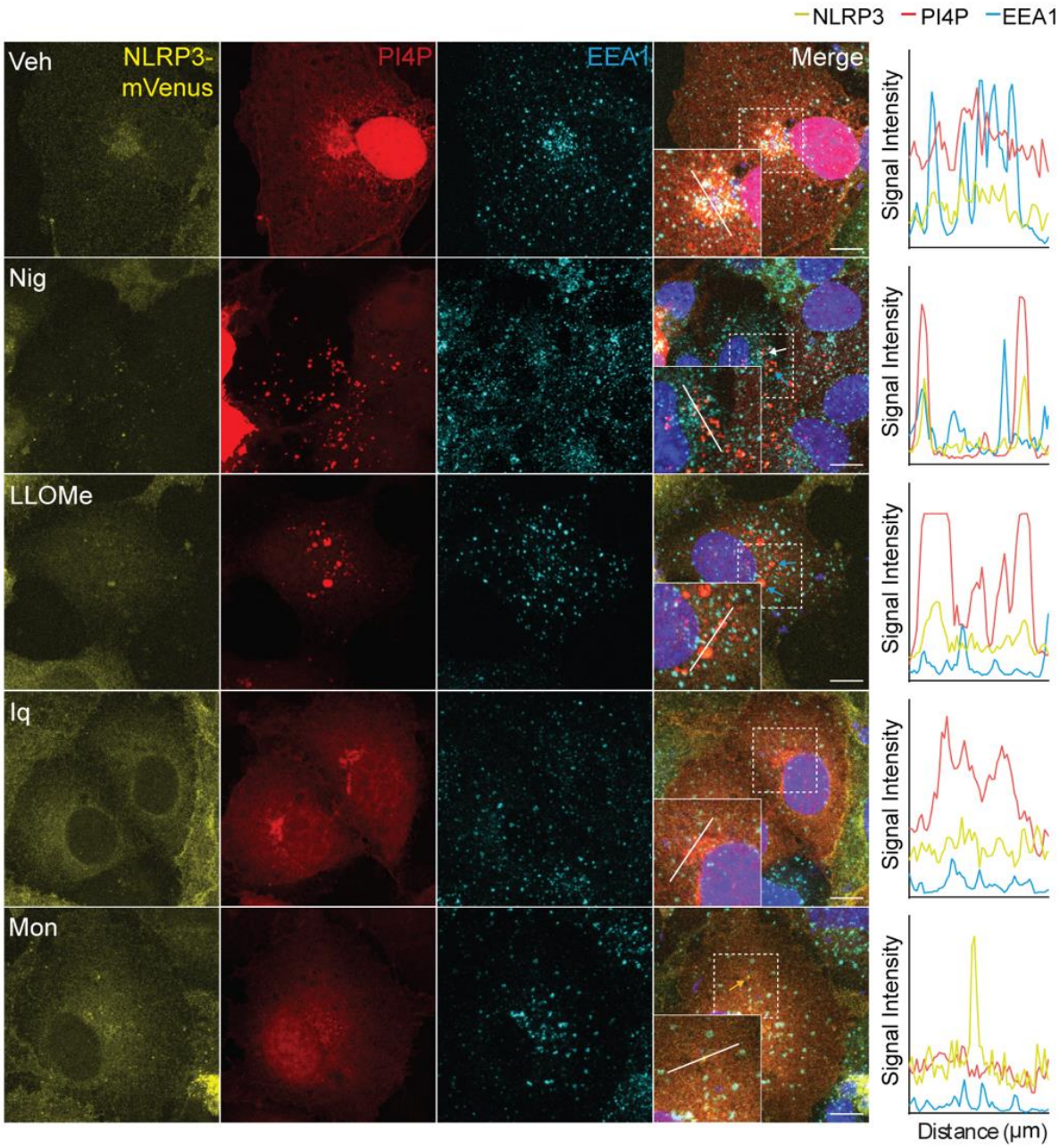

Figure 3.12. Localisation of NLRP3-mVenus with PI4P and EEA1 following stimulation with NLRP3-activating stimuli. Fluorescence and immunofluorescence images of COS7 cells stably expressing NLRP3-mVenus (yellow), transiently transfected with PI4P probe SidM-mCherry (red) and stimulated for 90 minutes with either vehicle (Veh), nigericin (Nig, 10 µM), LeuLeu-OMe (LLOMe, 1 mM), imiquimod (Iq, 75 µM), or monensin (Mon, 10 µM). Co-stained for EEA1 (cyan). Blue represents nuclei staining by DAPI. Scale bars are 10 µm. Images are representative of three independent experiments. Line graphs depicting changes in fluorescence intensity (min = 0 and max = 250) over 10 µm for each stimulus and stain are shown.

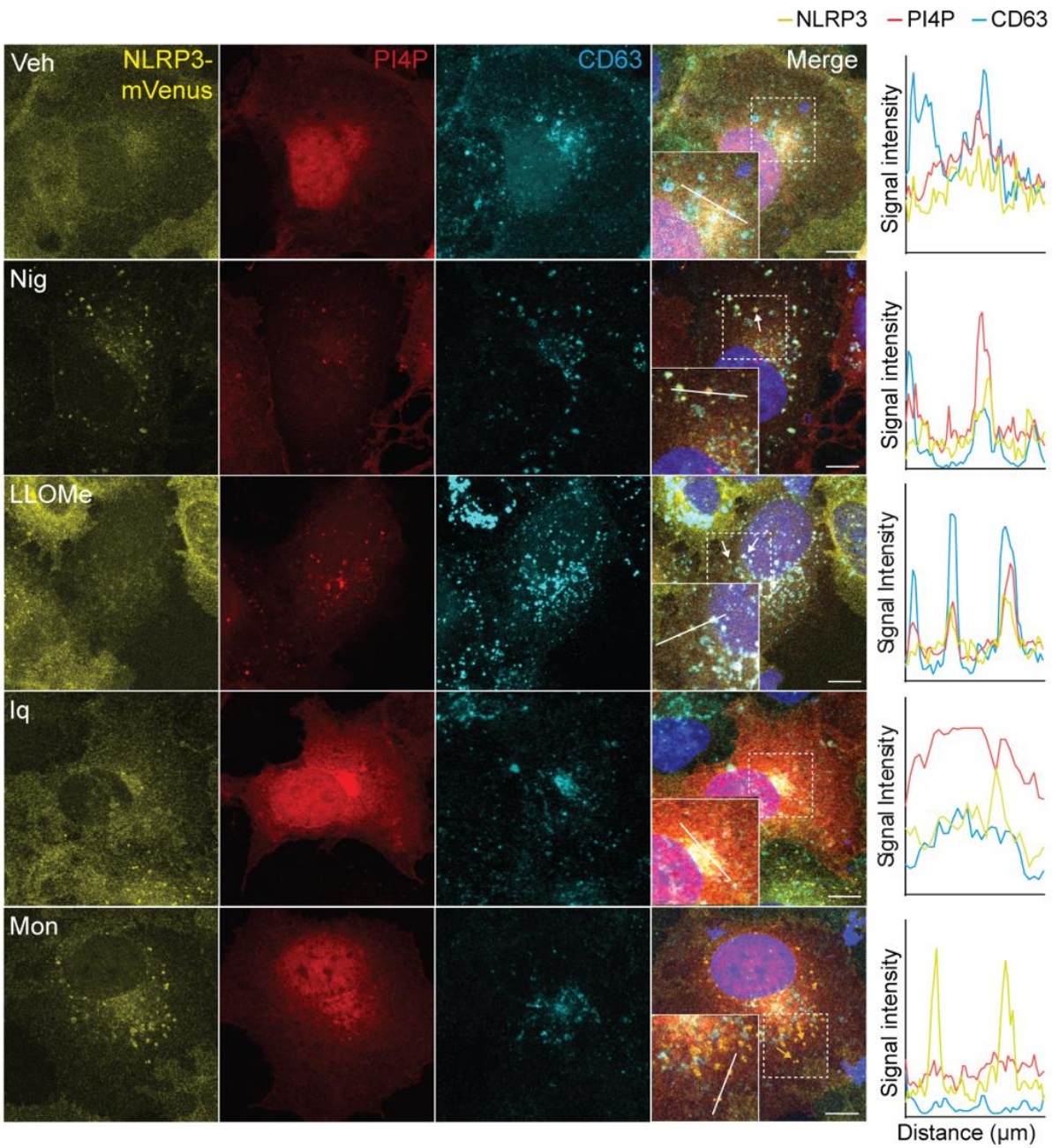

Figure 3.13. Localisation of NLRP3-mVenus with PI4P and CD63 following stimulation with NLRP3-activating stimuli. Fluorescence and immunofluorescence images of COS7 cells stably expressing NLRP3-mVenus (yellow), transiently transfected with PI4P probe SidM-mCherry (red) and stimulated for 90 minutes with either vehicle (Veh), nigericin (Nig, 10 µM), LeuLeu-OMe (LLOMe, 1 mM), imiquimod (Iq, 75 µM), or monensin (Mon, 10 µM). Co-stained for CD63 (cyan). Blue represents nuclei staining by DAPI. Scale bars are 10 µm. Images are representative of three independent experiments. Line graphs depicting changes in fluorescence intensity (min = 0 and max = 250) over 10 µm for each stimulus and stain are shown.

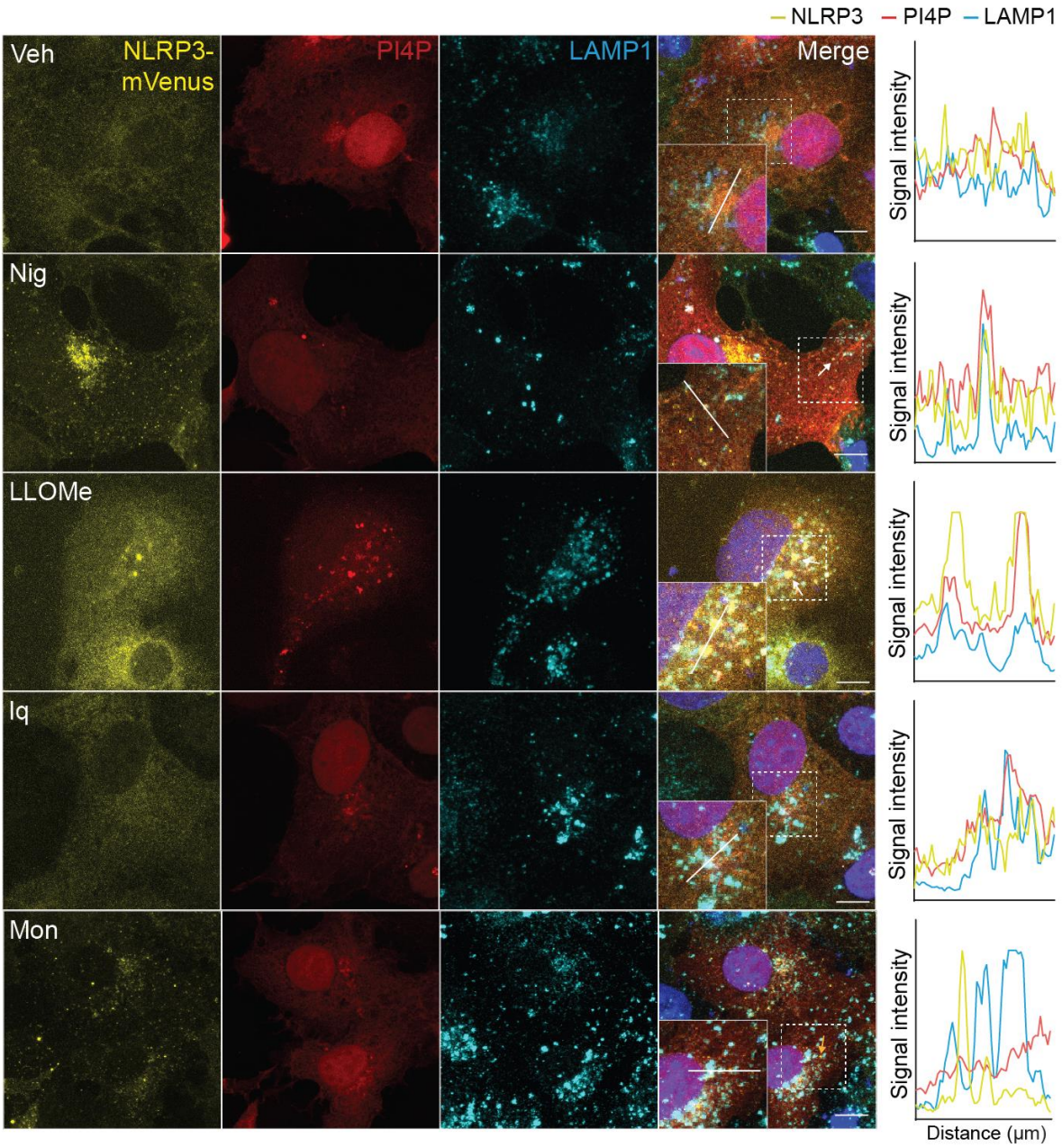

Figure 3.14. Localisation of NLRP3-mVenus with PI4P and LAMP1 following stimulation with NLRP3-activating stimuli. Fluorescence and immunofluorescence images of COS7 cells stably expressing NLRP3-mVenus (yellow), transiently transfected with PI4P probe SidM-mCherry (red) and stimulated for 90 minutes with either vehicle (Veh), nigericin (Nig, 10 µM), LeuLeu-OMe (LLOMe, 1 mM), imiquimod (Iq, 75 µM), or monensin (Mon, 10 µM). Co-stained for LAMP1 (cyan). Blue represents nuclei staining by DAPI. Scale bars are 10 µm. Images are representative of three independent experiments. Line graphs depicting changes in fluorescence intensity (min = 0 and max = 250) over 10 µm for each stimulus and stain are shown.

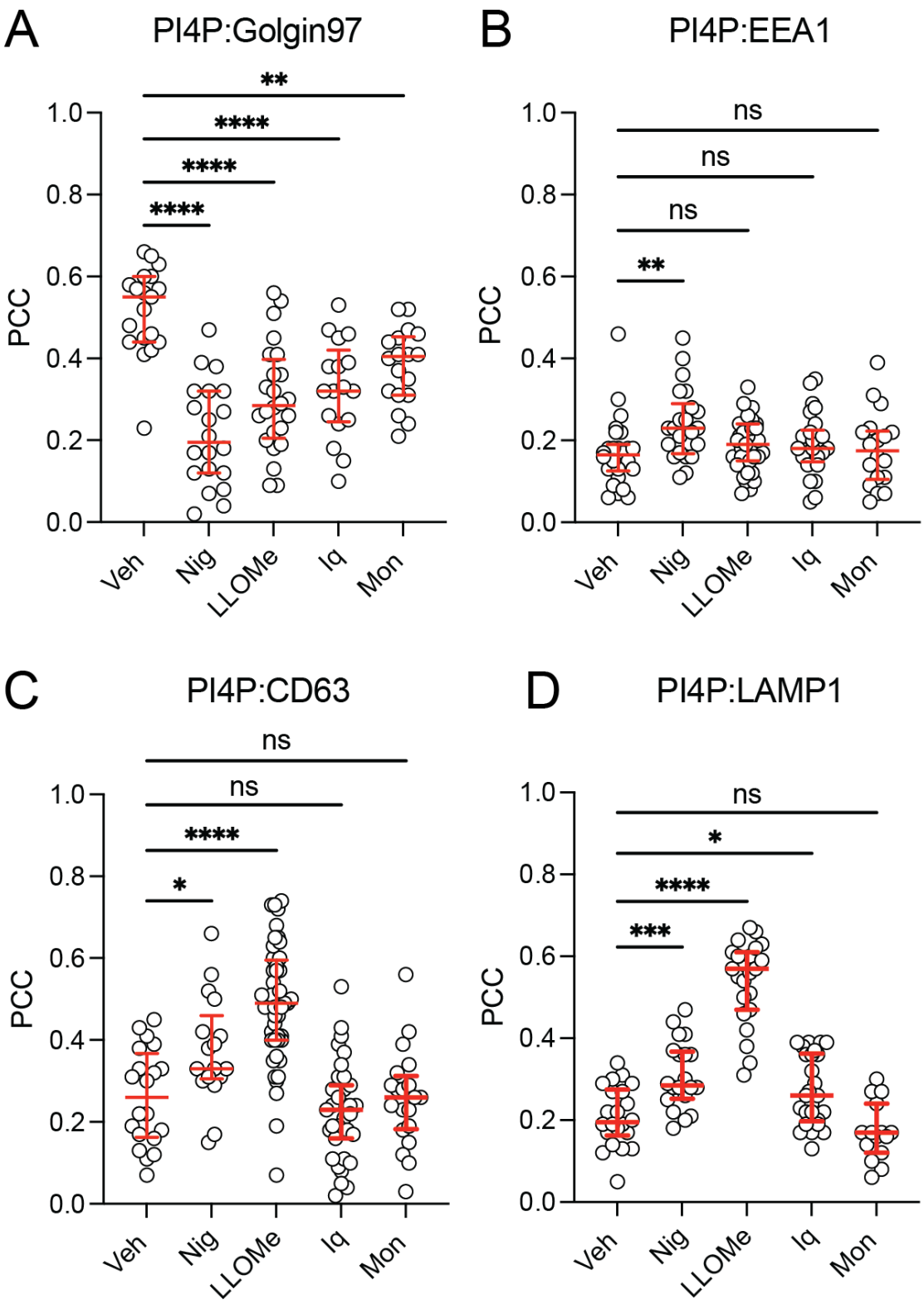
A
PI4P:Golgin97
B
PI4P:EEA1
C
PI4P:CD63
D
PI4P:LAMP1
PCC
1.0
0.8
0.6
0.4
0.2
0.0
**
****
****
****
ns
ns
ns
**
ns
ns
****
*
ns
ns
*
***
****
*
Veh
Nig
LLOMe
Iq
Mon

Figure 3.15. Co-localisation between PI4P and endolysosomal markers following stimulation with NLRP3-activating stimuli. COS7 cells stably expressing NLRP3-mVenus, transiently transfected with PI4P probe SidM-mCherry and stimulated for 90 minutes with either vehicle (Veh), nigericin (Nig, 10 µM), LeuLeu-OMe (LLOMe, 1 mM), imiquimod (Iq, 75 µM), or monensin (Mon, 10 µM). Quantification of stimulus-induced co-localisation of PI4P and **(A)** Golgin97, **(B)** EEA1, **(C)** CD63 or **(D)** LAMP1, with the Pearson's correlation coefficient (PCC). For **(A)** n = 17 to 24 cells per group from three random fields of view from three independent experiments. For **(B)** n = 18 to 35 cells per group from three random fields of view from three independent experiments. For **(C)** n = 17 to 48 cells per group from three random fields of view from four independent experiments. For **(D)** n = 15 to 26 cells per group from three random fields of view from three independent experiments. Values are median ± IQR. Data were analysed using One-way ANOVA followed by Dunnett's multiple comparison test (compared to vehicle). *, P≤0.05, **, P≤0.01 ***, P≤0.001, ****, P≤0.0001 ns= not significant.

3.2.4 Monensin alters imiquimod-induced NLRP3-mVenus and PI4P localisation

Thus far, imiquimod had caused the mildest perturbation of endosomal trafficking and mildest effect on NLRP3 and PI4P redistribution. Lee and Hoyle *et al.* hypothesised that the effects of NLRP3 activating stimuli could be potentiated by disrupting endosome trafficking. In those experiments, we treated LPS-primed BMDMs were treated with monensin for 2 hours before treatment with imiquimod for a further 2 hours. These experiments showed that monensin pre-treatment greatly potentiated imiquimod-induced IL-1β release, cell death and ASC oligomerisation (Lee and Hoyle et al., 2023). Therefore, I explored whether preceding imiquimod treatment with monensin altered the distribution and localisation of NLRP3 and PI4P. Imiquimod and monensin treatment alone showed no significant co-localisation between PI4P and NLRP3, or PI4P and EEA1-, CD63- or LAMP1-positive compartments (Figure 3.17A, C-E). Upon observation, treatment with monensin and subsequently imiquimod, caused the loss of PI4P from the perinuclear region and the formation of cytoplasmic puncta (Figure 3.16), although the loss of co-localisation between PI4P and Golgin97 was not significant following Pearson's colocalisation analysis (Figure 3.17B). Treatment with monensin then imiquimod stimulated the localisation of PI4P with NLRP3-mVenus (Figure 3.17A) and PI4P with LAMP1 (Figure 3.17E). Therefore, this may suggest that the enhanced IL-1β release overserved in macrophages when imiquimod stimulation is preceded by monensin, may be due to the co-localisation of PI4P with NLRP3 on lysosomal membranes, an event that is not observed following monensin or imiquimod treatment alone.

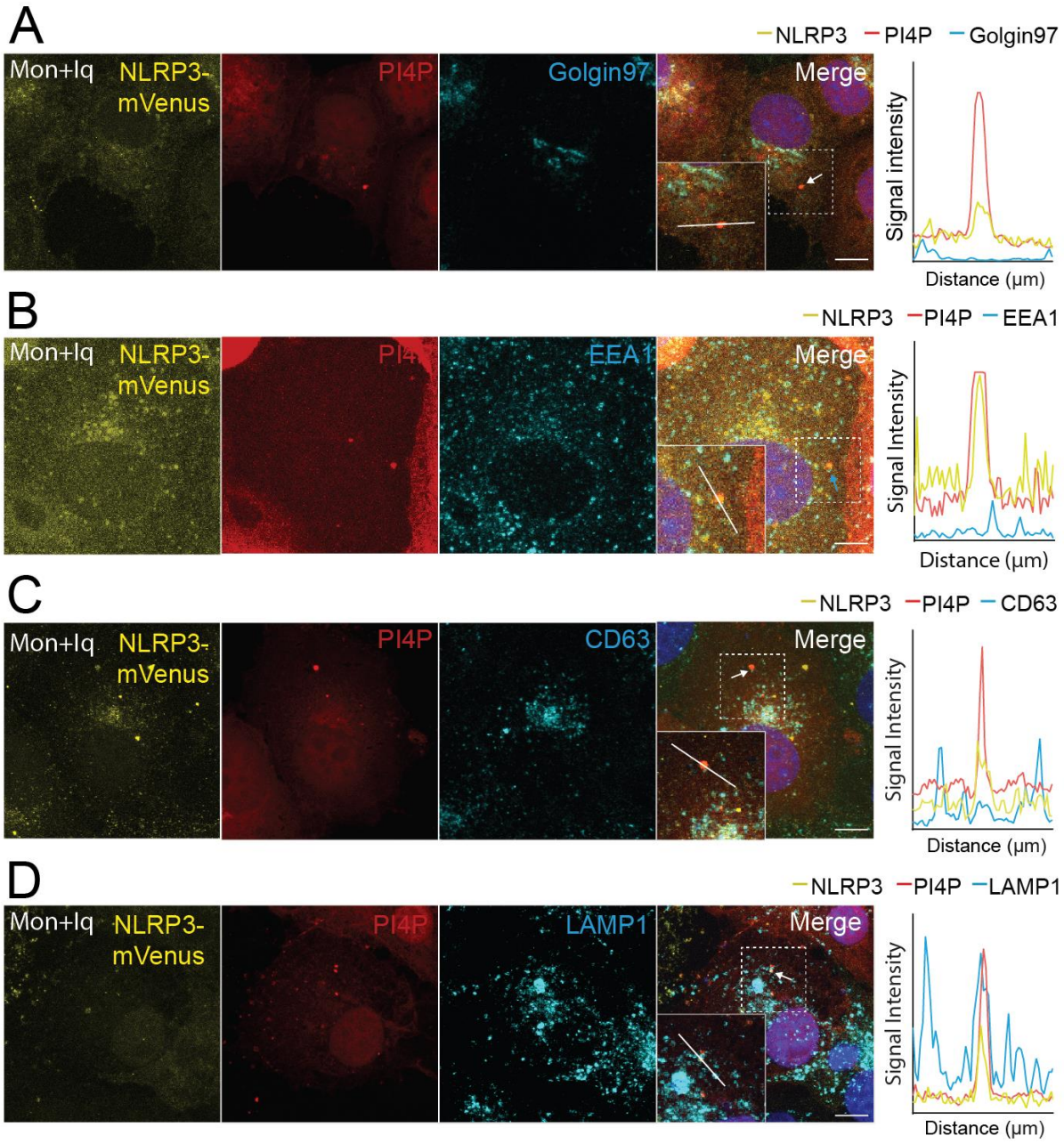

Figure 3.16. Localisation of NLRP3-mVenus with PI4P and endolysosomal markers following co-stimulation with monensin and imiquimod. Fluorescence and immunofluorescence images of COS7 cells stably expressing NLRP3-mVenus (yellow), transiently transfected with PI4P probe SidM-mCherry (red) and stimulated for 90 minutes with monensin (10 µM) before being stimulated with imiquimod (75 µM) for 90 minutes (Mon + Iq). Co-stained (cyan) for **(A)** Gogin97, **(B)** EEA1, **(C)** CD63, **(D)** LAMP1. Blue represents nuclei staining by DAPI. Scale bars are 10 µm. Images are representative of three **(A, B, D)** or four **(C)** independent experiments. Line graphs depicting changes in fluorescence intensity (min = 0 and max = 250) over 10 µm for each stimulus and stain are shown.

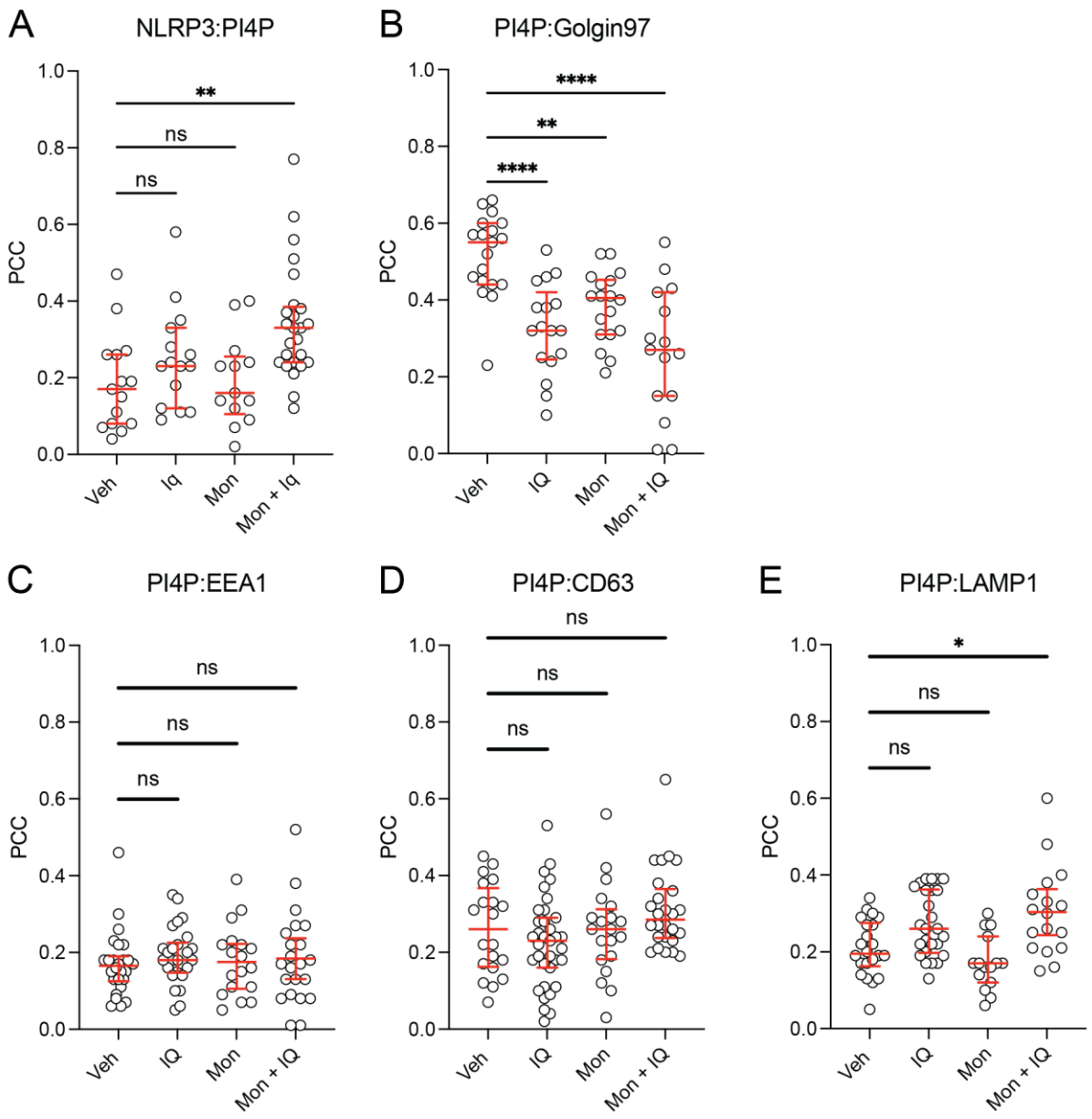
A
NLRP3:PI4P
PCC
1.0
0.8
0.6
0.4
0.2
0.0
**
ns
ns
Veh
Iq
Mon
Mon + Iq
B
PI4P:Golgin97
PCC
****
**
****
Veh
IQ
Mon
Mon + IQ
C
PI4P:EEA1
PCC
ns
ns
ns
Veh
IQ
Mon
Mon + IQ
D
PI4P:CD63
PCC
ns
ns
ns
Veh
IQ
Mon
Mon + IQ
E
PI4P:LAMP1
PCC
*
ns
ns
Veh
IQ
Mon
Mon + IQ

Figure 3.17. Co-localisation between PI4P and NLRP3-mVenus or endolysosomal markers following co-stimulation with monensin and imiquimod. COS7 cells stably expressing NLRP3-mVenus, transiently transfected with PI4P probe SidM-mCherry and stimulated for 90 minutes with vehicle (Veh), imiquimod (Iq, 75 µM), monensin (Mon, 10 µM) or monensin (10 µM) before being stimulated with imiquimod (75 µM) for 90 minutes (Mon + Iq). Quantification of stimulus-induced co-localisation of PI4P and **(A)** NLRP3, **(B)** Golgin97, **(C)** EEA1, **(D)** CD63 or **(E)** LAMP1, with the Pearson's correlation coefficient (PCC). For **(A)** n = 13 to 25 cells per group from three random fields of view from three independent experiments. For **(B)** n = 15 to 19 cells per group from three random fields of view from three independent experiments. For **(C)** n = 18 to 26 cells per group from three random fields of view from four independent experiments. For **(D)** n = 20 to 35 cells per group from three random fields of view from three independent experiments. For **(D)** n = 15 to 26 cells per group from three random fields of view from three independent experiments. Values are median ± IQR. Data were analysed using One-way ANOVA followed by Dunnett's multiple comparison test (compared to vehicle). *, P≤0.05, **, P≤0.01, ****, P≤0.0001 ns= not significant.

3.2.5 PI4P synthesis is important for NLRP3 activation

I established that NLRP3 co-localised with PI4P on endolysosomal membranes following stimulation with NLRP3 inflammasome activating stimuli. This evidence and previous work suggested that PI4P is important for NLRP3 inflammasome activation. I therefore wanted to investigate whether depleting levels of PI4P altered NLRP3 activation. A major route of PI4P synthesis is via phosphorylation of phosphatidylinositol (PI) by PI4 kinases (PI4K) (Balla, 2013). Inhibitors of PI4K, such as phenyl arsine oxide (PAO), deplete cellular PI4P (Hammond et al., 2009, Balla et al., 2008). Therefore, to investigate the role of PI4P in NLRP3 activation I treated LPS-primed mouse primary BMDMs with PAO for 15 minutes prior to stimulation with nigericin for 1 hour and assayed IL-1β release and cell death. Here, I observed a complete inhibition of nigericin-induced IL-1β release following pre-treatment with PAO, comparable to that of the direct NLRP3 inhibitor MCC950 (Figure 3.18A). I observed a slight potentiation in cell death with PAO pre-treatment, compared to a slight inhibition with MCC950 (Figure 3.18B). Previous studies have described that PAO causes a depletion of PI4P pools at the Golgi (Hammond et al., 2009). Therefore, depleting Golgi-derived PI4P may cause a loss of PI4P localisation to endolysosomal compartments, however, further experiments investigating the intracellular levels and localisation of PI4P following PAO treatment are required to confirm this. With this hypothesis in mind, these data suggest that depletion of PI4P by inhibiting PI4K, may perturb the activation of the NLRP3 inflammasome.

In addition to its role in depleting cellular levels of PI4P, PAO is also described to inhibit tyrosine dephosphorylation of the inflammasome adaptor protein ASC (Mambwe et al., 2019). Through this mechanism, inhibiting dephosphorylation of ASC inhibits both NLRP3 and AIM2-mediated IL-1β release *in vitro.* I therefore wanted to determine whether the inhibition

I observed here from PAO pre-treatment in my NLRP3-activation assay was due somewhat to PI4P depletion and not exclusively via modifications of ASC. Like NLRP3, activation of the AIM2 inflammasome is dependent upon ASC, but is not suggested to rely on PI4P for its activation. I therefore investigated the impact of PAO in an AIM2 inflammasome activation assay. To do this, LPS-primed BMDMs were treated with PAO for 15 minutes, prior to transfection with the synthetic double stranded (ds)DNA sequence poly dA:dT (Fernandes-Alnemri et al., 2009). I also used 4-sulfonic calixarene pre-treatment as a characterised inhibitor of the AIM2 inflammasome (Green et al., 2023). PAO pre-treatment showed a trend for inhibition in poly dA:dT-mediated IL-1β release, however, in contrast to calixarene pre-treatment, the inhibition of IL-1β release with PAO pre-treatment was not significant (Figure 3.18C). PAO appeared to have a greater inhibitory effect in NLRP3-mediated IL-β release compared to AIM2-mediated IL-β release (Figure 3.18 A and C). Overall, these data suggest that PAO may in fact be inhibiting ASC-dependent inflammasomes via dephosphorylation of the ASC adaptor protein. However, PAO-mediated inhibition of the NLRP3 inflammasome is greater here than that observed in the AIM2 inflammasome. Therefore, this may suggest that the depletion of PI4P is also playing a role in the inhibition of the NLRP3 inflammasome. Further characterisation the impact of PAO on PI4P levels in macrophages is required here to fully elucidate the mechanisms at play. Future studies will utilise the models optimised in this study to investigate the recruitment of NLRP3 to endolysosomal compartments following treatment with PAO.

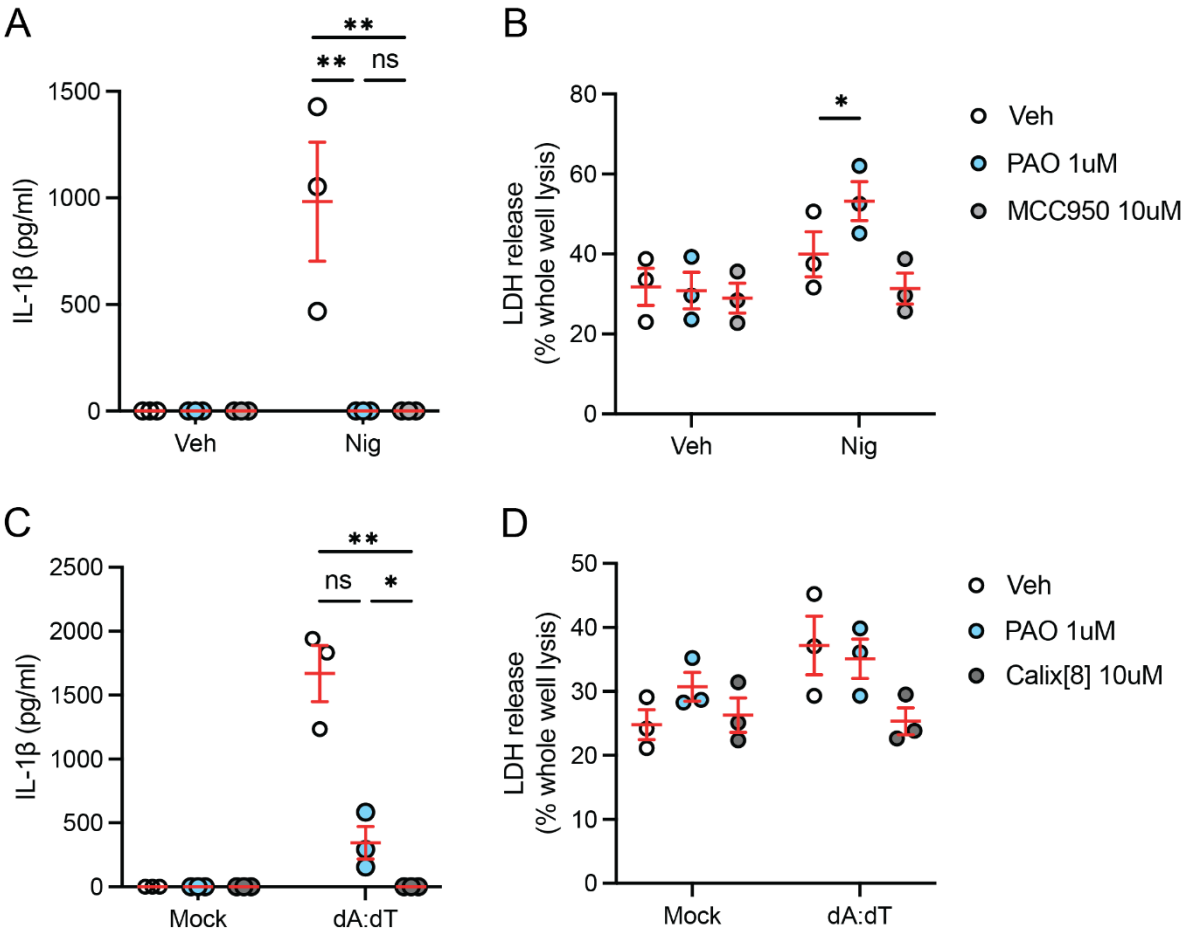

Figure 3.18. Phenyl arsine oxide (PAO) inhibits inflammasome-mediated IL-1β release. (A and B) LPS-primed primary BMDMs were pre-treated with vehicle (Veh), phenyl arsine oxide (PAO; 1 µM) or MCC950 (10 µM) for 15 minutes before being stimulated with vehicle (Veh) or nigericin (Nig; 10 µM) for 2 hours. Supernatants were assessed for **(A)** IL-1β (measured by ELISA) and **(B)** LDH release (n=3 independent experiments). **(C and D)** LPS-primed primary BMDMs were pre-treated with vehicle (Veh), phenyl arsine oxide (PAO; 1 µM) or 4-sulfonic calix[8]arene (10 µM) for 15 minutes before transfection with poly dA:dT (1 mg/ml, 4 h) or lipofectamine 3000 alone (mock). Supernatants were assessed for **(A)** IL-1β (measured by ELISA) and **(B)** LDH release (n=3 independent experiments Data underwent y=log(y+1) transformation (**A and C)** and analysed by two-way ANOVA followed by Sidak's multiple comparison test (compared between means). *, P≤0.05, **, P≤0.01, ns= not significant.

3.3 Discussion

There is a wealth of literature describing a link between organelle stress and NLRP3 inflammasome activation (Seoane et al., 2020). The NLRP3 inflammasome is distinct among inflammasomes in its ability to respond to a broad range of stimuli, all of which are now proposed to cause stress to subcellular organelles (Rahman et al., 2020, Seoane et al., 2020). Our recent review suggested that these stresses manifest themselves in organelle dysfunction, which is then integrated by NLRP3 to trigger NLRP3 inflammasome activation and subsequent inflammation (Seoane et al., 2020). However, the organelle dysfunction elicited by NLRP3-activating stimuli is still wide-ranging and may vary greatly depending on cell type, and the extent and type of stimulation. Therefore, a unifying mechanism of NLRP3 inflammasome activation is yet to be defined. Here, I propose a disruption in endocytic trafficking as an interesting unifier in the link between organelle stress and NLRP3 inflammasome activation. I established that wide-ranging NLRP3-activating stimuli all disrupt endosome to plasma membrane recycling. These results suggest that a disruption in endosomal trafficking is a common downstream effect of NLRP3-activating stimuli. However, disruption of endosomal trafficking alone is insufficient to activate the NLRP3 inflammasome, as observed with monensin stimulation in macrophages (Lee et al., 2023, Zhang et al., 2023). This suggests that endosomal trafficking dysfunction requires another concomitant stimulus to achieve activation of the NLRP3 inflammasome. These data suggest that the localisation of PI4P with NLRP3 on endolysosomal membranes provides explanation of an important step required to achieve NLRP3 inflammasome activation, as this is achieved with NLRP3-activating stimuli but not monensin.

The cycling of endosomal cargoes such as TGN38/46, which are trafficked from the *trans*-Golgi to the plasma membrane, have been reported to be disrupted by K^+ ionophores, leading to the cargo being trapped in endolysosomal compartments (Reaves et al., 1993, Chapman and Munro, 1994). Lee et al. (2023) show that nigericin, a potent activator of the NLRP3 inflammasome and a K^+ ionophore, indeed causes TGN38/46 to localise with endosomal and lysosomal markers (Lee et al., 2023). Further to this, NLRP3 has previously been reported to co-localise with TGN38/46 following cell stimulation with NLRP3 activators (Chen and Chen, 2018). Therefore, I wanted to test the hypothesis that a broad range of NLRP3 inflammasome activating stimuli elicit a common disruption in endosomal cargo trafficking. Here, I used fluorescently tagged transferrin (transferrin-488) to model endosome to plasma membrane recycling in HeLa cells (Kauppi et al., 2002). Transferrin-488 was readily recycled in the absence of stimulation following saturation of the media with unlabelled transferrin. Therefore, this assay was an effective model to characterise the effect of NLRP3 activating stimuli upon endosomal recycling.

To investigate the impact of NLRP3-activating stimuli upon the recycling of transferrin, I first tested whether these stimuli had any impact upon transferrin uptake. I observed that nigericin stimulation increased the amount of internalised transferrin in this assay, whereas Leu-LeuOMe and monensin decreased the amount of intracellular transferrin. A decrease in internalised fluorescent transferrin, compared to vehicle, may suggest a perturbation in endocytosis. However, as the impact upon internalised fluorescent transferrin did not appear to be consistent amongst the panel of NLRP3 inflammasome activating stimuli, I could conclude from this result that a disruption in transferrin uptake and therefore endocytosis is not a defining feature of NLRP3 inflammasome activating stimuli.

I then investigated the impact of NLRP3 inflammasome activating stimuli upon endosomal recycling. Here, I established that all NLRP3 inflammasome activating stimuli tested, to some extent, caused a retention in fluorescent transferrin and therefore a disruption of endosomal trafficking. In this assay of endosomal trafficking, nigericin had the greatest effect, followed by LeuLeu-OMe and imiquimod the mildest. Interestingly, the effectiveness of these stimuli in disrupting endosomal trafficking was matched in their potency to drive NLRP3-mediated IL-1β release in macrophages. This may suggest that stimuli with a robust mechanism to disrupt endosomal trafficking may result in greater inflammasome activation. However, monensin, a well-established and potent disruptor of endosomal trafficking, by itself has minimal effects on NLRP3 inflammasome activation. This suggested that a disruption in endosomal trafficking was important but not sufficient for NLRP3 inflammasome activation, and that additional events are necessary.

Research continues to suggest the importance of NLRP3 on organelle membranes. Previous work has shown co-localisation of NLRP3 to TGN38/46-positive compartments (Chen and Chen, 2018). Work by our group identified TGN38/46 positive structures co-localising with the early endosome marker EEA1, the late endosome marker CD63, and the lysosome marker LAMP1, under NLRP3 activating stimulation (Lee et al., 2023). In macrophages, caspase-1 cleaves the early endosome marker EEA1, and active caspase-1 is observed to co-localise to early endosomes following hypotonicity, an NLRP3 inflammasome activating stimulus (Baroja-Mazo et al., 2019). Recently, NLRP3 has been shown to interact with the Lamtor1 on the surface of lysosomes, and that Lamtor1-deficient mice showed an attenuation of NLRP3 activation and NLRP3-associated inflammatory disease (Tsujimoto et al., 2023). Following

stimulation with nigericin and Leu-LeuOMe, NLRP3 formed cytoplasmic puncta that co-localised with EEA1-, CD63- and LAMP1-positive compartments to varying extents. Interestingly, monensin still caused NLRP3 to form cytoplasmic puncta however, unlike nigericin and Leu-LeuOMe, these puncta showed little co-localisation with endolysosomal markers. This may suggest that to be activated, NLRP3 must be localised to an endosomal or lysosomal membrane. However, following stimulation with imiquimod, NLRP3 remained localised to the TGN and was not present on endolysosomal membranes, despite activating NLRP3. These data suggest that, in addition to endolysosomal membrane localisation, there is an additional signal that is necessary for NLRP3 activation. Due its known ability to interact with NLRP3, we propose the localisation of PI4P together with NLRP3 at subcellular membrane compartments as an interesting candidate.

PI4P is negatively charged and can interact with the conserved polybasic region of NLRP3 (Chen and Chen, 2018). PI4P is also reported to accumulate on TGN38/46-positive compartments following NLRP3 inflammasome activation (Chen and Chen, 2018). Recently, the importance of PI4P accumulation on endosomes and lysosomes has become an area of great interest. LeuLeu-OMe has been shown to cause accumulation of PI4P on damaged lysosomes (Tan and Finkel, 2022). PI4P is also reported to accumulate on endosomes following NLRP3 activation, and that depleting endosomal PI4P levels prevents endosomal association of NLRP3 and inhibits inflammasome activation (Zhang et al., 2023). In my experiments, PI4P was lost from the TGN and accumulated on both CD63-positive late endosomes and LAMP1-positive lysosomes in response to the NLRP3 inflammasome activating stimuli nigericin and Leu-LeuOMe. Here, PI4P on CD63- and LAMP1-positive compartments also co-localised with NLRP3. Following imiquimod stimulation, NLRP3

remained localised to the TGN. Interestingly, imiquimod also stimulated PI4P to accumulate at the TGN. It is important to consider that although NLRP3 and PI4P appear to be located at the TGN, there is still a proportion of CD63- and LAMP1-positive compartments localised to this area. This may suggest that NLRP3 and PI4P are localised to these compartments following imiquimod stimulation, in a similar fashion to nigericin and Leu-LeuOMe stimulated cells. This supports the hypothesis that NLRP3 accumulation to endolysosomal compartments must occur concomitantly with PI4P accumulation to allow NLRP3 activation. Indeed, in monensin treated cells, PI4P remained localised to the TGN and was separated from the punctate formation observed with NLRP3.

Imiquimod had the mildest effect on PI4P redistribution in my experiments and showed little co-localisation between NLRP3 and PI4P on endolysosomal compartments. However, when combined with monensin, imiquimod stimulated PI4P and NLRP3 to both redistribute from the TGN to cytoplasmic puncta. These puncta showed some co-localisation with LAMP1-positive lysosomes. Imiquimod was the only NLRP3-activating stimuli in this panel that works in a potassium efflux-independent manner. Monensin facilitates the exchange of sodium ions for protons across the endosomal membrane, therefore alkalinising the endosome and disrupting trafficking. However, monensin is also capable of transporting potassium ions, but has a ten times greater affinity for sodium over potassium (Mollenhauer et al., 1990). Data from our group show that in primary mouse macrophages, monensin pre-treatment potentiates imiquimod-induced IL-1β release, but not potassium-dependent stimuli such as nigericin (Lee et al., 2023). Further to this, the addition of high potassium containing media following monensin pre-treatment reduces the potentiation of imiquimod-induced NLRP3 activation (*unpublished data*). This suggests that monensin can potentiate the effects of

potassium-efflux independent stimuli, but this capacity is prevented in the presence of high extracellular potassium. Monensin is also an antimicrobial agent (Dawson and Boling, 1983). It has been suggested that increasing extracellular potassium levels attenuates the antimicrobial activity of monensin. It is possible therefore that increasing the extracellular potassium concentration in our experiments may perturb the activity of monensin in our assay and therefore prevent its ability to potentiate imiquimod-induced IL-1β release. Therefore, the redistribution of NLRP3 and PI4P observed here following monensin and imiquimod co-treatment could be due to a further perturbation in endocytic traffic that cannot be achieved with potassium-efflux dependent stimuli.

I have discovered here that accumulation of PI4P, concomitantly with NLRP3, occurred at endosomal and lysosomal compartments following treatment with NLRP3 activating stimuli. Therefore, I wanted to explore whether pharmacologically depleting levels of PI4P affected NLRP3 activation. The phosphatidylinositol 4-kinase (PI4K) inhibitor PAO inhibits the synthesis of PI4P and depletes PI4P pools at the Golgi (Hammond et al., 2009, Balla et al., 2008). Pre-treatment with PAO in LPS-primed macrophages inhibited nigericin-induced IL-1β release. This suggested that synthesis of PI4P was important for NLRP3 activation. However, further validation is required to determine whether in fact PAO is depleting cellular levels of PI4P, and what impact PAO has on other events upstream of IL-1β secretion, including caspase-1 cleavage and ASC speck formation. Recently, it has been shown that deleting the phosphatidylinositol 4-kinases, *PI4KIIIβ,* dampens nigericin-induced NLRP3 recruitment to endosomes and reduces NLRP3 activation in human monocyte THP-1 cells (Zhang et al., 2023). This further supports the hypothesis that attenuating PI4P levels alters NLRP3 inflammasome activation. However, it is important to consider that PAO is also reported to inhibit ASC-

dependent inflammasomes (Mambwe et al., 2019), therefore knock-out studies represent a cleaner mode of investigation here compared to pharmacological inhibition.

Understanding the cellular mechanisms involved in the activation of the NLRP3 inflammasome remains a persistent question in the field of inflammasome research. These data contribute to the ever-growing observations that a disruption in endosomal trafficking may contribute to an overall cellular stress that is sensed by NLRP3. Here, I show that NLRP3 can localise to endolysosomal membranes and that its concomitant localisation with PI4P may be an important step in the activation of the NLRP3 inflammasome. Further insight into these mechanisms will create a clearer picture as to how the NLRP3 inflammasome is activated and may identify new ways to target the NLRP3 inflammasome in disease.

Chapter 4:

The subcellular regulation of the NLRP3 inflammasome

Chapter 4. The subcellular regulation of the NLRP3 inflammasome

4.1 Introduction

A diverse range of damage- and pathogen-associated cellular stresses drive inflammation by activation of the NLRP3 inflammasome (Leemans et al., 2011). How exactly the NLRP3 inflammasome senses and integrates multiple different stimuli to signal inflammation is an area of great interest. NLRP3 has been suggested to sense a disruption in endosomal trafficking (Chapter 3 The cell biology of NLRP3 activation) (Lee et al., 2023, Zhang et al., 2023) . Previous work by our group and others has shown that NLRP3-activating stimuli cause a disruption in endosomal cargo trafficking (Lee et al., 2023, Zhang et al., 2023). NLRP3-activating stimuli have been shown to trigger the re-localisation of NLRP3 from the Golgi to vesicles positive for the endolysosomal markers EEA1, CD63 and LAMP1 (Lee et al., 2023). Further to this, NLRP3 has also been shown to localise to endolysosomal compartments positive for the inositol lipid PI4P (Chen and Chen, 2018, Lee et al., 2023, Zhang et al., 2023). Together these data suggest that NLRP3 can sense disruptions in endosomal cargo trafficking, and this may explain in part the spatial activation of the NLRP3 inflammasome complex. Investigating the NLRP3 protein interactome under stimulatory conditions is an essential next step to further elucidate the mechanisms by which NLRP3 senses and reacts to a disruption in endosomal trafficking.

Enzyme-catalysed proximity labelling is a method to screen protein-protein interactions and subcellular proteomes in live cell models (Kim et al., 2016). A method of enzyme-catalysed proximity labelling called TurboID allows rapid and non-toxic biotin labelling of proximal proteins (Cho et al., 2020). In this chapter, HeLa cells stably expressing the fusion protein NLRP3-TurboID were generated by lentiviral transfection (Chapter 2 Materials and Methods)

and used as a model to investigate the NLRP3 interactome in response to the activating stimulus nigericin. Bioinformatic analysis of the NLRP3 interactome allows the characterisation of the subcellular location of NLRP3-interacting proteins. I tested the hypothesis that proteins interacting with NLRP3 at rest and under stimulatory conditions may be important in canonical activation of the NLRP3 inflammasome. Specifically knocking down the expression of NLRP3-interacting proteins located on the Golgi apparatus or endocytic compartments in a monocyte cell model may build on our current understanding of how NLRP3 senses a disruption in endocytic traffic.

4.2 Results

4.2.1 Characterisation of model

HeLa cells stably expressing NLRP3-TurboID were generated by lentiviral transduction (Chapter 2 Materials and Methods). Immunocytochemistry was carried out using antibodies to NLRP3 and TurboID (BirA) to characterise the subcellular distribution of NLRP3-TurboID at rest (vehicle; ethanol 0.5% v/v) and following nigericin stimulation (10 μM) for 90 minutes. Addition of biotin (500 μM) for the final 60 minutes of vehicle or nigericin stimulation allowed analysis of the localisation of biotinylated proteins by streptavidin-HRP labelling. Consistent with previous observations of the intracellular localisation of NLRP3 (Chapter 3 The cell biology of NLRP3 activation) (Lee and Hoyle et al., 2023), at rest NLRP3-TurboID was predominantly diffuse in the cytosol with some concentration around the perinuclear region. Following nigericin stimulation, NLRP3-TurboID localised to distinct puncta throughout the cytosol (Figure 4.1A). Pearson's correlation coefficient (PCC) analysis revealed a strong co-localisation between NLRP3 and TurboID in both vehicle- (mean PCC= 0.88) and nigericin-

treated cells (mean PCC= 0.85) (Figure 4.1B). There was no difference in the co-localisation of NLRP3 and TurboID between vehicle and nigericin stimulation, highlighting that the localisation of TurboID in both vehicle- and nigericin-treated cells was an effective read-out of the localisation of NLRP3. This suggests that TurboID-mediated biotinylation of proteins in this model may be an effective method to analyse the NLRP3 interactome in HeLa cells.

Many endogenously biotinylated proteins can be found in the cytosol and mitochondria of mammalian cells and can therefore be labelled by streptavidin-HRP in the absence of biotin treatment (Coene et al., 2008). Biotinylated proteins were visualised by streptavidin-HRP labelling in both DMSO- (0.5% v/v) and biotin-treated cells (500 μM) by immunofluorescence microscopy (Figure 4.1C) and the co-localisation of TurboID and biotin was analysed by PCC (Figure 4.1D). PCC analysis showed that co-localisation of TurboID and biotinylated proteins was significantly increased in biotin-treated cells compared to DMSO for both vehicle and nigericin (Figure 4.1E). This confirmed that the biotinylation of proteins in this HeLa NLRP3-TurboID model is specific to the localisation of NLRP3-TurboID and not simply a result of endogenous biotinylated proteins. Western blotting was also used to validate protein expression and biotin ligase efficacy of NLRP3-TurboID (Figure 4.1E and F). NLRP3-TurboID protein expression was not affected by treatment with nigericin or biotin (Figure 4.1E). Western blots probed for streptavidin-HRP showed self-biotinylation of NLRP3-TurboID following biotin treatment, highlighting that TurboID is functional in our HeLa NLRP3-TurboID cell model, and is unaffected by nigericin treatment (Figure 4.1F). In summary, these data confirm that NLRP3-TurboID was expressed correctly, localised as expected and that the biotin ligase activity of the TurboID was functional in this stably expressing HeLa cell model.

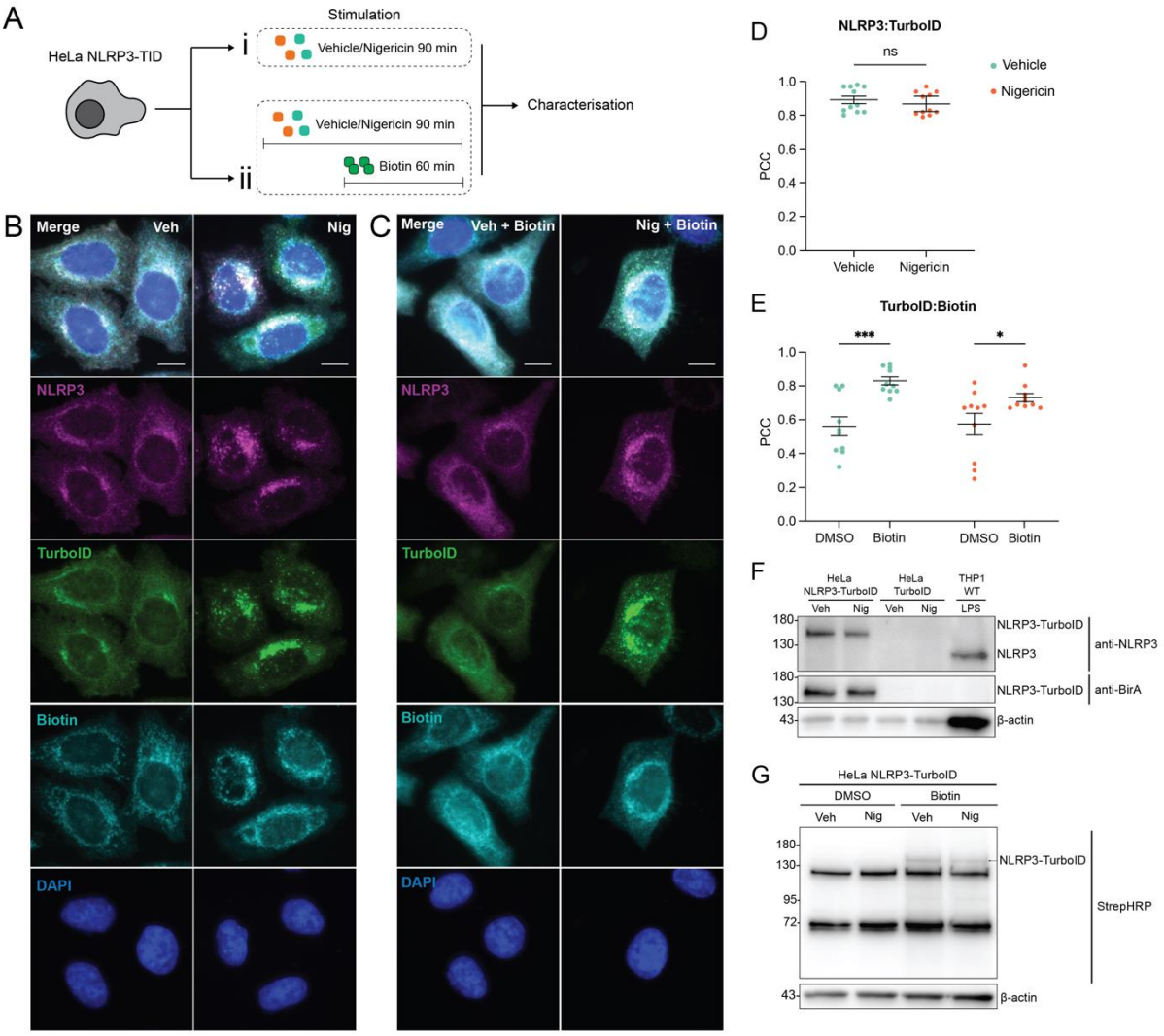
A
Stimulation
HeLa NLRP3-TID
i
Vehicle/Nigericin 90 min
Vehicle/Nigericin 90 min
Biotin 60 min
ii
Characterisation
B
Merge
Veh
Nig
NLRP3
TurboID
Biotin
DAPI
C
Merge
Veh + Biotin
Nig + Biotin
NLRP3
TurboID
Biotin
DAPI
D
NLRP3:TurboID
ns
Vehicle
Nigericin
PCC
1.0
0.8
0.6
0.4
0.2
0.0
Vehicle
Nigericin
E
TurboID:Biotin
***
*
PCC
1.0
0.8
0.6
0.4
0.2
0.0
DMSO
Biotin
DMSO
Biotin
F
HeLa NLRP3-TurboID
HeLa TurboID
THP1 WT
Veh
Nig
Veh
Nig
LPS
180
130
NLRP3-TurboID
NLRP3
anti-NLRP3
180
130
NLRP3-TurboID
anti-BirA
43
β-actin
G
HeLa NLRP3-TurboID
DMSO
Biotin
Veh
Nig
Veh
Nig
180
130
95
72
NLRP3-TurboID
StrepHRP
43
β-actin

Figure 4.1. Characterisation of HeLa NLRP3-TurboID cells. (A) Schematic illustrating the stimulation protocol for HeLa cells stably expressing NLRP3-TurboID. **(i)** HeLa NLRP3-TurboID cells are stimulated with vehicle (ethanol, 0.5% v/v) or nigericin (10 μM) for 90 minutes. **(ii)** HeLa NLRP3-TurboID cells are stimulated with vehicle or nigericin for 30 minutes before the addition of biotin (500 μM) for 60 minutes in the presence of vehicle or nigericin. **(B)** HeLa NLRP3-TurboID cells were simulated as in **Ai**, **(C)** HeLa NLRP3-TurboID were stimulated as in **Aii**. **(B, C)** Cells were analysed by immunofluorescence microscopy (n=4). Anti-NLRP3 labels NLRP3, anti-BirA labels TurboID, streptavidin-HRP labels biotinylated proteins. Blue represents nuclei stained by DAPI. Scale bars are 10 μm. **(D)** Quantification of co-localisation of NLRP3 and TurboID with the Person's correlation coefficient (PCC). Data are n=11 fields of view from four independent experiments. Data were analysed using unpaired two-tailed Mann-Whitney test, ns= not significant. **(E)** Quantification of co-localisation of TurboID and biotin with the Pearson's correlation coefficient (PCC). Data are n=10 fields of view from four independent experiments. Data were analysed using two-way ANOVA followed by Šidák's multiple comparisons test (compared with DMSO) *P ≤ 0.05 and ***P ≤ 0.001. **(F)** HeLa NLRP3-TurboID cells or HeLa cells stably expressing TurboID alone were stimulated as in **Ai** and wild-type (Mariathasan et al.) THP-1 monocytes were stimulated with LPS 1ug/ml for 4 hours as an NLRP3 expression control. Cell lysates were probed for NLRP3 (anti-NLRP3), TurboID (anti-BirA) (n=3). **(F)** HeLa NLRP3-TurboID cells were stimulated as in **Aii**. Cell lysates were probed for biotinylated proteins (StrepHRP) (n=3).

4.2.2 Mass spectrometry analysis

To establish an interactome for NLRP3-TurboID, HeLa NLRP3-TurboID cells were treated with vehicle (ethanol, 0.5% v/v; 90 min) or nigericin (10 µM; 90 min). Biotin (500 µM, 60 min) was added for the final 60 minutes of vehicle or nigericin stimulation. Four independent experiments were conducted for each treatment and samples were analysed for biotinylated proteins by mass spectrometry (Figure 4.2A). Principal component analysis (PCA) established that the NLRP3 interactome for vehicle differed from the NLRP3 interactome for nigericin (Figure 4.2B). The variance for both groups could be explained by 36.3% of principal component 1 (PC1) and 24.1% of PC2. Following filtering (Chapter 2 Materials and methods), a two-sample t-test was carried out on LFQ intensities between the vehicle and nigericin NLRP3 interactome. For this analysis, the minimal fold change for significance was 2 (s0=1) and a false discovery rate (FDR)=0.05. Here, seven proteins were significantly enriched with vehicle and 21 proteins were significantly enriched with nigericin (Table 4.1, Figure 4.2C).

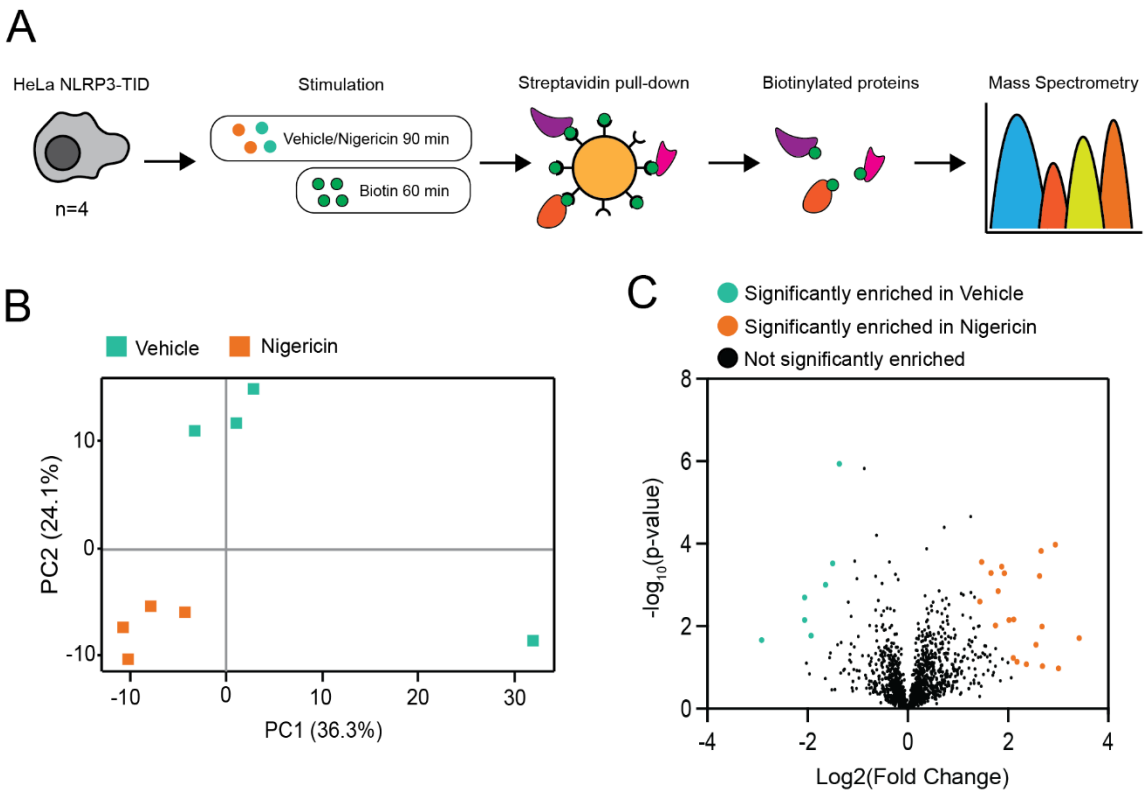

Figure 4.2. Mass spectrometry analysis of the NLRP3 interactome. (A) Schematic illustrating the pipeline of biotinylation enrichment analysis by mass spectrometry. HeLa cells stably expressing NLRP3-TurboID were treated with vehicle (ethanol, 0.5% v/v, 90 min) or nigericin (10 µM, 90 min) and biotin (500 µM) was added for the final 60 minutes (n=4). Streptavidin pull-down of biotinylated proteins was performed; illustration shows streptavidin-coated magnetic beads (yellow) bound to biotin (green) and biotinylated proteins. Biotinylated proteins were analysed by mass spectrometry. **(B)** Principal component analysis of LFQ intensities. Each single square denotes an independent experiment, with experimental groups (vehicle or nigericin) grouped by colour. **(C)** Volcano plot of proteins enriched in vehicle (green) and nigericin (orange) following two-sample t-test of LFQ intensity values (significance determined as Fold change ≤ -2 or ≥ 2; p ≤0.05).

Table 4.1. Significantly enriched proteins of the NLRP3 interactome. A table of the 28 proteins significantly enriched with NLRP3-TurboID interaction, seven proteins enriched in vehicie (green; Fold change ≤ -2; p ≤0.05), 21 proteins enriched in nigericin (orange; Fold change ≥ 2; p ≤0.05). Table shows gene name, protein name, Log2 fold change (FC) and -log10 (p-value).

Gene name	Protein name	Log2 FC	-Log10 p-value
Enriched in Vehicle			
AHCYL1	Adenosyl homocysteinase Like 1	-1.37	5.94
SHTN1	Shootin 1	-1.50	3.52
NMD3	NMD3 Ribosome Export Adaptor	-1.64	3.00
DEGS1	Delta 4-Desaturase, Sphingolipid 1	-1.93	1.77
GOLGA3	Golgin A3	-2.06	2.15
CEP350	Centrosomal protein 350	-2.06	2.70
TOMM5	Translocase Of Outer Mitochondrial Membrane 5	-2.92	1.66
Enriched in Nigericin			
ATP5F1E	ATP Synthase F1 Subunit Epsilon	3.42	1.71
PLP2	Proteolipid Protein 2	3.01	0.97
SNX3	Sorting nexin-3	2.94	3.98
MT-ATP8	Mitochondrially Encoded ATP Synthase Membrane Subunit 8	2.69	1.03
BAZ1B	Bromodomain Adjacent To Zinc Finger Domain 1B	2.68	1.99
GORASP2	Golgi Reassembly Stacking Protein 2	2.66	3.83
UQCRFS1	Ubiquinol-Cytochrome C Reductase, Rieske Iron-Sulfur Polypeptide 1	2.63	3.22
MIEF1	Mitochondrial Elongation Factor 1	2.56	1.55
NUFIP2	Nuclear FMR1 Interacting Protein 2	2.37	1.08
P4HB	Prolyl 4-Hydroxylase Subunit Beta	2.18	1.13
POLR1A	RNA Polymerase I Subunit A	2.11	2.17
LAMA1	Laminin subunit alpha-1	2.11	1.23

RAB11FIP5	Rab11 family-interacting protein 5	2.02	2.15
SDHA	Succinate dehydrogenase flavoprotein subunit A	1.93	3.28
MCM4	Minichromosome Maintenance Complex Component 4	1.87	3.44
TPD52L2	Tumour protein D54	1.80	2.85
ICAM1	Intercellular adhesion molecule 1	1.75	2.02
MTERF3	Mitochondrial Transcription Termination Factor 3	1.66	3.29
SURF1	Surfeit locus protein 1	1.47	3.56
ATP2B4	Plasma membrane calcium-transporting ATPase 4	1.44	2.60
MARCKS	Myristoylated alanine-rich C-kinase substrate	1.25	4.65

4.2.3 Functional analysis

4.2.3.1 Subcellular location

Ingenuity pathway analysis (Qiagen) was used to understand the 28 significantly enriched proteins in the context of their subcellular location. The seven proteins significantly enriched in vehicle were localised to the plasma membrane (SHTN1, DEGS1), mitochondria (AHCYL1, TOMM5), Golgi apparatus (GOLGA3), cytoskeleton/centrosome/centriole (CEP350) and nucleus (NMD3). Within the NLRP3 interactome with vehicle stimulation, two proteins were classified as enzymes (AHCYL1, DEGS1), one as a transporter (GOLGA3) and four as "other" (SHTN1, CEP350, NMD3, TOMM5). Following from previous literature on the localisation of NLRP3 to intracellular organelles following activation, the subcellular location of the NLRP3 interactome following nigericin stimulation was of particular interest here. Proteins enriched following nigericin stimulation were located to the mitochondria (SURF1, SDHA, UQCRFS1, MTERF3, MT-ATP8, ATP5F1E, MIEF1), Golgi apparatus (GORASP2, P4HB, RAB11FIP5), endoplasmic reticulum (PLP2, GORASP2, P4HB), phagosomes (SNX3, RAB11FIP5, P4HB), plasma membrane (MARCKS, ICAM1, ATP2B4), nucleus (POLR1A, MCM4, BAZ1B), endosomes

(SNX3, RAB11FIP5), centrosome (RAB11FIP5), cytoskeleton (P4HB), extracellular space (LAMA1) and “other cytoplasmic locations” (NUFIP2, TPD52L2). Of these proteins, seven were classified as enzymes (P4HB, SURF1, SDHA, UQCRFS1, MT-ATP8, MCM4, POLAR1A), four were classified as transporters (ATP2B4, PLP2, SNX3, ATP5F1E), one as a transmembrane receptor (ICAM1), one as a transcriptional regulator (BAZ1B) and eight as “other” (LAMA1, MARCKS, GORASP2, RAB11FIP5, MIEF1, MTERF3, TPD52L2, NUFIP2) (Figure 4.3).

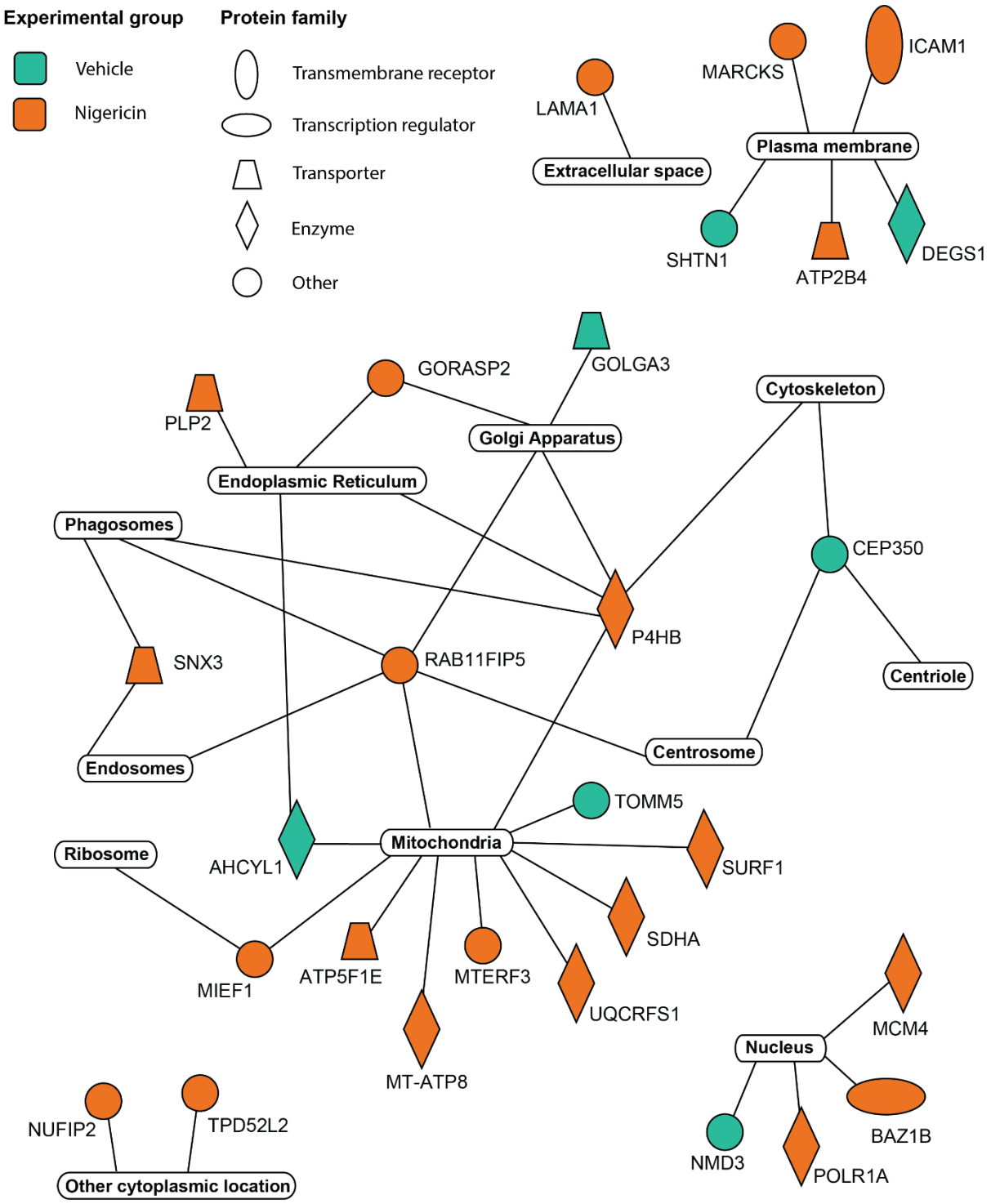

Figure 4.3. Subcellular location of NLRP3 interactome. Ingenuity pathway analysis (IPA) of the subcellular location of proteins significantly enriched in the NLRP3 interactome. Proteins enriched following treatment with vehicle (green) or nigericin (orange) are represented by symbol colour. Protein family is represented by symbol shape.

Based on previous work by our group and others showing that a disruption in endocytic traffic contributes to NLRP3 inflammasome activation (Lee et al., 2023, Zhang et al., 2023), I wanted to further explore proteins reported to be associated with endocytic compartments and involved in endosome-Golgi trafficking. I identified a panel of five proteins with evidence in the literature to support their cellular function in the endosome to Golgi trafficking pathway (Table 4.2).

Table 4.2. Endosome-Golgi traffic proteins of interest. Five proteins of interest in the NLRP3 interactome were selected for further investigation. Table shows gene name, protein name, subcellular location, functional annotations, and references that explain the rationale for selection.

Gene name	Protein Name	Subcellular Location	Functional Annotations	References
GOLGA3	Golgin subfamily A member 3	Cytosol, Golgi Apparatus	Protein associated with the cytoplasmic face of the Golgi membrane	(Misumi et al., 1997)
SNX3	Sorting nexin-3	Cytosol, Phagosomes, Endosomes	Binds phosphatidylinositols. Mediates endosome-to-TGN receptor transport. Mediates transferrin receptor recycling.	(Xu et al., 2001, Harterink et al., 2011, Chen et al., 2013, Harrison et al., 2014)
GORASP2	Golgi reassembly-stacking protein 2	Golgi Apparatus, Endoplasmic Reticulum	Regulates mature IL-1β release.	(Chiritoiu et al., 2019)
RAB11FIP5	Rab11 family-interacting protein 5	Phagosomes, Golgi Apparatus, Centrosome, Endosomes, Mitochondria	Involved in protein trafficking from recycling endosomes to plasma membrane.	(Schonteich et al., 2008, Prekeris et al., 2000)
TPD52L2	Tumour protein D54	Cytoplasm, Other	Involved in multiple membrane trafficking pathways: anterograde traffic, recycling, and Golgi integrity. Slower transferrin recycling and TGN46 dispersal in TPD54-depleted cells. Marker for intracellular nanovesicles (INVs)	(Larocque et al., 2020)

4.2.4 Characterisation of THP-1 monocyte cell lines containing knockdowns of NLRP3-TurboID proteins of interest

I identified 28 proteins significantly enriched in the NLRP3-TurboID interactome in HeLa cells. From these 28 proteins, five candidate proteins were selected due to their association with endocytic traffic and the endosome-Golgi organelle system (Table 4.2). The localisation of NLRP3 to endolysosomal compartments has been suggested as an important step in NLRP3 inflammasome activation (Lee et al., 2023, Zhang et al., 2023). Moreover, the five proteins identified in this panel provide greater insight to the protein interactions that may occur between NLRP3 at endocytic compartments. Therefore, I hypothesised that the five proteins identified here may be important in canonical activation of the NLRP3 inflammasome. Knocking down each of these proteins individually in a THP-1 monocyte cell line would allow investigation into canonical NLRP3 activation in their absence. Due to the lack of a suitable antibody to assess effective knockdown by western blot, Rab11FIP5 was later excluded from the panel of proteins.

The Genome Editing Unit (GEU) at The University of Manchester generated polyclonal pools of THP-1 monocytes by CRISPR/Cas9 protein knockdown. Editing efficiency of each gene was assessed by inference of CRISPR edits (ICE) analysis (percentage denotes the editing efficiency i.e., the proportion of cells within the pool with a non-wild type sequence); GOLGA3 (83%), GORASP2 (56%), SNX3 (61%) and TPD52L2 (79%) (Figure 4.4A and B). Assessment of protein expression by western blot confirmed that knockdown of the four target genes was successful. Each THP-1 monocyte knockdown (KD) cell line expressed their respective protein to a lesser level that was observed in wild type THP-1 monocytes (Figure 4.4C).

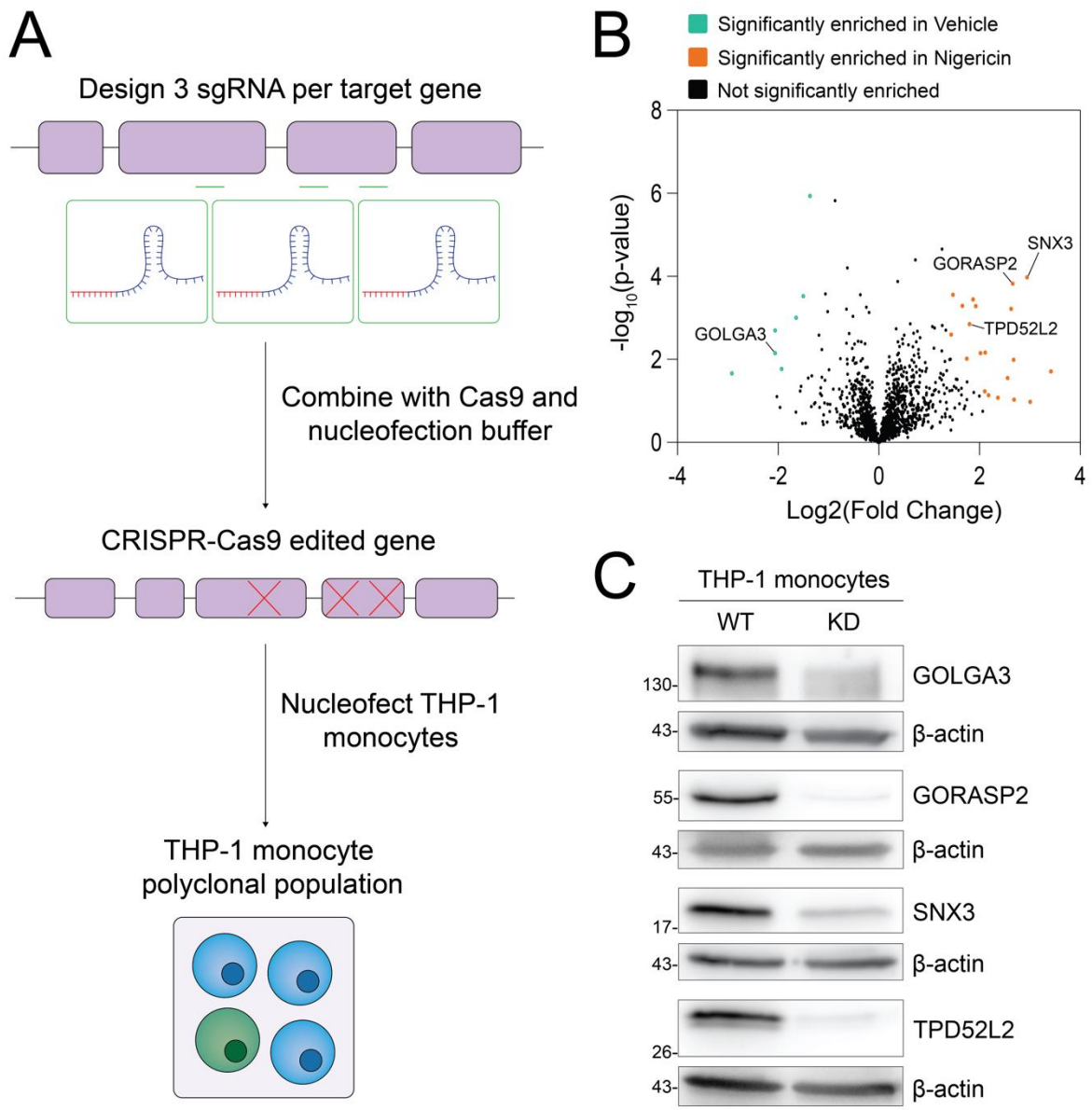

Figure 4.4. Generation of THP-1 monocytes with NLRP3-TurboID protein of interest knockdown (A) Schematic illustrating CRISPR/Cas9 knockdown process by nucleofection in THP-1 monocytes carried out by Genome Editing Unit (GEU) at The University of Manchester. Three single guide RNAs (sgRNA) were designed for each candidate gene (GOLGA3, GORASP2, SNX3, TPD52L2). CRISPR/Cas9 nucleofection into THP-1 monocytes was carried out to generate a polyclonal knockdown population. **(B)** Volcano plot of proteins enriched in vehicle (green) and nigericin (orange) (Figure 4.2B). Candidate genes selected for knockdown are labelled. **(C)** Western blot of cell lysates of wild type (Mariathasan et al.) and knockdown (KD) THP-1 monocytes probed for the protein encoded by the candidate knockdown gene; GOLGA3, GORASP2, SNX3 and TPD52L2 (n=3).

To assess the role that GOLGA3, GORASP2, SNX3 and TPD52L2 play in canonical activation of the NLRP3 inflammasome, wild type and THP-1 monocytes with the target protein knockdown were PMA-differentiated to monocyte-derived macrophages and primed with LPS, prior to stimulation with vehicle or nigericin (Figure 4.5A). Supernantants were assessed for IL-1β as a read-out of NLRP3 inflammasome activation. LPS-priming alone induced a small amount of IL-1β release (Figure 4.5B). In LPS-primed wild type cells, nigericin stimulation elicited a strong IL-1β release, suggesting effective activation of the NLRP3 inflammasome. In THP-1 macrophages with depleted TPD52L2, IL-1β release was significantly potentiated following nigericin stimualtion, compared to wild-type. Knockdown of GOLGA3, GORASP2 and SNX3 showed a trend for an increase in IL-1β release compared to wild type, but this increase was not statistically significant (Figure 4.5B). LDH release was unaffected by GOLGA3, GORASP2, SNX3 or TPD52L2 knockdown compared to wild type in all treatment groups (Figure 4.5C). These data suggest that THP-1 monocyte-derived macrophages with depleted TPD52L2 protein levels have an enhanced canonical NLRP3 inflammasome response.

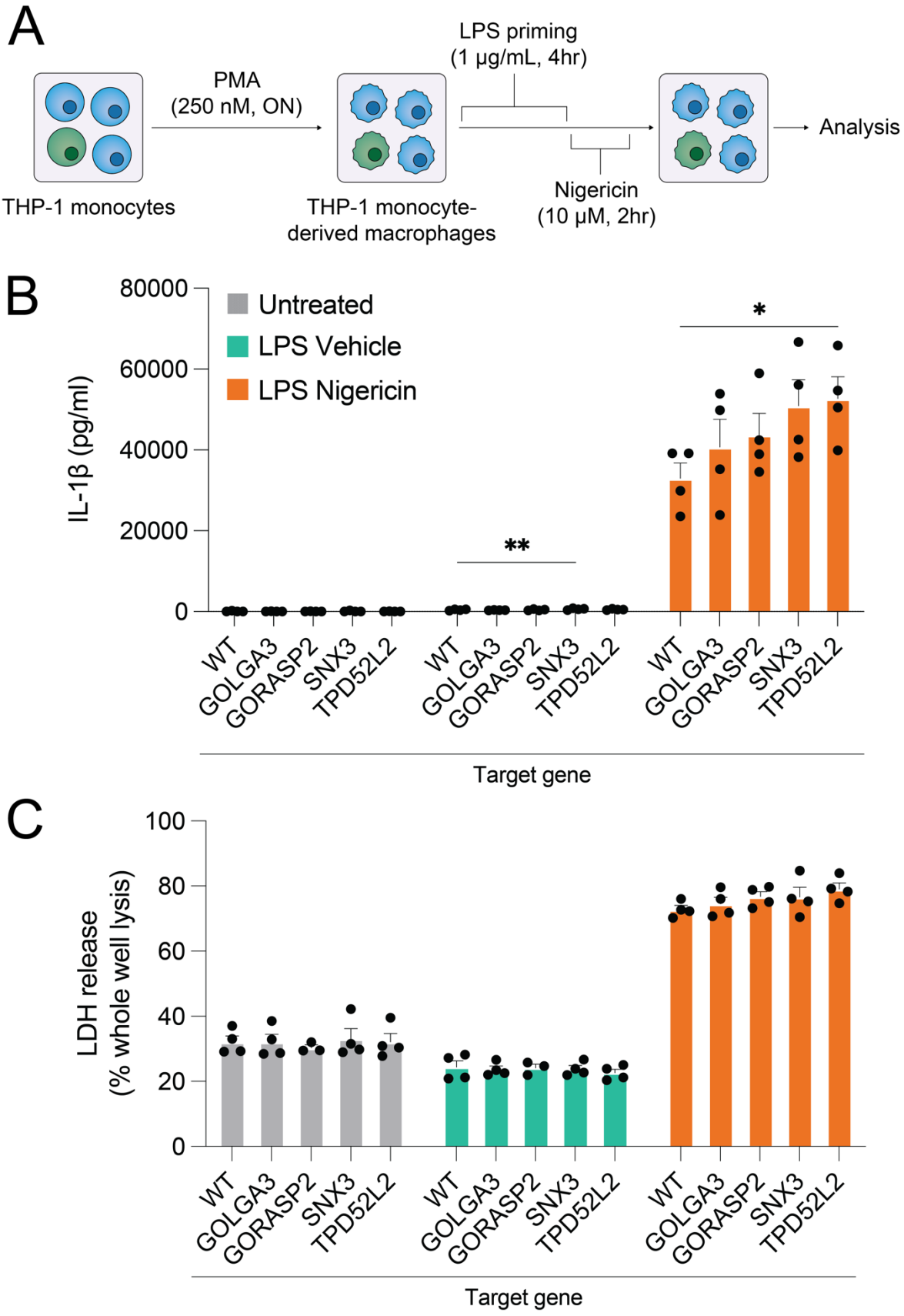
A
LPS priming
(1 µg/mL, 4hr)
PMA
(250 nM, ON)
Analysis
THP-1 monocytes
THP-1 monocyte-
derived macrophages
Nigericin
(10 µM, 2hr)
B
Untreated
LPS Vehicle
LPS Nigericin
IL-1β (pg/ml)
80000
60000
40000
20000
0
*
**
WT
GOLGA3
GORASP2
SNX3
TPD52L2
Target gene
C
LDH release
(% whole well lysis)
100
80
60
40
20
0
Target gene

Figure 4.5. Characterisation of NLRP3-TurboID target protein knockdown in THP-1 macrophages. (A) Schematic describing the experimental protocol leading to canonical NLRP3 inflammasome activation of THP-1 monocyte-derived macrophages. THP-1 monocytes were differentiated by Phorbol-12-myristate-13-acetate (PMA, 250 nM) overnight (ON). THP-1 monocyte-derived macrophages were primed with lipopolysaccharide (LPS, 1 μg/ml) for 4 hours prior to vehicle (ethanol, 0.5% v/v) or nigericin (10 μM) stimulation for 2 hours. Supernatants were assessed for **(B)** IL-1β and **(C)** LDH release (n=4). Data were analysed using two-way ANOVA with Dunnett's multiple comparison test. *P ≤ 0.05 and **P ≤ 0.01. Non-significance not shown.

4.3 Discussion

Thus far, data in Chapter 3 and further published work has suggested that a disruption in endocytic traffic is implicated in canonical activation of the NLRP3 inflammasome (Chapter 3 The cell biology of NLRP3 activation) (Lee et al., 2023, Zhang et al., 2023). Work in these studies shows that NLRP3 co-localises with endolysosomal markers following stimulation with NLRP3-activating stimuli, suggesting that the localisation of NLRP3 to endolysosomal compartments may be an important step in the activation of the inflammasome. I hypothesised that NLRP3 is interacting with proteins expressed on endocytic compartments following stimulation with NLRP3-activating stimuli, and that these interactions may be important in the activation of the NLRP3 inflammasome. Therefore, the aim of this chapter was to investigate the protein interactome of NLRP3 under NLRP3-activating conditions. Using TurboID, an efficient method of enzyme-catalysed proximity labelling (Cho et al., 2020), I determined the protein interaction profile of NLRP3 at rest (vehicle) and following stimulation with an NLRP3 activating stimulus (nigericin) in a HeLa cell model (Figure 4.2, Table 4.1). Following on from this unbiased method of investigation, I determined the subcellular location of the proteins enriched in vehicle and nigericin and identified proteins that have been characterised as integral members of the endocytic-Golgi pathway (Figure 4.3, Table 4.2). I proceeded to investigate the four proteins: Golgin subfamily A member 3, Sorting nexin-3, Golgi reassembly-stacking protein 2 and Tumour protein D54 (TPD54) by knocking down their corresponding genes in a THP-1 monocyte cell line (Figure 4.4). Interestingly, depletion of TPD54 in monocyte-derived macrophages results in potentiated NLRP3 inflammasome activation (Figure 4.5). TPD54 is involved in multiple membrane trafficking pathways, therefore its depletion disrupts normal endocytic traffic, which may be sensed by NLRP3 and potentiate inflammasome activation as a result (Larocque et al., 2020). These data

build on our previous research and support the hypothesis that a disruption in endocytic traffic is sensed by NLRP3 and further explains the spatial activation of the NLRP3 inflammasome.

Creating a HeLa NLRP3-TurboID cell model began with cloning the NLRP3-TurboID vector to express the flexible Waldo linker (GSW), with the aim to avoid any functional interference between NLRP3 and TurboID (Chapter 2 Materials and Methods)(Waldo et al., 1999). The Waldo linker is a glycine and serine rich linker that, many glycine and serine rich linkers, is flexible and We have previously shown that following treatment with NLRP3-activating stimuli, NLRP3 localises to endocytic compartments in non-immune cell lines, such as COS7 cells, in a similar fashion to cells that endogenously express NLRP3, such as bone marrow-derived macrophages (Lee et al., 2023). Therefore, to investigate the spatial interactome of NLRP3 under stimulatory conditions, I used lentiviral transfection to generate a HeLa cell line that stably expressed NLRP3-TurboID. Due to the absence of essential inflammasome components including the adaptor protein ASC, HeLa NLRP3-TurboID cells allowed investigation of the intracellular location of NLRP3 under stimulatory conditions without the formation of an active inflammasome and initiation of pyroptotic cell death (Yang et al., 2019). The expression, localisation and biotinylation efficacy of NLRP3-TurboID was characterised in this HeLa cell model (Figure 4.1). Immunofluorescence microscopy revealed that at rest, NLRP3 was largely cytosolic with some concentration to the perinuclear region, and under nigericin stimulation NLRP3 formed distinct cytoplasmic puncta (Figure 4.1B). NLRP3 appeared to co-localise with TurboID under both conditions, assessed by immunofluorescence microscopy and a high Pearson's Correlation Coefficient (PCC) (Figure 4.1B and D). Mitochondria contain endogenous biotinylated proteins that are observed

following streptavidin labelling, therefore, I wanted to assess whether addition of biotin resulted in specific biotinylation of proteins by TurboID. The co-localisation between TurboID and biotinylated proteins significantly increased following the addition of biotin, suggesting that biotinylated proteins in the presence of biotin is specific to the location of TurboID (Figure 4.1C and E). Therefore, it was convincing that the potential interactome of NLRP3-TurboID would mirror what would be expected of NLRP3 in this cell model.

Mass spectrometry analysis of biotinylated proteins revealed a 28 protein interactome for NLRP3-TurboID; seven proteins were enriched with vehicle and 21 proteins were enriched with nigericin. Gene ontology (GO) and ingenuity pathway analysis (IPA) allowed investigation into the subcellular localisation of these proteins according to current literature (Thomas et al., 2022, Kramer et al., 2014). In this study, the NLRP3 interactome is located across a range of subcellular organelles, which comes as no surprise considering the wide range of research implicating the location of organelles in NLRP3 inflammasome activation (Seoane et al., 2020). As mentioned previously, the focus of this study was to investigate the endocytic pathway with respect to the spatial activation of NLRP3. However, it would be amiss to not mention that several proteins present here are enriched on the mitochondria, endoplasmic reticulum, and centrosome. These organelles have all been highly studied with regards to NLRP3 inflammasome activation and may represent interesting targets for future studies (Zhou et al., 2011, Menu et al., 2012, Shi et al., 2016).

To investigate how the NLRP3 interactome is implicated in canonical activation of the inflammasome, five candidate proteins (GOLGA3, GORASP2, RAB11FIP5, SNX3 and TPD52L2) were selected for CRISPR/Cas9 knockdown in THP-1 monocytes based on previous literature

describing their expression on endocytic or Golgi compartments, association with phosphatidylinositols, role in endocytic trafficking, or association with IL-1β release (Table 4.2). It was important to include a protein enriched in NLRP3-TurboID under vehicle treatment, and so GOLGA3 was selected due to its location at the TGN, and previous work showing that NLRP3 resides on the TGN at rest (Chapter 3 The cell biology of NLRP3 activation) (Misumi et al., 1997, Chen and Chen, 2018, Lee et al., 2023, Zhang et al., 2023). Investigating knock-down of GOLGA3 with respect to canonical NLRP3 inflammasome activation may increase understanding of the functional biology of NLRP3 prior to activation.

SNX3 and RAB11FIP5 were the only two proteins in the NLRP3 interactome reported to be present on endosomes and were therefore interesting candidates. SNX3 is present on early endosomes and is suggested to be important in membrane trafficking, specifically retrograde endosome-TGN traffic and the regulation of endosomal cargo cycling such as the transferrin receptor and epidermal growth factor (EGF) receptor trafficking (Harterink et al., 2011, Xu et al., 2001, Chen et al., 2013). In addition, SNX3 is reported to possess a phox (PX) domain, which is a phosphatidylinositol binding domain (Xu et al., 2001). Interaction of NLRP3 with the phosphatidylinositol PI4P is important in the activation of the inflammasome, however, it is worth noting that currently, studies only describe an interaction between SNX3 and PI3P via the PX domain (Chen and Chen, 2018, Zhang et al., 2023, Xu et al., 2001, Chandra et al., 2019). Nevertheless, the clear association with membrane trafficking and phosphatidylinositol binding, and the importance of these functional pathways in NLRP3 inflammasome activation, provided enough evidence to select SNX3 as an important candidate for further study. Rab11FIP5 is located at recycling endosomes and the plasma membrane and regulates endosome-plasma membrane recycling (Prekeris et al., 2000). As NLRP3-activating stimuli

disrupt endosome-plasma membrane recycling, Rab11FIP5 appeared to be an interesting candidate for further investigation (Chapter 3 The cell biology of NLRP3 activation) (Lee et al., 2023, Zhang et al., 2023). However, Rab11FIP5 was eliminated from the panel due to the lack of a suitable antibody to probe for the protein in future experiments.

GORASP2 is a TGN-resident protein that plays an integral role in the maintenance of Golgi structure (Zhang and Seemann, 2021), however, this role did not form the primary rationale for its inclusion in the panel of proteins. Interestingly, GORASP2 is characterised as regulating the secretion of mature IL-1β through its role in the unfolded protein response (UPR) (Chiritoiu et al., 2019). Knockout of GORASP2 caused intracellular aggregation of mature IL-1β and affected secretion of the cytokine as a result (Chiritoiu et al., 2019). However, the role of GORASP2 in NLRP3 inflammasome activation was not explored in this study, therefore GORASP2 emerged as an interesting candidate for further study.

TPD54 was initially investigated for its role in the prognosis of several cancers (Kato et al., 2017, Ren et al., 2017, Zhuang et al., 2019). More recently, TPD54 is suggested to be involved in multiple membrane trafficking pathways including anterograde traffic, endosome recycling and the maintenance of Golgi integrity (Larocque et al., 2020). In this study by Larocque et al., a fluorescent transferrin assay was used to measure endosome-plasma membrane recycling, much like was carried out here in Chapter 3 (Larocque et al., 2020). Interestingly, depletion of TPD54 in HeLa cells causes a slowing of transferrin recycling, in line with what was observed following treatment of HeLa cells with NLRP3-activating stimuli (Larocque et al., 2020, Lee et al., 2023). In addition to a slowing of transferrin recycling, TPD54 depletion also causes a dispersal of TGN46 (Larocque et al., 2019). As observed in previous studies, a disruption in

endosomal trafficking results in the cycling trans-Golgi protein TGN46 to become trapped in endosomes and lysosomes, resulting in the presence of dispersed TGN46-positive puncta (Lee and Hoyle et al., 2023; Zhang et al., 2023). This therefore suggests that much like NLRP3-activating stimuli, TPD54 depletion in HeLa cells causes a disruption in endocytic traffic. In addition, TPD54 is present on membrane trafficking compartments termed intracellular nanovesicles (INVs), which may represent a novel membrane trafficking pathway that is implicated in the activation of the NLRP3 inflammasome (Larocque et al., 2020). From this evidence in previous literature, TPD54 was also selected as a candidate for knockdown in THP-1 monocytes.

CRISPR/Cas9 knockdown in THP-1 monocytes was carried out individually for each of the four candidate genes (GOLGA3, GORASP2, SNX3 and TPD52L2). THP-1 monocytes were selected as they would not only provide the opportunity to investigate a circulating monocyte cell line, but they can also be differentiated into macrophages (Bosshart and Heinzelmann, 2016). In addition, THP-1 monocytes represent a clinically relevant human cell model that are implicated in sterile inflammation that drives disease (Shi and Pamer, 2011).

To assess the role of each candidate protein in canonical activation of the NLRP3 inflammasome, THP-1 monocytes were differentiated into monocyte-derived macrophages by PMA treatment, then LPS primed prior to stimulation with vehicle of nigericin (Figure 4.5A). Following LPS priming, nigericin-induced IL-1β release was potentiated in THP-1 monocyte-derived macrophages with depleted levels of TPD54 compared to wild type (Figure 4.5B). LDH release was unchanged between each between each cell line within each treatment compared to wild type (Figure 4.5C). These data suggest that knockdown of TPD54

potentiates NLRP3 inflammasome activation without altering cell death. As TPD54 has previously been shown to cause a disruption in membrane trafficking pathways, and endocytic traffic dysfunction contributes to NLRP3 inflammasome activation, it is likely that the enhanced NLRP3 inflammasome response observed here is due to a further potentiation of disruptions in endocytic traffic (Larocque et al., 2020, Lee et al., 2023, Zhang et al., 2023). Indeed, data in chapter 3 suggest that more potent NLRP3-activating stimuli, such as nigericin, appear to be more effective disruptors of endosome-plasma membrane recycling, whereas imiquimod, the least potent NLRP3-activating stimuli, had the mildest effect on transferrin recycling (Chapter 3 The cell biology of NLRP3 activation). This could somewhat be explained by the fact that the doses of NLRP3-acting stimuli used in chapter 3 were not matched in terms of their efficacy at activating NLRP3, and higher doses of imiquimod may induce a further disruption in endocytic traffic. However, it is possible that that the level of endocytic traffic disruption may be proportional to the potency of NLRP3 inflammasome activation, and therefore this requires further investigation. Subsequent studies will aim to characterise endosome-plasma membrane recycling following nigericin stimulation in both wild type and TPD54 knockdown THP-1 monocytes.

Understanding how the NLRP3 inflammasome is activated is a prevailing question in the field. Creating a more comprehensive picture of how NLRP3 senses cellular stress may be key to understanding how the inflammasome propagates an inflammatory response. These data build on previously published observations that a disruption in endocytic traffic likely elicits a cellular stress that is sensed by NLRP3. Further, the localisation of NLRP3 to subcellular endocytic compartments has been shown to be important for its activation. Here I have shown that NLRP3 interacts with multiple proteins involved in endocytic traffic, including

TPD54. TPD54 knockdown results in potentiated NLRP3 inflammasome activation, which may be a result of disrupted endocytic traffic. Further investigation into these mechanisms will allow greater insight into NLRP3 biology and the development of more effective therapeutics to target NLRP3 in disease.

Chapter 5:

The intracellular role of pro-IL-1α

Chapter 5. The intracellular role of pro-IL-1α

5.1 Introduction

Members of the interleukin-1 (IL-1) family of cytokines, namely IL-1α and IL-1β, are important mediators of the innate immune response (Dinarello, 2018). IL-1α and IL-1β are pro-inflammatory cytokines that aim to protect against pathogenic infection. However, when dysregulated and in the absence of infection, IL-1α- and IL-1β-mediated inflammation can be detrimental to the host (Lukens et al., 2012). To gain greater insight into inflammatory mechanisms we must increase our understanding how IL-1α and IL-1β are regulated intracellularly. Currently, studies predominately centre on the regulation of IL-1β, with less research into IL-1α.

Inflammation is, in early life, a beneficial response that protects the host from pathogenic infection. Inflammation is a coordinated response of immune cells with communication between them driven by signalling molecules called cytokines (Kany et al., 2019). Cytokines are, in general, secreted proteins that bind to receptors on target cells to elicit a signalling response (Netea et al., 2017). There are examples however, where some cytokines appear to have dual function and have an additional intracellular role such as high-mobility group box 1 protein (HMGB1) and interleukin-33 (IL-33) (Bertheloot and Latz, 2017). One of the most important cytokine families in the host response to infection is the IL-1 family, which consists of 11 members of both pro- and anti-inflammatory cytokines. Pro-inflammatory members of the IL-1 family include the well-studied cytokines IL-1α and IL-1β. IL-1β is an ancient protein conserved throughout vertebrates, while IL-1α arose as a gene duplication of IL-1β and is present only in mammals (Rivers-Auty et al., 2018).

Like IL-1β, IL-1α is produced as a less active 31 kDa precursor (pro-IL-1α). However, the pro-domains of IL-1α and IL-1β appear to have evolved separate biological roles. There is limited sequence conservation within the pro- domain of IL-1β in mammals and it is considered simply to stop the secretion and activation of IL-1β (Monteleone et al., 2018). The pro- domain of IL-1α on the other hand is highly conserved amongst mammals and has a number of domains which may have evolved through a functional specialisation driving the divergence of IL-1α from IL-1β (Rivers-Auty et al., 2018). Highly conserved domains within the IL-1α pro-piece include a nuclear localisation sequence (NLS), a motif of basic amino acids that facilitates trafficking to the nucleus, and histone acetyl transferase (Chen et al.) binding domains (Rivers-Auty et al., 2018). Previously published studies have identified a possible role for pro-IL-1α in the regulation of gene expression via binding to histone acetyltransferase (Chen et al.) complexes (Shvedunova and Akhtar, 2022, Lee and Workman, 2007, Buryskova et al., 2004). The 17 kDa mature domain of IL-1α has potent pro-inflammatory actions as a secreted cytokine in common with IL-1β (Zamostna et al., 2012). The idea of IL-1α as a dual function cytokine has been around for many years (Bertheloot and Latz, 2017, McCarthy et al., 2013), although the exact nature of its role remains to be fully explored.

5.2 Results

5.2.1 Characterisation of model

HeLa cells were transiently transfected to express either human pro-IL-1α, pro-IL-1α-TurboID, or TurboID alone (Figure 5.1A). Immunocytochemistry was carried out using antibodies to IL-1α or TurboID (BirA) to characterise the sub-cellular distribution of expressed proteins (Figure 5.1B). Addition of biotin (500µM, 30min) to transfected cells followed by streptavidin-HRP

labelling allowed analysis of the localisation of biotinylated proteins by immunofluorescent microscopy in these cells (Figure 5.1B). Pro-IL-1α was largely localised to the nucleus consistent with previous reports of ectopically and endogenously expressed IL-1α (Luheshi et al., 2009a; Luheshi et al., 2009b) (Figure 5.1B). The expression pattern of pro-IL-1α-TurboID closely matches that of untagged pro-IL-1α, confirming that the TurboID tag did not affect expression or distribution of the protein (Figure 5.1B). Here, the localisation of biotinylated proteins by streptavidin-HRP labelling closely matches that of pro-IL-1α-TurboID by IL-1α. When expressed alone, TurboID was diffusely present throughout the entire cell, as were biotinylated proteins revealed by streptavidin-HRP labelling (Figure 5.1B). Western blot was used to validate protein expression and biotin labelling (Figure 5.1C and D). Labelling with IL-1α and BirA confirmed that pro-IL-1α-TurboID and TurboID were expressed in these cells (Figure 5.1C). Addition of biotin (500μM, 30min) to transfected cells followed by streptavidin-HRP labelling of protein gels confirmed the activity of the TurboID biotin ligase (Figure 5.1D). Treatment of pro-IL-1α- and pro-IL-1α-TurboID-expressing cells with the calcium ionophore ionomycin, an established activator of calpain-dependent pro-IL-1α processing (Tapia et al., 2019), confirmed that the TurboID tag did not interfere with IL-1α processing, or the kinetics of IL-1α processing, suggesting normal trafficking and processing (Figure 5.1E). In summary these data confirm that pro-IL-1α-TurboID was expressed correctly, trafficked normally, and that the biotin ligase activity of the TurboID was functional.

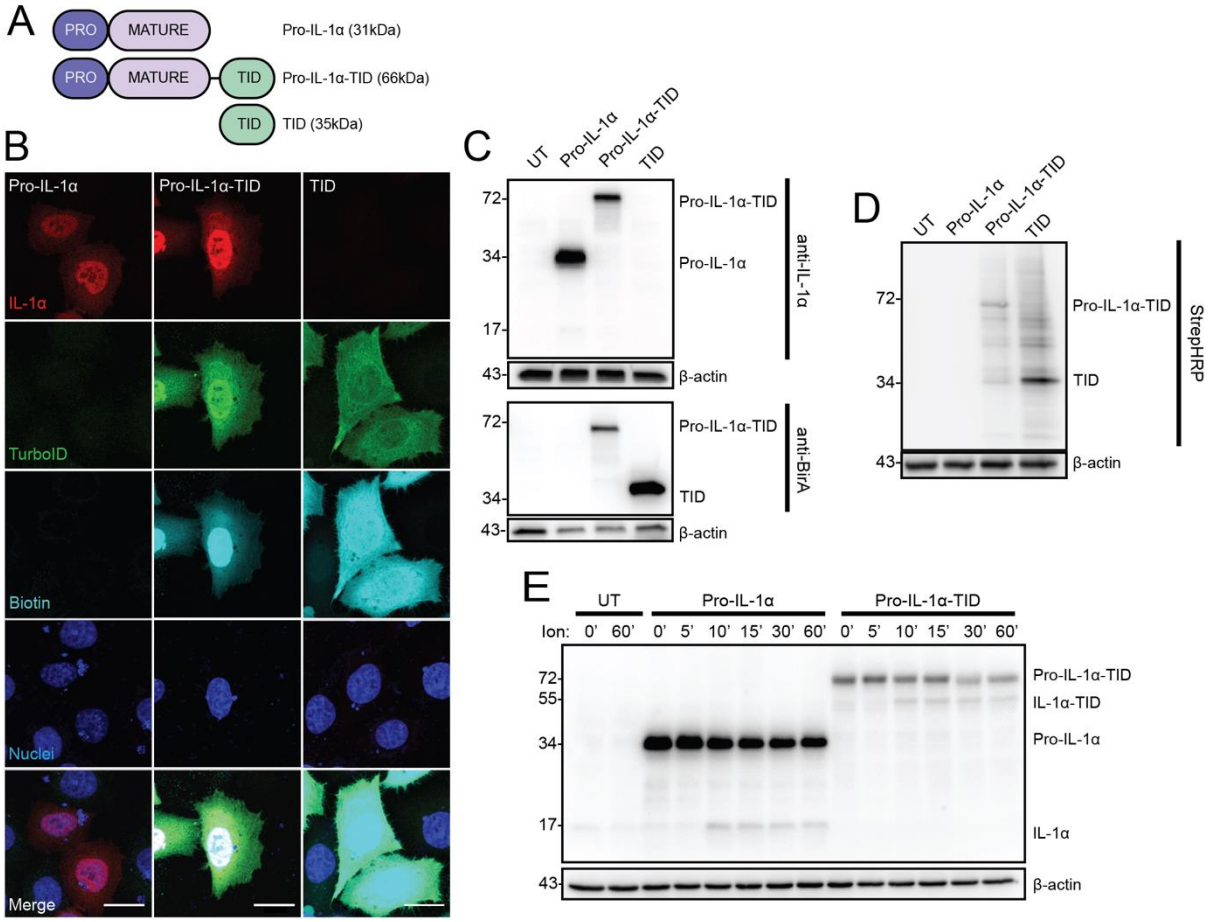

Figure 5.1. Characterisation of pro-IL-1α-TurboID in HeLa cells. (A) Schematic of pro-IL-1α, pro-IL-1α-TurboID (pro-IL-1α-TID) and TurboID (TID) constructs. (B) HeLa cells were transfected with constructs in (A), then treated with biotin (500 µM, 30 min), and analysed by immunofluorescence microscopy (n=2). Anti-IL-1α labels pro-IL-1α and mature IL-1α, anti-BirA labels TurboID, streptavidin-HRP labels biotinylated proteins. Dark blue represents nuclei stained by DAPI. Scale bars are 10 µm. (C, D) HeLa cells were untransfected (UT) or transfected with constructs in (A), then treated with biotin (500 µM, 30 min). Cell lysates were probed for (C) IL-1α (anti-IL-1α), TurboID (anti-BirA) (n=4), and (D) biotin (StrepHRP) (n=4). (E) HeLa cells were untransfected (UT) or transfected with pro-IL-1α or pro-IL-1α-TID and were then treated with ionomycin (Ion) for 0, 5, 10, 15, 30 or 60 minutes (n=4). Cell lysates were probed for IL-1α by western blotting. 0 and 60 minutes were used as representatives for UT cells.

5.2.2 Mass spectrometry analysis

To establish an interactome for pro-IL-1α-TurboID two experimental groups were prepared. These were 1) Pro-IL-1α-TurboID treated with biotin (500µM, 30min) and, 2) TurboID treated with biotin (500µM, 30min). Four independent experiments were conducted for each treatment and samples were analysed for biotinylated proteins by mass spectrometry (Figure 5.2A).

Principal component analysis (PCA) established that the pro-IL-1α interactome was significantly different from the TurboID interactome (Figure 5.2B). The variance for both groups could be explained by 32.4% of principal component 1 (PC1) and 14.4% of PC2. Following filtering (Chapter 2 Materials and methods), a two-sample t-test was carried out on LFQ intensities between pro-IL-1α-TurboID and TurboID interactome. For this analysis, minimal fold change for significance was 2 (s0=2) and FDR=0.01 (Figure 5.2C). Here, 56 proteins were significantly enriched with pro-IL-1α-TurboID (Table 5.1), and 169 proteins (not highlighted) were significantly enriched with the TurboID control (Figure 5.2C).

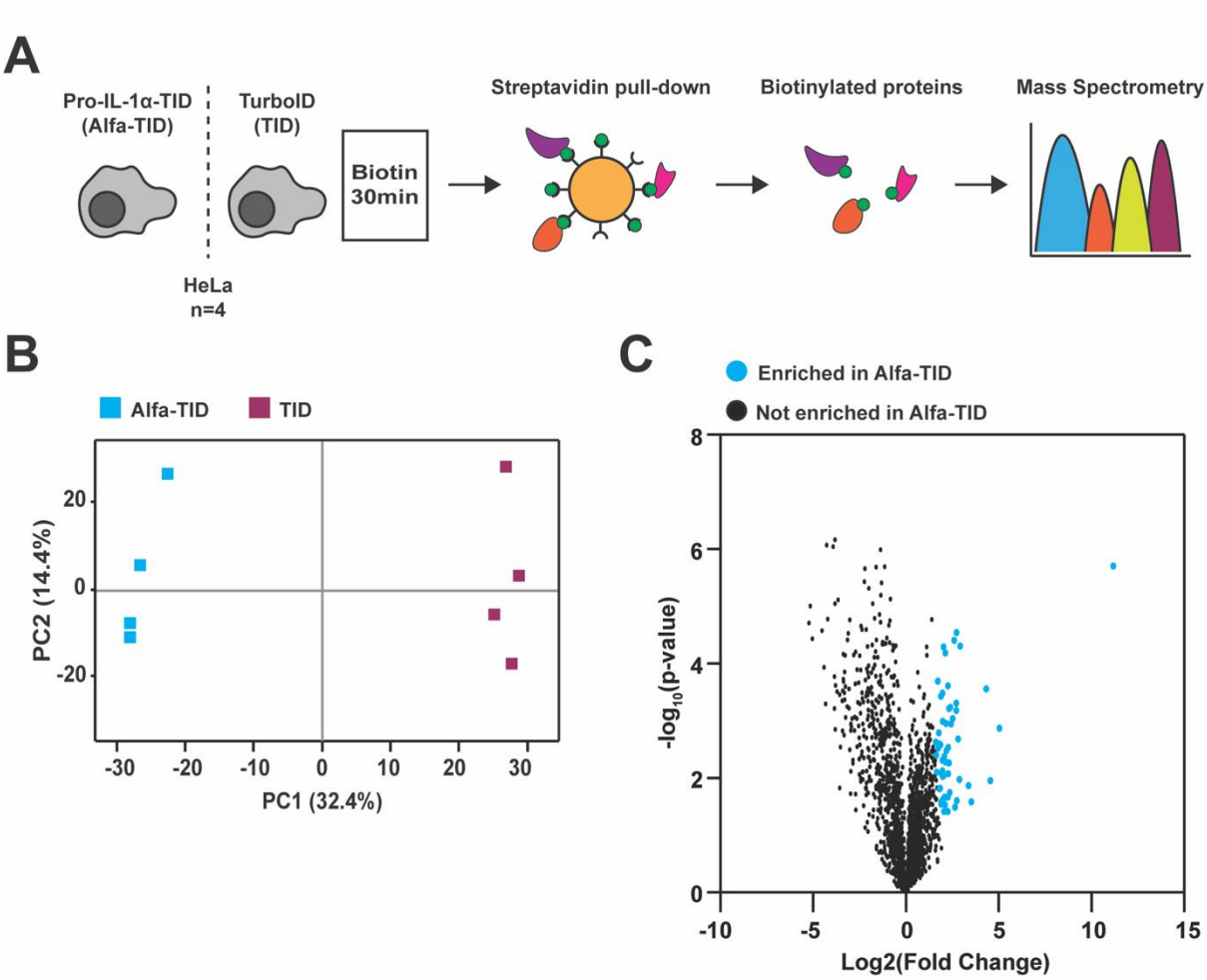

Figure 5.2. Mass Spectrometry analysis of the pro-IL-1α-TurboID interactome. (A) Schematic illustrating the two experimental groups prepared for biotinylation enrichment analysis by mass spectrometry: (1) Pro-IL-1α-TurboID (Alfa-TID) treated with biotin (500µM, 30min, n=4) and (2) TurboID (TID) treated with biotin (500µM, 30min, n=4). Streptavidin pull-down of biotinylated proteins was performed; illustration shows streptavidin coated magnetic beads (yellow) bound to biotin (green) and biotinylated proteins. Biotinylated proteins were analysed by mass spectrometry. **(B)** Principal component analysis of LFQ intensities. A single square denotes an independent experiment, experimental groups (Alfa-TID or TID) are grouped by colour. **(C)** Volcano plot of proteins enriched in Alfa-TID (blue) compared to TID following two-sample t-test of LFQ intensity values (significance determined as s0=2; FDR=0.05).

Table 5.1. Pro-IL-1α-TurboID significantly enriched proteins. 56 proteins significantly enriched via pro-IL-1α-TurboID-mediated biotinylation. Significance calculated using Perseus computational platform statistical analysis (s0=2 and FDR=0.01). Table shows gene name, protein name, log2 fold change (FC) and -log10 (p-value).

Gene name	Protein name	Log2 FC	-Log10 p-value
IL1A	Interleukin-1 alpha	11.16	5.67
EP300	Histone acetyltransferase p300	2.72	4.54
YEATS2	YEATS domain-containing protein 2	2.60	4.41
CRTC2	CREB-regulated transcription coactivator 2	2.92	4.30
DMAP1	DNA methyltransferase 1-associated protein 1	2.03	4.30
ZFHX3	Zinc finger homeobox protein 3	2.12	4.18
ARID2	AT-rich interactive domain-containing protein 2	1.72	3.69
KMT2D	Histone-lysine N-methyltransferase 2D	2.26	3.61
ZZZ3	ZZ-type zinc finger-containing protein 3	4.32	3.56
SMTN	Smoothelin	1.96	3.48
QSER1	Glutamine and serine-rich protein 1	1.89	3.43
TRPS1	Zinc finger transcription factor Trps1	2.71	3.31
MYBL2	Myb-related protein B	2.39	3.24
JMJD1C	Probable JmjC domain-containing histone demethylation protein 2C	2.32	3.22
NCOA3	Nuclear receptor coactivator 3	2.71	3.18
MAML1	Mastermind-like protein 1	2.51	3.04
CIC	Protein capicua homolog	1.99	3.00
SUPT20H	Transcription factor SPT20 homolog	2.17	2.95
ARNT	Aryl hydrocarbon receptor nuclear translocator	2.43	2.94
KMT2C	Histone-lysine N-methyltransferase 2C	5.03	2.88
BCORL1	BCL-6 corepressor-like protein 1	1.77	2.79
SMARCE1	SWI/SNF-related matrix-associated actin-dependent regulator of chromatin subfamily E member 1	2.80	2.68

ATN1	Atrophin-1	1.60	2.63
KDM3A	Lysine-specific demethylase 3A	1.81	2.59
BCL9L	B-cell CLL/lymphoma 9-like protein	1.86	2.58
HIVEP1	Zinc finger protein 40	2.27	2.53
ARID1A	AT-rich interactive domain-containing protein 1A	1.73	2.52
NCOA5	Nuclear receptor coactivator 5	2.18	2.48
EP400	E1A-binding protein p400	1.63	2.40
C15orf39	Uncharacterized protein C15orf39	2.07	2.38
ASXL2	Putative Polycomb group protein ASXL2	1.97	2.32
EPC1	Enhancer of polycomb homolog 1	2.13	2.28
BCL9	B-cell CLL/lymphoma 9 protein	2.32	2.27
ELMSAN1	ELM2 and SANT domain-containing protein 1	1.97	2.12
UBR2	E3 ubiquitin-protein ligase UBR2	1.66	2.11
MAD1L1	Mitotic spindle assembly checkpoint protein MAD1	1.91	2.08
POLDIP3	Polymerase delta-interacting protein 3	2.28	2.08
IRF2BP1	Interferon regulatory factor 2-binding protein 1	2.03	2.05
CFAP20	Cilia- and flagella-associated protein 20	1.98	2.03
SAP130	Histone deacetylase complex subunit SAP130	2.88	1.97
SETD1B	Histone-lysine N-methyltransferase SETD1B	4.55	1.96
JUND	Transcription factor jun-D	3.37	1.87
SRSF2	Serine/arginine-rich splicing factor 2	1.84	1.82
KIAA0907	UPF0469 protein KIAA0907	1.80	1.81
GSE1	Genetic suppressor element 1	2.36	1.75
NCOA2	Nuclear receptor coactivator 2	2.27	1.67
FOXK2	Forkhead box protein K2	2.08	1.67
ARL6IP1	ADP-ribosylation factor-like protein 6-interacting protein 1	1.98	1.62
IRF2BP2	Interferon regulatory factor 2-binding protein 2	2.73	1.61
RAB10	Ras-related protein Rab-10	3.53	1.58

PSMB4	Proteasome subunit beta type-4	1.89	1.58
PCYT1A	Choline-phosphate cytidylyltransferase A	1.90	1.54
RNF40	E3 ubiquitin-protein ligase BRE1B	2.11	1.53
GTF2A1	Transcription initiation factor IIA subunit 1	2.64	1.49
NCBP2	Nuclear cap-binding protein subunit 2	2.25	1.42
MGA	MAX gene-associated protein	2.06	1.41

5.2.3 Functional analysis

5.2.3.1 Subcellular Location

The Ingenuity pathway analysis (IPA) bioinformatics resource (QIAGEN; (Kramer et al., 2014)) was used to understand the 56 significantly enriched proteins in the context of biological systems obtained from a manually curated database of the literature. These proteins will be referred to throughout this text as the pro-IL-1α interactome. IPA was used to investigate the subcellular location of each protein within the pro-IL-1α interactome. Of the 56 proteins, 42 (75%) were nuclear, 9 (16.1%) cytoplasmic, 4 (7.1%) in the extracellular space and 1 protein (1.8%) classed as "other" by IPA (Figure 5.3). It is important to note that IPA initially categorised IL1A as an extracellular protein due to its well characterised role as a secreted cytokine. However, as the intracellular role of IL1A in its precursor form (pro-IL-1α) is of interest in this study, and not the secreted mature form (IL-1α), it was left uncategorised. Using the IPA knowledgebase, proteins were grouped by protein family, allowing a greater insight into their role within each subcellular location. Here, 31 proteins were classed as transcription regulators, accounting for 55% of all significant proteins and 72% of nuclear proteins, with GTF2A1 as the only non-nuclear protein to be classed as a transcription factor.

6 proteins (11%) were categorised as enzymes, 1 (1.8%) as a peptidase and the 17 (30.4%) proteins left ungrouped by protein family were categorised as “other” by IPA.

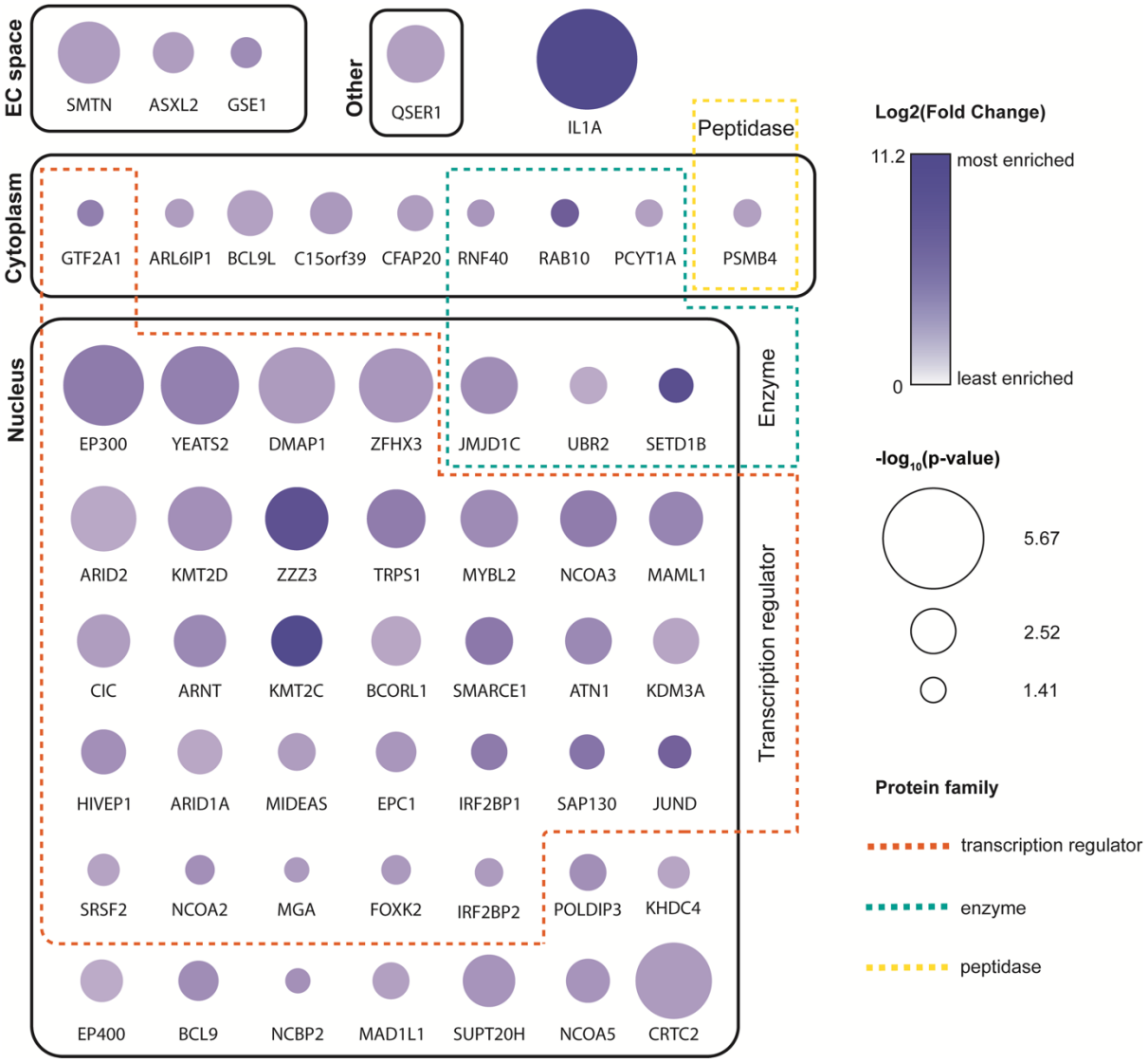

Figure 5.3. Subcellular location and protein family groups of pro-IL-1α-TurboID interactome. Proteins are clustered by subcellular location and protein family as described by IPA. Those proteins with no assigned protein family group were categorised as "other" by IPA. Gene symbol name is used to annotate each protein. Proteins are coloured by fold change in enrichment, displayed as Log2 (Fold Change), and sized by p-value, displayed as $-\log_{10}$ (p-value), determined by two-sample t-test of LFQ intensity values (significance determined as s0=2; FDR=0.05). Fold change and p-value are calculated following comparison with TID control. Subcellular locations are determined by IPA and grouped by solid boxes (EC space: extracellular space). Protein families are grouped by dashed lines; transcription regulator (orange); enzyme (green); peptidase (yellow).

5.2.3.2 Canonical Pathways

To investigate the functionality of the pro-IL-1α interactome, their representation within canonical pathways present on the IPA knowledgebase was analysed. Here, each pathway is assigned a p-value of overlap, which describes whether there is a significant overlap between proteins from the pro-IL-1α interactome and all proteins in that pathway; $p<0.01$ was used as a significance threshold for the pathways shown here (Figure 5.4). IPA also provides a predicted activation (orange) or inhibition (blue) of a pathway based on the expression levels of overlapping proteins within that pathway. If there is not sufficient information within the IPA knowledgebase to make an accurate prediction of the activity of a given pathway, IPA displays this as "no activity pattern available" (grey). 12 canonical pathways were identified with a p-value of overlap <0.01 (Figure 5.4). Of these pathways, four were predicted to be activated: "Aryl hydrocarbon receptor signalling", "Xenobiotic metabolism AHR signalling", "Ribonucleotide reductase signalling" and "Senescence pathway". From our 12 canonical pathways, only four were already reported to contain IL1A (Table 5.2), these were "Aryl hydrocarbon receptor signalling", "Xenobiotic metabolism AHR signalling", "Glucocorticoid receptor signalling" and "Senescence pathway". Currently, there is no literature supporting the role of IL1A within the eight other pathways identified here. Therefore, novel pathways important in IL1A signalling may have been revealed here. However, it is important to note that IPA categorises IL1A as a secreted cytokine and therefore this must be factored into the interpretation of the role of pro-IL-1α in these pathways.

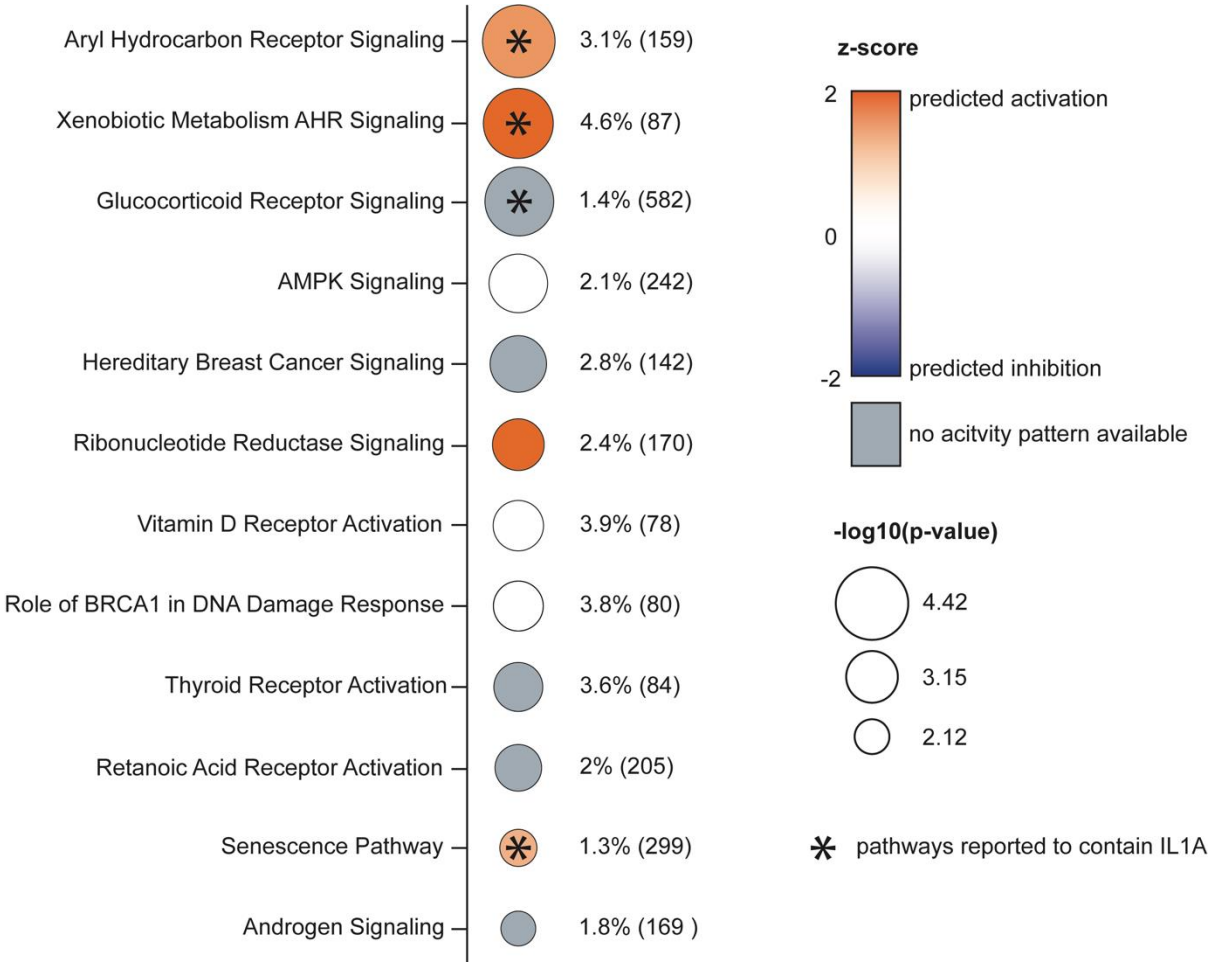

Figure 5.4. Canonical pathways associated with the pro-IL-1α interactome. Significant canonical pathways obtained from IPA are displayed with circle annotations to describe z-score and p-value. Pathways are coloured by z-score which denotes the predicted activation (orange), inhibition (blue) or no change in activation state (white) of that given pathway based on the presence of pro-IL-1α interactome proteins within that pathway. Grey indicates no activity pattern available due to the lack of information available to make a prediction. Pathways are sized by -$\log_{10}$ (p-value). Number of pro-IL-1α interactome proteins within each pathway is displayed as a percentage, followed by total number of proteins within that pathway in parentheses. Pathways displayed have a p-value<0.01. Pathways that were reported to contain IL1A are indicated by an asterisk.

Table 5.2. Proteins associated with significant canonical pathways. Proteins associated with each significant ($p<0.01$) canonical pathway are shown. Pro-IL-1α interactome proteins are represented by gene symbol.

Canonical Pathway	**Pro-IL-1α interactome proteins**
Aryl Hydrocarbon Receptor Signalling	ARNT, EP300, IL1A, NCOA2, NCOA3
Xenobiotic Metabolism AHR Signalling Pathway	ARNT, EP300, IL1A, NCOA2
Glucocorticoid Receptor Signalling	ARID1A, ARID2, EP300, GTF2A1, IL1A, NCOA2, NCOA3, SMARCE1
AMPK Signalling	ARID1A, ARID2, CRTC2, EP300, SMARCE1
Hereditary Breast Cancer Signalling	ARID1A, ARID2, EP300, SMARCE1
Ribonucleotide Reductase Signalling Pathway	ARID1A, ARID2, MYBL2, SMARCE1
Vitamin D Receptor Activation	EP300, NCOA2, NCOA3
Role of BRCA1 in DNA Damage Response	ARID1A, ARID2, SMARCE1
Thyroid Receptor Activation	EP300, NCOA2, NCOA3
Retinoic Acid Receptor Activation	ARID1A, ARID2, EP300, SMARCE1
Senescence Pathway	ASXL2, EP300, EP400, IL1A
Androgen Signalling	EP300, GTF2A1, NCOA2

5.2.3.3 Downstream Effects

Biological Function

IPA was used to investigate the predicted downstream effects of the proteins identified in the pro-IL-1α interactome. To achieve this, "biological functions" and "diseases and disorders" that had a significant p-value of overlap between the pro-IL-1α interactome and the proteins involved in these downstream processes were analysed. Biological functions and diseases and disorders can be described by terms that fit into three hierarchal levels: level 1 – high-level functional category (e.g., post-translational modification), level 2 – mid-level functional category (e.g., acetylation) and level 3 – specific functions that are significantly represented in the data (e.g., acetylation of histone h2a). Note, level 2 and 3 terms can belong to multiple level 1 terms.

The ten most significant biological functions (level 1) predicted to be associated with the pro-IL-1α interactome and the number of proteins associated with each function are: gene expression (38), cellular compromise (3), post-translational modification (4), cell signalling (3), cell growth (32), cell death and survival (30), carbohydrate metabolism (10), cellular development (32), cell cycle (24) and cell morphology (16) (Figure 5.5A). Gene expression is the most significant function (mean p-value= 1.58E-12); this indicates that, based on the literature, the association between the pro-IL-1α interactome and proteins involved in gene expression is greater than would be expected by random association. In line with this result, the five pathways (level 3) with the most significant p-values (Figure 5.5B) all belong to the gene expression biological function (level 1). Post-translational modification is the third most significant biological function identified here (mean p-value=5E-05). The post-translational

modification pathways involved in this enrichment are “acetylation of proteins” (p=2.2E-06), “acetylation of histone h2a” (p=1.19E-05) and “acetylation of L-lysine” (p=4.74E-03).

Analysis of the pro-IL-1α interactome with respect to biological function allowed investigation into which functions are predicted to be activated or inhibited. The top five pathways are highlighted here (level 2&3) with z-scores for predicted activation (z>0) (Figure 5.5C) and predicted inhibition (z<0) (Figure 5.5D). The pathways that are predicted to be activated are: transactivation (z-score=3), transactivation of RNA (z-score=2.9), binding of DNA (z-score=2.93), cell survival (z-score=2.83) and call viability (z-score=2.64). The pathways predicted to be inhibited are apoptosis (z-score=-2.1), cell proliferation of squamous cell carcinoma cell lines (z-score=-1.1), apoptosis of connective tissue cells (z-score=-0.73), necrosis (z-score=-0.9) and cell death of connective tissue cells (z-score=-0.56). Note that, although the pathways here are trending towards inhibition, a z-score<2 or >2 can only be deemed as significantly predicted to be activated or inhibited.

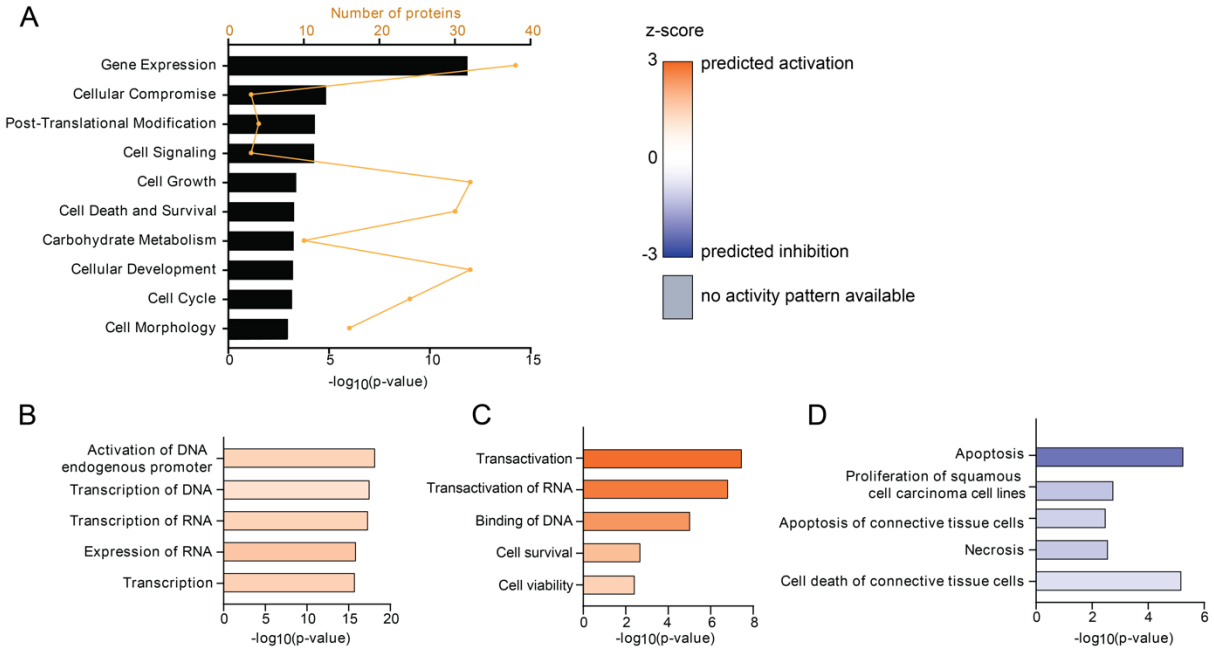

Figure 5.5. Biological Functions associated with the pro-IL-1α interactome. (A) The ten most significant biological functions (obtained by IPA) associated with the 56 proteins of the pro-IL-1α interactome. Bars (Groelly et al.) show mean p-value for all pathways within the biological function described, functions are ordered by p-value. Line (yellow) shows number of proteins from the 56 protein pro-IL-1α interactome included within each biological function. Level 3 biological functions **(B)** top 5 p-values (ranked by p-value), **(C)** top 5 z-scores (ranked by z-score highest to lowest) and **(D)** bottom 5 z-scores (ranked by z-score lowest to highest).

Diseases and Disorders

Next, analysis was carried out on the downstream effects of the pro-IL-1α interactome, looking at pathways associated diseases and disorders. As with biological functions, diseases and disorders are categorised into three hierarchical levels. The ten most significant diseases and disorders (level 1) predicted to be associated with our pro-IL-1α interactome and the number of proteins associated with each function are: haematological disease (37), immunological disease (35), renal and urological disease (26), cancer (55), organismal injury and abnormalities (55), gastrointestinal disease (55), neurological disease (42), developmental disorder (21), hereditary disorder (21), and skeletal and muscular disorders (24) (Figure 5.6A). Haematological disease was our most significant disease and disorder pathway (mean p-value= 7.94E-06). Cancer, organismal injury and abnormalities, and gastrointestinal disease were associated with 55 of the 56 proteins from the pro-IL-1α interactome (Figure 5.6A). Looking at more specific disease and disorder pathways (level 2&3), the four of our most significant pathways (Figure 5.6B) show an overlap between cancer and haematological disease.

Diseases and disorders predicted to be activated or inhibited based on the enrichment of our pro-IL-1α interactome were investigated. The top 5 pathways (level 2&3) are highlighted with z-scores for predicted activation (z>0) (Figure 5.6C) and predicted inhibition (z<0) (Figure 5.6D). The pathways that are predicted to be activated are: infection by HIV-1 (z-score=2.4), infection of cells (z-score=2.4), infection of cervical cancer cell lines (z-score=1.7), growth of tumour (z-score=1.2) and metastasis of tumour cell lines (z-score=0.56). The pathways predicted to be inhibited are liver lesion (z-score=-2.77), extra-pancreatic malignant tumour

(z-score=-2.1), abdominal carcinoma (z-score=-1.95), hepatobiliary carcinoma (z-score=-1.95) and liver tumour (z-score=-1.95).

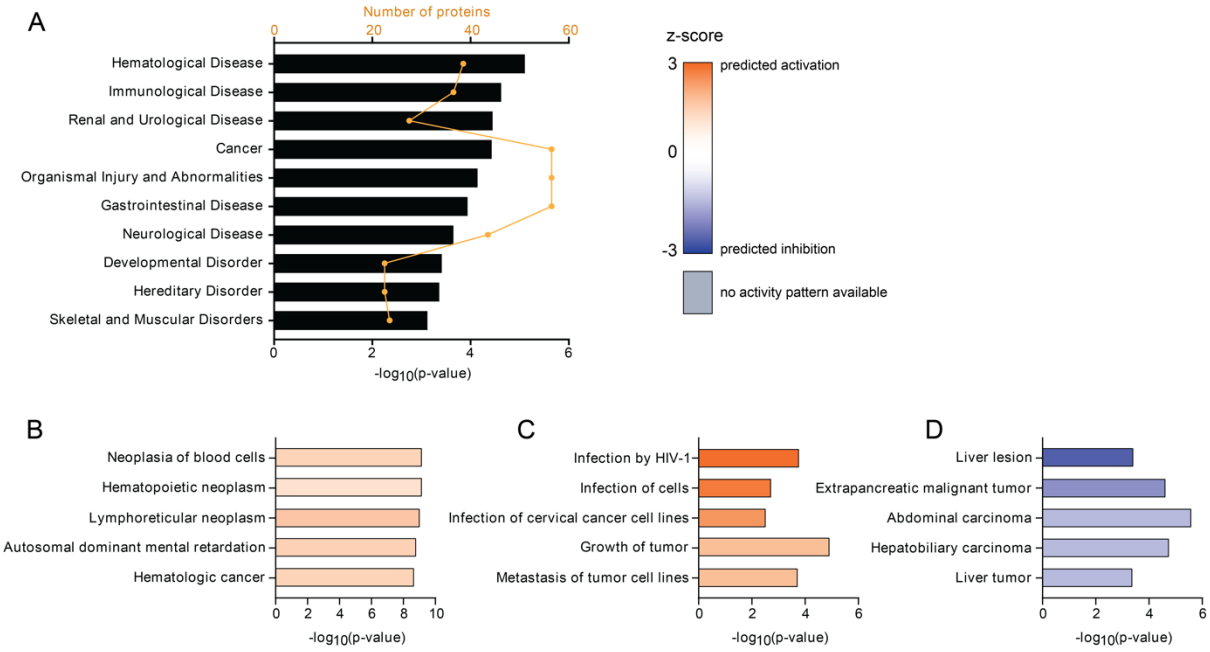

Figure 5.6. Diseases and disorders associated with the pro-IL-1α interactome. (A) The ten most significant diseases and disorders (obtained by IPA) associated with the 56 proteins of the pro-IL-1α interactome. Bars (Groelly et al.) show mean p-value for all pathways within the disease or disorder described, diseases and disorders are ordered by p-value. Line (yellow) shows number of proteins from the 56 protein pro-IL-1α interactome included within each disease or disorder group. Level 3 diseases and disorders **(B)** top 5 p-values (ranked by p-value), **(C)** top 5 z-scores (ranked by z-score highest to lowest) and **(D)** bottom 5 z-scores (ranked by z-score lowest to highest).

5.2.4 STRING analysis

In addition to carrying out assessment of the pro-IL-1α interactome by IPA, STRING was used to further investigate interactor of pro-IL-1α. Based on a database of the current literature, STRING (https://string-db.org/) analysis determined known interacting partners within the pro-IL-1α interactome and used Gene Ontology (GO) terms to identify functions of the pro-IL-1α interactome proteins. This analysis identified many members of the pro-IL-1α interactome as HAT proteins (Figure 5.7). The interaction between pro-IL-1α and the HAT protein, EP300 was previously identified (Buryskova et al., 2004, Luheshi et al., 2009a). Other HAT proteins identified here that have not previously been recorded to interact with pro-IL-1α are CRT2C, NCOA2, NCOA3, ZZZ3, SUPT20H, EPC1, DMAP1, YEATS2 and EP400 (Figure 5.7). These data highlight an association with pro-IL-1α and HAT proteins and is therefore a strong indication of an intracellular role of pro-IL-1α.

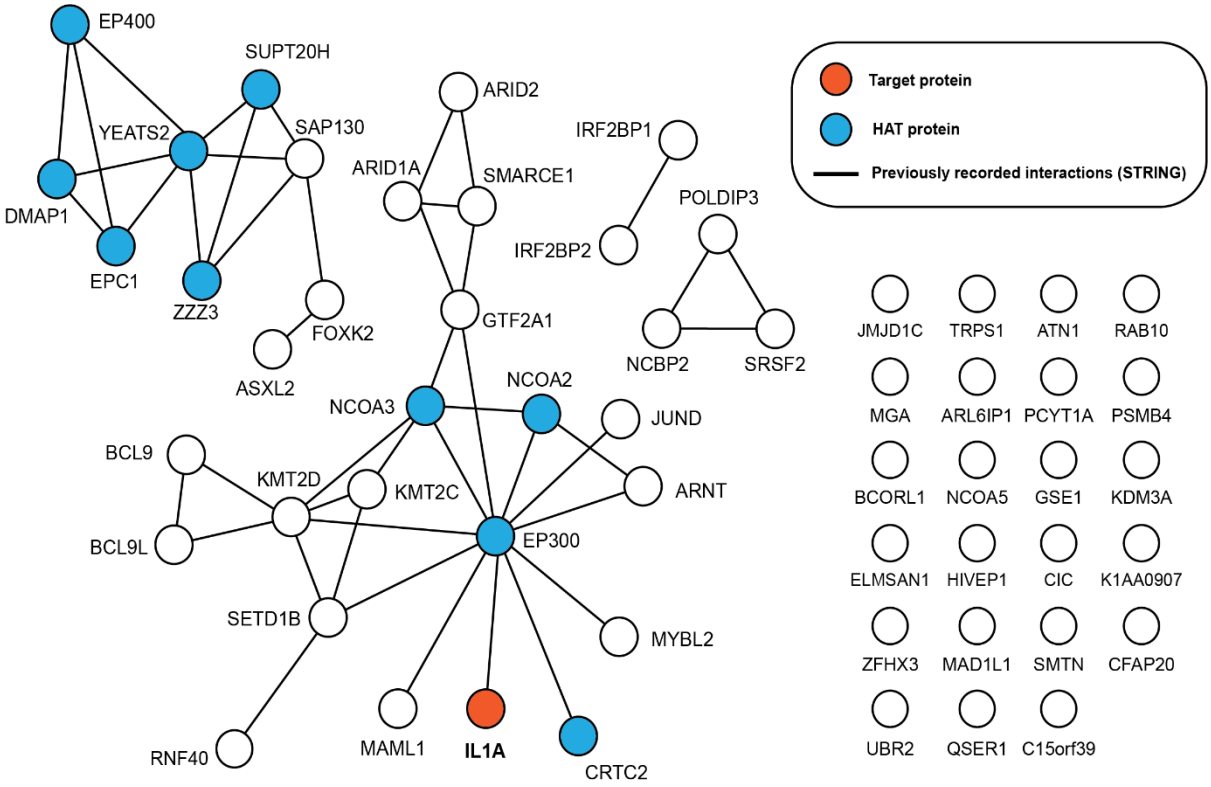

Figure 5.7. STRING analysis of pro-IL-1α-TurboID biotinylated proteins highlighting prominent proximity to HAT proteins. STRING network analysis (generated via https://string-db.org/) of proteins significantly enriched in pro-IL-1α-TurboID. Lines represent previously recorded physical interactions identified by STRING, unconnected proteins have no previously recorded interactions with significantly enriched proteins. Histone acetyltransferase (Chen et al.) proteins were identified through gene ontology (GO) analysis. Proteins are displayed using gene symbol label. Gene symbol for the target protein (IL1A; pro-IL-1α) represents the target protein of this experiment.

5.3 Discussion

IL-1α is a pro-inflammatory cytokine and is implicated in the inflammation that contributes to many conditions including respiratory, cardiovascular, and neurological disease (Cavalli et al., 2021). Interestingly, the pro-domain of IL-1α contains a nuclear localisation sequence (NLS) (Wessendorf et al., 1993). Therefore, pro-IL-1α may have additional functions that relate to its nuclear subcellular localisation. In this study, an interactome for pro-IL-1α is defined and bioinformatic analysis is used to place these proteins within the context of biological systems. Therefore, this study builds on current understanding, and provides further insight into the potential intracellular role of pro-IL-1α.

To identify protein interactors of pro-IL-1α, a method of enzyme-catalysed proximity labelling called TurboID was used (Cho et al., 2020). Pro-IL-1α-TurboID was characterised *in vitro,* and its expression and processing were investigated with respect to wild-type unlabelled pro-IL-1α. The expression of TurboID alone was also characterised, as this was used as a control for non-specific protein biotinylation. Transient transfection in HeLa cells revealed that both pro-IL-1α and pro-IL-1α-TurboID were largely nuclear, and that TurboID was cytoplasmic (Figure 5.1B). The location of biotinylated proteins in pro-IL-1α-TurboID and TurboID transfected cells matched the location of their respective proteins as observed by IL-1α and/or TurboID labelling (Figure 5.1B). Therefore, it was convincing that the potential interactome of pro-IL-1α-TurboID would effectively mirror that what would be expected of wild-type pro-IL-1α. Pro-IL-1α-TurboID was also effectively processed to IL-1α-TurboID following ionomycin treatment, albeit to a lesser degree than the wild-type (Figure 5.1E). This indicates that the TurboID tag does not substantially interfere with the cleavage or processing kinetics of pro-IL-1α-TurboID. This model, therefore, could be used to investigate the pro-IL-1α interactome

in response to a processing stimulus in future experiments. As mentioned, TurboID alone was used as a biotinylation control. However, a limitation of this study is the comparative localisation of TurboID and pro-IL-1α-TurboID. TurboID is predominantly cytoplasmic and pro-IL-1α-TurboID predominantly nuclear. Were this study to be repeated, a version of TurboID with a nuclear localisation sequence may provide a more effective control for comparison with pro-IL-1α-TurboID.

Mass spectrometry analysis of biotinylated proteins revealed a 56 protein interactome for pro-IL-1α (Figure 5.2; Table 5.1). Ingenuity pathway analysis (IPA) and gene ontology (GO) allowed investigation into the subcellular location of these proteins and their known interactions according to current literature (Kramer et al., 2014, Thomas et al., 2022). The pro-IL-1α interactome is predominantly nuclear with 46 of the 56 proteins located in the nucleus (Figure 5.3). This conclusion comes as no surprise given the presence of the pro-IL-1α NLS and well characterised nuclear localisation by immunocytochemistry (Wessendorf et al., 1993)(Figure 5.1B). What remains to be revealed is the functional relevance of the nuclear pro-IL-1α interactome. It has often been suggested that pro-IL-1α is sequestered into the nucleus as a mechanism to dampen sterile inflammation and protect against release (Luheshi et al., 2009a). Therefore, the proteins that pro-IL-1α interacts with in the nucleus may be integral in facilitating this mechanism. Interestingly, previous work by our group shows that IL-1α is immobilised to nuclear specks containing EP300, a member of our pro-IL-1α interactome (Luheshi et al., 2009a). In this study, pro-IL-1α is retained in the nucleus following necrosis, limiting its release (Luheshi et al., 2009a). Downstream analysis predicted an inhibition of necrosis, based on the enrichment of the pro-IL-1α interactome. These data highlight an association between the pro-IL-1α interactome and cell death mechanisms,

revealing a potential new avenue for study with regards to IL-1α nuclear localisation and cell death.

Interestingly, EP300 is the only protein here that has previously been shown to interact with IL1α physically and functionally (Luheshi et al., 2009a, Buryskova et al., 2004). Buryskova et al. (2004), were the first to show that the pro-domain of IL-1α interacts with EP300 and increase transcriptional expression as a result. IPA identified multiple nuclear receptor signalling pathways that are associated with the pro-IL-1α interactome including the aryl hydrocarbon receptor, glucocorticoid receptor, vitamin D receptor, thyroid receptor and retinoic acid receptor signalling pathways. In the nucleus, these receptors form complexes and bind to DNA response elements, acting as transcriptional regulators as a result. Proteins within the interactome that are associated with nuclear receptor signalling all play an integral role in chromatin remodelling (Trotter and Archer, 2007). This further validates the role of pro-IL-1α and its interactome as key players in transcriptional regulation (Werman et al., 2004, Buryskova et al., 2004).

Nine HAT proteins, including EP300 which is already suggested to interact with IL-1α, were identified as part of the pro-IL-1α interactome (Table 5.1; Figure 5.8)(Luheshi et al., 2009a). Alignment of the mammalian pro-IL-1α sequence has shown that HAT binding domains within the IL-1α pro-domain are highly conserved and show overlap with the NLS (Rivers-Auty et al., 2018). This may suggest the involvement of HATs in the nuclear function of pro-IL-1α. Acetylation of pro-IL-1α itself has been shown to be important for its nuclear localisation (Cohen et al., 2015). However, further investigation is required to determine whether pro-IL-1α can also act to facilitate the acetylation of histones and other proteins in the nucleus via

its HAT binding capacity. Post-translational modifications play an integral role in signalling cellular stress, specifically DNA damage (Huen and Chen, 2008). Exposing keratinocytes to UV radiation triggers IL-1α release, and in the presence of HDAC inhibitors which prevents IL-1α deacetylation, IL-1α secretion is dampened (Cohen et al., 2015). Therefore, pro-IL-1α acetylation may represent a mechanism to signal genotoxic stress and limit inflammation to neighbouring cells. Unresolved DNA damage is a critical factor in the pathogenesis of cancer (Groelly et al., 2023). The downstream analysis of the interactome predict cancer pathways as upregulated. Genotoxic stress has been shown to trigger EP300-mediated acetylation of the tumour suppressor protein p53, and p53 has also been shown to associate with IL-1α itself following DNA damage (Ito et al., 2001, Novak et al., 2020). Keratinocytes are amongst the only cells characterised to express basal levels of pro-IL-1α and are often subject to pathological DNA damage by UV radiation and wound formation (Groß et al., 2012). Therefore, exploring the nuclear pro-IL-1α interactome in this cell model, may advance understanding in the treatment of skin cancer and wound healing.

Senescence is a protective mechanism that causes cell cycle arrest in response to oncogene activation, DNA damage or oxidative stress (Munoz-Espin and Serrano, 2014). In aged tissue or disease state, senescent cells are not effectively cleared, thereby resulting in a chronic inflammatory microenvironment (Grivennikov et al., 2010). Senescent cells develop an altered secretory state known as senescence-associated secretory phenotype (SASP), releasing chemokines, proteases, and pro-inflammatory cytokines, including IL-1α. The senescence pathway was predicted to be upregulated based on the enrichment of the pro-IL-1α interactome (Figure 5.4). Secretion of IL-1α following its processing by caspase-5/11 has been shown to be essential for SASP (Wiggins et al., 2019). Therefore, the high levels of

enrichment of IL-1α may drive this prediction. However, nuclear proteins within our interactome, EP300, EP400 and ASXL2, are also associated with this pathway and may play a role in the regulation of senescence (Munoz-Espin and Serrano, 2014). As discussed previously, acetylation of the tumour suppressor protein p53, is achieved through interaction with EP300. P53 is an essential component in regulating senescence (Mijit et al., 2020). Interestingly, EP300-mediated acetylation of p53 has been shown to drive a pro-senescent response whereas phosphorylation of p53 is associated with pro-apoptotic signalling (Donninger et al., 2015). Apoptosis was predicted to be inhibited downstream of the pathways associated with the pro-IL-1α interactome, indicating that a senescent phenotype associated with acetylation may be favoured here.

Nuclear enrichment of pro-IL-1α is enhanced by an NLS within its pro-domain (Wessendorf et al., 1993, Tapia et al., 2019). Our lab previously reported that whilst the NLS within the pro-domain of pro-IL-1α is conserved amongst many mammalian sequences, it is lost in the toothed whale clade (Rivers-Auty et al., 2018). Unpublished work shows that mutating the mouse NLS to mimic that of the toothed whale results in a cytoplasmic localisation of pro-IL-1α. This therefore validates that the toothed whale pro-IL-1α does not possess a functional NLS. As discussed previously, pro-IL-1α may be sequestered into the nucleus to limit innate immune signalling. Infection by HIV-1 and infection of cells are the top diseases and disorders predicted to be upregulated downstream of the pro-IL-1α interactome. Therefore, proteins associated with nuclear pro-IL-1α may serve to regulate these pathways and initiate an anti-viral response. Toothed whales are reported to have lost Mx1 and Mx2 anti-viral proteins (Braun et al., 2015). Therefore, localisation of pro-IL-1α to the cytoplasm in these animals may have provided a selective advantage and allow an IL-1α-mediated immune response to

compensate for the loss of anti-viral Mx proteins. Further studies utilising the NLS mutant mouse model in response to viral infection will allow a greater understanding of the mechanisms at play here.

Investigation into the pro-IL-1α interactome has both improved understanding of the intracellular role of pro-IL-1α and identified numerous interacting proteins to direct further study. Future experiments will look to validate novel interactors of pro-IL-1α *in vitro* and explore their functional role with respect to associated pathways and downstream mechanisms identified by IPA. Gaining greater insight into the role of human pro-IL-1α may also elucidate its function in mammals that lack a functional NLS.

Chapter 6:

General discussion

Chapter 6. General Discussion

6.1 Summary

NLRP3 inflammasome activation and subsequent inflammation is an essential line of defence to protect against infectious organisms or other potential threats to the host. However, NLRP3 inflammasome activation can contribute to the chronic inflammation that underlies a vast array of non-communicable diseases (Mangan et al., 2018). The NLRP3 inflammasome regulates the activation of IL-1β and indirectly regulates IL-1α processing and release (Groß et al., 2012, Tapia et al., 2019). The pro-inflammatory cytokines, IL-1α and IL-1β, are key players in driving harmful inflammation (Dinarello, 2018). NLRP3 inflammasome activation, therefore, must be tightly regulated to avoid disease, and subcellular localisation of NLRP3 may prove important in its regulation (Mangan et al., 2018, Seoane et al., 2020). In addition to its role as a secreted cytokine, the IL-1α precursor may have an additional intracellular role in the nucleus (Rivers-Auty et al., 2018). A key take-home of this thesis is that investigating the subcellular location of inflammatory proteins, such as NLRP3 and pro-IL-1α, provides important insight into their function and regulation. Gaining a greater understanding of the fundamental biology of inflammasome activation and its regulated cytokines will form the building blocks for development of more effective treatments for non-communicable disease.

A major aim of this thesis was to advance our understanding of the cell biology of NLRP3 inflammasome activation and utilise a method of proximity labelling to investigate the NLRP3 protein interactome with respect to membrane trafficking organelles. Moreover, I also aimed to investigate the interactome of the precursor cytokine pro-IL-1α, whilst exploring its

localisation to the nucleus as a potentially novel intracellular role. Specifically, this thesis aimed to:

1. Investigate how endocytic traffic contributes to NLRP3-inflammasome activation, specifically focusing on the impact of NLRP3-activating stimuli on endosomal cargo trafficking and the subcellular location of NLRP3 with the phosphatidylinositol PI4P, in the context of endocytic trafficking organelles.

2. Identify novel interactors of NLRP3 using TurboID proximity labelling. Using a bioinformatics approach, identify interactors of NLRP3 and use a genetic approach to investigate the role of cargo trafficking proteins in the canonical activation of the NLRP3 inflammasome.

3. Investigate the nuclear role of pro-IL-1α by characterising its protein interactome using TurboID proximity labelling. Using a bioinformatics approach, investigate the subcellular and functional profile of the pro-IL-1α interactome and discuss the rationale for an intracellular role of the precursor protein.

6.2 General Discussion

6.2.1 The common cellular event in NLRP3 inflammasome activation

It is widely discussed that the NLRP3 inflammasome is unique among inflammasomes in its ability to respond to a plethora of diverse activating stimuli, including ionophores, lysosomal destabilising agents and sterile particulates; examples include nigericin, Leu-LeuOMe and

silica, respectively (Perregaux and Gabel, 1994, Mariathasan et al., 2006, Hornung et al., 2008). As the structure and mechanisms of action of NLRP3-activating stimuli differ so much between each other, it is unlikely that the NLRP3 receptor can sense them directly. Therefore, it is suggested that NLRP3-activating stimuli converge on a common cellular event that is subsequently detected by NLRP3 to trigger assembly and activation of the inflammasome. This principle forms the basis for one of the great unanswered questions in NLRP3 inflammasome research: what is the common cellular event that triggers activation of the NLRP3 inflammasome?

A wealth of research has been carried out in pursuit of a unifying hypothesis for the activation of the NLRP3 inflammasome. A seminal paper by Munoz-Planillo et al. (2013), suggests that potassium efflux, and a subsequent decrease in cytosolic potassium, is the common step necessary for NLRP3 inflammasome activation (Munoz-Planillo et al., 2013). However, the identification of a potassium-efflux independent mechanism of NLRP3 inflammasome activation, through the action of small molecules imiquimod and CL097, suggests that the shared mode of action of NLRP3-activating stimuli may not solely converge on potassium efflux (Groß et al., 2016). In addition to its response to ion flux, research suggests that subcellular localisation of NLRP3 is an important factor in its activation (Hamilton and Anand, 2019). This is illustrated by the spatial redistribution of ASC following NLRP3 inflammasome activation, where ASC specks form at the perinuclear region, and that perinuclear localisation of ASC is essential for inflammasome function (Bryan et al., 2009). In addition, numerous studies have described the interaction of NLRP3 with subcellular organelles and that organelle dysfunction is associated with NLRP3 inflammasome activation (Seoane et al., 2020). How NLRP3 can sense organelle dysfunction is yet to be defined. It is possible that NLRP3-activating

stimuli bring about stress to a range of organelles and that overall organelle dysfunction and therefore cellular stress may be the trigger for NLRP3 inflammasome activation. Equally, it is possible that stress brought about by NLRP3-activating stimuli may converge on the activation of NLRP3 at a single organelle (Akbal et al., 2022). A disassembly of the *trans*-Golgi network (TGN) and recruitment of NLRP3 to dispersed TGN (dTGN) via binding to the phosphatidylinositol-4-phosphate (PI4P) is suggested as a common cellular event in NLRP3 inflammasome activation (Chen and Chen, 2018). Here, dTGN is defined by the presence of the cycling TGN protein TGN46 (the human homolog of TGN38) on cytoplasmic puncta (Chen and Chen, 2018). Following re-examination of TGN46-positive vesicles, it is suggested that many NLRP3- and PI4P-containing vesicles are in fact endosomes and lysosomes, and that TGN46-positive vesicles also contain markers for early endosomes (EEA1, Rab5), late endosome (CD63) and lysosomes (LAMP1) (Lee et al., 2023, Zhang et al., 2023). TGN46 does not permanently reside at the TGN and cycles to the plasma membrane via endosomes before returning to the TGN (Ladinsky and Howell, 1992, Reaves et al., 1993). Therefore, the accumulation of TGN46 on endolysosomal compartments is suggested to be a by-product of a disruption in endocytic traffic (Chapman and Munro, 1994). This evidence forms the basis of the hypothesis that a disruption in endocytic traffic may be the common cellular event in NLRP3 inflammasome activation (Lee et al., 2023, Zhang et al., 2023).

The localisation of NLRP3 to PI4P-containing endosomes and lysosomes may be important in understanding the spatial regulation and activation of the NLRP3 inflammasome (Lee et al., 2023, Zhang et al., 2023). It is logical that NLRP3 must be localised near endolysosomal compartments to sense a disruption in endocytic traffic, however, the specific signal that allows NLRP3 to integrate endocytic traffic dysfunction requires further investigation. The

accumulation of PI4P on endolysosomal compartments may be a likely candidate (Lee et al., 2023, Zhang et al., 2023). Increased lipid presentation on organelles under cellular stress has been previously associated with inflammasome activation. (Elliott et al., 2018). Under homeostatic conditions, PI4P is largely localised to the Golgi and plasma membrane (Hammond et al., 2014). However, following treatment with NLRP3 inflammasome activating stimuli, PI4P accumulates at compartments positive for endolysosomal markers (Lee et al., 2023, Zhang et al., 2023). Phosphoinositides (PIs) cluster in distinct intracellular membranes due to the precise location of different PI-modifying enzymes throughout the cell, therefore the localisation of PIs in a healthy cell can serve as specific organelle markers (Kutateladze, 2010). The aberrant accumulation of PI4P on endosomes and lysosomes following treatment with NLRP3-activting stimuli may be an important signal of cellular stress that is sensed by NLRP3 (Lee et al., 2023, Zhang et al., 2023). This hypothesis is supported further due to the physical interaction that occurs between NLRP3 and PI4P through ionic bonding between the negatively charged PI4P and NLRP3 polybasic motif (Chen and Chen, 2018).

As endocytic traffic disruption is suggested to mediate NLRP3 inflammasome activation, the behaviour of key endosomal and lysosomal membrane markers have been characterised in response to NLRP3-activating stimuli (Chapter 3. Figures 3.7-3.9). Further work shows that NLRP3 interacts with TPD54 (Chapter 4. Table 4.1), a membrane trafficking protein which defines a new class of intracellular transport vesicle termed intracellular nanovesicles (INVs) (Larocque et al., 2020). Knock-down of the TPD54 gene, TPD52L2, disrupts endosome-plasma membrane recycling (Larocque et al., 2020), and potentiates canonical NLRP3 inflammasome activation (Chapter 4. Figure 4.5), further supporting the hypothesis that a disruption in endocytic traffic mediates NLRP3 inflammasome activation. Therefore, TPD54-positive INVs

reveal an attractive new candidate to investigate the localisation of NLRP3 and endosomal trafficking dysfunction in the context of NLRP3 inflammasome activation. Interestingly, INVs have also been suggested to associate with the PI4P converting enzyme phosphatidylinositol 4-kinase (PI4KB), therefore whether PI4P can present on INVs is a question for further study (Nakajima et al., 2019, Larocque and Royle, 2022).

The search for a unifying mechanism of NLRP3 inflammasome activation is not limited to canonical activation; an understanding of the mechanisms that are shared between canonical, noncanonical and alternative inflammasome activation is important in creating a more complete picture of how NLRP3 senses and reacts to wide-ranging stimuli. Organelle function and more specifically, endocytic traffic, are controlled by ion flux and ion concentrations both extracellularly and intracellularly. This is highlighted in my experiments investigating the disruption in endocytic traffic following stimulation with potassium-dependent (nigericin) or potassium-independent (imiquimod) NLRP3 activating stimuli, where a disruption in endocytic traffic is less so with imiquimod, in the absence of potassium efflux. Noncanonical NLRP3 inflammasome activation is potassium-dependent, and following activation of casaspe4/5/11, GSDMD is cleaved to allow potassium efflux and NLRP3 activation. This therefore suggests that an imbalance in ion homeostasis achieved here may also result in endocytic trafficking dysfunction, further suggesting a role for endosomes in NLRP3 activation. To investigate the mechanisms of endosome dysfunction in noncanonical inflammasome activation, activation of the noncanonical inflammasome in macrophages and subsequent staining for TGN38 to determine whether noncanonical inflammasome activation leads to a disruption in TGN38 trafficking and formation of TGN38-positive puncta is a logical first step. In contrast to canonical and noncanonical inflammasome activation, alternative

NLRP3 inflammasome activation occurs in the absence of potassium efflux and ASC speck formation. Similarly, the formation of TGN38-positive puncta following alternative inflammasome activation should be investigated here. As endocytic trafficking dysfunction can still occur in the absence of potassium efflux, as with imiquimod, this doesn't rule out a similar mechanism occurring in alternative inflammasome activation.

Endocytic trafficking dysfunction has emerged as a likely common mechanism that contributes to NLRP3 inflammasome activation. However, further characterisation of both the membrane trafficking pathway in response to NLRP3 inflammasome activating stimuli, and how NLRP3 senses a disruption in endocytic traffic is required to fully elucidate this mechanism. The search for a unifying hypothesis of NLRP3 inflammasome activation is not only important in developing our understanding of inflammasome biology but may reveal important targets for treatments against NLRP3-driven disease.

6.2.2 A novel intracellular role of pro-IL-1α

IL-1α is a pro-inflammatory cytokine that is indirectly regulated by the NLRP3 inflammasome, has been considered to act as a DAMP upon release from damaged cells, and is implicated in the inflammation that underlies many diseases including cancer, atherosclerosis and neurological disease (Groß et al., 2012, Martin, 2016, Cavalli et al., 2021). IL-1α also propagates an inflammatory phenotype during cellular senescence, where it promotes the senescence-associated secretory phenotype (SASP) (Wiggins et al., 2019). IL-1α originated as a gene duplication event of IL-1β around 320 million years ago, and despite sharing many structural and functional similarities with IL-1β, IL-1α was retained. Unlike IL-1β, IL-1α

possesses a highly conserved pro-domain, which is suggested to play a role in its functional divergence. Conserved regions within the pro-domain include a nuclear localisation sequence (NLS) and histone acetyltransferase (Chen et al.) binding domains; these conserved domains may point to an additional intracellular role of IL-1α. The role of IL-1α nuclear localisation is suggested as a mechanism to limit inflammation following cell death or signal genotoxic stress to the surrounding tissue (Luheshi et al., 2009a, Cohen et al., 2015), however, further investigation into the nuclear function of pro-IL-1α is required. Therefore, investigating the protein interactome of pro-IL-1α allowed further development in our understanding of the potential novel role of nuclear IL-1α.

Using TurboID, a method of enzyme-catalysed proximity labelling, I characterised the pro-IL-1α interactome in HeLa cells as a method to further develop our understanding of the potential novel role of nuclear IL-1α (Cho et al., 2020). Following a bioinformatics approach, I identified nine histone-modifying enzymes as part of the pro-IL-1α interactome, in addition to the HAT protein, EP300, which is previously reported to interact with pro-IL-1α in the nucleus (Buryskova et al., 2004, McCarthy et al., 2013, Luheshi et al., 2009a). Histone modification plays an important role in gene expression (Lawrence et al., 2016). In Chapter 5, gene expression and many nuclear receptor pathways involved in gene expression, were associated with the pro-IL-1α interactome. This suggests that pro-IL-1α may play an important role in regulating gene expression via its association with proteins involved in histone modification, further supporting its role as a dual functioning protein.

Previous, and unpublished work by our group reports that toothed whales, amongst other mammals, possess a non-functional NLS (Rivers-Auty et al., 2018). This suggests that in these

animals, a cytoplasmic localisation of pro-IL-1α may have conferred an evolutionary advantage. Toothed whales have also been reported to have lost the antiviral proteins, Mx1 and Mx2 (Braun et al., 2015). Nuclear localisation of IL-1α has been suggested as a mechanism to protect against sterile inflammation (Luheshi et al., 2009a). Therefore, in this context, the cytosolic localisation of pro-IL-1α may serve as a mechanism to mount a potentiated inflammatory response to compensate for the lack of antiviral proteins. This hypothesis, however, requires further investigation. Despite the lack of a functional NLS in some mammalian species, the nuclear localisation of pro-IL-1α should not be completely discounted in these animals. Passive diffusion of pro-IL-1α can still occur across the nuclear membrane, suggesting that pro-IL-1α may interact with nuclear proteins even in the presence of a non-functional NLS. In addition, acetylation of Lys82 within the mammalian NLS has been shown to increase nuclear localisation of pro-IL-1α (Cohen et al., 2015).

Importantly, in those species with a non-functional NLS, at least one pro-IL-1α HAT binding domain remained highly conserved, suggesting that HAT binding may be key selection pressure for the intracellular role of pro-IL-1α (Wellens et al., 2023 *pre-print*). A possible explanation for the conservation of HAT domains, despite the loss of a functional NLS, is that cytosolic pro-IL-1α may interact with cytosolic HATs in these species. Multiple non-histone substrates of HATs have been identified in both the nucleus and the cytosol, highlighting their wide-ranging role in regulating a plethora of proteins within the cell (Lee and Workman, 2007). In fact, pro-IL-1α itself has been shown to be acetylated, suggesting that HATs may not only bind to, but also acetylate pro-IL-1α to regulate its localisation and function (Cohen et al., 2015). In addition, EP300 has been reported to be present in the cytosol and has been reported to exhibit E3 and E4 ubiquitin ligase activity (Grossman et al., 2003). Interestingly,

this ligase activity is only functional when EP300 is in the cytosolic fraction of the cell (Shi et al., 2009). Pro-IL-1α itself is reported to be polyubiquitinated, however, whether this process is dependent upon interaction with EP300 requires further investigation. Moreover, I have shown here that pro-IL-1α interacts with two other E3 ubiquitin ligase proteins, indicating an additional avenue of investigation in the function of pro-IL-1α.

Although cytosolic interactions of HAT proteins may be important, humans and many other mammals possess the pro-IL-1α protein with a functional NLS. Here, I have shown that HAT proteins and other gene regulatory proteins such as transcription factors are highly enriched in the pro-IL-1α interactome. This suggests that understanding the nuclear interactors of pro-IL-1α and what consequences this has upon the cell, tissue and in the context of disease is an important next step in understanding IL-1α.

6.3 Limitations

6.3.1 Cell biology of NLRP3 activation

Following an *in vitro* approach to investigating the cell biology of NLRP3 activation, it is important to consider the limitations of this study. Firstly, this chapter primarily used non-immune cell lines, including HeLa and COS7, to investigate the impact of NLRP3-activating stimuli on endosomal traffic and NLRP3 localisation. As these cells do not physiologically express NLRP3, they can only be taken as a model for investigation. COS7 NLRP3-mVenus cells were generated to visualise the localisation of the NLRP3 protein prior to the formation of an inflammasome speck and do not express the adaptor protein ASC. A stimulation of 90 minutes was used in these experiments; however, ASC speck formation is reported to occur following

a 20-minute stimulation with NLRP3-activating stimuli in LPS-primed BMDMs (Lee et al., 2023). ASC has also been reported to localise to endosomes following nigericin stimulation, albeit in HeLa cells (Zhang et al., 2023). Therefore, localisation of NLRP3 during inflammasome activation is likely impacted by the presence of ASC or formation of an ASC speck, and NLRP3 may exhibit a different subcellular distribution in immune cells as a result. Experiments carried out using BMDMs or THP-1 monocytes may prove as a better mode of investigation to accurately assess how NLRP3-activating stimuli impact endocytic traffic and NLRP3 localisation.

The Pearson's correlation coefficient (PCC) was used extensively here to quantify subcellular co-localisation of organelle markers, NLRP3 and PI4P. However, the use of PCC across all experiments represents another potential limitation of this study. PCC assumes a normal distribution of variance for the measurements carried out in its analysis (Janse et al., 2021). However, I did not test for this assumption and so the PCC may not be the correct tool to use for co-localisation analysis in all cases. Spearman's rank correlation coefficient is a non-parametric method of co-localisation analysis and therefore it is important to consider its use in future studies (Schober et al., 2018). Another note to consider with regards to PCC is that it does distinguish between background non-specific staining and specific antibody binding, therefore, co-localisation quantification in a whole field of view may be skewed by the presence of background signal.

The organelle marker panel (Chapter 3, Figure 3.4) was selected here with the aim to accurately plot the endocytic pathway, and identify key players involved in membrane trafficking. However, it is important to note that organelle markers are not unique to one

compartment. In fact, a springboard for this study was the misidentification of TGN46-positive vesicles as dTGN rather than endosomes. Therefore, this must be considered when charactering the localisation of NLRP3 to specific organelles based on the expression of membrane marker proteins at these compartments.

6.3.2 The subcellular regulation of the NLRP3 inflammasome

The use of TurboID to investigate the NLRP3 interactome was one that provided high spatial resolution of interacting proteins (TurboID biotinylation radius is approx. 15nm) with efficient labelling following the addition of biotin (Cho et al., 2020). However, one considerable limitation of TurboID is the presence of non-specific biotinylation of proteins within the same subcellular localisation as the bait protein i.e., NLRP3. A possible resolution to this issue is the use of a TurboID only control, not conjugated to NLRP3, that will allow the subtraction of proteins that are non-specifically labelled by TurboID. As discussed previously, conducting these experiments in an immune cell line, as appose to HeLa cells, may more accurately represent the physiological behaviour of NLRP3.

HeLa cells were chosen for lentiviral transduction of NLRP3-TurboID in the initial mass spectrometry experiments here. These cells were selected as I was interested in investigating the subcellular localisation of NLRP3 following NLRP3 activating stimuli that also disrupted endosomal traffic. However, it is important to recognise that because these cells do not naturally express NLRP3 and cannot form an active inflammasome, the interactome determined from these experiments may not be representative of that in a primed and activated macrophage for example. The protocol for lentiviral transduction in THP-1

monocytes has since been optimised. Therefore, transducing THP-1 monocytes, deficient in wild-type NLRP3, with NLRP3-TurboID may be a logical next step to elucidate the NLRP3 interactome under conditions that allow formation of an activate inflammasome.

Ingenuity pathway analysis was used to investigate the subcellular localisation of the protein interactome identified with NLRP3-TurboID (Kramer et al., 2014). Subcellular location is assigned from a database of literature which is curated by QIAGEN; this method of analysis provides both a strength and limitation to this study. As QIAGEN review and curate the literature which subsequently forms the evidence for their findings, this suggests that the results are more robust than a simple gene ontology search carried out by programmes such as STRING (https://string-db.org/). Conversely, for a paper to be included in the database, it must of course be reviewed first, therefore creating a potential delay in new research being part of the database and possibly leading to some important research being missed. Another possible limitation of IPA's subcellular localisation tool is the lack of specificity that it has regarding intracellular compartments. For example, the subcellular location of protein TPD52L2 was determined by IPA as "other cytoplasmic location" and it was only following a manual literature search that TPD52L2 was identified as a marker of intracellular membrane vesicles termed intracellular nanovesicles. Therefore, teaming efficient, high throughput tools such as IPA with a comprehensive investigation of the literature is important.

Finally, it must be considered that although I have concluded here that TPD54 KD in THP-1 monocytes potentiates NLRP3 activation due to a disruption in endocytic traffic, the only read-out currently investigated is IL-1β release (Chapter 4. Figure 5). Therefore, to conclusively reveal that TPD54 KD leads to potentiated inflammasome activation, further

components of NLRP3 inflammasome activation must be studied. These will be explored further in the future directions of this study. In addition, it was a surprising result that all cell lines displayed a trend for an increase in IL-1β release following NLRP3 inflammasome activation. A limitation here may be that knocking down a protein by CRISPR-Cas9 nucleofection may potentiate NLRP3-mediated IL-1β release by an undefined mechanism. The THP-1 WT control used in these experiments also underwent nucleofection, and therefore it is not simply the method of nucleofection that has brought about this response. Activating the NLRP3 inflammasome in a THP-1 monocyte cell line with knockdown of a random protein would be a useful control to determine whether protein knockdown itself affects NLRP3 inflammasome activation.

6.3.3 The intracellular role of pro-IL-1α

As discussed previously, including a TurboID only control is an important factor in proximity labelling experiments to eliminate non-specifically biotinylated proteins. In chapter 5, TurboID alone was used to compare against pro-IL-1α-TurboID, however, a limitation of this experimental design is that TurboID is mostly cytoplasmic, whereas pro-IL-1α-TurboID is primarily localised to the nucleus (Chapter 5. Figure 5.1). Development of a TurboID plasmid with a functional NLS motif may provide a resolution to this issue; nuclear localised TurboID would allow non-specific biotinylated proteins in the nucleus to be subtracted from the analysis. In addition, and as discussed above, the mass spectrometry experiments carried out here were exclusively in HeLa cells which do not express endogenous IL-1α. An important next step in this study is to repeat the investigation of the IL-1α interactome in a more biologically relevant cell line, such as keratinocytes which endogenously express IL-1α. IL-1α

and keratinocytes have been implicated in the pathogenesis of diseases such as skin cancer and therefore may improve the transnationality of this study (Cohen et al., 2015).

The statistical analysis carried out by IPA in determining the p-value of canonical pathways, biological processes and diseases and disorders assumes that all genes inputted for analysis are independent. However, when investigating biological systems, this clearly is not the case, and it is extremely likely that proteins biotinylated by pro-IL-1α-TurboID are structurally and functionally related to each other. Therefore, significance assigned to certain pathways, such as gene expression for example, may be inflated due to the presence of pro-IL-1α in the nucleus. IPA is a very useful tool to carry out efficient and high throughput proteomic analysis, however, the pathways and processes that it deems as significant must be validated experimentally and investigated in reference to the whole biological system.

6.4 Future directions

The overarching aim of chapters 3 and 4 is to investigate the role of endocytic trafficking dysfunction in NLRP3 inflammasome activation. As the final experiments in chapter 4 suggest that TPD54 knockdown potentiates NLRP3 inflammasome activation in THP-1 macrophages, future experiments will look to investigate this mechanism further and characterise the behaviour of TPD54 membrane trafficking in NLRP3 inflammasome activation.

6.4.1 NLPR3 inflammasome activation in THP-1 TPD54 KD cells

Prior to any experiments investigating mechanisms of endocytic traffic that may be at play here, I first need to comprehensively characterise the potentiation of NLRP3 inflammasome

activation observed here. Firstly, I will investigate whether the increase in IL-1β release is an effect of increased inflammasome activation or an increase in pro-IL-1β and NLRP3 expression following LPS-priming. To do this, I will assess cell lysates of untreated and LPS-primed cells for pro-IL-1β and NLRP3. To better characterise NLRP3 inflammasome activation, I will also assess cell lysates for caspase-1 and GSDMD to investigate their cleavage. I will also investigate ASC speck formation as a read-out of NLRP3 inflammasome activation by carrying out an ASC crosslinking assay and assess for ASC oligomers and therefore speck formation.

6.4.2 Endocytic trafficking characterisation in THP-1 TPD54 KD cells

I have suggested here that the mechanisms of NLRP3 inflammasome potentiation in TPD54 KD THP-1 macrophages is due to a disruption in endocytic traffic (Larocque et al., 2020). Therefore, I will use immunocytochemistry and fluorescence microscopy to characterise the endocytic trafficking pathway in these cells. Using the transferrin-488 cycling assay characterised in chapter 3, I will determine whether endosome-plasma membrane trafficking is disrupted in TPD54 KD cells and whether the trafficking disruption induced by nigericin stimulation is exacerbated in these cells. In addition to this, I will also stain for the cycling TGN protein TGN46 in THP-1 TPD54 KD cells, as the presence of TGN46-positive puncta across the cytoplasm is a marker of disrupted endocytic traffic (Lee et al., 2023, Zhang et al., 2023). If TGN46-positive puncta are observed, a polyclonal pool of knockdown cells will be a useful tool here; co-staining cells for TGN46 and TPD54 will allow investigation into whether the formation of TGN46-positive puncta occur in the absence of TPD54.

6.4.3 NLRP3 and PI4P localisation to intracellular nanovesicles

TPD54 has been characterised as a marker of a new class of membrane trafficking vesicles called intracellular nanovesicles (INVs). NLRP3 and PI4P have been characterised to localise to other membrane trafficking compartments including EEA1- and CD63-positive endosomes, and LAMP-1-positive lysosomes (Lee et al., 2023, Zhang et al., 2023). Therefore, investigating whether NLRP3 and/or PI4P localises to TPD54-positive INVs is a novel and interesting avenue of study. Therefore, staining for TPD54 in COS7 NLRP3-mVenus cells, transfected for the PI4P probe, SidM-mCherry, is a logical next step. In addition, I will also investigate the localisation of TPD54-positive compartments in these cells under stimulation with NLRP3 inflammasome activating stimuli.

Chapter 5 looks to investigate the interactome of pro-IL-1α to allow further elucidate its possible intracellular function. This chapter primarily took a bioinformatics approach to this question and therefore, future directions will look to experimentally validate members of the pro-IL-1α interactome and further explore some of the pathways and processes identified by IPA.

6.4.4 Validation of pro-IL-1α interactome

Immunoprecipitation (IP) pull-downs of biotinylated proteins and IL-1α to assess for interaction with proteins in the pro-IL-1α interactome is a necessary first step; specifically focusing on the interaction with HAT proteins, as they may serve as interesting targets for further study. These experiments should be carried out firstly in the HeLa pro-IL-1α-TurboID cell model and pull-downs should be carried out using streptavidin coated beads to assess for biotinylated proteins. Following this, pull-down of IL-1α in more physiologically relevant cells

such as THP-1 monocytes or BMDMs will allow the interaction profile of IL-1α to be characterised further. As discussed, the HAT proteins identified here are also able to acetylate non-histone substrates and so assessing IL-1α pull-downs for acetylated proteins will assess whether IL-1α itself is acetylated.

6.4.5 Nuclear localisation as a mechanism to protect against release

As pro-IL-1α is localised to the nucleus, the functional importance of this mechanism is an area of great interest. Studies following on from this will look to characterise whether nuclear localisation of IL-1α is a mechanism to protect against release and therefore is an important mechanism in immunity and inflammation. The Genome Editing Unit at The University of Manchester have developed a mouse model that expresses a version of IL-1α with a non-functional NLS. Preliminary experiments have shown that the localisation of IL-1α is cytosolic in primary BMDMs from these mice. Further characterisation of the IL-1α immune response in these animals in response infection will allow investigation into the functional importance of nuclear localised IL-1α.

6.5 Concluding remarks

This thesis offers new insight into the subcellular regulation of the NLRP3 inflammasome and pro-IL-1α, and will contribute to further research increasing our understanding of the fundamental biology of inflammation. In turn, this study enhances the prospect to develop therapeutic targets for harmful inflammation in disease. Specifically, I have:

- Identified that endocytic trafficking dysfunction is a common mechanism of a range of NLRP3 inflammasome activating stimuli, and that following stimulation with NLRP3-activating stimuli, NLRP3 localises to PI4P-positive endocytic compartments.
- Characterised the NLRP3 interactome and its subcellular localisation, and subsequently identified that genetic knockdown of TPD54 causes potentiation of NLRP3 inflammasome activation.
- Characterised the pro-IL-1α interactome and identified HAT proteins as a key group of pro-IL-1α interacting proteins suggesting an additional intracellular role of pro-IL-1α.

Appendix 2: Other contributions

Wellens, R., Tapia, V.S., Bennett, H., Adamson, A., Rivers-Auty, J., Green, J.P., Lopez-Castejon, G., Brough, D. and Hoyle, C., 2023. Proximity labelling and evolutionary evidence reveal insights into IL-1α nuclear networks and function. bioRxiv, pp.2023-06.

https://www.biorxiv.org/content/10.1101/2023.06.26.546506v1.abstract

Lee, B., Hoyle, C., **Wellens, R**., Green, J.P., Martin-Sanchez, F., Williams, D.M., Matchett, B.J., Seoane, P.I., Bennett, H., Adamson, A. and Lopez-Castejon, G., 2023. Disruptions in endocytic traffic contribute to the activation of the NLRP3 inflammasome. Science Signaling, 16(773), p.eabm7134.

https://www.science.org/doi/10.1126/scisignal.abm7134

Wellens, R., Matchett, B., Brough, D. and Hoyle, C., 2023. Cellular signaling, molecular activation, and regulation of the NLRP3 inflammasome. In *Inflammasome Biology* (pp. 51-65). Academic Press.

https://www.sciencedirect.com/science/article/pii/B9780323918022000025

Yu, S., Green, J., **Wellens, R**., Lopez-Castejon, G. and Brough, D., 2021. Bafilomycin A1 enhances NLRP3 inflammasome activation in human monocytes independent of lysosomal acidification. *The FEBS Journal*, *288*(10), pp.3186-3196.

https://febs.onlinelibrary.wiley.com/doi/10.1111/febs.15619

References

AFONINA, I. S., TYNAN, G. A., LOGUE, S. E., CULLEN, S. P., BOTS, M., LUTHI, A. U., REEVES, E. P., MCELVANEY, N. G., MEDEMA, J. P., LAVELLE, E. C. & MARTIN, S. J. 2011. Granzyme B-dependent proteolysis acts as a switch to enhance the proinflammatory activity of IL-1alpha. *Mol Cell,* 44**,** 265-78.

AKBAL, A., DERNST, A., LOVOTTI, M., MANGAN, M. S. J., MCMANUS, R. M. & LATZ, E. 2022. How location and cellular signaling combine to activate the NLRP3 inflammasome. *Cell Mol Immunol,* 19**,** 1201-1214.

ANDREI, C., DAZZI, C., LOTTI, L., TORRISI, M. R., CHIMINI, G. & RUBARTELLI, A. 1999. The secretory route of the leaderless protein interleukin 1beta involves exocytosis of endolysosome-related vesicles. *Mol Biol Cell,* 10**,** 1463-75.

BALDWIN, A. G., RIVERS-AUTY, J., DANIELS, M. J. D., WHITE, C. S., SCHWALBE, C. H., SCHILLING, T., HAMMADI, H., JAIYONG, P., SPENCER, N. G., ENGLAND, H., LUHESHI, N. M., KADIRVEL, M., LAWRENCE, C. B., ROTHWELL, N. J., HARTE, M. K., BRYCE, R. A., ALLAN, S. M., EDER, C., FREEMAN, S. & BROUGH, D. 2017. Boron-Based Inhibitors of the NLRP3 Inflammasome. *Cell Chem Biol,* 24**,** 1321-1335 e5.

BALLA, A., KIM, Y. J., VARNAI, P., SZENTPETERY, Z., KNIGHT, Z., SHOKAT, K. M. & BALLA, T. 2008. Maintenance of hormone-sensitive phosphoinositide pools in the plasma membrane requires phosphatidylinositol 4-kinase IIIalpha. *Mol Biol Cell,* 19**,** 711-21.

BALLA, T. 2013. Phosphoinositides: tiny lipids with giant impact on cell regulation. *Physiol Rev,* 93**,** 1019-137.

BAROJA-MAZO, A., COMPAN, V., MARTIN-SANCHEZ, F., TAPIA-ABELLAN, A., COUILLIN, I. & PELEGRIN, P. 2019. Early endosome autoantigen 1 regulates IL-1beta release upon caspase-1 activation independently of gasdermin D membrane permeabilization. *Sci Rep,* 9**,** 5788.

BERTHELOOT, D. & LATZ, E. 2017. HMGB1, IL-1alpha, IL-33 and S100 proteins: dual-function alarmins. *Cell Mol Immunol,* 14**,** 43-64.

BIANCO, F., PRAVETTONI, E., COLOMBO, A., SCHENK, U., MOLLER, T., MATTEOLI, M. & VERDERIO, C. 2005. Astrocyte-derived ATP induces vesicle shedding and IL-1 beta release from microglia. *J Immunol,* 174**,** 7268-77.

BOSSHART, H. & HEINZELMANN, M. 2016. THP-1 cells as a model for human monocytes. *Ann Transl Med,* 4**,** 438.

BRAUN, B. A., MARCOVITZ, A., CAMP, J. G., JIA, R. & BEJERANO, G. 2015. Mx1 and Mx2 key antiviral proteins are surprisingly lost in toothed whales. *Proc Natl Acad Sci U S A,* 112**,** 8036-40.

BROUGH, D., LE FEUVRE, R. A., WHEELER, R. D., SOLOVYOVA, N., HILFIKER, S., ROTHWELL, N. J. & VERKHRATSKY, A. 2003. Ca2+ stores and Ca2+ entry differentially contribute to the release of IL-1 beta and IL-1 alpha from murine macrophages. *J Immunol,* 170**,** 3029-36.

BROUGH, D. & ROTHWELL, N. J. 2007. Caspase-1-dependent processing of pro-interleukin-1beta is cytosolic and precedes cell death. *J Cell Sci,* 120**,** 772-81.

BRYAN, N. B., DORFLEUTNER, A., ROJANASAKUL, Y. & STEHLIK, C. 2009. Activation of inflammasomes requires intracellular redistribution of the apoptotic speck-like protein containing a caspase recruitment domain. *J Immunol,* 182**,** 3173-82.

BURYSKOVA, M., POSPISEK, M., GROTHEY, A., SIMMET, T. & BURYSEK, L. 2004. Intracellular interleukin-1alpha functionally interacts with histone acetyltransferase complexes. *J Biol Chem,* 279**,** 4017-26.

CARROLL, T. P., GREENE, C. M., TAGGART, C. C., BOWIE, A. G., O'NEILL, S. J. & MCELVANEY, N. G. 2005. Viral inhibition of IL-1- and neutrophil elastase-induced inflammatory responses in bronchial epithelial cells. *J Immunol,* 175**,** 7594-601.

CAVALLI, G., COLAFRANCESCO, S., EMMI, G., IMAZIO, M., LOPALCO, G., MAGGIO, M. C., SOTA, J. & DINARELLO, C. A. 2021. Interleukin 1alpha: a comprehensive review on the role of IL-1alpha in the pathogenesis and treatment of autoimmune and inflammatory diseases. *Autoimmun Rev,* 20**,** 102763.

CHANDRA, M., CHIN, Y. K., MAS, C., FEATHERS, J. R., PAUL, B., DATTA, S., CHEN, K. E., JIA, X., YANG, Z., NORWOOD, S. J., MOHANTY, B., BUGARCIC, A., TEASDALE, R. D., HENNE, W. M., MOBLI, M. & COLLINS, B. M. 2019. Classification of the human phox homology (PX) domains based on their phosphoinositide binding specificities. *Nat Commun,* 10**,** 1528.

CHAPMAN, R. E. & MUNRO, S. 1994. Retrieval of TGN proteins from the cell surface requires endosomal acidification. *EMBO J,* 13**,** 2305-12.

CHEN, C., GARCIA-SANTOS, D., ISHIKAWA, Y., SEGUIN, A., LI, L., FEGAN, K. H., HILDICK-SMITH, G. J., SHAH, D. I., COONEY, J. D., CHEN, W., KING, M. J., YIEN, Y. Y., SCHULTZ, I. J., ANDERSON, H., DALTON, A. J., FREEDMAN, M. L., KINGSLEY, P. D., PALIS, J., HATTANGADI, S. M., LODISH, H. F., WARD, D. M., KAPLAN, J., MAEDA, T., PONKA, P. & PAW, B. H. 2013. Snx3 regulates recycling of the transferrin receptor and iron assimilation. *Cell Metab,* 17**,** 343-52.

CHEN, J. & CHEN, Z. J. 2018. PtdIns4P on dispersed trans-Golgi network mediates NLRP3 inflammasome activation. *Nature,* 564**,** 71-76.

CHEN, K. W., MONTELEONE, M., BOUCHER, D., SOLLBERGER, G., RAMNATH, D., CONDON, N. D., VON PEIN, J. B., BROZ, P., SWEET, M. J. & SCHRODER, K. 2018. Noncanonical inflammasome signaling elicits gasdermin D-dependent neutrophil extracellular traps. *Sci Immunol,* 3.

CHIRITOIU, M., BROUWERS, N., TURACCHIO, G., PIROZZI, M. & MALHOTRA, V. 2019. GRASP55 and UPR Control Interleukin-1beta Aggregation and Secretion. *Dev Cell,* 49**,** 145-155 e4.

CHO, K. F., BRANON, T. C., UDESHI, N. D., MYERS, S. A., CARR, S. A. & TING, A. Y. 2020. Proximity labeling in mammalian cells with TurboID and split-TurboID. *Nat Protoc,* 15**,** 3971-3999.

CHRIST, A., LAUTERBACH, M. & LATZ, E. 2019. Western Diet and the Immune System: An Inflammatory Connection. *Immunity,* 51**,** 794-811.

CHU, L. H., INDRAMOHAN, M., RATSIMANDRESEY, R. A., GANGOPADHYAY, A., MORRIS, E. P., MONACK, D. M., DORFLEUTNER, A. & STEHLIK, C. 2018. The oxidized phospholipid oxPAPC protects from septic shock by targeting the non-canonical inflammasome in macrophages. *Nat Commun,* 9**,** 996.

CLANCY, D. M., SULLIVAN, G. P., MORAN, H. B. T., HENRY, C. M., REEVES, E. P., MCELVANEY, N. G., LAVELLE, E. C. & MARTIN, S. J. 2018. Extracellular Neutrophil Proteases Are Efficient Regulators of IL-1, IL-33, and IL-36 Cytokine Activity but Poor Effectors of Microbial Killing. *Cell Rep,* 22**,** 2937-2950.

COENE, E. D., SHAW, M. K. & VAUX, D. J. 2008. Anti-biotin antibodies offer superior organelle-specific labelling of mitochondria over avidin or streptavidin. *Methods Mol Biol,* 418**,** 157-70.

COHEN, I., RIDER, P., VORNOV, E., TOMAS, M., TUDOR, C., WEGNER, M., BRONDANI, L., FREUDENBERG, M., MITTLER, G., FERRANDO-MAY, E., DINARELLO, C. A., APTE, R. N. & SCHNEIDER, R. 2015. IL-1alpha is a DNA damage sensor linking genotoxic stress signaling to sterile inflammation and innate immunity. *Sci Rep,* 5**,** 14756.

COPPE, J. P., DESPREZ, P. Y., KRTOLICA, A. & CAMPISI, J. 2010. The senescence-associated secretory phenotype: the dark side of tumor suppression. *Annu Rev Pathol,* 5**,** 99-118.

DANIELS, M. J., RIVERS-AUTY, J., SCHILLING, T., SPENCER, N. G., WATREMEZ, W., FASOLINO, V., BOOTH, S. J., WHITE, C. S., BALDWIN, A. G., FREEMAN, S., WONG, R., LATTA, C., YU, S., JACKSON, J., FISCHER, N., KOZIEL, V., PILLOT, T., BAGNALL, J., ALLAN, S. M., PASZEK, P., GALEA, J., HARTE, M. K., EDER, C., LAWRENCE, C. B. & BROUGH, D. 2016. Fenamate NSAIDs inhibit the NLRP3 inflammasome and protect against Alzheimer's disease in rodent models. *Nat Commun,* 7**,** 12504.

DAWSON, K. A. & BOLING, J. A. 1983. Monensin-resistant bacteria in the rumens of calves on monensin-containing and unmedicated diets. *Appl Environ Microbiol,* 46**,** 160-4.

DI, A., XIONG, S., YE, Z., MALIREDDI, R. K. S., KOMETANI, S., ZHONG, M., MITTAL, M., HONG, Z., KANNEGANTI, T. D., REHMAN, J. & MALIK, A. B. 2018. The TWIK2 Potassium Efflux Channel in Macrophages Mediates NLRP3 Inflammasome-Induced Inflammation. *Immunity,* 49**,** 56-65 e4.

DIAMOND, C. E., LEONG, K. W. K., VACCA, M., RIVERS-AUTY, J., BROUGH, D. & MORTELLARO, A. 2017. Salmonella typhimurium-induced IL-1 release from primary human monocytes requires NLRP3 and can occur in the absence of pyroptosis. *Sci Rep,* 7**,** 6861.

DIAZ-DEL-OLMO, I., WORBOYS, J., MARTIN-SANCHEZ, F., GRITSENKO, A., AMBROSE, A. R., TANNAHILL, G. M., NICHOLS, E. M., LOPEZ-CASTEJON, G. & DAVIS, D. M. 2021. Internalization of the Membrane Attack Complex Triggers NLRP3 Inflammasome Activation and IL-1beta Secretion in Human Macrophages. *Front Immunol,* 12**,** 720655.

DINARELLO, C. A. 2018. Overview of the IL-1 family in innate inflammation and acquired immunity. *Immunol Rev,* 281**,** 8-27.

DONNINGER, H., CALVISI, D. F., BARNOUD, T., CLARK, J., SCHMIDT, M. L., VOS, M. D. & CLARK, G. J. 2015. NORE1A is a Ras senescence effector that controls the apoptotic/senescent balance of p53 via HIPK2. *J Cell Biol,* 208**,** 777-89.

ELLIOTT, E. I., MILLER, A. N., BANOTH, B., IYER, S. S., STOTLAND, A., WEISS, J. P., GOTTLIEB, R. A., SUTTERWALA, F. S. & CASSEL, S. L. 2018. Cutting Edge: Mitochondrial Assembly of the NLRP3 Inflammasome Complex Is Initiated at Priming. *J Immunol,* 200**,** 3047-3052.

FADEEL, B. & GRZYBOWSKA, E. 2009. HAX-1: a multifunctional protein with emerging roles in human disease. *Biochim Biophys Acta,* 1790**,** 1139-48.

FERNANDES-ALNEMRI, T., YU, J. W., DATTA, P., WU, J. & ALNEMRI, E. S. 2009. AIM2 activates the inflammasome and cell death in response to cytoplasmic DNA. *Nature,* 458**,** 509-13.

FURMAN, D., CAMPISI, J., VERDIN, E., CARRERA-BASTOS, P., TARG, S., FRANCESCHI, C., FERRUCCI, L., GILROY, D. W., FASANO, A., MILLER, G. W., MILLER, A. H., MANTOVANI, A., WEYAND, C. M., BARZILAI, N., GORONZY, J. J., RANDO, T. A., EFFROS, R. B., LUCIA, A., KLEINSTREUER, N. & SLAVICH, G. M. 2019. Chronic inflammation in the etiology of disease across the life span. *Nat Med,* 25**,** 1822-1832.

GAIDT, M. M., EBERT, T. S., CHAUHAN, D., RAMSHORN, K., PINCI, F., ZUBER, S., O'DUILL, F., SCHMID-BURGK, J. L., HOSS, F., BUHMANN, R., WITTMANN, G., LATZ, E., SUBKLEWE,

M. & HORNUNG, V. 2017. The DNA Inflammasome in Human Myeloid Cells Is Initiated by a STING-Cell Death Program Upstream of NLRP3. *Cell,* 171**,** 1110-1124 e18.

GAIDT, M. M., EBERT, T. S., CHAUHAN, D., SCHMIDT, T., SCHMID-BURGK, J. L., RAPINO, F., ROBERTSON, A. A., COOPER, M. A., GRAF, T. & HORNUNG, V. 2016. Human Monocytes Engage an Alternative Inflammasome Pathway. *Immunity,* 44**,** 833-46.

GAIDT, M. M. & HORNUNG, V. 2017. Alternative inflammasome activation enables IL-1beta release from living cells. *Curr Opin Immunol,* 44**,** 7-13.

GBD, G. B. O. D. C. N. 2019. Global Burden of Disease Study 2019. Institute for Health Metrics and Evaluation (IHME).

GOLL, D. E., THOMPSON, V. F., LI, H., WEI, W. & CONG, J. 2003. The calpain system. *Physiol Rev,* 83**,** 731-801.

GREEN, J. P., EL-SHARKAWY, L. Y., ROTH, S., ZHU, J., CAO, J., LEACH, A. G., LIESZ, A., FREEMAN, S. & BROUGH, D. 2023. Discovery of an inhibitor of DNA-driven inflammation that preferentially targets the AIM2 inflammasome. *iScience,* 26**,** 106758.

GREEN, J. P., YU, S., MARTIN-SANCHEZ, F., PELEGRIN, P., LOPEZ-CASTEJON, G., LAWRENCE, C. B. & BROUGH, D. 2018. Chloride regulates dynamic NLRP3-dependent ASC oligomerization and inflammasome priming. *Proc Natl Acad Sci U S A,* 115**,** E9371-E9380.

GRIVENNIKOV, S. I., GRETEN, F. R. & KARIN, M. 2010. Immunity, inflammation, and cancer. *Cell,* 140**,** 883-99.

GROELLY, F. J., FAWKES, M., DAGG, R. A., BLACKFORD, A. N. & TARSOUNAS, M. 2023. Targeting DNA damage response pathways in cancer. *Nat Rev Cancer,* 23**,** 78-94.

GROS, C. J., MISHRA, R., SCHNEIDER, K. S., MEDARD, G., WETTMARSHAUSEN, J., DITTLEIN, D. C., SHI, H., GORKA, O., KOENIG, P. A., FROMM, S., MAGNANI, G., CIKOVIC, T., HARTJES, L., SMOLLICH, J., ROBERTSON, A. A. B., COOPER, M. A., SCHMIDT-SUPPRIAN, M., SCHUSTER, M., SCHRODER, K., BROZ, P., TRAIDL-HOFFMANN, C., BEUTLER, B., KUSTER, B., RULAND, J., SCHNEIDER, S., PEROCCHI, F. & GROSS, O. 2016. K(+) Efflux-Independent NLRP3 Inflammasome Activation by Small Molecules Targeting Mitochondria. *Immunity,* 45**,** 761-773.

GROSS, O., POECK, H., BSCHEIDER, M., DOSTERT, C., HANNESSCHLAGER, N., ENDRES, S., HARTMANN, G., TARDIVEL, A., SCHWEIGHOFFER, E., TYBULEWICZ, V., MOCSAI, A., TSCHOPP, J. & RULAND, J. 2009. Syk kinase signalling couples to the Nlrp3 inflammasome for anti-fungal host defence. *Nature,* 459**,** 433-6.

GROS, O., YAZDI, A. S., THOMAS, C. J., MASIN, M., HEINZ, L. X., GUARDA, G., QUADRONI, M., DREXLER, S. K. & TSCHOPP, J. 2012. Inflammasome activators induce interleukin-1alpha secretion via distinct pathways with differential requirement for the protease function of caspase-1. *Immunity,* 36**,** 388-400.

GROSSMAN, S. R., DEATO, M. E., BRIGNONE, C., CHAN, H. M., KUNG, A. L., TAGAMI, H., NAKATANI, Y. & LIVINGSTON, D. M. 2003. Polyubiquitination of p53 by a ubiquitin ligase activity of p300. *Science,* 300**,** 342-4.

GUO, C., CHI, Z., JIANG, D., XU, T., YU, W., WANG, Z., CHEN, S., ZHANG, L., LIU, Q., GUO, X., ZHANG, X., LI, W., LU, L., WU, Y., SONG, B. L. & WANG, D. 2018. Cholesterol Homeostatic Regulator SCAP-SREBP2 Integrates NLRP3 Inflammasome Activation and Cholesterol Biosynthetic Signaling in Macrophages. *Immunity,* 49**,** 842-856 e7.

HAFNER-BRATKOVIC, I., BENCINA, M., FITZGERALD, K. A., GOLENBOCK, D. & JERALA, R. 2012. NLRP3 inflammasome activation in macrophage cell lines by prion protein fibrils as the source of IL-1beta and neuronal toxicity. *Cell Mol Life Sci,* 69**,** 4215-28.

HALLE, A., HORNUNG, V., PETZOLD, G. C., STEWART, C. R., MONKS, B. G., REINHECKEL, T., FITZGERALD, K. A., LATZ, E., MOORE, K. J. & GOLENBOCK, D. T. 2008. The NALP3 inflammasome is involved in the innate immune response to amyloid-beta. *Nat Immunol,* 9**,** 857-65.

HAMILTON, C. & ANAND, P. K. 2019. Right place, right time: localisation and assembly of the NLRP3 inflammasome. *F1000Res,* 8.

HAMMOND, G. R., MACHNER, M. P. & BALLA, T. 2014. A novel probe for phosphatidylinositol 4-phosphate reveals multiple pools beyond the Golgi. *J Cell Biol,* 205**,** 113-26.

HAMMOND, G. R., SCHIAVO, G. & IRVINE, R. F. 2009. Immunocytochemical techniques reveal multiple, distinct cellular pools of PtdIns4P and PtdIns(4,5)P(2). *Biochem J,* 422**,** 23-35.

HARRISON, M. S., HUNG, C. S., LIU, T. T., CHRISTIANO, R., WALTHER, T. C. & BURD, C. G. 2014. A mechanism for retromer endosomal coat complex assembly with cargo. *Proc Natl Acad Sci U S A,* 111**,** 267-72.

HARTERINK, M., PORT, F., LORENOWICZ, M. J., MCGOUGH, I. J., SILHANKOVA, M., BETIST, M. C., VAN WEERING, J. R. T., VAN HEESBEEN, R., MIDDELKOOP, T. C., BASLER, K., CULLEN, P. J. & KORSWAGEN, H. C. 2011. A SNX3-dependent retromer pathway mediates retrograde transport of the Wnt sorting receptor Wntless and is required for Wnt secretion. *Nat Cell Biol,* 13**,** 914-923.

HE, W. T., WAN, H., HU, L., CHEN, P., WANG, X., HUANG, Z., YANG, Z. H., ZHONG, C. Q. & HAN, J. 2015. Gasdermin D is an executor of pyroptosis and required for interleukin-1beta secretion. *Cell Res,* 25**,** 1285-98.

HE, Y., ZENG, M. Y., YANG, D., MOTRO, B. & NUNEZ, G. 2016. NEK7 is an essential mediator of NLRP3 activation downstream of potassium efflux. *Nature,* 530**,** 354-7.

HENEKA, M. T., KUMMER, M. P., STUTZ, A., DELEKATE, A., SCHWARTZ, S., VIEIRA-SAECKER, A., GRIEP, A., AXT, D., REMUS, A., TZENG, T. C., GELPI, E., HALLE, A., KORTE, M., LATZ, E. & GOLENBOCK, D. T. 2013. NLRP3 is activated in Alzheimer's disease and contributes to pathology in APP/PS1 mice. *Nature,* 493**,** 674-8.

HOFFMAN, H. M., WANDERER, A. A. & BROIDE, D. H. 2001. Familial cold autoinflammatory syndrome: phenotype and genotype of an autosomal dominant periodic fever. *J Allergy Clin Immunol,* 108**,** 615-20.

HOLLEY, C. L. & SCHRODER, K. 2020. The rOX-stars of inflammation: links between the inflammasome and mitochondrial meltdown. *Clin Transl Immunology,* 9**,** e01109.

HORNUNG, V., BAUERNFEIND, F., HALLE, A., SAMSTAD, E. O., KONO, H., ROCK, K. L., FITZGERALD, K. A. & LATZ, E. 2008. Silica crystals and aluminum salts activate the NALP3 inflammasome through phagosomal destabilization. *Nat Immunol,* 9**,** 847-56.

HU, Y. B., DAMMER, E. B., REN, R. J. & WANG, G. 2015. The endosomal-lysosomal system: from acidification and cargo sorting to neurodegeneration. *Transl Neurodegener,* 4**,** 18.

HUANG, B., QIAN, Y., XIE, S., YE, X., CHEN, H., CHEN, Z., ZHANG, L., XU, J., HU, H., MA, S., HEROUX, P., WANG, D., SHEN, H. M., WU, Y. & XIA, D. 2021. Ticagrelor inhibits the NLRP3 inflammasome to protect against inflammatory disease independent of the P2Y(12) signaling pathway. *Cell Mol Immunol,* 18**,** 1278-1289.

HUANG, L. S., HONG, Z., WU, W., XIONG, S., ZHONG, M., GAO, X., REHMAN, J. & MALIK, A. B. 2020. mtDNA Activates cGAS Signaling and Suppresses the YAP-Mediated Endothelial Cell Proliferation Program to Promote Inflammatory Injury. *Immunity,* 52**,** 475-486 e5.

HUEN, M. S. & CHEN, J. 2008. The DNA damage response pathways: at the crossroad of protein modifications. *Cell Res,* 18**,** 8-16.

ICHINOHE, T., YAMAZAKI, T., KOSHIBA, T. & YANAGI, Y. 2013. Mitochondrial protein mitofusin 2 is required for NLRP3 inflammasome activation after RNA virus infection. *Proc Natl Acad Sci U S A,* 110**,** 17963-8.

ITO, A., LAI, C. H., ZHAO, X., SAITO, S., HAMILTON, M. H., APPELLA, E. & YAO, T. P. 2001. p300/CBP-mediated p53 acetylation is commonly induced by p53-activating agents and inhibited by MDM2. *EMBO J,* 20**,** 1331-40.

IYER, S. S., HE, Q., JANCZY, J. R., ELLIOTT, E. I., ZHONG, Z., OLIVIER, A. K., SADLER, J. J., KNEPPER-ADRIAN, V., HAN, R., QIAO, L., EISENBARTH, S. C., NAUSEEF, W. M., CASSEL, S. L. & SUTTERWALA, F. S. 2013. Mitochondrial cardiolipin is required for Nlrp3 inflammasome activation. *Immunity,* 39**,** 311-323.

JANSE, R. J., HOEKSTRA, T., JAGER, K. J., ZOCCALI, C., TRIPEPI, G., DEKKER, F. W. & VAN DIEPEN, M. 2021. Conducting correlation analysis: important limitations and pitfalls. *Clin Kidney J,* 14**,** 2332-2337.

KANG, L., YU, H., YANG, X., ZHU, Y., BAI, X., WANG, R., CAO, Y., XU, H., LUO, H., LU, L., SHI, M. J., TIAN, Y., FAN, W. & ZHAO, B. Q. 2020. Neutrophil extracellular traps released by neutrophils impair revascularization and vascular remodeling after stroke. *Nat Commun,* 11**,** 2488.

KANKKUNEN, P., TEIRILA, L., RINTAHAKA, J., ALENIUS, H., WOLFF, H. & MATIKAINEN, S. 2010. (1,3)-beta-glucans activate both dectin-1 and NLRP3 inflammasome in human macrophages. *J Immunol,* 184**,** 6335-42.

KANNEGANTI, T. D., BODY-MALAPEL, M., AMER, A., PARK, J. H., WHITFIELD, J., FRANCHI, L., TARAPOREWALA, Z. F., MILLER, D., PATTON, J. T., INOHARA, N. & NUNEZ, G. 2006. Critical role for Cryopyrin/Nalp3 in activation of caspase-1 in response to viral infection and double-stranded RNA. *J Biol Chem,* 281**,** 36560-8.

KANY, S., VOLLRATH, J. T. & RELJA, B. 2019. Cytokines in Inflammatory Disease. *Int J Mol Sci,* 20.

KARASAWA, T., KOMADA, T., YAMADA, N., AIZAWA, E., MIZUSHINA, Y., WATANABE, S., BAATARJAV, C., MATSUMURA, T. & TAKAHASHI, M. 2022. Cryo-sensitive aggregation triggers NLRP3 inflammasome assembly in cryopyrin-associated periodic syndrome. *Elife,* 11.

KATO, K., MUKUDAI, Y., MOTOHASHI, H., ITO, C., KAMOSHIDA, S., SHIMANE, T., KONDO, S. & SHIROTA, T. 2017. Opposite effects of tumor protein D (TPD) 52 and TPD54 on oral squamous cell carcinoma cells. *Int J Oncol,* 50**,** 1634-1646.

KATSNELSON, M. & DUBYAK, G. 2013. Cytosolic K+ and extracellular Na+ as regulators of NLRP3 inflammasome activation and the IL-1β secretion response of macrophages to crystalline stimuli. Wiley Online Library.

KATSNELSON, M. A., RUCKER, L. G., RUSSO, H. M. & DUBYAK, G. R. 2015. K+ efflux agonists induce NLRP3 inflammasome activation independently of Ca2+ signaling. *J Immunol,* 194**,** 3937-52.

KAUPPI, M., SIMONSEN, A., BREMNES, B., VIEIRA, A., CALLAGHAN, J., STENMARK, H. & OLKKONEN, V. M. 2002. The small GTPase Rab22 interacts with EEA1 and controls endosomal membrane trafficking. *J Cell Sci,* 115**,** 899-911.

KAWAGUCHI, Y., NISHIMAGI, E., TOCHIMOTO, A., KAWAMOTO, M., KATSUMATA, Y., SOEJIMA, M., KANNO, T., KAMATANI, N. & HARA, M. 2006. Intracellular IL-1alpha-binding proteins contribute to biological functions of endogenous IL-1alpha in systemic sclerosis fibroblasts. *Proc Natl Acad Sci U S A,* 103**,** 14501-6.

KAYAGAKI, N., KORNFELD, O. S., LEE, B. L., STOWE, I. B., O'ROURKE, K., LI, Q., SANDOVAL, W., YAN, D., KANG, J., XU, M., ZHANG, J., LEE, W. P., MCKENZIE, B. S., ULAS, G., PAYANDEH, J., ROOSE-GIRMA, M., MODRUSAN, Z., REJA, R., SAGOLLA, M., WEBSTER, J. D., CHO, V., ANDREWS, T. D., MORRIS, L. X., MIOSGE, L. A., GOODNOW, C. C., BERTRAM, E. M. & DIXIT, V. M. 2021. NINJ1 mediates plasma membrane rupture during lytic cell death. *Nature,* 591**,** 131-136.

KAYAGAKI, N., STOWE, I. B., LEE, B. L., O'ROURKE, K., ANDERSON, K., WARMING, S., CUELLAR, T., HALEY, B., ROOSE-GIRMA, M., PHUNG, Q. T., LIU, P. S., LILL, J. R., LI, H., WU, J., KUMMERFELD, S., ZHANG, J., LEE, W. P., SNIPAS, S. J., SALVESEN, G. S., MORRIS, L. X., FITZGERALD, L., ZHANG, Y., BERTRAM, E. M., GOODNOW, C. C. & DIXIT, V. M. 2015. Caspase-11 cleaves gasdermin D for non-canonical inflammasome signalling. *Nature,* 526**,** 666-71.

KAYAGAKI, N., WARMING, S., LAMKANFI, M., VANDE WALLE, L., LOUIE, S., DONG, J., NEWTON, K., QU, Y., LIU, J., HELDENS, S., ZHANG, J., LEE, W. P., ROOSE-GIRMA, M. & DIXIT, V. M. 2011. Non-canonical inflammasome activation targets caspase-11. *Nature,* 479**,** 117-21.

KELLEY, N., JELTEMA, D., DUAN, Y. & HE, Y. 2019. The NLRP3 Inflammasome: An Overview of Mechanisms of Activation and Regulation. *Int J Mol Sci,* 20.

KIM, B., LEE, Y., KIM, E., KWAK, A., RYOO, S., BAE, S. H., AZAM, T., KIM, S. & DINARELLO, C. A. 2013. The Interleukin-1alpha Precursor is Biologically Active and is Likely a Key Alarmin in the IL-1 Family of Cytokines. *Front Immunol,* 4**,** 391.

KIM, D. I., JENSEN, S. C., NOBLE, K. A., KC, B., ROUX, K. H., MOTAMEDCHABOKI, K. & ROUX, K. J. 2016. An improved smaller biotin ligase for BioID proximity labeling. *Mol Biol Cell,* 27**,** 1188-96.

KIM, S., KIM, S. & RHEE, K. 2011. NEK7 is essential for centriole duplication and centrosomal accumulation of pericentriolar material proteins in interphase cells. *J Cell Sci,* 124**,** 3760-70.

KOBAYASHI, Y., YAMAMOTO, K., SAIDO, T., KAWASAKI, H., OPPENHEIM, J. J. & MATSUSHIMA, K. 1990. Identification of calcium-activated neutral protease as a processing enzyme of human interleukin 1 alpha. *Proc Natl Acad Sci U S A,* 87**,** 5548-52.

KRAMER, A., GREEN, J., POLLARD, J., JR. & TUGENDREICH, S. 2014. Causal analysis approaches in Ingenuity Pathway Analysis. *Bioinformatics,* 30**,** 523-30.

KUTATELADZE, T. G. 2010. Translation of the phosphoinositide code by PI effectors. *Nat Chem Biol,* 6**,** 507-13.

KUTSCH, M., SISTEMICH, L., LESSER, C. F., GOLDBERG, M. B., HERRMANN, C. & COERS, J. 2020. Direct binding of polymeric GBP1 to LPS disrupts bacterial cell envelope functions. *EMBO J,* 39**,** e104926.

LADINSKY, M. S. & HOWELL, K. E. 1992. The trans-Golgi network can be dissected structurally and functionally from the cisternae of the Golgi complex by brefeldin A. *Eur J Cell Biol,* 59**,** 92-105.

LAMKANFI, M. & KANNEGANTI, T. D. 2010. Nlrp3: an immune sensor of cellular stress and infection. *Int J Biochem Cell Biol,* 42**,** 792-5.

LAROCQUE, G., LA-BORDE, P. J., CLARKE, N. I., CARTER, N. J. & ROYLE, S. J. 2020. Tumor protein D54 defines a new class of intracellular transport vesicles. *J Cell Biol,* 219.

LAROCQUE, G. & ROYLE, S. J. 2022. Integrating intracellular nanovesicles into integrin trafficking pathways and beyond. *Cell Mol Life Sci,* 79**,** 335.

LAWRENCE, M., DAUJAT, S. & SCHNEIDER, R. 2016. Lateral Thinking: How Histone Modifications Regulate Gene Expression. *Trends Genet,* 32**,** 42-56.

LEE, B., HOYLE, C., WELLENS, R., GREEN, J. P., MARTIN-SANCHEZ, F., WILLIAMS, D. M., MATCHETT, B. J., SEOANE, P. I., BENNETT, H., ADAMSON, A., LOPEZ-CASTEJON, G., LOWE, M. & BROUGH, D. 2023. Disruptions in endocytic traffic contribute to the activation of the NLRP3 inflammasome. *Sci Signal,* 16**,** eabm7134.

LEE, G. S., SUBRAMANIAN, N., KIM, A. I., AKSENTIJEVICH, I., GOLDBACH-MANSKY, R., SACKS, D. B., GERMAIN, R. N., KASTNER, D. L. & CHAE, J. J. 2012. The calcium-sensing receptor regulates the NLRP3 inflammasome through Ca2+ and cAMP. *Nature,* 492**,** 123-7.

LEE, K. K. & WORKMAN, J. L. 2007. Histone acetyltransferase complexes: one size doesn't fit all. *Nat Rev Mol Cell Biol,* 8**,** 284-95.

LEEMANS, J. C., CASSEL, S. L. & SUTTERWALA, F. S. 2011. Sensing damage by the NLRP3 inflammasome. *Immunol Rev,* 243**,** 152-62.

LERNER, A. G., UPTON, J. P., PRAVEEN, P. V., GHOSH, R., NAKAGAWA, Y., IGBARIA, A., SHEN, S., NGUYEN, V., BACKES, B. J., HEIMAN, M., HEINTZ, N., GREENGARD, P., HUI, S., TANG, Q., TRUSINA, A., OAKES, S. A. & PAPA, F. R. 2012. IRE1alpha induces thioredoxin-interacting protein to activate the NLRP3 inflammasome and promote programmed cell death under irremediable ER stress. *Cell Metab,* 16**,** 250-64.

LI, X., THOME, S., MA, X., AMRUTE-NAYAK, M., FINIGAN, A., KITT, L., MASTERS, L., JAMES, J. R., SHI, Y., MENG, G. & MALLAT, Z. 2017. MARK4 regulates NLRP3 positioning and inflammasome activation through a microtubule-dependent mechanism. *Nat Commun,* 8**,** 15986.

LISTON, A. & MASTERS, S. L. 2017. Homeostasis-altering molecular processes as mechanisms of inflammasome activation. *Nat Rev Immunol,* 17**,** 208-214.

LUHESHI, N. M., MCCOLL, B. W. & BROUGH, D. 2009a. Nuclear retention of IL-1 alpha by necrotic cells: a mechanism to dampen sterile inflammation. *Eur J Immunol,* 39**,** 2973-80.

LUHESHI, N. M., ROTHWELL, N. J. & BROUGH, D. 2009b. The dynamics and mechanisms of interleukin-1alpha and beta nuclear import. *Traffic,* 10**,** 16-25.

LUKENS, J. R., GROSS, J. M. & KANNEGANTI, T. D. 2012. IL-1 family cytokines trigger sterile inflammatory disease. *Front Immunol,* 3**,** 315.

MACKENZIE, A., WILSON, H. L., KISS-TOTH, E., DOWER, S. K., NORTH, R. A. & SURPRENANT, A. 2001. Rapid secretion of interleukin-1beta by microvesicle shedding. *Immunity,* 15**,** 825-35.

MAGUPALLI, V. G., NEGRO, R., TIAN, Y., HAUENSTEIN, A. V., DI CAPRIO, G., SKILLERN, W., DENG, Q., ORNING, P., ALAM, H. B., MALIGA, Z., SHARIF, H., HU, J. J., EVAVOLD, C. L., KAGAN, J. C., SCHMIDT, F. I., FITZGERALD, K. A., KIRCHHAUSEN, T., LI, Y. & WU, H. 2020. HDAC6 mediates an aggresome-like mechanism for NLRP3 and pyrin inflammasome activation. *Science,* 369.

MAMBWE, B., NEO, K., JAVANMARD KHAMENEH, H., LEONG, K. W. K., COLANTUONI, M., VACCA, M., MUIMO, R. & MORTELLARO, A. 2019. Tyrosine Dephosphorylation of ASC Modulates the Activation of the NLRP3 and AIM2 Inflammasomes. *Front Immunol,* 10**,** 1556.

MAN, S. M., KARKI, R., SASAI, M., PLACE, D. E., KESAVARDHANA, S., TEMIROV, J., FRASE, S., ZHU, Q., MALIREDDI, R. K. S., KURIAKOSE, T., PETERS, J. L., NEALE, G., BROWN, S. A., YAMAMOTO, M. & KANNEGANTI, T. D. 2016. IRGB10 Liberates Bacterial Ligands for Sensing by the AIM2 and Caspase-11-NLRP3 Inflammasomes. *Cell,* 167**,** 382-396 e17.

MANGAN, M. S. J., OLHAVA, E. J., ROUSH, W. R., SEIDEL, H. M., GLICK, G. D. & LATZ, E. 2018. Targeting the NLRP3 inflammasome in inflammatory diseases. *Nat Rev Drug Discov,* 17**,** 588-606.

MARIATHASAN, S., WEISS, D. S., NEWTON, K., MCBRIDE, J., O'ROURKE, K., ROOSE-GIRMA, M., LEE, W. P., WEINRAUCH, Y., MONACK, D. M. & DIXIT, V. M. 2006. Cryopyrin activates the inflammasome in response to toxins and ATP. *Nature,* 440**,** 228-32.

MARTIN, S. J. 2016. Cell death and inflammation: the case for IL-1 family cytokines as the canonical DAMPs of the immune system. *FEBS J,* 283**,** 2599-615.

MARTINON, F., PÉTRILLI, V., MAYOR, A., TARDIVEL, A. & TSCHOPP, J. 2006. Gout-associated uric acid crystals activate the NALP3 inflammasome. *Nature,* 440**,** 237-241.

MAYES-HOPFINGER, L., ENACHE, A., XIE, J., HUANG, C. L., KOCHL, R., TYBULEWICZ, V. L. J., FERNANDES-ALNEMRI, T. & ALNEMRI, E. S. 2021. Chloride sensing by WNK1 regulates NLRP3 inflammasome activation and pyroptosis. *Nat Commun,* 12**,** 4546.

MCCARTHY, D. A., RANGANATHAN, A., SUBBARAM, S., FLAHERTY, N. L., PATEL, N., TREBAK, M., HEMPEL, N. & MELENDEZ, J. A. 2013. Redox-control of the alarmin, Interleukin-1alpha. *Redox Biol,* 1**,** 218-25.

MENG, G., ZHANG, F., FUSS, I., KITANI, A. & STROBER, W. 2009. A mutation in the Nlrp3 gene causing inflammasome hyperactivation potentiates Th17 cell-dominant immune responses. *Immunity,* 30**,** 860-74.

MENU, P., MAYOR, A., ZHOU, R., TARDIVEL, A., ICHIJO, H., MORI, K. & TSCHOPP, J. 2012. ER stress activates the NLRP3 inflammasome via an UPR-independent pathway. *Cell Death Dis,* 3**,** e261.

MEUNIER, E., DICK, M. S., DREIER, R. F., SCHURMANN, N., KENZELMANN BROZ, D., WARMING, S., ROOSE-GIRMA, M., BUMANN, D., KAYAGAKI, N., TAKEDA, K., YAMAMOTO, M. & BROZ, P. 2014. Caspase-11 activation requires lysis of pathogen-containing vacuoles by IFN-induced GTPases. *Nature,* 509**,** 366-70.

MIJIT, M., CARACCIOLO, V., MELILLO, A., AMICARELLI, F. & GIORDANO, A. 2020. Role of p53 in the Regulation of Cellular Senescence. *Biomolecules,* 10.

MISUMI, Y., SOHDA, M., YANO, A., FUJIWARA, T. & IKEHARA, Y. 1997. Molecular characterization of GCP170, a 170-kDa protein associated with the cytoplasmic face of the Golgi membrane. *J Biol Chem,* 272**,** 23851-8.

MOLLENHAUER, H. H., MORRE, D. J. & ROWE, L. D. 1990. Alteration of intracellular traffic by monensin; mechanism, specificity and relationship to toxicity. *Biochim Biophys Acta,* 1031**,** 225-46.

MONTELEONE, M., STANLEY, A. C., CHEN, K. W., BROWN, D. L., BEZBRADICA, J. S., VON PEIN, J. B., HOLLEY, C. L., BOUCHER, D., SHAKESPEAR, M. R., KAPETANOVIC, R., ROLFES, V., SWEET, M. J., STOW, J. L. & SCHRODER, K. 2018. Interleukin-1beta Maturation Triggers Its Relocation to the Plasma Membrane for Gasdermin-D-Dependent and -Independent Secretion. *Cell Rep,* 24**,** 1425-1433.

MUNOZ-ESPIN, D. & SERRANO, M. 2014. Cellular senescence: from physiology to pathology. *Nat Rev Mol Cell Biol,* 15**,** 482-96.

MUNOZ-PLANILLO, R., KUFFA, P., MARTINEZ-COLON, G., SMITH, B. L., RAJENDIRAN, T. M. & NUNEZ, G. 2013. K(+) efflux is the common trigger of NLRP3 inflammasome activation by bacterial toxins and particulate matter. *Immunity,* 38**,** 1142-53.

MURAKAMI, T., OCKINGER, J., YU, J., BYLES, V., MCCOLL, A., HOFER, A. M. & HORNG, T. 2012. Critical role for calcium mobilization in activation of the NLRP3 inflammasome. *Proc Natl Acad Sci U S A,* 109**,** 11282-7.

MUSHEGIAN, A. & MEDZHITOV, R. 2001. Evolutionary perspective on innate immune recognition. *J Cell Biol,* 155**,** 705-10.

NAKAHIRA, K., HASPEL, J. A., RATHINAM, V. A., LEE, S. J., DOLINAY, T., LAM, H. C., ENGLERT, J. A., RABINOVITCH, M., CERNADAS, M., KIM, H. P., FITZGERALD, K. A., RYTER, S. W. & CHOI, A. M. 2011. Autophagy proteins regulate innate immune responses by inhibiting the release of mitochondrial DNA mediated by the NALP3 inflammasome. *Nat Immunol,* 12**,** 222-30.

NAKAJIMA, K., NOZAWA, T., MINOWA-NOZAWA, A., TOH, H., YAMADA, S., AIKAWA, C. & NAKAGAWA, I. 2019. RAB30 regulates PI4KB (phosphatidylinositol 4-kinase beta)-dependent autophagy against group A Streptococcus. *Autophagy,* 15**,** 466-477.

NETEA, M. G., BALKWILL, F., CHONCHOL, M., COMINELLI, F., DONATH, M. Y., GIAMARELLOS-BOURBOULIS, E. J., GOLENBOCK, D., GRESNIGT, M. S., HENEKA, M. T., HOFFMAN, H. M., HOTCHKISS, R., JOOSTEN, L. A. B., KASTNER, D. L., KORTE, M., LATZ, E., LIBBY, P., MANDRUP-POULSEN, T., MANTOVANI, A., MILLS, K. H. G., NOWAK, K. L., O'NEILL, L. A., PICKKERS, P., VAN DER POLL, T., RIDKER, P. M., SCHALKWIJK, J., SCHWARTZ, D. A., SIEGMUND, B., STEER, C. J., TILG, H., VAN DER MEER, J. W. M., VAN DE VEERDONK, F. L. & DINARELLO, C. A. 2017. A guiding map for inflammation. *Nat Immunol,* 18**,** 826-831.

NOVAK, J., ZAMOSTNA, B., VOPALENSKY, V., BURYSKOVA, M., BURYSEK, L., DOLECKOVA, D. & POSPISEK, M. 2020. Interleukin-1alpha associates with the tumor suppressor p53 following DNA damage. *Sci Rep,* 10**,** 6995.

O'REGAN, L. & FRY, A. M. 2009. The Nek6 and Nek7 protein kinases are required for robust mitotic spindle formation and cytokinesis. *Mol Cell Biol,* 29**,** 3975-90.

ORLOWSKI, G. M., COLBERT, J. D., SHARMA, S., BOGYO, M., ROBERTSON, S. A. & ROCK, K. L. 2015. Multiple Cathepsins Promote Pro-IL-1beta Synthesis and NLRP3-Mediated IL-1beta Activation. *J Immunol,* 195**,** 1685-97.

PERREGAUX, D. & GABEL, C. A. 1994. Interleukin-1 beta maturation and release in response to ATP and nigericin. Evidence that potassium depletion mediated by these agents is a necessary and common feature of their activity. *J Biol Chem,* 269**,** 15195-203.

PERREGAUX, D. G. & GABEL, C. A. 1998. Post-translational processing of murine IL-1: evidence that ATP-induced release of IL-1 alpha and IL-1 beta occurs via a similar mechanism. *J Immunol,* 160**,** 2469-77.

PÉTRILLI, V., PAPIN, S., DOSTERT, C., MAYOR, A., MARTINON, F. & TSCHOPP, J. 2007. Activation of the NALP3 inflammasome is triggered by low intracellular potassium concentration. *Cell Death Differ,* 14**,** 1583-9.

PIZZIRANI, C., FERRARI, D., CHIOZZI, P., ADINOLFI, E., SANDONA, D., SAVAGLIO, E. & DI VIRGILIO, F. 2007. Stimulation of P2 receptors causes release of IL-1beta-loaded microvesicles from human dendritic cells. *Blood,* 109**,** 3856-64.

PREKERIS, R., KLUMPERMAN, J. & SCHELLER, R. H. 2000. A Rab11/Rip11 protein complex regulates apical membrane trafficking via recycling endosomes. *Mol Cell,* 6**,** 1437-48.

RAHMAN, T., NAGAR, A., DUFFY, E. B., OKUDA, K., SILVERMAN, N. & HARTON, J. A. 2020. NLRP3 Sensing of Diverse Inflammatory Stimuli Requires Distinct Structural Features. *Front Immunol,* 11**,** 1828.

REAVES, B., HORN, M. & BANTING, G. 1993. TGN38/41 recycles between the cell surface and the TGN: brefeldin A affects its rate of return to the TGN. *Mol Biol Cell,* 4**,** 93-105.

REN, L., CHEN, J. & ZHANG, X. 2017. Increased expression of tumor protein D54 is associated with clinical progression and poor prognosis in patients with prostate cancer. *Oncol Lett,* 14**,** 7739-7744.

RIVERS-AUTY, J., DANIELS, M. J. D., COLLIVER, I., ROBERTSON, D. L. & BROUGH, D. 2018. Redefining the ancestral origins of the interleukin-1 superfamily. *Nat Commun,* 9**,** 1156.

ROTH FLACH, R. J. & CZECH, M. P. 2015. NETs and traps delay wound healing in diabetes. *Trends Endocrinol Metab,* 26**,** 451-2.

RUBARTELLI, A., COZZOLINO, F., TALIO, M. & SITIA, R. 1990. A novel secretory pathway for interleukin-1 beta, a protein lacking a signal sequence. *EMBO J,* 9**,** 1503-10.

SANTOS, J. C., BOUCHER, D., SCHNEIDER, L. K., DEMARCO, B., DILUCCA, M., SHKARINA, K., HEILIG, R., CHEN, K. W., LIM, R. Y. H. & BROZ, P. 2020. Human GBP1 binds LPS to initiate assembly of a caspase-4 activating platform on cytosolic bacteria. *Nat Commun,* 11**,** 3276.

SCHMACKE, N. A., O'DUILL, F., GAIDT, M. M., SZYMANSKA, I., KAMPER, J. M., SCHMID-BURGK, J. L., MADLER, S. C., MACKENS-KIANI, T., KOZAKI, T., CHAUHAN, D., NAGL, D., STAFFORD, C. A., HARZ, H., FROHLICH, A. L., PINCI, F., GINHOUX, F., BECKMANN, R., MANN, M., LEONHARDT, H. & HORNUNG, V. 2022. IKKbeta primes inflammasome formation by recruiting NLRP3 to the trans-Golgi network. *Immunity,* 55**,** 2271-2284 e7.

SCHMID-BURGK, J. L., CHAUHAN, D., SCHMIDT, T., EBERT, T. S., REINHARDT, J., ENDL, E. & HORNUNG, V. 2016. A Genome-wide CRISPR (Clustered Regularly Interspaced Short Palindromic Repeats) Screen Identifies NEK7 as an Essential Component of NLRP3 Inflammasome Activation. *J Biol Chem,* 291**,** 103-9.

SCHOBER, P., BOER, C. & SCHWARTE, L. A. 2018. Correlation Coefficients: Appropriate Use and Interpretation. *Anesth Analg,* 126**,** 1763-1768.

SCHONTEICH, E., WILSON, G. M., BURDEN, J., HOPKINS, C. R., ANDERSON, K., GOLDENRING, J. R. & PREKERIS, R. 2008. The Rip11/Rab11-FIP5 and kinesin II complex regulates endocytic protein recycling. *J Cell Sci,* 121**,** 3824-33.

SCHORN, C., FREY, B., LAUBER, K., JANKO, C., STRYSIO, M., KEPPELER, H., GAIPL, U. S., VOLL, R. E., SPRINGER, E., MUNOZ, L. E., SCHETT, G. & HERRMANN, M. 2011. Sodium overload and water influx activate the NALP3 inflammasome. *J Biol Chem,* 286**,** 35-41.

SEOANE, P. I., LEE, B., HOYLE, C., YU, S., LOPEZ-CASTEJON, G., LOWE, M. & BROUGH, D. 2020. The NLRP3-inflammasome as a sensor of organelle dysfunction. *J Cell Biol,* 219.

SHI, C. & PAMER, E. G. 2011. Monocyte recruitment during infection and inflammation. *Nat Rev Immunol,* 11**,** 762-74.

SHI, D., POP, M. S., KULIKOV, R., LOVE, I. M., KUNG, A. L. & GROSSMAN, S. R. 2009. CBP and p300 are cytoplasmic E4 polyubiquitin ligases for p53. *Proc Natl Acad Sci U S A,* 106**,** 16275-80.

SHI, F., YANG, L., KOUADIR, M., YANG, Y., WANG, J., ZHOU, X., YIN, X. & ZHAO, D. 2012. The NALP3 inflammasome is involved in neurotoxic prion peptide-induced microglial activation. *J Neuroinflammation,* 9**,** 73.

SHI, H., WANG, Y., LI, X., ZHAN, X., TANG, M., FINA, M., SU, L., PRATT, D., BU, C. H., HILDEBRAND, S., LYON, S., SCOTT, L., QUAN, J., SUN, Q., RUSSELL, J., ARNETT, S., JUREK, P., CHEN, D., KRAVCHENKO, V. V., MATHISON, J. C., MORESCO, E. M., MONSON, N. L., ULEVITCH, R. J. & BEUTLER, B. 2016. NLRP3 activation and mitosis are mutually

exclusive events coordinated by NEK7, a new inflammasome component. *Nat Immunol,* 17**,** 250-8.

SHI, J., ZHAO, Y., WANG, K., SHI, X., WANG, Y., HUANG, H., ZHUANG, Y., CAI, T., WANG, F. & SHAO, F. 2015. Cleavage of GSDMD by inflammatory caspases determines pyroptotic cell death. *Nature,* 526**,** 660-5.

SHI, J., ZHAO, Y., WANG, Y., GAO, W., DING, J., LI, P., HU, L. & SHAO, F. 2014. Inflammatory caspases are innate immune receptors for intracellular LPS. *Nature,* 514**,** 187-92.

SHIMADA, K., CROTHER, T. R., KARLIN, J., DAGVADORJ, J., CHIBA, N., CHEN, S., RAMANUJAN, V. K., WOLF, A. J., VERGNES, L., OJCIUS, D. M., RENTSENDORJ, A., VARGAS, M., GUERRERO, C., WANG, Y., FITZGERALD, K. A., UNDERHILL, D. M., TOWN, T. & ARDITI, M. 2012. Oxidized mitochondrial DNA activates the NLRP3 inflammasome during apoptosis. *Immunity,* 36**,** 401-14.

SHVEDUNOVA, M. & AKHTAR, A. 2022. Modulation of cellular processes by histone and non-histone protein acetylation. *Nat Rev Mol Cell Biol,* 23**,** 329-349.

SUBRAMANIAN, N., NATARAJAN, K., CLATWORTHY, M. R., WANG, Z. & GERMAIN, R. N. 2013. The adaptor MAVS promotes NLRP3 mitochondrial localization and inflammasome activation. *Cell,* 153**,** 348-61.

SWANSON, K. V., DENG, M. & TING, J. P. 2019. The NLRP3 inflammasome: molecular activation and regulation to therapeutics. *Nat Rev Immunol,* 19**,** 477-489.

SWANTON, T., BESWICK, J. A., HAMMADI, H., MORRIS, L., WILLIAMS, D., DE CESCO, S., EL-SHARKAWY, L., YU, S., GREEN, J., DAVIS, J. B., LAWRENCE, C. B., BROUGH, D. & FREEMAN, S. 2020. Selective inhibition of the K(+) efflux sensitive NLRP3 pathway by Cl(-) channel modulation. *Chem Sci,* 11**,** 11720-11728.

TAN, J. X. & FINKEL, T. 2022. A phosphoinositide signalling pathway mediates rapid lysosomal repair. *Nature,* 609**,** 815-821.

TANG, T., LANG, X., XU, C., WANG, X., GONG, T., YANG, Y., CUI, J., BAI, L., WANG, J., JIANG, W. & ZHOU, R. 2017. CLICs-dependent chloride efflux is an essential and proximal upstream event for NLRP3 inflammasome activation. *Nat Commun,* 8**,** 202.

TAPIA, V. S., DANIELS, M. J. D., PALAZON-RIQUELME, P., DEWHURST, M., LUHESHI, N. M., RIVERS-AUTY, J., GREEN, J., REDONDO-CASTRO, E., KALDIS, P., LOPEZ-CASTEJON, G. & BROUGH, D. 2019. The three cytokines IL-1beta, IL-18, and IL-1alpha share related but distinct secretory routes. *J Biol Chem,* 294**,** 8325-8335.

TAPIA-ABELLAN, A., ANGOSTO-BAZARRA, D., ALARCON-VILA, C., BANOS, M. C., HAFNER-BRATKOVIC, I., OLIVA, B. & PELEGRIN, P. 2021. Sensing low intracellular potassium by NLRP3 results in a stable open structure that promotes inflammasome activation. *Sci Adv,* 7**,** eabf4468.

THOMAS, P. D., EBERT, D., MURUGANUJAN, A., MUSHAYAHAMA, T., ALBOU, L. P. & MI, H. 2022. PANTHER: Making genome-scale phylogenetics accessible to all. *Protein Sci,* 31**,** 8-22.

TROTTER, K. W. & ARCHER, T. K. 2007. Nuclear receptors and chromatin remodeling machinery. *Mol Cell Endocrinol,* 265-266**,** 162-7.

TSUCHIYA, K., HOSOJIMA, S., HARA, H., KUSHIYAMA, H., MAHIB, M. R., KINOSHITA, T. & SUDA, T. 2021. Gasdermin D mediates the maturation and release of IL-1alpha downstream of inflammasomes. *Cell Rep,* 34**,** 108887.

TSUJIMOTO, K., JO, T., NAGIRA, D., KONAKA, H., PARK, J. H., YOSHIMURA, S. I., NINOMIYA, A., SUGIHARA, F., HIRAYAMA, T., ITOTAGAWA, E., MATSUZAKI, Y., TAKAICHI, Y., AOKI, W., SAITA, S., NAKAMURA, S., BALLABIO, A., NADA, S., OKADA, M., TAKAMATSU, H. &

KUMANOGOH, A. 2023. The lysosomal Ragulator complex activates NLRP3 inflammasome in vivo via HDAC6. *EMBO J,* 42**,** e111389.

TYANOVA, S., TEMU, T., SINITCYN, P., CARLSON, A., HEIN, M. Y., GEIGER, T., MANN, M. & COX, J. 2016. The Perseus computational platform for comprehensive analysis of (prote)omics data. *Nat Methods,* 13**,** 731-40.

VERHOEF, P. A., KERTESY, S. B., LUNDBERG, K., KAHLENBERG, J. M. & DUBYAK, G. R. 2005. Inhibitory effects of chloride on the activation of caspase-1, IL-1beta secretion, and cytolysis by the P2X7 receptor. *J Immunol,* 175**,** 7623-34.

VIGANO, E., DIAMOND, C. E., SPREAFICO, R., BALACHANDER, A., SOBOTA, R. M. & MORTELLARO, A. 2015. Human caspase-4 and caspase-5 regulate the one-step non-canonical inflammasome activation in monocytes. *Nat Commun,* 6**,** 8761.

WALDO, G. S., STANDISH, B. M., BERENDZEN, J. & TERWILLIGER, T. C. 1999. Rapid protein-folding assay using green fluorescent protein. *Nat Biotechnol,* 17**,** 691-5.

WANDEL, M. P., KIM, B. H., PARK, E. S., BOYLE, K. B., NAYAK, K., LAGRANGE, B., HEROD, A., HENRY, T., ZILBAUER, M., ROHDE, J., MACMICKING, J. D. & RANDOW, F. 2020. Guanylate-binding proteins convert cytosolic bacteria into caspase-4 signaling platforms. *Nat Immunol,* 21**,** 880-891.

WANG, W., HU, D., WU, C., FENG, Y., LI, A., LIU, W., WANG, Y., CHEN, K., TIAN, M., XIAO, F., ZHANG, Q., SHEREEN, M. A., CHEN, W., PAN, P., WAN, P., WU, K. & WU, J. 2020. STING promotes NLRP3 localization in ER and facilitates NLRP3 deubiquitination to activate the inflammasome upon HSV-1 infection. *PLoS Pathog,* 16**,** e1008335.

WARNATSCH, A., IOANNOU, M., WANG, Q. & PAPAYANNOPOULOS, V. 2015. Inflammation. Neutrophil extracellular traps license macrophages for cytokine production in atherosclerosis. *Science,* 349**,** 316-20.

WERMAN, A., WERMAN-VENKERT, R., WHITE, R., LEE, J. K., WERMAN, B., KRELIN, Y., VORONOV, E., DINARELLO, C. A. & APTE, R. N. 2004. The precursor form of IL-1alpha is an intracrine proinflammatory activator of transcription. *Proc Natl Acad Sci U S A,* 101**,** 2434-9.

WESSENDORF, J. H., GARFINKEL, S., ZHAN, X., BROWN, S. & MACIAG, T. 1993. Identification of a nuclear localization sequence within the structure of the human interleukin-1 alpha precursor. *J Biol Chem,* 268**,** 22100-4.

WIGGINS, K. A., PARRY, A. J., CASSIDY, L. D., HUMPHRY, M., WEBSTER, S. J., GOODALL, J. C., NARITA, M. & CLARKE, M. C. H. 2019. IL-1alpha cleavage by inflammatory caspases of the noncanonical inflammasome controls the senescence-associated secretory phenotype. *Aging Cell,* 18**,** e12946.

XIE, C. B., QIN, L., LI, G., FANG, C., KIRKILES-SMITH, N. C., TELLIDES, G., POBER, J. S. & JANE-WIT, D. 2019. Complement Membrane Attack Complexes Assemble NLRP3 Inflammasomes Triggering IL-1 Activation of IFN-gamma-Primed Human Endothelium. *Circ Res,* 124**,** 1747-1759.

XIE, S., BAHL, K., REINECKE, J. B., HAMMOND, G. R., NASLAVSKY, N. & CAPLAN, S. 2016. The endocytic recycling compartment maintains cargo segregation acquired upon exit from the sorting endosome. *Mol Biol Cell,* 27**,** 108-26.

XU, Y., HORTSMAN, H., SEET, L., WONG, S. H. & HONG, W. 2001. SNX3 regulates endosomal function through its PX-domain-mediated interaction with PtdIns(3)P. *Nat Cell Biol,* 3**,** 658-66.

YANG, Y., WANG, H., KOUADIR, M., SONG, H. & SHI, F. 2019. Recent advances in the mechanisms of NLRP3 inflammasome activation and its inhibitors. *Cell Death Dis,* 10**,** 128.

ZAMOSTNA, B., NOVAK, J., VOPALENSKY, V., MASEK, T., BURYSEK, L. & POSPISEK, M. 2012. N-terminal domain of nuclear IL-1alpha shows structural similarity to the C-terminal domain of Snf1 and binds to the HAT/core module of the SAGA complex. *PLoS One,* 7**,** e41801.

ZANONI, I., TAN, Y., DI GIOIA, M., BROGGI, A., RUAN, J., SHI, J., DONADO, C. A., SHAO, F., WU, H., SPRINGSTEAD, J. R. & KAGAN, J. C. 2016. An endogenous caspase-11 ligand elicits interleukin-1 release from living dendritic cells. *Science,* 352**,** 1232-6.

ZHANG, Y. & SEEMANN, J. 2021. Rapid degradation of GRASP55 and GRASP65 reveals their immediate impact on the Golgi structure. *J Cell Biol,* 220.

ZHANG, Z., MESZAROS, G., HE, W. T., XU, Y., DE FATIMA MAGLIARELLI, H., MAILLY, L., MIHLAN, M., LIU, Y., PUIG GAMEZ, M., GOGINASHVILI, A., PASQUIER, A., BIELSKA, O., NEVEN, B., QUARTIER, P., AEBERSOLD, R., BAUMERT, T. F., GEORGEL, P., HAN, J. & RICCI, R. 2017. Protein kinase D at the Golgi controls NLRP3 inflammasome activation. *J Exp Med,* 214**,** 2671-2693.

ZHANG, Z., VENDITTI, R., RAN, L., LIU, Z., VIVOT, K., SCHURMANN, A., BONIFACINO, J. S., DE MATTEIS, M. A. & RICCI, R. 2023. Distinct changes in endosomal composition promote NLRP3 inflammasome activation. *Nat Immunol,* 24**,** 30-41.

ZHENG, Y., HUMPHRY, M., MAGUIRE, J. J., BENNETT, M. R. & CLARKE, M. C. 2013. Intracellular interleukin-1 receptor 2 binding prevents cleavage and activity of interleukin-1alpha, controlling necrosis-induced sterile inflammation. *Immunity,* 38**,** 285-95.

ZHONG, Z., LIANG, S., SANCHEZ-LOPEZ, E., HE, F., SHALAPOUR, S., LIN, X. J., WONG, J., DING, S., SEKI, E., SCHNABL, B., HEVENER, A. L., GREENBERG, H. B., KISSELEVA, T. & KARIN, M. 2018. New mitochondrial DNA synthesis enables NLRP3 inflammasome activation. *Nature,* 560**,** 198-203.

ZHOU, R., YAZDI, A. S., MENU, P. & TSCHOPP, J. 2011. A role for mitochondria in NLRP3 inflammasome activation. *Nature,* 469**,** 221-5.

ZHUANG, Y., LY, R. C., FRAZIER, C. V., YU, J., QIN, S., FAN, X. Y., GOETZ, M. P., BOUGHEY, J. C., WEINSHILBOUM, R. & WANG, L. 2019. The novel function of tumor protein D54 in regulating pyruvate dehydrogenase and metformin cytotoxicity in breast cancer. *Cancer Metab,* 7**,** 1.